2014-09-30

Characterization and Asphaltene Precipitation Modeling of Native and Reacted Crude Oils

Powers, Diana Paola

UNIVERSITY OF CALGARY

Characterization and Asphaltene Precipitation Modeling of Native and Reacted Crude Oils

by

Diana Paola Powers

A THESIS
SUBMITTED TO THE FACULTY OF GRADUATE STUDIES
IN PARTIAL FULFILMENT OF THE REQUIREMENTS FOR THE
DEGREE OF DOCTOR OF PHILOSOPHY

DEPARTMENT OF CHEMICAL AND PETROLEUM ENGINEERING

CALGARY, ALBERTA
SEPTEMBER, 2014

Abstract

The prediction and mitigation of asphaltene precipitation is an ongoing issue in upstream operations with native oils and in refinery processes of fluids from thermocracking and hydrocracking processes. Asphaltenes can precipitate with changes in pressure, temperature and composition, promoting problems with deposition and fouling during crude oil operations. Fouling problems are a key concern in the oil industry because of their associated cost due to shut downs that decrease production and increase cost for maintenance for cleaning or replacing equipment. Hence, reliable methods are needed to predict asphaltene precipitation at different conditions during upstream and downstream crude oil operations.

The modified regular solution approach (RSM) has been successfully applied to predict asphaltene precipitation from native oils or upstream processes. This approach requires mole fractions, molar volumes, and solubility parameters for the pseudo-components representing the crude oil mixture. The pseudo-components used in the RSM, based on a solubility fractionation method (modified ASTM D4124 technique), are namely saturates, aromatics, resins, and asphaltenes (SARA). SARA fractionation applies to heavy oils and bitumens which do not have significant amounts of volatile compounds distillable at atmospheric pressure. However, the reactions in refinery processes convert a significant amount of the bitumen and heavy oil into lighter compounds creating a significant amount of distillables in the product streams. These reactions also alter the chemical structure of the crude oil and, therefore, the properties and correlations used in the RSM must be modified for these oils.

The objective of this thesis is to characterize several native and reacted oils and develop a general model for asphaltene precipitation from both native and reacted oils using the standard SARA characterization method for the heavy fraction and distillation assays for the lighter fraction of the oils. The oils investigated included native, thermocracked (*in situ* converted and visbreaker samples), and hydrocracked samples.

Each of the distillable fractions and SARA fractions were characterized in detail to identify the changes with reaction in comparison with native oils and to estimate the properties required for

the regular solution model. Properties including densities, molecular weight, and solubilities were measured for the SAR fractions. Asphaltenes tend to self-associate and form nano-aggregates and, therefore, a more detailed characterization was required to determine the asphaltene property distributions. Molecular weight and density distributions of asphaltenes in toluene were obtained from a previous study. Solubility parameter distributions were determined by fitting the RSM to asphaltene precipitation yield data measured for "pure" asphaltenes in mixtures of n-heptane and toluene (heptol). Yield data was also measured for the heavy fractions of the oils and whole oils diluted with *n*-heptane and used to tune the model.

The updated model is applicable to both native and reacted oils and includes a new correlation for the solubility parameter of the distillables as a function of their boiling point, and new asphaltene density and solubility parameter correlations, as a function of mass fraction and molecular weight, respectively. The required input data are: a distillation assay of the oil, SARA assay of the non-distillable residue, and density of the asphaltenes. Distillables, if present, are represented with 5 pseudo-components which are added to the SARA characterization. The density and molecular weight of the saturates, aromatics and Resins (SAR) fractions can be estimated from average values from this study. The asphaltene nano-aggregate molecular weight distribution in the crude oil cannot be measured or estimated *a priori* and is represented with a gamma distribution which requires the average molecular weight of asphaltenes nano-aggregates and the distribution shape factor. The two unknown molecular weight distribution parameters are found by tuning the model to fit the heavy oil (or heavy fraction) solubility data. Once the model is tuned to fit the solubility data of the heavy fraction of the oil, the model predicts the whole crude oil (distillables + SARA) stability.

The model and the property correlations developed in this project can potentially be implemented in a simulation software to predict asphaltene precipitation for different crude oil samples. A predictive model for asphaltene precipitation is an important tool for production and refinery engineers to find operating conditions that avoid asphaltene precipitation and the consequent lost production and increased costs from fouling and plugging of production and refinery equipment. Additionally, the characterization data for the pseudo-components of native and reacted oils can

be used to develop models for other fluid modeling applications including property correlations and fouling models.

Acknowledgements

I would like to express my sincere and deepest gratitude to my supervisor, Dr. H.W. Yarranton for his excellent guidance, encouragement and valuable advice during my studies; there are no words to describe his enormous unconditional support. I also want to thank Ms. Elaine Baydak for all of her assistance, help, support and invaluable words not only as a coworker but also as a friend; additionally, all of her help with extra collection of experimental data. Thanks to Florian Schoeggl for his extra help anytime I asked for it. Thanks to the summer students that contributed to this work, Nick Dalgliesh, Jeff Horton, Lana Huynh and Andrezza Ribeiro. I also thank the Master students, now graduated, that participated in this project: Diana Barrera, Jane Okafor and Hassan Sadeghi contributed to different aspects and during different stages of this project. I am also grateful to the Asphaltene and Emulsion Research members at the University of Calgary.

I also want to thank Shell Global Solutions International for the financial support. Special thanks to Dr. Frans van den Berg for his valuable discussions, contributions and support during the development of this project. I also thank Zhongxin Zuo from Shell Global, Cecile Siewe, Michael Zenaitis, Xiaohui Zhang and Haiyong Cai from Shell Canada who collaborated in this project by organizing and sending samples, providing discussions and feedback and with the elemental analysis required for some of the samples or fractions.

Finally, I would like to thank to my family, especially my mom, Marlene Gonzalez, my husband, Tyler Powers and my sister, Carolina Ortiz who were always encouraging and supporting me throughout my studies

Dedication

Dedicada a mi mami, Marlene Gonzalez; mi esposo, Tyler Powers, y mi futuro hijo (Noviembre 2014)

Table of Contents

List of Tables

List of Figures

Nomenclature

Symbols

A	Coefficient in VPO calibration equation
a	Constant
B	Bitumen
b	Fitting Parameter
C	Solute concentration
cP	Centipoise
C5	*n*-pentane
C7	*n*-heptane
dJ	Deci Joules
E	Voltage
f	Fugacity
FRI	Function of the refraction index (n) defined as follows, $\left(\frac{n^2-1}{n^2+2}\right)$.
g	grams
h	Planck's constant
H	Heptane volume fraction
ΔH_V	Enthalpy of vaporization
K	VPO calibration constant in Eq. 3-1, Equilibrium ratio in Eq.4-7 and association constant in Eq 4-22.
Kg	Kilograms
MPa	Mega Pascals
MW	Molecular Weight
n_D	Refractive index measured at Sodium D-line
N_a	Avogadro's number
P_c	Critical pressure

R	Universal gas constant
r	Distance between molecules
SG	Specific gravity
SR	Short residue – Vacuum residue from refinery process
T	Temperature
T_b	Boiling point temperature
T_c	Critical temperature
V	Voltage
VB	Vacuum bottoms or vacuum residue
v	Molar volume
w	mass fraction
x	Mole fraction

Greek Letters

α	Polarizability
α	Shape factor of the Gamma Distribution
β_{12}	Binary interaction parameter between components 1 and 2
γ	Activity coefficient
Δ	Difference
δ	Solubility Parameter
π	Mathematical constant (3.1416)
ρ	Density
φ	Intermolecular potential energy function
ϕ	Volume fraction

Subscripts

$_A$	Asphaltenes
$_{aro}$	Aromatics
$_{avg}$	Average
$_b$	Boiling point

H	Heavy
L	Light
mono	Monomer
r	reduced
s	Solvent
sat	saturates
T	Temperature
v	Vaporization

Superscripts

°	Standard state
h	Heavy liquid phase
l	Light liquid phase
ppt	Precipitated
s	Solution
V	Vaporization
T	Temperature

Abbreviations

AAD	Average absolute deviation
ADC	Advance Distillation Curve
API	American Petroleum Institute
AR	Atmospheric residue
AARD	Average absolute relative deviation
ARD	Average relative deviation
ASTM	American Society for Testing Materials
AT	Atmospheric residue from refinery process.
B	Bitumen
CPA	Cubic plus association
DB	Diluted bitumen
DCB	o-Dichlorobenzene

DCM	Dichloromehtane
DVFA	Deep Vacuum Fractionation Apparatus
EOS	Equation of state
ELSD	Evaporative light scattering detector
FRI	Function of the refractive index
Heptol	Solvent mixture of *n*-heptane and toluene
HNMR	High proton nuclear magnetic resonance spectroscopy
HOS B	Heavy oil stripper bottoms
H/C	Hydrogen to carbon atomic ratio
LC-Fining	Ebullated bed hydrocracking processes by Chevron Lummus Global.
MN	Methylnaphthalene
NIST	National Institute of Standards and Technology
PAH's	Poly-aromatic hydrocarbons
PDF	Probability density function
PIONA	*n*-paraffins, *iso*-paraffins, olefins, naphthene and aromatics
RCF	Relative centrifugal force
RICO	Ruthenium ions catalyzed oxidation
RSM	Regular Solution Model
SAFT	Statistical associating fluid theory
SANS	Small angle neutron scattering
SAR	Saturates, aromatics and resins
SARA	Saturates, aromatics, resins and asphaltenes
SBD	Spinning band distillation
SR	Short residue
TBP	True boiling point
TI	Toluene insolubles
VB	Vacuum bottoms
VPO	Vapour pressure osmometer
WC	Western Canada
XANES	X-ray absorption near-edge spectroscopy

Chapter One: Introduction

1.1 Overview

As conventional oil reserves have depleted over the past few decades, refineries have been adapting their processes to treat heavy oils, bitumen, blends and heavy residues feedstocks (Huc, 2011). These feedstocks have a high content of asphaltenes, the heaviest and most aromatic fraction of crude oils. Asphaltenes can precipitate due to changes in pressure, temperature, and composition. Crude oil production and refinery process streams undergo changes in these conditions creating the potential for asphaltene precipitation leading to the formation of deposits which foul production and refinery equipment (Macchietto *et al*., 2011). The associated loss of production time to clean or replace equipment is a significant cost for the oil industry. Hence, there is an ongoing incentive to understand and model asphaltene precipitation in order to avoid or mitigate its effects during crude oil operations including refinery conversion processes such as visbreakers and hydrocrackers which are fed with heavy feedstocks and resdiues with high asphaltene content.

Asphaltene precipitation has been intensely studied and several thermodynamic precipitation models have been developed for upstream operation; that is, for native oils that have not been processed or converted. In particular, the regular solution approach, which is a thermodynamic model to predict/describe phase behaviour of mixtures, in this case a liquid-liquid equilibrium, has been successfully used to model asphaltene precipitation from native oils, live oils, and blends of native oils (Akbarzadeh *et al.*, 2005; Tharanivasan *et al.*, 2011). As with all thermodynamic phase behavior models, the oil must first be characterized into pseudo-components representing the distribution of physical properties in the oil. The regular solution model requires mole fractions, molar volumes, and solubility parameters for each pseudo-component. These properties have been measured and correlated for native heavy oils (Akbarzadeh *et al*., 2005; Alboudwarej *et al.*, 2003) but the model has not been tested on converted crude oils.

There are two major challenges in applying the model to processed crude oils: 1) the characterization of distillable components; 2) chemical alterations from reactive processes. Unlike

heavy oils, converted oils contain significant amounts of light ends or distillables. To date, most oil characterizations for the regular solution model have been based on SARA (saturates, aromatics, resins and asphaltenes) assays. The SARA fractionation methodology is exclusively applied to heavy fractions (bitumen or heavy residues) with no volatiles; otherwise, high losses and errors are introduced into the procedure. Some progress has been made in characterizing the volatile fraction of a live oil using gas chromatographic assays (Tharanivasan *et al.*, 2011) although this approach has not been rigorously tested. The characterization of distillables for a regular solution model based on a distillation assay has not yet been attempted. A methodology is required to combine a conventional characterization of distillables with the SARA-based characterization to model asphaltene precipitation for oils with significant amounts of light ends.

During thermocracking refinery processes, crude oils are exposed to high temperatures causing thermocracking reactions which break some crude oil molecules into smaller molecules. Hydrocracking processes crack (break chemical bounds) and introduce hydrogen into the crude oil. All of the SARA fractions can undergo cracking reactions to a higher or lesser extent altering the original properties of each fraction. For instance, conversion processes decrease the molecular weight and increase the aromaticity (decrease the H/C ratio) of asphaltenes (Trejo *et al.*, 2007). Therefore, the property correlations that have been developed for the SARA fractions from native oils will not apply to the reacted refinery streams. A more comprehensive set of property correlations that include the effect of reaction is required to extend the model to converted oils.

1.2 Objectives

The main objectives of this thesis are to measure asphaltene precipitation from upstream (non-reactive) and downstream (reactive) processes and to adapt the regular solution based characterization and modeling methodology previously developed for upstream native petroleum to reacted oils. Specific objectives of this thesis are to:

1. Measure asphaltene precipitation from native and reacted crude oils.
2. Develop a characterization methodology for downstream fluids which combines traditional characterization methods such as distillation assays for the light components and SARA fractionation for the residua.

3. Develop property distributions and correlations (as applicable) for asphaltenes from native and reacted oils. Note, asphaltenes self-associate and the property distributions of the aggregated system are required for the regular solution model.
    a. Determine the asphaltene molecular weight and density distributions based on previously collected molecular weight and density data of asphaltene solubility cuts.
    b. Since the asphaltene aggregate size (apparent molecular weight) depends on temperature, determine and develop a correlation for the effect of temperature on the aggregated molecular weight of asphaltenes.
    c. Determine the asphaltene solubility parameters by fitting the regular solution model to asphaltene solubility data. Develop a correlation for the solubility parameter of asphaltenes that applies to both reacted and native samples.
4. Determine and correlate (as applicable) the properties of SAR (saturate, aromatic, resin) fractions from the distillation residue of native and reacted oils.
    a. Perform measurements to complete an existing dataset of molecular weights and densities of the SAR fractions from reacted oils.
    b. Determine the solubility parameter of the SAR fractions by fitting the regular solution model to asphaltene solubility data from solutions including the SAR fractions.
    c. Identify the main changes in SARA properties (density, molecular weight, solubility parameter, refractive index and elemental analysis) due to reaction processes.
5. Characterize the distillable fraction (where applicable) from reacted and native crude oils using standard distillation assays.
    a. Measure the distillation assays and divide into pseudo-components of known boiling point.
    b. Use, adapt, or develop correlations for the molecular weight, density, and solubility parameter of each pseudo-component.

6. Adapt/develop the thermodynamic model based on the regular solution approach to predict asphaltene stability for converted (and native) oils using the characterization data and proposed methodology.
7. Complete: a) an extensive experimental database of native and reacted oils properties that can be used to characterize fluids for property and asphaltene precipitation modeling in production or refining processes, and; b) a prototype software program that can be used or adapted by refinery, production, or flow assurance engineers in process simulators to predict (or semi-predict) asphaltene precipitation from native or reacted oils.

Note, this thesis is the culmination of a larger project involving three Masters students: Diana Barrera, Jane Okafor, and Hassan Sadeghi. Barrera and Sadeghi collected most of the data on asphaltene property distributions and Okafor collected the data on SAR properties from native oils, in-situ converted oils and HOS Bottoms. Experimental data from the three Master thesis were used in this thesis with different purposes and analysis that the one performed in each of the three thesis. Experimental data collected exclusively as part of this thesis include: distillation assays, all SARA compositions, SAR properties of thermocracked (X-#) and hydrocracked (RHC-#) samples (and additional data from two more native oils), asphaltene yields from heavy fractions and whole crude oils. Note that data analysis included in this document, new property correlations, and modifications to the regular solution model were done exclusively as part of this thesis.

1.3 General Methodology

The general methodology of this thesis can be summarized in the following four steps (see Figure 1.1.):

1. Step 1 covers the characterization of asphaltenes (density, molecular weight, refractive index, elemental analysis, reconstructing property distributions) and using the modified regular solution model (RSM) to determine the solubility parameter of asphaltenes from solubility measurements of asphaltene model systems (asphaltenes from heptane extractions in mixtures of toluene and heptane).
2. Step 2 involves to the characterization of saturates, aromatics and resins (density, molecular weight, refractive index) and using the RSM to find the solubility parameter of

saturates and aromatics from solubility measurements of asphaltenes in mixtures of a) toluene and saturates and b) aromatics and heptane.

3. Step 3 applies the regular solution model with the characterization data from Steps 1 and 2 along with the SARA composition to fit the RSM to experimental solubility curve of the heavy fraction of the crude oil. The crude oil solubility curve shows the asphaltene precipitation yields from a crude oil versus the mass fraction of added solvent, usually *n*-heptane. The fitting parameters in Step 3 are the average molecular weight of asphaltene nano-aggregates in the oil and the shape factor a gamma distributions used to represent the molecular weight distribution of asphaltenes.
4. Step 4 includes the distillable fraction in the RSM. A distillation assay is required to estimate the properties of the distillable fraction (light fraction in the crude oil). The fitting parameters from Step 3 are used in the RSM to predict the stability of the "whole" crude oil. Note that the "whole" crude oil is defined as the crude oil before distillation; hence, it includes both the light and heavy fraction of the oil.

Each of these steps is the subject of a different chapter as outlined in the next section.

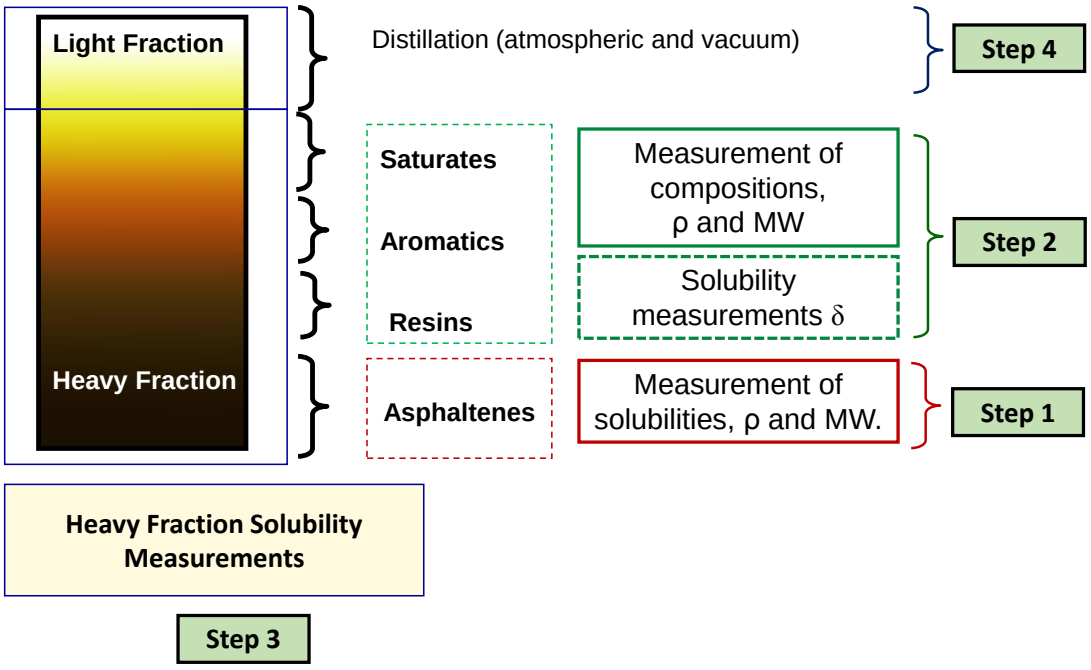

Figure 1-1. General methodology of the characterization and modeling of native and reacted oils applied in this thesis.

1.4 Thesis Outline

This thesis is organized in nine chapters.

- Chapter 1 introduces of the relevance of the thesis research topic and the main objectives proposed for this study.
- Chapter 2 presents a literature survey in the main topics related to this thesis including: crude oil definition and standard characterization methods, characterization of SARA fractions, asphaltene properties, and approaches for asphaltene precipitation modeling. It also includes a brief review on the main conversion processes applied in refineries and their effect on crude oil and asphaltene properties.
- Chapter 3 describes the characterization methodology and experimental methods used in this thesis.
- Chapter 4 reviews the models applied in this thesis, including the regular solution model for asphaltene precipitation and the self-association model for the asphaltene molecular weight distribution.
- Chapter 5 presents the characterization of asphaltenes from native and reacted oils. It includes the analysis of the molecular weight data to determine molecular weight distributions and the effect of temperature in aggregation. The development of the density distribution is shown and a solubility parameter correlation for asphaltenes is proposed (Step 1 in general methodology).
- Chapter 6 presents the characterization of saturates, aromatics and resins in terms of density, molecular weight, refractive index, and elemental composition. The determination of the solubility parameters of saturates and aromatics from reacted oils is also discussed (Step 2 in general methodology).
- Chapter 7 presents the application of the regular solution model to the heavy fractions of the crude oils samples using the asphaltene and SAR characterizations presented in Chapters 5 and 6 (Step 3 in general methodology).
- Chapter 8 shows how the regular solution model was modified to include a combined characterization (distillation assay and SARA assay) to predict crude oil stability in terms of asphaltene precipitation (Step 4 in general methodology).

- Chapter 9 summarizes the major conclusions of this thesis and presents recommendations for future research.

Chapter Two: Literature Review

An understanding of the nature of crude oil, oil refinery processes, oil characterization, asphaltene precipitation, and phase behavior modeling is required in order to be able to model asphaltene precipitation in downstream processes. Each of these topics is reviewed below.

2.1 Crude Oil Definition.

Hydrocarbons occur naturally as gas, gas condensate, crude oil from light oils to extra-heavy oils, bitumen, and coal. Crude oils are classified in terms of their physical properties (viscosity and density/API) as indicated with the UNITAR classification given in Table 2-1.

Table 2-1. UNITAR classification of oils by their physical properties at 15.6°C (Gray, 1994)**.**

	Viscosity mPa.s	Density kg/m³	API Gravity
Conventional oil	$<10^2$	< 934	>20°
Heavy oil	$10^2 – 10^4$	934 – 1000	20° – 10°
Bitumen	$>10^4$	>1000	<10°

Crude oil is a mixture of hundreds of thousands of different hydrocarbon based molecules many of which also contain non-hydrocarbon components such as nitrogen, oxygen, sulfur and sometimes organometallic compounds. Crude oil can be thought of as a distribution of paraffinic, naphthenic, and aromatic species of increasing molecular weight and complexity as described in Altgelt *et al*. (1994). As seen in Figure 2-1, crude oil boiling point increases as the complexity of the components making up the oil increases. The left boundary (Paraffins solid line) in Figure 2-1 represents the boiling point of paraffins (*n*-alkanes) for which molar mass rapidly increases at higher boiling points. The right boundary at higher boiling points (>300°C for Polar Polyfunctional compounds dash line) in Figure 2-1 represent complex multi-aromatic ring structures and polyfunctional compounds. The largest and most complex components are the asphaltenes which make up 5 to 20 wt% of native heavy oils and bitumen and up to 50 wt% or 60 wt% of vacuum residues in refineries.

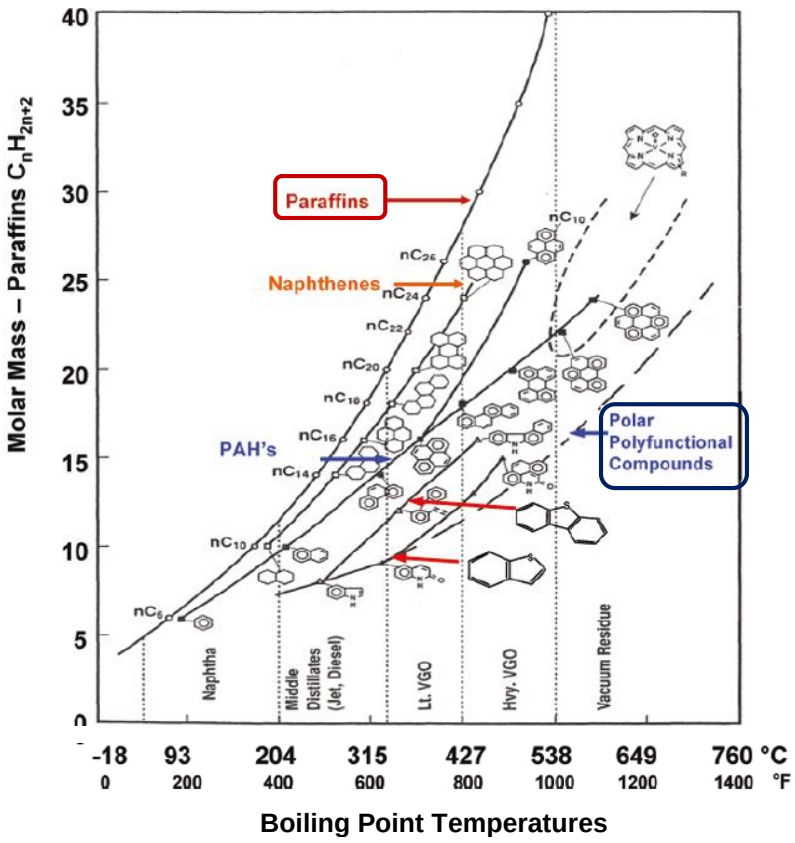

Figure 2-1. Effect of molecular weight and structure on boiling (Altgelt and Boduszynski, 1994).

In comparison with conventional oils, heavy oils have high viscosity, high asphaltene content, and relatively high heavy metals, sulfur, and nitrogen contents, usually out of market specifications. Heavy oils are further classified into three different categories according to specific gravity and viscosity at reservoir conditions (Huc, 2011):

1. Heavy oil: API degree higher than 10, ambient viscosity lower than 10,000 cP, and flows at reservoir conditions
2. Extra-heavy oil: API degree less than 10, *in situ* viscosity less than 10,000 cP, some mobility at reservoir conditions
3. Natural Bitumen: API degree less than 10, *in situ* viscosity greater than 10,000 cP, and does not flow at reservoir conditions.

Conventional oils, bitumen, and vacuum residues are used in this project as well as *in situ* reacted oils and converted oils from a visbreaker and a hydrocracking process.

2.2 Crude Oil Conversion Processes

Crude oils, heavy oils, and bitumen are refined to obtain high-value products, such as liquefied fuels, solvents, lubricants and petrochemical streams (Speight, 1998). The basic refinery process is distillation which fractionates the crude oil into products of differing volatility. After distillation some streams are further fractionated by other physical methods such as absorption, adsorption, and solvent extraction. The bottom products from these separations (usually atmospheric or vacuum residua) are sent to conversion processes to increase the yield of lighter higher value products. These conversion processes are based on either carbon rejection or hydrogen addition reactions.

Carbon rejection processes, such as visbreaking, involve the redistribution of hydrogen among the various components via thermal or catalytic cracking. During carbon rejection processes, the concentration of high molecular weight and high polarity material increases until a sufficient concentration is reached to form a separate dense, aromatic liquid phase termed coke (Trejo *et al*., 2009). Hydrogen addition processes, such as hydroconversion (hydrocracking or hydrotreatment), supply an external source of hydrogen to increase the hydrogen to carbon atomic ratio (H/C) of the feedstock (Ancheyta *et al.,* 2010). Hydrogen addition processes decrease the yield of coke formation (Rana *et al.,* 2007) and increase the H/C ratio in comparison with carbon rejection processes. For both carbon rejection and hydrogen addition processes, the severity of the treatment (reaction time and temperature) determines the extent of reaction and the final product composition.

During the last few years, many approaches to upgrading bitumen and heavy oils and improving upgrading process efficiency have been developed and some of them have been implemented in the oil industry. A brief description of the main processes for heavy oils and residues is provided below.

2.2.1 In-Situ Upgrading

In situ upgrading, usually referred to as in-situ heat treatment, is a process to reduce the viscosity and density of the oil in a subsurface formation. In-situ upgrading consists of thermal treatment of the oil in the reservoir using a heating device such as electrical heaters. During in-situ heat treatment, pyrolysis reactions occur where high temperature is maintained in the formation. This process produces a lower density, lower viscosity oil, synthesis gas (H_2, CO_2, H_2O, N_2, CH_4 and other gases in lower proportions), and a coke-like residue. The amount and properties of the products depends on the temperature and the type of oil (Roes *et al.*, 2009).

In situ combustion processes can also upgrade part of the in-situ oil. In-situ combustion consists of injecting an oxidizing agent, such as air or oxygen enriched air, into the reservoir to burn a portion of the oil and promote mobility and higher production of the remaining oil. Part of the oil close to the burning zone is also cracked into lighter components. The oxidizing agent is injected for "short" periods of time (days or few weeks) sometime with the aid of steam (Castanier and Brigham, 2003). Mass transport and several chemical reactions occur as the process progresses and temperature gradients develop in the reservoir. Some of the chemical reactions are combustion, oxidation, cracking, and pyrolysis (Castanieret *et al*., 2003; Jia *et al*, 2013). In-situ combustion can also lower sulfur, metals and asphaltene content depending on the conditions and additives added during the operation.

2.2.2 Thermocracking

The main objective of thermocracking processes is to mildly crack the heavy hydrocarbon molecules (high molecular weight) to produce more distillates (naphtha and gasoline) from atmospheric and vacuum residues, extra heavy oils, and bitumen. The main processes are visbreaking, catalytic cracking, and coking.

Visbreaking, one of the basic processes in refining resids, is a non-catalytic thermal process used to reduce the viscosity of residue fractions and produce limited amounts of distillables. It is an inexpensive upgrading process especially used for residues of conventional oils and bitumen (Lababidi *et al*., 2014; Xu *et al*., 2013). The operating conditions of a visbreaker are critical to

attain a high degree of conversion without worsening the stability of the resid. Operating conditions are also very important to attain large operation times before cleaning maintenance is required to remove coke deposits from the reactor (Vezirov, 2011).

Catalytic cracking uses catalyst to promote faster and more effective cracking reactions with higher cracking rates (Corma and Wojciechowski, 1985). Different type of catalyst beds have been developed according to the needs and research of major oil companies. The main reaction is thermocracking of carbon-carbon bonds into a lighter paraffins and olefin.

Coking is used to reduce the carbon-to-hydrogen ratio. Residues are transformed at higher temperatures than the visbreaking process. Coking is also used to reduce the viscosity of extra heavy oils in production fields so that the product can be easily transported to the refinery for further downstream treatment (Huc, 2011)

2.2.3 Catalytic Hydroconversion: Hydrocracking and Hydrotreatment

Catalytic hydrotreatment and hydrocracking involve thermal-processing of a feedstock, such as a vacuum residue, with a catalyst and hydrogen at pressure to produce lighter and more valuable products from a large variety of feedstocks (Altgelt *et al*., 1994; Kaes, 2000; Speight, 1998). They are very important processes in the refinery because they convert heavy and/or sulfur and aromatic-rich feedstocks into middle distillates of high quality within market specifications including low sulfur, minimum impurities, and lower aromatic content (Minderhoud and van Veen 1993). The process is referred as hydrotreatment instead of hydrocracking when the main purpose is to reduce the organometallic compounds (hydrodemetalization) (Huc, 2011)

There are several configurations for commercial hydrocracking processes which can be classified into four main categories: fixed bed, moving bed (co- or counter-current), ebullated bed, and entrained bed reactors (Huc, 2011). One of the most common processes configurations is a two-stage process with one or more reactors for each stage. The first stage is usually where the cracking reactions occur; the second stage serves to reduce sulfur, nitrogen, oxygen and aromatic content of the feedstock. Hydrocracking processes play an important role converting bitumen, heavy

feedstocks or resids into lighter and more valuable synthetic oils and are nowadays used by major oil companies in Alberta and worldwide (Huc, 2011; Roes *et al.*, 2009).

2.3 Crude Oil Characterization

Crude oil characterization is the identification and quantification of the main compounds or pseudo-components making up the crude oil mixture. Characterization of crude oil feedstocks and product streams is required for the design and operation of all refinery processes including conversion processes. One objective of the characterization is to: 1) evaluate the potential of a feedstock (processing costs and market values for the associated products); 2) identify the required treatment for a feedstock; 3) evaluate the quality of the products after the conversion process. A second objective of the characterization is to determine the thermophysical property distributions representing the crude oil or petroleum fraction. These properties are used as inputs to thermodynamic phase behavior and physical property models. The two most commonly used characterization methods in refinery applications are based on distillation and solubility assays.

2.3.1 Distillation Curves and Boiling Point Distributions

Crude oils and petroleum streams are typically characterized starting from a fractionation of the petroleum into a number of components and pseudo-components that represent boiling point intervals. True boiling point (ASTM Standard D2892 2009) distillation is the most accurate method to determine boiling point intervals for a petroleum stream. The true boiling point (TBP) refers to a distillation performed at high reflux ratio (≥5) and a large number of theoretical stages (≥14). Under these operation conditions, TBP distillation achieves a sharp separation of the components making up the crude oil. Therefore, the distribution of boiling points obtained with the TBP distillation describes the distribution of the components or pseudo-components in the crude oil mixture in order of boiling point.

However, TBP is not practical for most applications because the assay is time consuming and costly. TBP is instead approximated from other types of assays using empirical correlations. Examples of boiling point assays are ASTM standards D86, D1160 and D 5236. TBP can also be estimated from chromatographic analysis such as simulated distillation. Recently, a spinning band

distillation (SBD) method has been adapted to measure the boiling point distribution of crude oils equivalent to TBP. SBD has a large number of theoretical stages, depending on the length of the band in the column, and it can be performed at both atmospheric and vacuum pressures at any desired reflux ratio. It takes shorter operation time and requires less sample than the standard TBP ASTM method. All of these distillation methods are briefly presented in Table 2-2.

Table 2-2. Description of different methods to determine boiling point distributions.

Method	Description
ASTM D2892 (TBP)	Vacuum distillation. Sharp separation of components by their boiling point. Uses 14 to 18 theoretical stages and reflux ratio of 5:1.
ASTM D5236	An extension of ASTM 2892. Allows measurements of real boiling points of the mixture at reduced pressure.
ASTM D86	Atmospheric distillation. Limited by the cracking temperature of the crude oil samples (~344°C). D86 is not practical for heavy oil samples. Temperatures are measured at the vapor phase.
ASTM D1160	Vacuum distillation for high boiling samples. Reduced pressure to avoid cracking. Samples can be distilled up to ~538°C. However, it is inadequate for heavy oils and bitumen.
Advanced Distillation Curve (Bruno 2006)	Atmospheric distillation. It is an improved setup of ASTM D86 that allows accurate measurements of real/instant boiling points of the mixture and provides accurate volume measurements.
Spinning Band Distillation (Adapted from ASTM 2892)	Atmospheric or vacuum distillation. The fractionation device is a spinning band which rotates at high speed giving efficiencies up to 50 theoretical plates and allowing high reflux ratios. Allows collection of fractions at desired pressure (>1 mmHg) and temperature intervals (Maximun pot temperature of 300°C to avoid cracking).
ASTM D3710, D2887, extended D2887 (SimDist, C30+, or SCN)	Gas chromatography assays used to predict boiling point distribution. The standard is usually a mixture of normal paraffins. Some "customized" aromatic corrections have been developed.

When the crude oil is characterized by any of the distillation methods except TBP, the distillation data must be converted to TBP. When the distillation is performed under vacuum, the temperature data also must be converted to atmospheric equivalent temperature. API has published standard procedures to interconvert data obtained from tests such as D86 and D1160 to an equivalent TBP curve, including the Riazi-Daubert method and the Maxwell and Bonnell method (ASTM Standard D5236, 2007.; Riazi, 2005). Note that the temperature measurements in most of the distillation methods, with the exception of ASTM 5236, do not represent a true thermodynamic state and the interconversion methods are empirically based correlations with no thermodynamic meaning. Therefore, inconsistencies are sometimes unavoidable. A new distillation method was developed by Bruno (2006) at NIST to measure thermodynamic boiling points of conventional oils and also have more accurate volume measurements. This method is known as the Advanced Distillation Curve (ADC) or composition-explicit approach. ADC distillation can be also used to medium oils and is being adapted to work under conventional vacuum for heavier oils.

Boiling point distributions have limited applicability for heavy oils and bitumen because they contain high molecular mass fractions that decompose before they boil with conventional vacuum. Heavy oil and bitumen contain up to 70 wt% of "non-distillable" components with conventional vacuum. Recently, Castellanos-Diaz *et al.* (2014) developed a static deep vacuum laboratory apparatus (DVFA) to measure saturation pressures of petroleum fractions from extra-heavy oils and bitumen. DVFA is currently being adapted to fractionate bitumen by volatility to extend the data from conventional vacuum distillation (Sánchez-Lemus *et al*., 2014).

2.3.2 Crude Oil Pseudo-Components from Boiling Point Distributions

In order to use the TBP data for material balances and phase behavior modeling, the TBP curve must be split into a number of components and pseudo-components to represent the distribution of properties in the mixture. Generally, two techniques are applied to split the distributions: 1) the pseudo-component approach; 2) the continuous mixture approach (Riazi, 2005).

In the pseudo-component approach, the TBP curve is divided into a number of subfractions with known boiling point, specific gravity, and molecular weight (T_b, *SG*, and *MW)*. This procedure is

also known as pseudoization. Note that, each fraction or pseudo-component is actually a mixture of many pure components that happen to boil at the same normal boiling point (or boiling point range). Therefore, each fraction may be further split into three (or more) pseudo-components to differentiate between chemical families such as paraffins, naphthenes, and aromatics if needed. Each fraction is assigned a unique set of properties such as density, molecular weight, critical properties, and elemental composition (Hay *et al.* 2013; Riazi, 2005).

In the continuous mixture approach, a probability distribution function (PDF) is defined to describe the composition of the mixture. The PDF can be defined in terms of a measurable property, such as boiling point, molecular weight, refractive index, or carbon number, and varies from the value of the lightest to the heaviest component present in the mixture. When a mixture is represented with a PDF, it must eventually be presented in terms of pseudo-components (pseudoization of the distribution function). Therefore, both the pseudo-component and the continuous mixture approaches are used simultaneously. Both approaches work well when modeling physical operations in which the volatility is the major property of interest and no reactions and/or complex association are involved.

2.3.3 Property Estimation and Prediction for TBP Crude Oil Pseudo-Components

Once the pseudo-components are defined, their properties must be measured or calculated. Typically, each pseudo-component from a boiling point distribution represents the average boiling temperature of the given interval on the boiling curve. The specific gravity and average molecular weight for each pseudo-component are determined from correlations. There are several correlations to estimate specific gravity based on Riazi-Daubert method using boiling point, molecular weight, or kinematic viscosity; however, the specific gravity of hydrocarbons and petroleum fractions is normally available from experimental data because it is easily measurable (Riazi, 2005).

Riazi-Daubert methods can be used to estimate the molecular weight of hydrocarbons with molecular weights up to 700 g/mol, using the constants recommended by Tsonopoulos *et al.*, (1986) as follows,

$$MW = 42.965\left[\exp\left(0.0002097 * T_b - 7.78712 * SG + 0.00208476 * T_b * SG\right)\right] T_b^{1.26007} SG^{4.98308} \quad \textbf{2-1}$$

where *MW* is molecular weight, *Tb* is the boiling point and *SG* is the specific gravity.

This equation is recognized as the standard method of estimating molecular weight of petroleum fractions in the industry. Other characterization parameters can be measured for the bulk crude oil and used to constrain the correlations, particularly the average specific gravity and average molecular weight.

Once the T_b, *MW*, and *SG* are defined for each pseudo-component, other thermodynamic properties needed for phase behavior modeling, such as critical temperature, critical pressure and acentric factor, are then determined using correlations. There are a number of property correlations in the open literature and the most commonly used are the Lee-Kesler, Twu, and Riazi-Daubert methods. For example, the critical temperature (T_c) and critical pressure (P_c) from the Riazi-Daubert method (Riazi, 2005) are given by:

$$T_c = 9.5233\left[\exp\left(-0.0009314T_b - 0.544442SG + 0.00064791T_b SG\right)\right] T_b^{0.81067} SG^{0.53691} \quad \textbf{2-2}$$

$$P_c = 3.1958 * 10^5\left[\exp\left(-0.008505T_b - 4.8014SG + 0.005749T_b SG\right)\right] T_b^{-0.4844} SG^{4.0846} \quad \textbf{2-3}$$

These correlations were also adopted by the API and have been commonly used for industrial applications such as process simulators (Riazi, 2005, VMGSim, 2012).

Another useful property, particularly when modeling asphaltene precipitation, is the solubility parameter. Barton (1991) and Hansen (2007) provided a table with solubility parameter data for several pure components. A correlation is required when the solubility parameter is unknown. The solubility parameter is related to the enthalpy of vaporization by definition as follows,

$$\delta_T = \left(\frac{\Delta H_{vT} - RT}{v_T}\right)^{0.5} \quad \textbf{2-4}$$

where δ is the solubility parameter, ΔH_{vT} is the enthalpy of vaporization at temperature *T*, *R* is the universal gas constant, and *v* is the molar volume. Measured data for enthalpy of vaporization are available in the literature for pure components. There are also several correlations in the open

literature to estimate enthalpy of vaporization at a given temperature and pressure for pure components or pseudo-components with unknown properties. Some of the correlations are based on vapor pressure correlations derived from clausius-clapeyron equation and/or EOS and others are empirically developed.

The enthalpy of vaporization at the boiling point, ΔH_{vb}, can be determined from the simplified Trouton's rule, Chen, or Vetere methods as shown below.

Chen Method (Poling *et al.*, 2001):

$$\Delta H_{vb} = RT_c T_{br} \frac{3.978T_{br} - 3.958 + 1.555 \ln P_c}{1.07 - T_{br}} \qquad \textbf{2-5}$$

where T_{br} is the reduced temperature at the boiling point (Temperature in K and pressure in bars).

Vetere Method (Poling *et al.*, 2001):

When T_c and P_c are available (Temperature in K and pressure in bars):

$$\Delta H_{vb} = RT_b \frac{(1-T_{br})^{0.38}\left(\ln P_c - 0.513 + 0.5066/\left(P_c T_{br}^2\right)\right)}{1 - T_{br} + \left(1-(1-T_{br})^{0.38}\right)\ln T_{br}} \qquad \text{(Vetere 1)} \qquad \textbf{2-6}$$

and when T_c and P_c are not available:

$$\Delta H_{vb} = RT_b\left(A + B\ln T_b + \frac{CT_b^{1.72}}{MW'}\right) \qquad \text{(Vetere 2)} \qquad \textbf{2-7}$$

where *A, B* and *C* are constants. For hydrocarbons, A=3.298, B=1.015, C=0.00352, and MW′ is a "fictitious" molecular weight that is equal to the true molecular weight for most compounds.

Trouton's Rule (Modified) (Hildenbrand and Scott, 1964)

$$\Delta H_{vb} = 87.5 * T_b \qquad \textbf{2-8}$$

Sometimes the enthalpy of vaporization is required at standard conditions and a temperature correction must be applied to ΔH_{vb}. A widely used correlation between ΔH_{vb} and temperature is the Watson correlation (Poling *et al.*, 2001) given by:

$$\Delta H_{v2} = \Delta H_{v1}\left(\frac{1-T_{r2}}{1-T_{r1}}\right)^{n} \qquad \textbf{2-9}$$

where T_r is the reduced temperature, the subscripts 1 and 2 refer to Temperatures 1 and 2, and n is a constant. Common values for n are 0.375 or 0.38 (Poling *et al.*, 2001; Weissberger, 1959). n can be also obtained with correlations (Viswanath and Kullor, 1965).

2.3.4 Solubility Based Methods for Crude Oil Characterization

The boiling point characterization approach usually fails when used to model complex processes involving chemical reactions or extractive separations based on polarity (Hay *et al.*, 2013) as well as asphaltene precipitation from heavy oils. A PIONA (n-paraffin, iso-paraffin, olefin, naphthene and aromatic) characterization technique has been developed by Hay *et al*., (2013) to capture the chemistry of a typical oil and was successfully used to track and estimate hydrocarbon mixture thermodynamic properties to be applied in chemical reaction processes in the refinery.

Other physical fractionation methods are also available to characterized heavy oils and bitumen based in solubility separation; for example, SARA analysis (adapted ASTM 4124 and ASTM D2007) where the oil is divided into four solubility and adsorption classes: saturates (S), aromatics (A), resins (R) and asphaltenes (A). One advantage of the SARA fractionation approach is that separation between chemical families is achieved allowing for a better description of the solubility parameter distribution used for asphaltene precipitation modeling. There are also modified procedures to the solubility or adsorption type separations to separate polar or acidic subfractions.

There are three general ASTM standard for separation of feedstocks into four or five pseudo-components, ASTM D2006, ASTMD2007, ASTM D4121. These methods use *n*-pentane as the solvent for the initial fractionation into asphaltenes and deasphalted oil; some have been modified to use *n*-heptane. Each assay separates the deasphaltened oil into different fractions: ASTM2006

into polar compounds, 1st acidic paraffins, 2nd acidic paraffins, and saturates; ASTM 2007 into resins, aromatics, and saturates; ASTM D4124 into polar aromatics (resins), naphthenic-aromatics (aromatics), and saturates (Speight, 1998).

2.3.5 Crude Oil Pseudo-Components from SARA Fractionation and their Properties

A commonly used method to characterized heavy oils and bitumen is SARA fractionation in which the oil is separated into saturates, aromatics, resins and asphaltenes depending on their solubility and polarity. Figure 2-2 shows typical SARA composition of heavy oils from different sources.

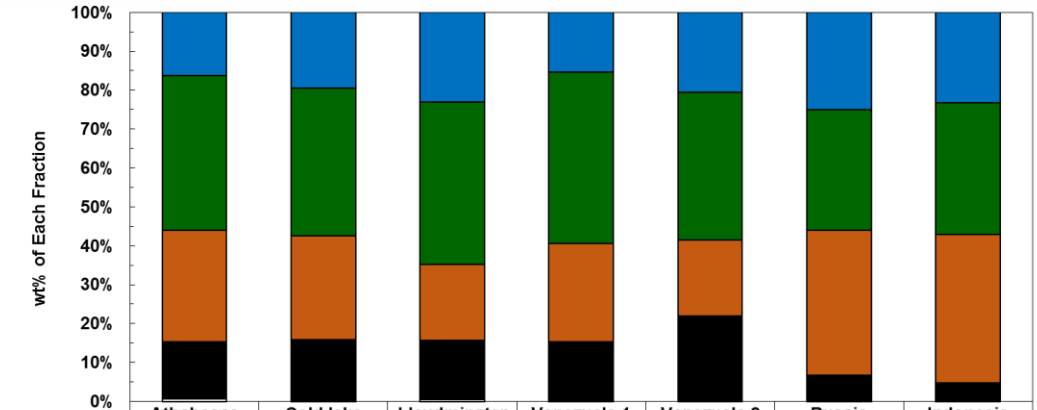

	Athabasca	Cold lake	Lloydminster	Venezuela 1	Venezuela 2	Russia	Indonesia
Saturates	16.3	19.4	23.1	15.4	20.5	25.0	23.2
Aromatics	39.8	38.1	41.7	44.4	38.0	31.1	33.9
Resins	28.5	26.7	19.5	25.5	19.6	37.1	38.2
Asphaltenes	14.7	15.5	15.3	15.2	21.8	6.8	4.7
Solids	0.7	0.3	0.4	0.2	0.1	0.0	0.0

Figure 2-2. SARA composition of crude and heavy oils from different sources (Data from (Akbarzadeh, *et al*. 2005a).

Properties of the SARA fractions such as molecular weight and density must be measured. Solubility parameters cannot be directly measured but have been determined from modeling experimental solubility data (Akbarzadeh *et al.*, 2005) or correlated to refractive index measurements (Wang *et al.*, 2001). Typical properties for SARA fractions from Athabasca bitumen are shown in Table 2-3.

Table 2-3. SARA properties for Athabasca bitumen (Akbarzadeh *et al.* 2005).

Bitumen fraction	Molecular Weight (kg/kmol)	Density (kg/m^3)	Solubility parameter $(MPa)^{0.5}$
Saturates	460	880	15.9
Aromatics	522	990	20.2
Resins	1040	1044	19.6
Asphaltenes	1800+	1080+	20.1+

SARA fractionation groups components of similar chemical family as described below.

Saturates are the least polar fraction and consist mostly of heavy paraffins and cycloparaffins (Speight, 2001). Their molecular weight ranges between 300 to 600 g/mol, densities between 800 and 900 kg/m^3, and solubility parameters between 15 and 16 $MPa^{0.5}$.

Aromatics consist mostly of compounds with one to a few aromatic rings with alkyl-chains. They can also have some naphthenic rings attached to the aromatic ring (Speight, 2001). Their molecular weight ranges between 300 and 800 g/mol, densities between 950 and 1050 kg/m^3, and solubility parameters between 19 and 20 $MPa^{0.5}$ (Akbarzadeh *et al*., 2005).

Resins consist of compounds with larger aromatic cores with naphthenic rings and paraffinic side chains. Resins have higher polarity and lower H/C ratio than aromatics (Yarranton *et al.*, 2013; Yarranton and Masliyah, 1996). Resin molecular weight ranges between 700 to 1300 g/mol. Their density is approximately 1050 kg/m^3 and their solubility parameters are 20 ±0.5 $MPa^{0.5}$. Resins can also be considered to be a lower molecular weight, non-associating fraction of the asphaltenes.

Asphaltenes are the most polar fraction in the crude oils and are larger and more aromatic than resins. Asphaltene property determination is more challenging because asphaltene molecules self-associate and is presented in more detail in next sections.

2.4 Asphaltenes from Native Oils

2.4.1 Definition and Composition

Asphaltenes are defined as a solubility class of crude oil components that can precipitate in an excess of n-alkanes, such as n-pentane and n-heptane, but remain soluble in aromatic solvents, such as toluene. They are a mixture of thousands of different species, generally large, polar, polynuclear molecules consisting of condensed aromatic rings, aliphatic side chains and various heteroatom groups (Payzant *et al*., 1991). Their elemental composition varies somewhat from source to source but falls within a relatively narrow range (Speight, 1998); for example, the H/C atomic ratio is known to fall between 1 to 1.2. However, the elemental composition of asphaltenes precipitated with different solvents can also vary. Asphaltenes precipitated with *n*-heptane have lower H/C ratio than precipitated with *n*-pentane indicating higher aromaticity for *n*-heptane asphaltenes.

Several studies have analyzed the structure of asphaltene molecules using fluorescence depolarization techniques or by cracking methods such as RICO (ruthenium-ions-catalyzed-oxidation) or pyrolysis methods for whole asphaltenes from different oil samples. These studies support the hypothesis that asphaltenes contain condensed polynuclear aromatic ring systems bearing alkyl side chains (Parkash *et al.*, 1979; Yen et al., 1984; Bandurski, 1982; Groenzin and Mullins, 1999; Mullins, 2008). The heteroelements (*e.g.*, nitrogen, oxygen and sulfur) are scattered in various locations both within the ring structures and on the side chains. X-ray absorption near-edge structure (XANES) spectroscopy indicates that the nitrogen in asphaltenes is likely in pyrrolic rather than pyridinic forms (Mitra-kirtley *et al*., 1993). Infrared spectroscopy investigations suggest that oxygen is present as carboxylic, ketone and phenol function locations (Speight and Moschopedis, 1979). Benzothiophenes and dibenzothiophenes are the common forms of sulfur in asphaltene structures (Rose and Francisco, 1988; Kelemen *et al.*, 1990). Nickel and vanadium has been observed in porphyrin (or methalporphyrin) forms (Gawrys et al.,2006; Galimov *et al.* 1993; Qian *et al.*, 2010).

Velásquez Rueda, (2013) cracked asphaltenes from different sources in the presence of hydrogen to ensure minimal change of the molecular structure of the fragments and additionally to minimize

coke formation and produce a high yield of distillates. They identified several molecular structures including saturates (mainly paraffins), aromatics with 1-3 rings, naphthenoaromatics species below 3wt%, and heteroatomic species such as alkylcarbazoles and cyclic compounds containing aliphatic sulfur. The unconverted asphaltene fraction was not studied. More complex structures such as large polyaromatics and large naphthenoaromatic structures were not identified but they could be present in the unconverted fraction.

2.4.2 Molecular Structure

While functional groups within the asphaltenes have been identified, molecular structures have been difficult to determine. It is accepted that the asphaltene structure is composed by aromatic rings, alkane chains and cyclic alkanes with some heteroatoms within the asphaltene structure. Two types of structures have been postulated: the "archipelago" structure (Figure. 2-3a) and the "continent" structure (Figure 2-3b).

The archipelago structure consists of small aromatic groups (up to four rings) which are connected to each other by aliphatic chains with carbon numbers up to 24 (Zhang *et al*., 2007; Murgich, 2003). Gel permeation, thermal degradation, oxidation and angle neutron scattering (SANS) data (Sheremata *et al*., 2004; Mullins *et al.*, 2012; Strausz *et al.*, 2002) show evidence of this structure. The continent structure represents asphaltene as relatively flat disk shape molecules with a dominantly aromatic core (usually consisting of more than seven rings) and a periphery of aliphatic chains (Kuznicki *et al.*, 2009; Sheremata *et al.*, 2004; Mullins, 2008; Murgich, 2003). HNMR spectroscopy, X-ray diffraction and fluorescence depolarization support this interpretation (Yen *et al.*, 1984; Sheremata *et al.*, 2004).

Several studies of asphaltenes behaviour and association with different methods suggests that both structures may co-exist within asphaltenes. Association, adsorption, and adhesion properties of asphaltenes can be justified when a range of architectures (e.g. archipelago and continent) are present simultaneously (Mullins *et al*., 2012; Gray *et al*., 2011).

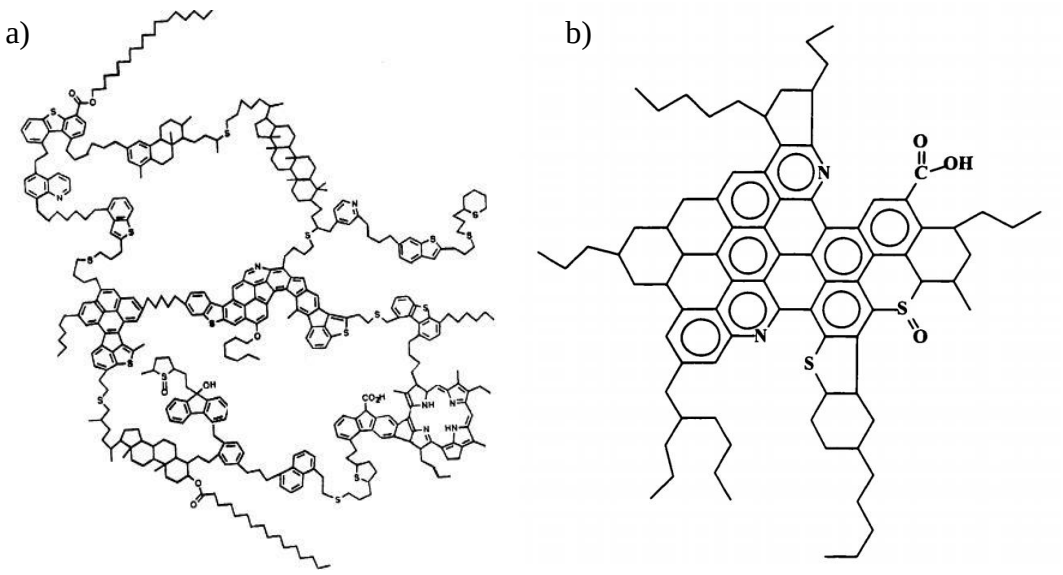

Figure 2-3. Hypothetical asphaltene structures: a) Archipelago: $C_{412}H_{509}S_{17}O_9N_7$ with a H/C ratio of 1.23 and a molecular weight of 6239 g/mol (Murgich *et al.*, 1999; Strausz *et al.*, 1992) b) Continent: $C_{84}H_{100}N_2S_2O_3$ with a H/C ratio of 1.19 and a molecular weight of 1276 g/mol (Dickie and Yen, 1967; Mullins, 2008).

2.4.3 Asphaltenes Molecular Weight and Self-association

The molecular weight of asphaltenes is much debated because asphaltenes self-associate and the apparent molecular weight of asphaltenes depends on concentration and temperature. Asphaltene self-association has been observed with a number of techniques including vapor pressure osmometry (Yarranton *et al.*, 2000), interfacial tension (Yarranton *et al.*, 2000; Yarranton *et al.*, 2013), small-angle X-ray and neutron scattering measurements (Barré *et al.*, 2009; Xu *et al.*, 1995) differential scanning calorimetry (Andersen and Birdi, 1991), dielectric spectroscopy (Maruska and Rao, 1987), on-column method (ELSD) (Rogel *et al.*, 2009),. The apparent molecular weight of asphaltenes increases with asphaltene concentration (Sztukowski *et al.*, 2003; Moschopedis *et al.*, 1976) indicating association of asphaltene into nanoaggregates of different sizes (Mullins *et al.*, 2012; Barré *et al*., 2009; Rogel *et al.*, 2009; Rogel *et al.*, 2012; Barrera *et al.*, 2013; Sheremata *et al.*, 2004).

The average molecular weight of asphaltene monomers is now thought to be on the order of 1000 ± 300 g/mol (Mullins, 2008; Akbarzadeh *et al.*, 2007; McKenna *et al.*, 2013). Recent studies (McKenna *et al*. 2013) show that asphaltenes may start forming nanoaggregates at concentrations lower than 50 µg/ml. The average nanoaggregate molecular weight in solution with toluene appears to consist of two to six monomers per aggregate (Yarranton, 2005) although they may range in size up to 30,000 g/mol (Barrera *et al.*, 2013; Yarranton *et al.*, 2013; Yarranton, 2005) or even 100,000 g/mol (Xu *et al.*, 1995).

Barrera *et al.*, (2013) reconstructed molecular weight distributions from MW measurements of asphaltene solubility fractions using an association model. The less soluble (heavy) asphaltenes had higher molecular weight than the more soluble (light) asphaltenes. They also found that asphaltene molecular weights were best represented as a combination of associating and non-associating material. Non-associating material, also called neutrals, has the lowest molecular weight within the asphaltene monomer distribution and are smaller and more aromatic than bulk asphaltenes. Reconstruction of density distributions to represent the density data from the same fractions confirmed the need to represent asphaltenes with these two types of material.

It is clear that asphaltenes cannot be defined as a single component but rather as a continuum of monomers and aggregates with a distribution of properties. In general, unimodal property distributions have been found for molecular weight (Barrera *et al*., 2013; Becker *et al.*, 2008), density (Barrera *et al.*, 2013; Peramanu *et al.*, 1999) and solubility (Rogel *et al.*, 2012) of non-reacted asphaltenes.

2.4.4 Other Properties of Asphaltenes

Other properties of asphaltenes have been also studied including some thermodynamic properties such as molar volume (or density) and solubility parameter (Akbarzadeh *et al.*, 2004; Wiehe, 2008; Wang and Buckley, 2001), and heat capacity (Laštovka *et al.*, 2008). The first two properties are important in this thesis because they are inputs to the model used to predict asphaltene precipitation; they are briefly described below and they will be explained in detail for the RSM in chapter 4.

Density

Gravimetric measurements are usually applied to asphaltene to obtain their densities. The densities of solid asphaltenes have been reported to be between 1100 and 1280 kg/m^3 (Rogel and Carbognani, 2003). The density of asphaltenes dissolved in a liquid has also been measured indirectly from asphaltene solutions in toluene by extrapolating to zero concentration assuming zero excess volume to obtain an average value of 1162 kg/m^3 (Yarranton and Masliyah, 1996). Barrera (2012) tested both regular and excess volume mixing rules for asphaltene toluene solutions for whole asphaltenes and their soluble and insoluble fractions from native oils. Barrera concluded that using the regular mixing rule for asphaltenes toluene solutions was more appropriate because crude oil aromatics had negligible excess volumes in aromatic solvents and there was no strong evidence that asphaltenes would behave differently. The extrapolated densities with the regular mixing rule were found to be between 1050 and 1200 kg/m^3.

Solubility Parameter

The solubility parameter of asphaltenes cannot be measured directly but is rather determined indirectly by modeling asphaltene solubility data. Hirschberg *et al*. (1984) reported asphaltene solubility parameters of 19.50 $MPa^{0.5}$. Lian *et al*. (1994) reported solubility parameters ranging from 17.6 to 21.3 $MPa^{0.5}$. Yarranton and Masliyah (1996) determined solubility parameters in the range of 19 to 21 $MPa^{0.5}$. Andersen (1999) calculated solubility parameters between 19 and 22 $MPa^{0.5}$. Wang and Buckley (2001) fitted solubility parameters between 20.0 and 20.5 $MPa^{0.5}$ depending on the oil. However, the solubility parameter of asphaltenes is still uncertain as it depends on the interpretation of the data and solubility model.

Empirical correlations have been developed to estimate the solubility parameters of asphaltenes or crude oils in general. Some of the correlations are based on the molecular weight of asphaltenes or the oil (Chung, 1992; Zhou *et al.*, 1996). More recently, solubility parameter has been correlated to the refractive index of the crude oils (Wang and Buckley, 2001; Creek *et al.*, 2009). Buckley (1998) postulated that the solubility parameter of pure paraffinic and alkyl-aromatic hydrocarbons

is linearly related to a function of their refractive index, FRI, and proposing the following correlation to be applied to crude oils components,

$$\delta = 52.042 FRI + 2.904 \qquad \textbf{2-10}$$

where FRI is defined as follows,

$$FRI = \frac{n_D^2 - 1}{n_D^2 + 2} \qquad \textbf{2-11}$$

where n_D is the refractive index. FRI is related to other fluid properties through the Lorentz-Lorenz equation as follows (Chartier 2005; Toralf 2007),

$$FRI = \alpha \frac{4\pi N_a \rho}{3MW} \qquad \textbf{2-12}$$

where α is polarizability, *Na* is Avogadro's number, and ρ is density. Hence, the solubility parameter correlation is valid when the relationship between polarizability, density, and molecular weight remains consistent; that is, for dispersion force dominant systems. The correlation was applied to asphaltenes and crude oils on the assumption that the crude oil constituents (including asphaltenes) are non-polar and dispersion forces are dominant in hydrocarbons. However, the complexity of crude oil and especially asphaltenes suggest that this assumption may be an over-simplification and may not be precise for the asphaltene fraction.

Note that refractive index is measured using conventional refractometers; however, as with density, it must be measured in asphaltene solutions in a solvent, usually aromatic solvents such as toluene, and a mixing rule must be applied. Volumetric mixing rules of the FRI are usually applied because the polarizability is roughly proportional to the molecular size of the molecule (Prausnitz *et al.*, 1999). However, molar mixing rules have also been proposed to be more appropriate for the refractive index (Brocos *et al*., 2003).

2.5 Effect of Reaction Processes in the Chemistry of Asphaltenes

Upgrading can have a significant impact on asphaltene structure and properties including the H/C ratio, metal content (Trejo *et al.*, 2005; Trejo and Ancheyta, 2007), aromaticity factor (Yen and

Chilingarian, 2000), molecular weight (Trejo *et al.*, 2004; Bartholdy and Andersen, 2000; Trejo *et al.*, 2007), and asphaltene size (Buch *et al*., 2003). Typically, aliphatic chains are cracked off the asphaltenes leaving aromatic cores. While cracking reactions of asphaltenes are predominant, there is evidence that some addition reactions can also occur with the formation of archipelago structures during thermal cracking leading to the formation of molecular weights higher than that of the starting material (Alshareef *et al*., 2011). When cracking asphaltenes in the presence of hydrogen, the yield of distillates may increase and the production of coke can decrease (Velásquez Rueda, 2013). Gray and McCaffrey (2002) explain that the presence of hydrogen-donor solvents in cracking reaction suppresses the polymerization of olefins. Polymerized olefins are believed to be responsible for coke formation.

At high conversions, highly condensed structures are expected with lower molecular weight and increased aromaticity. For both downstream asphaltenes or asphaltenes from partly reacted streams, conversion also appears to decrease the average molecular weight of the asphaltene aggregates (Ancheyta *et al.*, 2003). However, it is unknown if downstream asphaltenes self-associate in the same manner as upstream asphaltenes since their molecular structure has been altered. Conversion processes have also been shown to decrease asphaltene solubility by removal or reduction of the alkyl chains and the change in solubility is proportional to the percent conversion.

Rogel *et al.* (2012) and others (Schabron and Rovani, 2008) have shown that the stability of visbroken residues in terms of asphaltene precipitation, depends upon the changes in solubility parameter distribution of the asphaltenes upon processing. Rogel *et al* (2012) used the on-column method to examine the changes in asphaltene properties due to processing and considered vacuum and atmospheric residue, visbroken residue, LC-fining products, coker heavy oils and other hydro-thermally-treated materials. A significant difference was observed for processed asphaltenes, which showed bimodal and wider solubility distributions in comparison with the unimodal distributions observed for native asphaltenes. Lababidi *et al*. (2014) also found that thermal cracking reactions decreased the average molecular weight of asphaltenes and produced bimodal molecular weight distributions as measured by gel permeation chromatography. Bimodal

distributions suggest that there are two different association mechanisms (or two type of "species" in solution). For example, one group of components that self-associate and another group of either poorly soluble monomers or dimerized condensed aromatics.

2.6 Crude Oil Stability and Asphaltene Precipitation Models

Asphaltene precipitation, also known as crude oil instability, can be triggered by changes in composition (such as solvent addition), temperature and pressure (Andersen and Speight 1999; Altgelt, Klaus H and Boduszynski 1994; Wiehe and Liang 1996). During crude oil operations and processing where these changes take place, asphaltenes precipitation is likely to occur and a second asphaltene-rich phase is formed. In some crude oil operations asphaltenes are deliberately precipitated; however, in other processes such as distillation, hydroconversion and blending, asphaltene precipitation is not desirable. Hence, an understanding of asphaltene stability is a key issue for the optimization of crude oil recovery and refinery operations.

Asphaltenes usually precipitate as 1-2 micron diameter particles (Rastegari *et al.*, 2004). It is not known if the particles are flocculated colloids, a solid phase, or a liquid/glass phase. As a result, a number of precipitation models have been proposed but the two main approaches are: 1) colloidal models (Leontaritis, 1989; Pan and Firoozabadi, 1998) and; 2) thermodynamic models (Hirschberg *et al.*, 1984; Akbarzadeh *et al.*, 2005; Chung, 1992; Ting *et al.*, 2003; Gupta, 1986). Additionally to these two approaches, it is common in the industry to use empirical experimental techniques, such as the p-value, solubility/insolubility number, and spot test, to determine the overall crude oil stability. These latter empirical methods are not discussed in this thesis as they are not modeling tools.

2.6.1 Colloidal Models

In the colloidal model, asphaltenes are assumed to be dispersed in the crude oil in the form of colloids. The structures are tens of nanometers in diameter and are assumed to consist of an asphaltene core with a shell of resins that prevents flocculation and therefore disperses the asphaltenes. Precipitation occurs when the resins are stripped off, allowing the asphaltene cores to flocculate into particles. The colloidal model is partially supported by small-angle neutron

scattering measurements (SANS) although this interpretation of the SANS data has been challenged (Sirota, 2005). Additionally, nanofiltration experiments indicate that there is no preferential association of asphaltenes with resins or any of the other SARA fractions (Zhao and Shaw, 2007). This model does not provide a satisfactory explanation for dilution with aromatic solvents which would be expected to strip off resins and yet do not cause precipitation. Precipitation models based on this approach are not predictive and have only been tested on limited data.

2.6.2 Thermodynamic Models

The thermodynamic models assume that asphaltenes are part of a continuous mixture. Asphaltenes are assumed to self-associate into macromolecules that remain in solution. Asphaltene precipitation is then considered as a liquid-liquid or solid-liquid equilibrium. Thermodynamic models have also proven successful in fitting and predicting asphaltene precipitation over a wide range of conditions. The two types of thermodynamic models used for asphaltene precipitation are equations of state and regular solution theory.

Equations of state (EoS) approaches include the Peng-Robison cubic EoS (Agrawal *et al.*, 2011) , the cubic plus association (CPA) EoS (Li and Firoozabadi, 2010), and the statistical associating fluid theory (SAFT) EoS (Ting *et al.*, 2003). Equations of state require the estimation of the critical properties for asphaltenes well beyond any available data (asphaltenes decompose at temperatures below their critical point which is unattainable and therefore undefined). Cubic equations of state provide poor predictions of asphaltene yields at high dilutions (Castellanos-Díaz *et al.*, 2011). CPA and SAFT have provided better predictions of asphaltene yields but are more complex to apply and have not yet been widely applied.

The regular solution method is based on Scatchard-Hildebrand theory (Andersen and Speight, 1999; Hirschberg *et al.*, 1984). The model was adapted using the Flory-Huggins lattice theory (Kawanaka and Mansoori, 1991), which takes into account the entropy of mixing of molecules with different molecular sizes (Hildenbrand *et al.*, 1970). This model has been successively modified to improve its predictive capability (Akbarzadeh *et al*., 2005; Alboudwarej *et al.*, 2003;

Kawanaka and Mansoori, 1991; Wang and Buckley, 2001). The regular solution model has successfully predicted asphaltene precipitation yields for asphaltene-solvent (Akbarzadeh *et al*., 2004) and bitumen-solvent systems (Akbarzadeh *et al.*, 2005) over a range of temperature and pressures. More recently, (Tharanivasan *et al*., 2011) extended the model to asphaltene precipitation during the depressurizing of a live oil (a pressurized crude oil with light ends and a high gas-to-oil ratio). It is proposed to adapt the regular solution approach for refinery streams and therefore the model is reviewed in more detail in Chapter 4.

Chapter Three: Experimental Methods

This chapter describes the samples used in this study, the characterization methodology, and the experimental methods used to characterize the crude oil samples and their SARA fractions. The characterization methodology includes water content determination, water removal, distillation assays, SARA fractionation, and characterization of each of the fractions by measuring molecular weight, density, refractive index, and elemental analysis (C, H, S and N).

3.1 Crude Oil Samples

Twenty one crude oils samples from different sources, processes, and extents of reaction were obtained and characterized in this thesis. Note that the experimental data in this thesis also includes data collected in three M.Sc. projects (Barrera, 2012; Okafor, 2013; Sadeghi-Yamchi, 2014). The samples were supplied by Shell Global Solutions with the exception of WC-B-A1 which was supplied by Syncrude Canada Ltd. Table 3.1 lists the samples used in this thesis. For the native samples from Western Canada (WC), the terms B, DB, VB, SR, and AR denote bitumen, dilbit, vacuum bottoms, short residue, and atmospheric residue.

The *in-situ* converted oils were directly treated in the reservoir and Table 3-2 shows the reservoir conditions for each sample. The extent of reaction in *in-situ* converted samples depends on the duration of their exposure to heating; that is, time in the reservoir during the thermal process. Hence, the date of collection of the sample is also specified. The original untreated sample in the reservoir was WC-B-B2.

Table 3-1. Bitumen and crude oil samples used in this thesis.

Native Oils	*In Situ* Thermocracked Oils	Visbreaker Thermocracked Oils	Hydrocracked Oils	Unknown Origin
WC-B-A1	26845-38	X-1357	HOSBottoms	27-168-179
Arabian	27034-113	X-1359	RHC-19-03	
Gippsland*	27034-87	X-1360	RHC-18-19	
WC-B-C1			RHC-18-37	
WC-B-B2				
WC-DB-A2				
WC-VB-B2				
WC-SR-A3				
WC-B-CL2				
WC-AR-HA				

*The asphaltene content was very low (<2 wt%) and the co-precipitated wax was very high for this oil, therefore, its asphaltenes were not further analyzed.

Table 3-2. Reservoir conditions for *in-situ* samples.

Sample	Temperature °C	Pressure MPa	Extent of Reaction	Date m/d/y
***In situ* Conversion**			%	
27034-113	275	9.84	29.9	3/15/2007
27034-87	314	2.90	78.9	1/7/2008
26845	317	1.96	97.8	10/13/2008

The thermocracked (X-##) and hydrocracked (RHC-##) samples came from a visbreaker and a catalytic hydrocracking reactor pilot plant, respectively. The pilot plants were run at different conditions to obtain different extents of reaction. Table 3-3 shows the operating conditions for the visbreaker and the catalytic hydrocracking reactor. Note that the samples were received as short residues (vacuum distillation residue) for this project and no further details of the pilot plant

operations are known. The HOS Bottoms sample came from an industrial refinery reactor. The feed to the visbreaker was WC-VR-B2 and the feed to the hydrocracking reactor was WC-SR-A3. The latter sample is believed to also be the feed to the refinery reactor.

Table 3-3. Average run operation conditions for visbroken and hydrocracked samples.

Sample	Average Temperature ^{o}C	Pressure psig	Conversion
Visbreaker - Thermocracked			***Wt% (520^{o}C+)***
X-1357	395	150	17.3
X-1359	415	150	31
X-1360	426	150	50.8
Catalytic Hydrocracking Reactor			***vol%***
RHC-19-03	410	2100	56
RHC-18-19	432	1960	70
RCH-18-37	440	1960	80
HOS Bottoms*	*	*	77

*Unknown operation conditions.

3.2 Characterization Methodology

Crude oils from downstream processes contain a large amount of distillable components. Some of the samples for this thesis were unmodified and still contained the distillable components; other samples (short residues) were obtained after vacuum distillation in Shell Laboratories. Crude oil samples with distillables were separated into two fractions, a light fraction (distillable) and a heavy fraction (bottoms or residues). The light fraction was characterized based on its boiling point distribution (distillation assay) and the heavy fraction was characterized based on a SARA assay. The short residues consisted only of the heavy fraction and were characterized based on a SARA assay alone. The distillation assays were divided into pseudo-components representing boiling

intervals and their physical properties determined from correlations. For each SARA fraction, its density, molecular weight, refractive index, and elemental composition were measured. Asphaltene solubility curves were also measured and used to determine solubility parameters of saturates, aromatics, and asphaltenes. The characterization methodology is depicted in Figure 3-1. The experimental methods are described in the following sections.

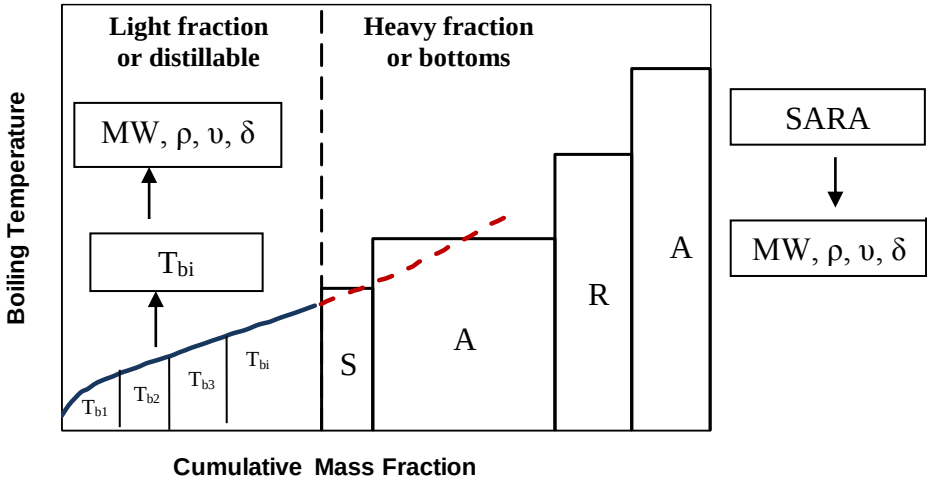

Figure 3-1. Schematic representation of the characterization methodology.

3.3 Sample Preparation - Dewatering

When the water content was higher than 4 wt%, the oil sample had to be dewatered before further characterization. If water is not removed, the compositions from the distillation assays and the SARA fractionations will be incorrect (modified trends distillation assays and it will report to the aromatic and resin fraction during SARA fractionation). The water content was determined using a Karl Fischer Titrator (Methohm 787 KF Titrino). The reagent was Aqualine Complete 5 by EMD from VWR International. The electrolyte solution was a mixture of 26 vol% 2-propanol and 74 vol% toluene, both solvents were ACS grade supplied by VWR International. Oil samples were diluted by mass with the electrolyte mixture and shaken until dissolved. Water percentage in the sample was calculated by interpolation of a calibration curve of volume of KF reagent used versus water content.

Crude oil samples 27034-113, WC-B-B2 and WC-B-C1 contained residual water greater than 4 wt%. These oils were dewatered using a batch distillation apparatus (Advanced Distillation Curve, ADC). The ADC distillation apparatus and procedure are described in Section 3.5. The procedure used for dewatering followed the same procedure but with a slower heating rate to a maximum temperature of 120°C.

3.4 Characterization of the Light Fraction: Distillation Assays

A crude oil distillation assay determines the boiling point distribution; that is, the boiling temperature versus cumulative volume fraction distilled (distillation curve). Two methods were used to measure the boiling point distributions: the Advanced Distillation Curve, ADC, and a spinning band distillation column, SBD. The ADC distillation allows the separation of all the light compounds that boil below 305°C and the distillation curve is based in the bulk temperature corresponding to the thermodynamic boiling temperature of the mixture; the SBD distillation fractionate the oil and provides the TBP distillation assays, the distillation assay is based in the temperature on the condensed vapours corresponding to the boiling temperature of the "pure" component. Figure 3-2 shows an example of both ADC and SBD distillation curves.

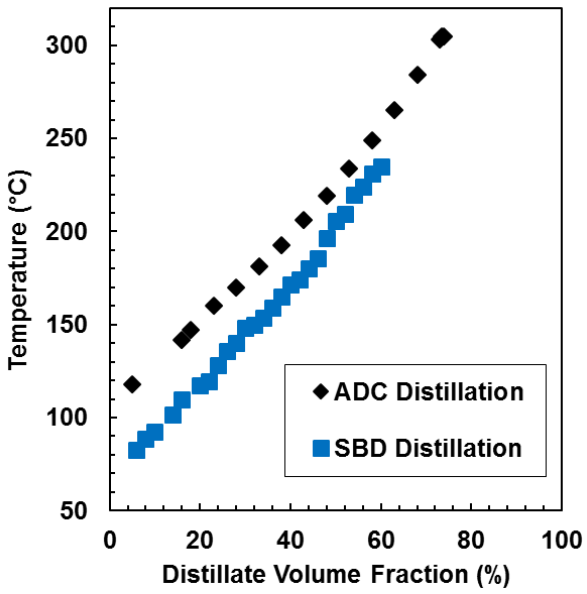

Figure 3-2. Distillation curves from ADC and SBD distillations for 27034-87 crude oil.

3.4.1 Spinning Band Distillation Column

Spinning band distillation, SBD, allows a sharp separation of fractions within a temperature range due to the presence of a fractionation device. The spinning band distillation apparatus (BR 36-100 fractional mini distillation system) was obtained from BR Instruments and is schematically presented in Figure 3-3. To perform a distillation, a known volume (from 50 to 100 mL) or mass of oil was placed in a 250 ml round bottom flask which contained a magnetic stirrer. The flask was placed in a heating mantle and secured to the column with a clamp. Two thermocouples were placed and secured in the system. The first was located in an adapter in the round bottom flask to measure the temperature of the fluid in the flask; the second was placed on top of the column to measure the temperature of the vapours taking off to the water-cooled condenser. Four calibrated receivers were placed and secured in the system after the condenser to collect the desired fractions.

The distillation was semi-automatically controlled with a BR M690 PC-interface. A heating rate was defined as an input in the software to bring the fluid to the initial boiling point. The reflux ratio (controlled with an automatic solenoid valve), temperature of each cut (temperature to change receivers), and final fluid temperature (temperature in the flask) were also input in the software. Once the oil was boiling, the column was left to stabilize for 90 to 120 minutes depending on the oil. After stabilization of the distillation column, that is, when pot and vapour (top) temperature reached a plateau, the distillables were collected according to the pre-determined inputs for the temperature range of each distillation cut. To avoid cracking, the distillation was stopped at 310^{o}C in the liquid. The data from the SBD distillation is equivalent to true boiling points (TBPs). TBPs are used to define the pseudo-components of a specific crude oil for modeling purposes. All the SBD distillations, hence the TBP data in this thesis, were performed at atmospheric pressure.

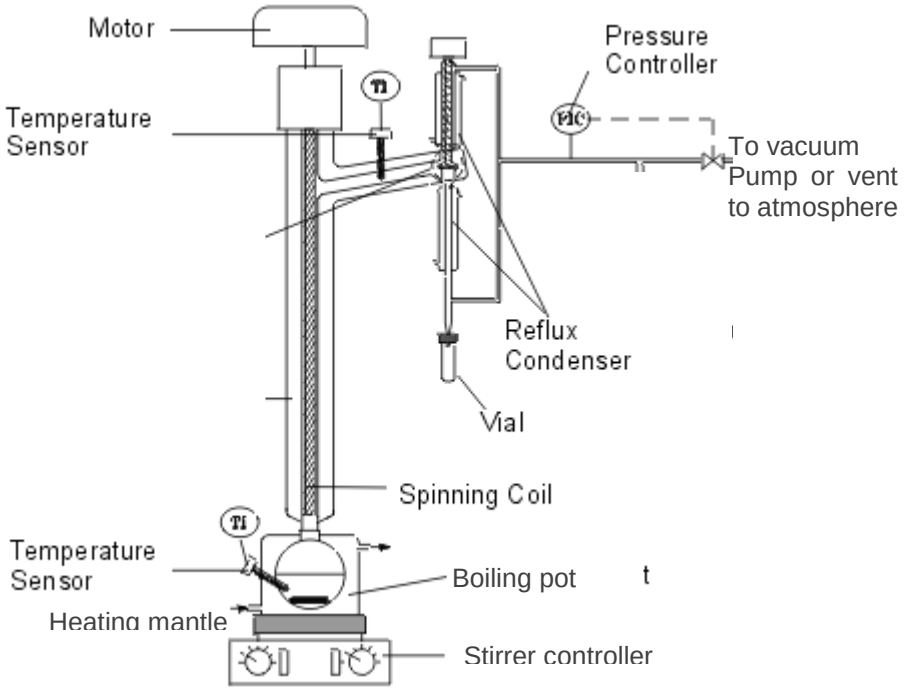

Figure 3-3. Schematic representation of the spinning band distillation column.

3.4.2 Advanced Distillation Curve, ADC

The ADC apparatus was designed by Bruno (2006) and is an improved procedure from ASTM D86. Figure 3-4 shows a schematic representation of the ADC apparatus. The apparatus was obtained from The National Institute of Standards and Technology, USA (NIST).

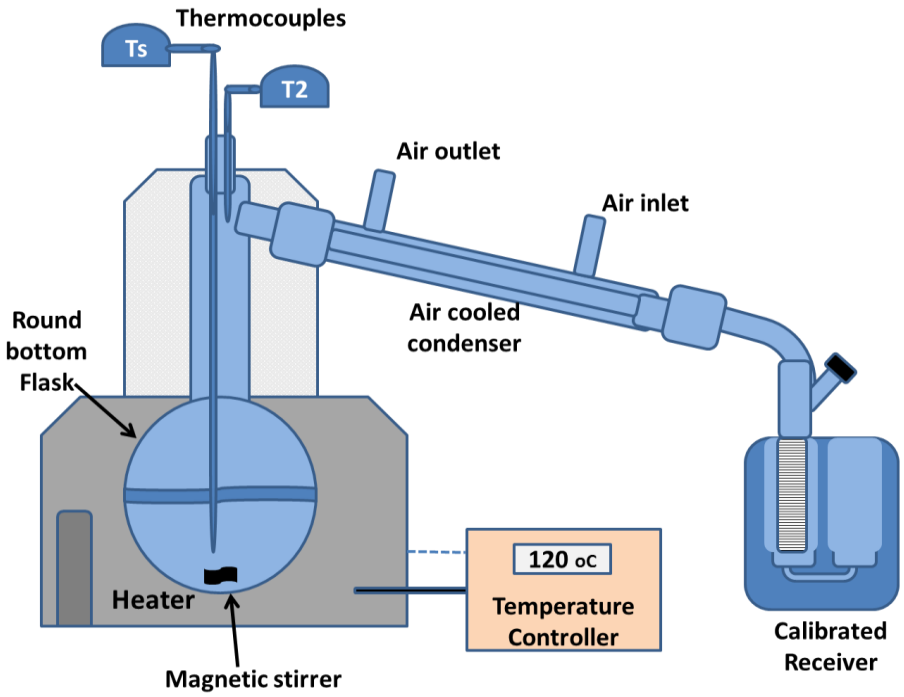

Figure 3-4. Schematic representation of the Advanced Distillation Curve apparatus (Ortiz, *et al.* 2013).

To perform an atmospheric distillation, an exact volume of sample was pipetted into a 500 ml round bottom flask containing a magnetic stirrer. If the oil sample was too viscous to be pipetted, the oil was poured directly into a tared round bottom flask and then weighed to determine the exact mass in the flask. The density of the oil was also measured to determine the volume added. The flask was placed in a heating mantle with a temperature controller to provide an appropriate heating rate for each fluid. The flask was connected to an air cooled condenser. The inlet air was cooled with a vortex tube (Bruno, 2006; Bruno, 1987) which was controlled with a manual valve to obtain the temperature required to condense the vaporized components (distillables). As the distillables became heavier and denser, the temperature of the air was increased. The condensed vapours flowed to a graduated receiver where the volume collected was recorded.

Two thermocouples were inserted through the top of the flask; Figure 3-4. One thermocouple measured the bulk fluid temperature which corresponds to the saturation temperature of the liquid in the still. The second thermocouple was placed on the take-off of the vapours. The top vapour

temperature can provide an insight on the presence of an azeotropic boiling point when it converges with the kettle temperature. This temperature can be also used to compare the results with standard ASTM D86. However, this top vapour temperature was not required for this thesis and only the bulk fluid temperature was used. To avoid cracking the oil, the distillation ended when the temperature in the bulk fluid reached 300 to 305ºC. The typical uncertainty in temperature measurements with the ADC apparatus is less than ±0.5ºC (Bruno, *et al.* 2010a; Bruno, *et al*. 2010b). All of the ADC data reported in the body of the thesis are from atmospheric distillations.

The ADC apparatus was also adapted by NIST to operate under vacuum (Bruno *et al*., 2011). The vacuum controller and instrumentation were obtained from NIST and the apparatus was commissioned in-house. Vacuum distillations were performed on a limited number of samples for more extensive characterization and modelling with the ADC distillation for future work. The ADC apparatus is a relatively new method and interconversion methods have not yet been developed for handling data collected at vacuum conditions. Therefore, an interconversion method was developed to convert the vacuum distillation data to normal boiling points using a trajectory optimization methodology (Ortiz *et al.,* 2013) for future work characterizing vacuum residues instead of atmospheric residues. However, vacuum distillation was not used for the work in this thesis and will not be discussed further.

3.5 Characterization of the Heavy Fraction: SARA Fractionation

SARA fractionation of the crude oil samples was performed using a modified ASTM D4124 procedure. SARA fractionation consists of a preliminary separation of asphaltenes with the addition of excess of *n*-alkane (*e.g.*, 40 to 1 *n*-alkane to oil). Saturates, aromatics, and resins were then separated using liquid chromatography. Technical grade (>99.5%) toluene was used for SARA analysis and solids removal. Acetone, *n*-pentane and *n*-heptane had a purity >99.5 and 99.7 wt%, respectively. Figure 3-5 shows the general procedure for SARA fractionation.

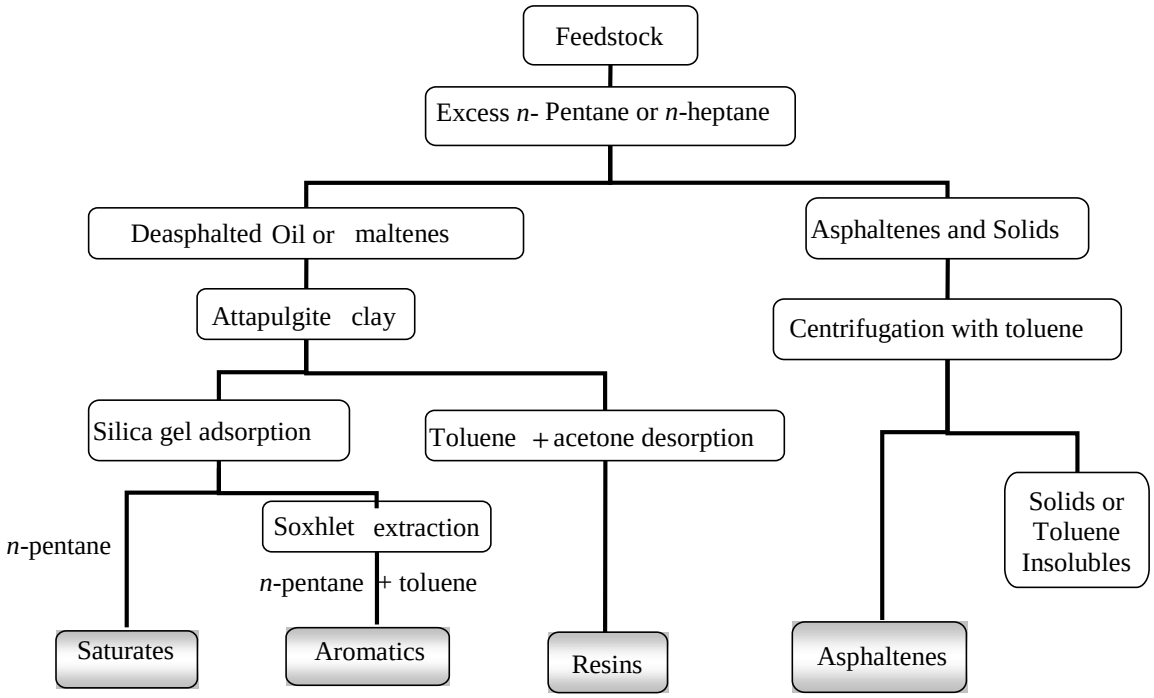

Figure 3-5. Schematic procedure of SARA fractionation.

3.5.1 Asphaltene Extraction: Precipitation and Solids Removal

The asphaltene precipitation procedure was a modified form of the ASTM D2007 standard. Asphaltenes were extracted from the heavy fraction (bitumen or bottoms of distillation) by addition of excess *n*-pentane or *n*-heptane at a ratio of 40 mL of solvent to 1 g of oil. The mixture was sonicated (non-intrusive mixing in a sonicator) for 60 minutes and left to settle at room temperature for a total contact time of 24 hours. Then, the supernatant was filtered through a Whatman #2 filter paper. The residue, approximately 20 to 25 vol% of the original mixture, was mixed with more solvent (4 to 1 ratio of solvent to original oil) and sonicated for 30 min. The mixture was left to settle overnight for up to 16 hours and then filtered using the same filter paper. The filter cake (precipitated asphaltenes) was washed on the filter paper at least three times a day by adding approximately 25 mL of solvent each time. After five days of washing the effluent from the filter was almost colorless.

The filter cake was dried in a closed fume hood until the total mass of the filter did not change significantly. The dry filter cake consisted of asphaltenes and solids; the material precipitated with

n-pentane and that precipitated with *n*-heptane were labeled "C5-asphaltenes+solids" and "C7-asphaltenes+solids", respectively. The residual filtrate was termed "diluted maltenes". Diluted maltenes from the *n*-pentane extraction (C5-maltenes) were recovered by evaporating the solvent using a rotary evaporator at 40°C to 60°C and atmospheric pressure. C5-maltenes were further dried in the oven at 60°C and vacuum (70 kPa vacuum) until the total mass did not significantly change.

Toluene insoluble material (such as clays and coke) were removed from the asphaltene-solids from native oils by dissolving the asphaltenes in toluene. The asphaltene-solids-toluene solution was sonicated for 40 to 60 minutes and settled for 45 minutes. Then, the solution was poured in centrifuge tubes and centrifuged for 6 minutes at 4000 rpm (1800 RCF). The centrifuged solution was decanted into a glass beaker and dried in a fume hood. However, asphaltene-solids from thermocracked and hydrocracked samples contained higher amounts of toluene insoluble materials which were not fully separated by centrifugation. Therefore, the solids removal procedure was modified by Sadeghi-Yamchi (2014) to effectively remove and recover these larger amounts of toluene insolubles. After centrifugation, the supernatant was filtered through a Whatman #2 filter paper. In this case, the toluene insolubles are the filter cake plus the solids in the centrifuge tubes. The repeatability of the standard solids removal procedure was ±6 wt% (Barrera, 2012; Sadeghi-Yamchi, 2014). The asphaltenes recovered after solids removal are termed "C5-" or "C7-asphaltenes". The average repeatability for C5-asphaltene extraction was ±2.1 wt% and ±2.8 wt% for C7-asphaltene extraction. Details in the error and repeatability analysis is presented in Appendix A.

Several asphaltene extractions were performed to be able to collect enough sample (C5-maltenes, C7-asphaltenes, and where possible toluene insolubles) for further fractionation and analysis. C5-maltenes were used for the liquid chromatographic fractionation. C5-asphaltenes were not analysed in this thesis. C7-asphaltenes were further used for extensive characterization through asphaltene fractionation in another project as explained elsewhere (Barrera, *et al.* 2013; Barrera 2012). Characterization of the toluene insoluble material is discussed in Chapter 5.

3.5.2 Chromatographic Separation of Saturates, Aromatics and Resins.

Saturates, aromatics, and resins (SAR) were fractionated from C5-maltenes using a modified ASTM D2887 procedure. Activated Attapulgus clay and silica gel were used as adsorbents in two glass separation columns mounted one above the other. The lower column was packed with approximately 200 g of activated silica gel and was topped with 50 g of clay; the upper column was packed with approximately 150 g of Attapulgus clay. Two upper columns were packed and used during the fractionation.

To start the procedure 5 g of C5-maltenes were dissolved in 25 mL of *n*-pentane. The two glass separation columns were initially wet with 25 mL of *n*-pentane and the maltene-*n*-pentane solution was poured into the top of the upper column. Then, 500 mL of *n*-pentane was added to the top of the columns at the same rate as elution from the lower column. Saturates did not adsorb in either of the adsorbents in the columns and passed through as a solution of saturates and *n*-pentane. After the elution stopped, the upper column was replaced by the second upper column and the procedure was repeated.

The aromatics and resins were adsorbed on the silica gel and attapulgus clay, respectively. To recover the aromatic fraction, the columns were eluted with 1600 mL of toluene-pentane mixture (1:1 vol). Then, the silica gel column was refluxed with 200 mL of toluene for 2 hours in a soxhlet apparatus. To recover the resin fraction, the two upper columns (clay columns) were connected and eluted with 800 ml of toluene-acetone mixture (1:1 vol). Saturates, aromatics and resins fractions were individually recovered by evaporating the solvent in a rotary evaporator and placing them in a fume hood overnight. The samples were further dried in an oven at 60^{o}C and vacuum (70 kPa vacuum) until there was no further change in mass. The SAR fractions were weighed and the yields were calculated. The average repeatability of the SAR fractionation was ±3.6 wt%, ±6.0 wt%, and ±5.5 wt% for saturates, aromatics and resins, respectively. The error analysis is presented in Appendix A.

3.6 Property Measurements of Crude Oil Fractions

The molecular weight, density and refractive index were measured for the fractions obtained from distillation and SARA fractionation. Elemental analysis was performed on the SARA fractions from the thermocracked and hydrocracked samples at the Shell Technology Center in Calgary.

3.6.1 Molecular Weight

Molecular weights were measured in a UIC Jupiter Model 833 vapour pressure osmometer (VPO) for samples dissolved in toluene at 50°C or dichlorobenzene at 110°C. The effect of temperature on molecular weight of asphaltenes was also studied in toluene at three different temperatures: 38, 77, and 88°C. A schematic representation of the VPO apparatus is shown in Figure 3-6.

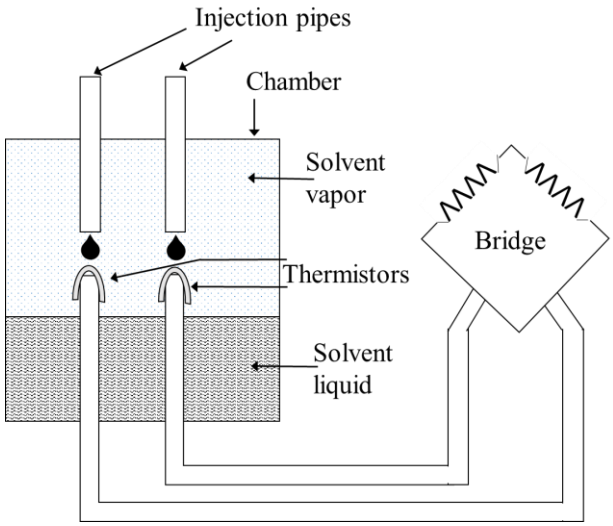

Figure 3-6. Schematic of a vapour pressure osmometer.

This technique is based on the difference of vapour pressure when a solute is added to a pure solvent at a defined temperature. The instrument has two thermistors in a closed chamber saturated with pure solvent vapour. Pure solvent is injected onto one thermistor and a solution of a solute in the same solvent is injected onto the second thermistor. The difference in vapour pressure between the two thermistors generates a difference in temperature which creates a different voltage at each thermistor. Equation 3-1 is used to relate the voltage difference with the molecular weight of the solute (Peramanu, *et al*. 1999).

$$\frac{\Delta E}{C_2} = K\left(\frac{1}{MW_2} + A_1 C_2 + A_2 C_2^{\,2} + \ldots\right) \qquad \textbf{3-1}$$

where ΔE is the voltage difference between the thermistors, C_2 is the solute concentration, K is the proportionality constant, and A_1 and A_2 are coefficients arising from the non-ideal behavior of the solution. Note that, the voltage difference is calculated from the absolute difference between the readings of a blank baseline (pure solvent in both syringes) and the sample measurements (solute-solvent solution in sample syringe) at each concentration.

To determine K, the proportionality or calibration constant, two solutes with known molecular weight are used, sucrose octaacetate (679 g/mol) and octacosane (395 g/mol). Concentrations from 1 to 5 g/L are prepared with each solute. The solutions prepared form nearly ideal mixtures with the solvent at low concentrations. In these cases, the higher order terms become negligible and Equation 3-1 is reduced to:

$$\frac{\Delta E}{C_2} = K\left(\frac{1}{MW_2} + A_1 C_2\right) \qquad \textbf{3-2}$$

Since MW_2 (molecular weight of the solute for calibration) is known, K can be easily determined by calculating the intercept in a plot of $\Delta E/C_2$ versus C_2. To calculate the molecular weight when the mixture solute-solvent is non-ideal, the slope in the plot $\Delta E/C_2$ versus C_2 had to be pre-defined, that is, the magnitude of A_1 must be known (Peramanu, *et al*. 1999). When the mixture solute-solvent is completely ideal, A_1 becomes zero and the molecular weight can be calculated as follows (Barrera 2012),

$$MW_2 = \frac{K}{\left(\Delta E / C_2\right)} \qquad \textbf{3-3}$$

Okafor (2013) determined the average magnitude of A_1 for saturates and aromatic fractions. The average slopes were found be 0.13 mV/(g/L)² and 0.09 mV/(g/L)² for saturates and aromatics, respectively. In this thesis, these slopes were applied to saturates and aromatics from native and *in-situ* converted oils (see Figures 3.7a and 3-78b). However, the slope changed for saturates and

aromatics from the thermocracked (X-##) and hydrocracked samples (RHC-##). Figure 3-8 compares the VPO data of saturates from native oils (closed symbols- Okafor 2013) and saturates from reacted oils (open symbols). The slopes are lower for both saturates and aromatics from thermo- and hydrocracked oils. The average value of *A* was found to be 0.04 mV/(g/L)^2 and 0.02 mV/(g/L)^2 for thermo- and hydrocracked saturates and aromatics, respectively.

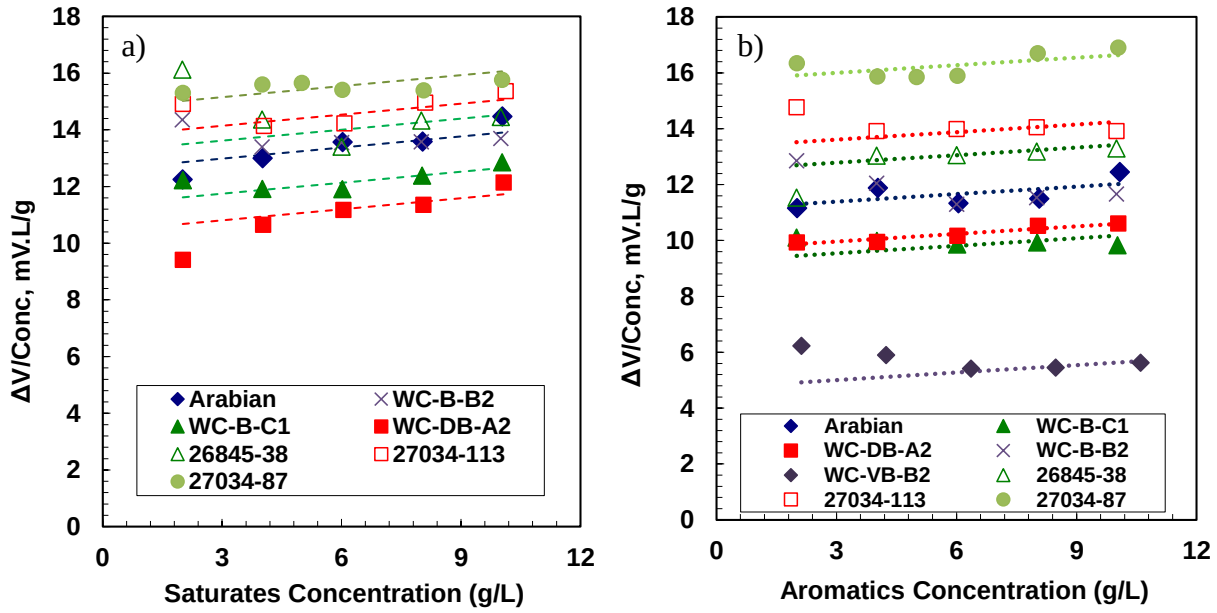

Figure 3-7. Measurements from the VPO for a) saturates and b) aromatics in toluene at 50°C.

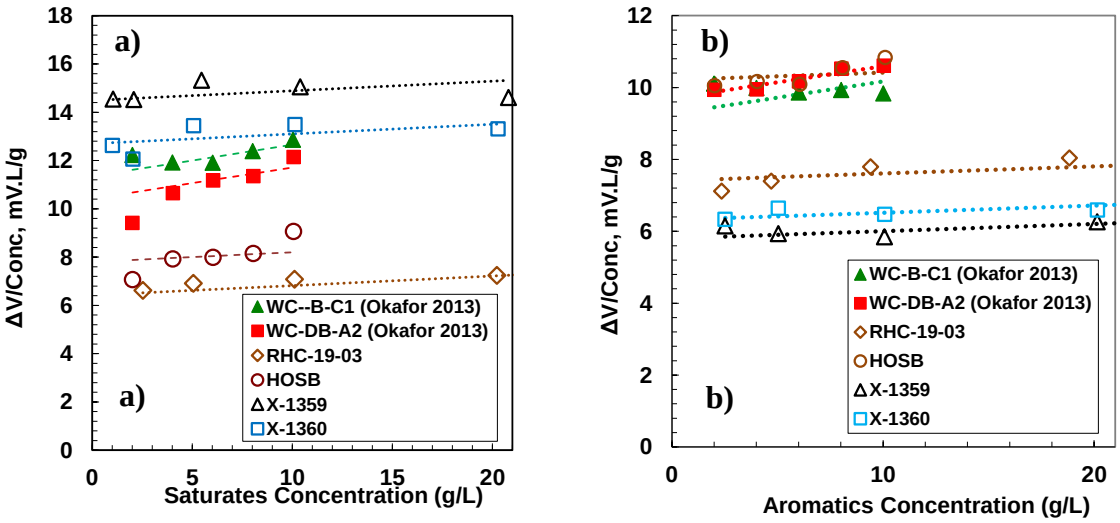

Figure 3-8. VPO measurements for a) saturate and b) aromatic fractions in toluene at 50°C.

Okafor (2013) also found that the slope was small and inconsistent for solutions of resins in toluene and assumed the slope for resins to be negligible in all cases. Note, in this thesis, the slope for aromatics from the reacted oils was even lower than the slope determined by Okafor. Hence, the slope was also assumed to be negligible for reacted resins and the average VPO response (Equation 3-3) to determine their molecular weight; that is, an A_1 of zero (Okafor, 2013). Barrera (2012) recommended using an A_1 of zero for asphaltene fractions. She found that even low values of A_1 (*e.g.*, -0.001) resulted in non-physical trends of MW with concentration. Therefore, Equation 3-3 was used for all resin and asphaltene samples.

During the molecular weight measurements, there were slight fluctuations in the voltage. These fluctuations are likely due to variations in local temperature, atmospheric pressure, and humidity. Therefore, a minimum of 3 to 5 readings were taken at each concentration to obtain a repeatable voltage response at each concentration. Concentrations between 1 to 50 g/L were used for each sample (crude oil fraction). Each sample was measured at least twice to reduce uncertainty and verify repeatability. The measured molecular weight of octacosane in toluene at 50°C was within 3% of the actual value. The repeatability of the molecular weight measurements in toluene at 50°C was approximately ±12% (Barrera, 2012; Okafor 2013).

Asphaltenes from hydrocracked (RHC-## and HOS) samples had limited solubility in toluene. Therefore, measurements of molecular weight in dichlorobenzene (DCB) at 110°C were performed by Sadeghi-Yamchi (2014) for asphaltenes from hydrocracked samples. A method was developed by Sadeghi-Yamchi (2014) to convert the measurements from DCB to toluene-equivalent molecular weights. His data are used in this work for modeling purposes. Molecular weight of toluene insolubles from hydrocracked samples were also measured in dichlorobenzene at 110°C and are discussed in Chapter 5.

3.6.2 Density

Densities were measured with an Anton Paar DM46 and a DMA 4500M density meter. These instruments apply the oscillating U-tube principle and are equipped with a U-tube sensor and an integrated reference oscillator. Most measurements were performed at 20°C and atmospheric pressure. The instrument precision is ±0.00001 g/cm³ with an accuracy of ±0.00005 g/cm^3.

The density of distillables, saturates and aromatics were measured directly. Resins and asphaltene densities cannot be measured directly because they are too viscous to handle or are a solid at ambient temperature. Instead, their densities were determined indirectly from the measured densities of solutions of resins or asphaltene in toluene at different concentrations (from 2 to 60 g/L for asphaltenes and 2 to 160 g/L for resins). The resin and asphaltene densities were determined from a mixing rule. The mixing rule for a regular solution is given by,

$$\frac{1}{\rho_{mix}} = \frac{w_1}{\rho_1} + \frac{w_2}{\rho_2} \qquad \textbf{3-4}$$

and a mixing rule for a solution with a non-zero excess volume is given by,

$$\frac{1}{\rho_{mix}} = \frac{w_1}{\rho_1} + \frac{w_2}{\rho_2} - w_S w_2 \left(\frac{1}{\rho_1} + \frac{1}{\rho_2} \right) \beta_{12} \qquad \textbf{3-5}$$

where ρ_{mix}, ρ_1 and ρ_2 are the mixture, solvent, and solute density (kg/m³), respectively; w_S and w_2 are the solvent and solute mass fraction, respectively; and β_{12} is a binary interaction parameter between the solute and the solvent.

Okafor (2013) determined the magnitude of the excess volumes, in particular the values of β_{12}, for solutions of saturates and aromatics in toluene and heptane. Figure 3-9 shows that the experimental specific volume (inverse density) data deviates from the linear regular solution trend for saturates and aromatics. Therefore, the excess volume mixing rule is required to determine their densities and the binary interaction parameters must be determined.

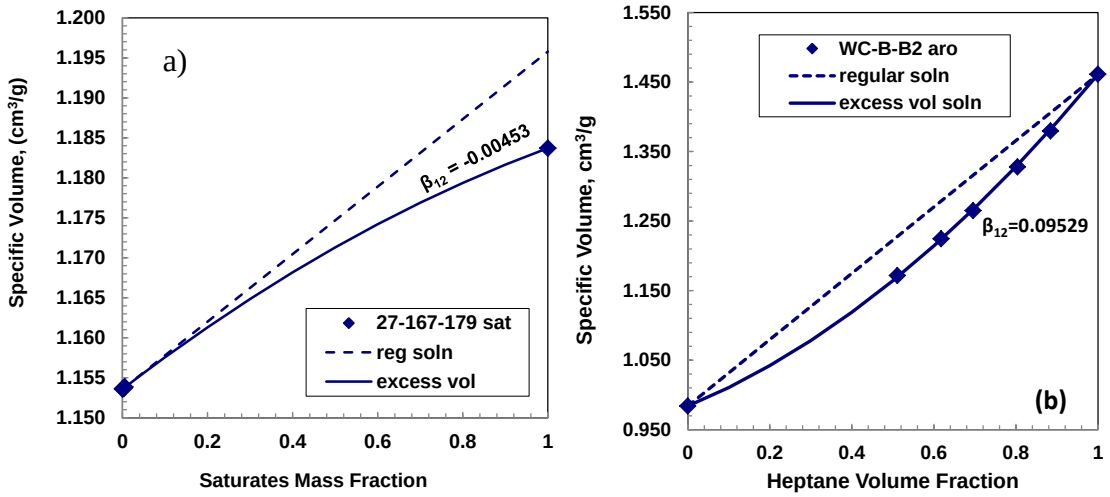

Figure 3-9. Density measurements of a) 27-168-179 saturates in toluene b) WC-B-B2 aromatics with heptane. Data from Okafor (2013). Note, Figure 3-9a a low concentration contain at least four data points which are not visible at the scale of the plot.

Saryazdi et al. (2013) found that the binary interaction parameters for the density of hydrocarbon mixtures correlates to the normalized difference between the mass specific volumes of the two components defined as follows:

$$v_N = \frac{2|v_1 - v_2|}{v_1 + v_2} \qquad \textbf{3-6}$$

where v_1 and v_2 are the mass specific volumes (inverse of density) of the two components. Okafor *et al* (2013) plotted the binary interaction parameters for saturates-toluene, saturates-heptane, aromatics-toluene, and aromatics-heptane (determined from fitting density data for saturates-solvent and aromatics-solvent mixtures) against v_N (see Figure 3-10). The interaction parameters follow a clear trend and were fitted with the following correlation:

$$\beta_{12} = -0.00754 + 0.05635\left(1 - \exp\left\{-1.5 v_N\right\}\right) \qquad \textbf{3-7}$$

The correlation fitted the majority of the data within 50% (Okafor, 2013).

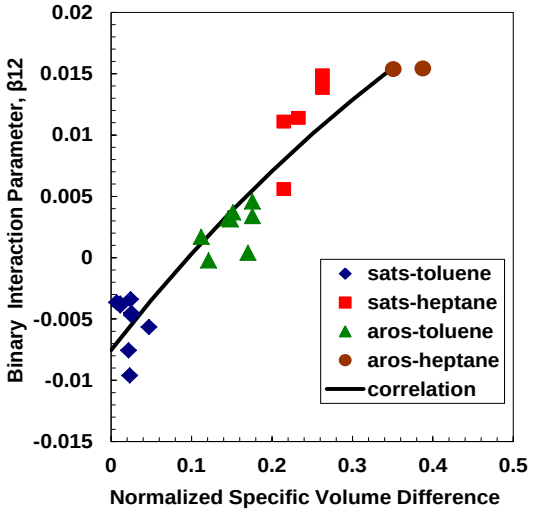

Figure 3-10. Binary interaction parameters of the excess volume of mixing of pseudo-binary mixtures saturate and aromatic with toluene and heptane. (Okafor, 2013).

When applied to resins, the correlation suggests that solutions of resins and toluene have non-zero excess volumes. However, Sadeghi (2014) measured the density of asphaltenes dissolved in both toluene and dichlorobenzene at 20°C and found that the asphaltene densities calculated with the regular mixing rule were the same for both solvents, Figure 3-11. The consistency of the results from the regular solution mixing rule indicate that there was no excess volume for asphaltene-toluene solutions. Data from Okafor (2013) and Sadeghi-Yamchi (2014) also suggests that mixtures of like-like solvents, such as aromatics-toluene, have very little or no excess volumes. Therefore, resins-toluene solutions which involve only aromatic components, may not have excess volumes.

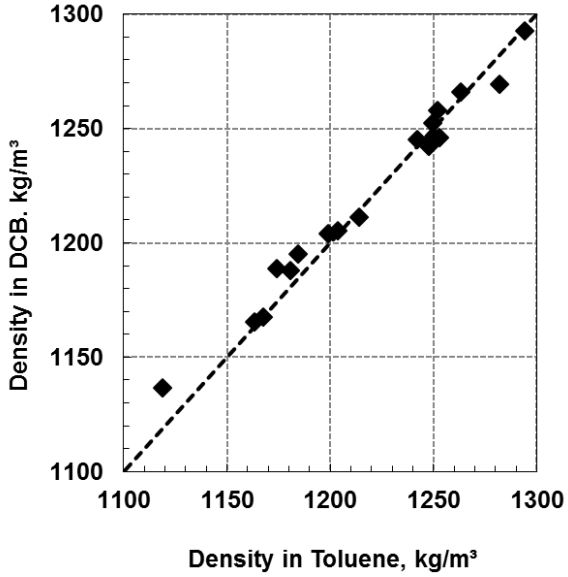

Figure 3-11. Comparison of densities measured in toluene and o-dichlorobenzene (DCB) for WC-VR-B2 and HOS Bottoms whole asphaltenes and their different solubility cuts. Data from Sadeghi –Yamchi (2014).

To resolve whether resin-toluene solutions have non-zero excess volumes, the density of three sample of resins were also measured in dichlorobenzene. Table 3-4 shows that the density from both toluene and DCB extrapolations are in excellent agreement for the three resins samples. Hence, it appears that mixtures of resins in aromatic solvents do not have excess volumes. The resin density extrapolations from all of the other samples were therefore performed using the regular mixing rule.

Table 3-4. Density values for resins from extrapolations using the regular solution mixing rule in toluene and dichlorobenzene (DCB) at 20°C.

Sample	Density from Toluene solutions	Density from DCB solutions	Reported Density
WC-VB-B2	1059.69	1058.95	1060
X-1359	1089.04	1090.45	1090
RHC-19-03	1050.16	1044.81	1050
RCH-18-37	1098.78	1097.79	1099

3.6.3 Refractive Index

Refractive indices (n_D) were measured with an Anton Paar Abbemat HP refractometer with a sodium D lamp (wavelength of 589.3 nm). The measurements were performed at 20ºC and atmospheric pressure. The instrument has a precision nD of ±0.00002 in refractive index.

The refractive index of distillables, saturates, and aromatics were measured directly. The sample was placed on the measuring prism and covered with a lid. The readings were taken after 5 to 60 seconds, depending on the sample, to wait for thermal equilibration and stable readings. Resins and asphaltenes samples were measured indirectly through toluene solutions at different concentrations, as explained earlier for density measurements. To extrapolate the value at zero solvent, rather than using the refractive index directly, the mixing rules usually use a correlation function of the refractive index (*FRI*) defined as follows,

$$FRI = \frac{n_D^2 - 1}{n_D^2 + 2} \qquad \textbf{3-6}$$

where n_D is the refractive index. All the refractive index measurements were converted to *FRI* and the extrapolations to zero solvent for resins and asphaltenes were performed. The repeatability of the *FRI* from direct measurements was ±0.00022 and ±0.00015 for saturates and aromatics, respectively (Okafor, 2013). The repeatability of the indirect *FRI* was found to be ±0.00261 for resins, and ±0.0035 for asphaltenes (Okafor, 2013).

As with density, either regular or excess *FRI* mixing rules were used for the *FRI* extrapolation in resins and asphaltenes. The *FRI* of a mixture is usually expressed as the volume average of the *FRI* components (Brocos *et al.*, 2003) for a regular mixture as follows,

$$FRI_{mix} = \phi_1 FRI_1 + \phi_2 FRI_2 \qquad \textbf{3-7}$$

where ϕ is volume fraction. Some mixtures exhibit excess *FRI* of mixing (due to excess molar refractions) and, in this case, the *FRI* of the mixture was calculated as follows,

$$FRI_{mix} = \phi_1 FRI_1 + \phi_2 FRI_2 - \phi_1 \phi_2 (FRI_1 + FRI_2) \beta_{12}^* \qquad \textbf{3-8}$$

where β_{12}^* is the binary interaction parameter for the refractive index.

Okafor (2013) measured the refractive index of several hydrocarbon mixtures (saturates-solvent and aromatics-solvent) and determined the excess *FRI* of each mixture, that is, the binary interaction parameter for refractive indexes. Figure 3-12 shows that, as with density, a clear trend was observed when the binary interaction parameter was plotted against the normalized *FRI* difference, FRI_N, defined as,

$$FRI_N = \frac{2\left|FRI_1 - FRI_2\right|}{FRI_1 + FRI_2} \qquad \textbf{3-9}$$

The following correlation fit the majority of the data in Figure 3-12 to within 60%,

$$\beta_{12}^{*} = 0.01699 - 0.04561\left(1 - \exp\left\{-5.71 FRI_N\right\}\right) \qquad \textbf{3-10}$$

The correlation could also be used to estimate the binary interaction parameters for solutions of resins and asphaltenes in toluene. However, the *FRI* in asphaltene mixtures were also analyzed to determine which mixing rule was more suitable for resins.

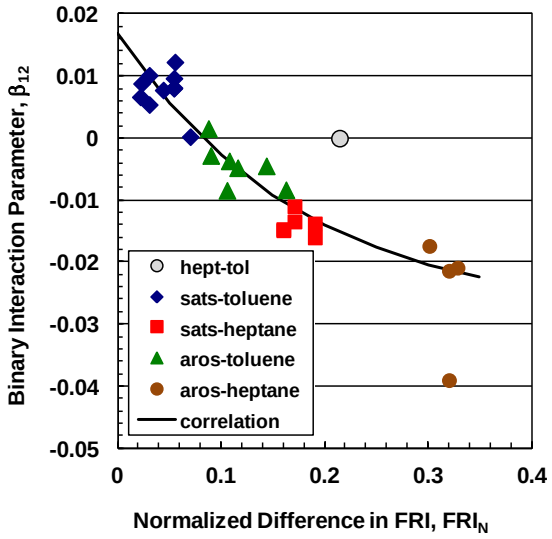

Figure 3-12. Relationship to normalized *FRI* of binary interaction parameters for the *FRI* of saturate and aromatic pseudo-binary mixtures with toluene and heptane (Okafor, 2013).

Sadeghi-Yamchi (2014) measured the refractive index of asphaltene solutions in toluene and dichlorobenzene. Recall that the regular density extrapolations for asphaltenes in both toluene and dichlorobenzene were found to match each other confirming regular solutions instead of excess volumes. Since refractive index is a correlated property of density, regular extrapolations were expected to match both solvents. Surprisingly, this was not the case for refractive index; the *FRI* regular extrapolations for asphaltenes in toluene and dichlorobenzene were not in agreement, as shown in Figure 3-13. However, when the excess *FRI* extrapolation in toluene was compared against the regular *FRI* extrapolation in DCB, the *FRI* was in very good agreement with both solvents. It is not clear why this difference exists between *FRI* results. One possible reason is that FRI mixing rules are not the most appropriate and other functions of the refractive index such as molar refractivity should be used for the mixing rules (Brocos *et al.*, 2003).

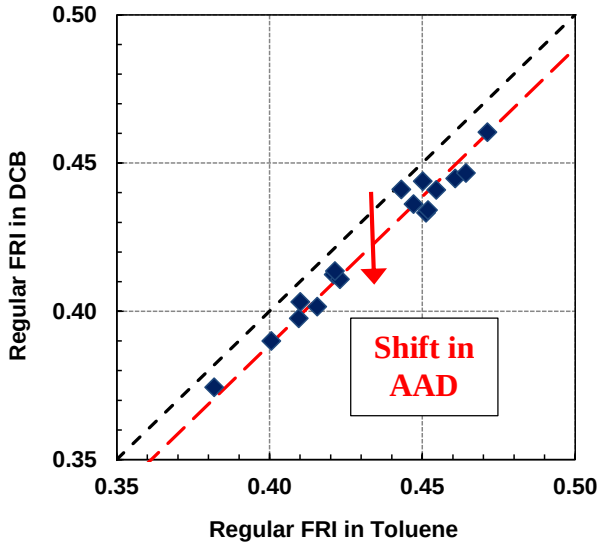

Figure 3-13. Average absolute deviation (Cross-plot) of asphaltene FRI from regular extrapolation of FRI in both DCB and toluene at 20°C and atmospheric pressure (Data from Sadeghi-Yamchi 2014).

In this thesis, refractive index measurements were performed for solutions of resins in both toluene and dichlorobenzene in order to determine the most suitable mixing rule to determine the FRI of resins. Figure 3-14 is a cross-plot of the FRIs obtained from resin-toluene and resin-DCB solutions using the regular mixing rule. The *FRI* appear to be shifted to slightly lower values in DCB but

the average absolute deviations (AAD: absolute difference between calculated FRI in toluene and FRI in DCB), Table 3-5, are small and no definite conclusion can be drawn.

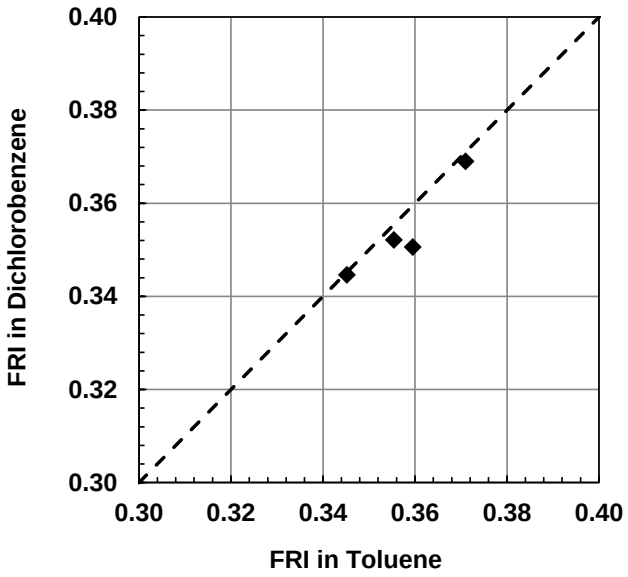

Figure 3-14. Comparison of FRI of resins from toluene and *o*-dichlorobenze solutions at 20°C and atmospheric pressure.

Table 3-5. Resin FRIs calculated with the regular mixing rule for toluene and dichlorobenzene and FRI average absolute deviation (AAD).

	FRI Toluene	**FRI DCB**	**AAD**
Toluene*	0.2926		
Dichlorobenzene*		0.3169	
WC-VB-B2	0.3452	0.3446	0.0006
X-1359	0.3595	0.3506	0.0089
RCH-19-03	0.3554	0.3521	0.0033
RHC-18-37	0.3710	0.3690	0.0020
		Average	0.0037

* Pure solvents

An alternative is to use the following mixing rule based on molar refractivities (FRI*molar volume) as recommended by Brocos *et al.* (2003):

$$R_m^{Mixture} = x_1\ R_m^1 + x_2\ R_m^2 + \Delta R_m^E \qquad \textbf{3-11}$$

where R_m is the molar refraction (or molar refractivity) of each compound, x is the mole fraction of each compound and ΔR_m^E is the excess molar refraction. Note that ΔR_m^E is zero if the mixture is regular. The molar refraction is defined as,

$$R_m = \left(\frac{n^2-1}{n^2+2}\right)\left(\frac{MW}{\rho}\right) = FRI\left(\frac{MW}{\rho}\right) \qquad \textbf{3-12}$$

where n is the refractive index of each compound or the mixture, MW is the molecular weight, and ρ is the density of each compound or the mixture.

Molar refractivities were applied to the resin data to investigate which type of solutions the resins formed. Figure 3-15 shows that the regular extrapolated molar refractivities in toluene and dichlorobenzene are in excellent agreement with very low AAD (Table 3-6). Therefore, regular extrapolations were performed for all the resins in this study.

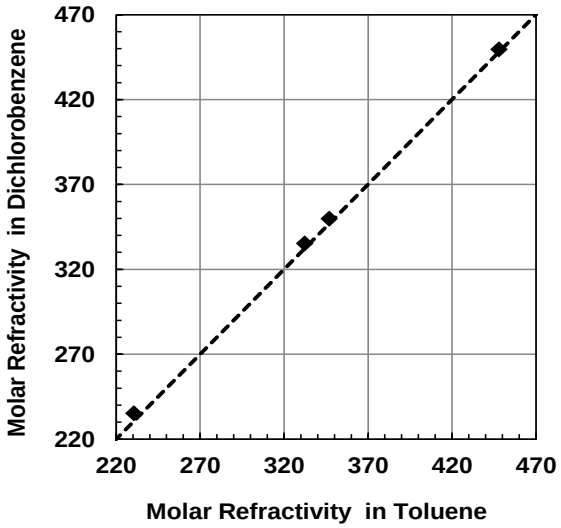

Figure 3-15. Comparison of the molar refractivity of resins from toluene and DCB solutions at 20°C and atmospheric pressure.

Table 3-6. Resins molar refractivities using Eq. 6-2 with $\Delta \boldsymbol{R_m^E}$=0 (regular mixing rule) in toluene and dichlorobenzene.

Sample	Molar Refractivity		AAD Rm
	Toluene Regular	DCB Regular	Tol-DCB
Toluene	31.1		
DCB		114.1	
WC-VB-B2	456.2	449.6	6.6
X-1359	356.3	349.9	6.4
RCH-19-03	338.6	335.3	3.3
RHC-18-37	236.4	235.2	1.2
		Average	4.4

Sadeghi's data for asphaltenes in solutions of either toluene or dichlorobenzene were reevaluated using molar refractivities to extrapolate asphaltene solution data. Asphaltenes have increasing molecular weight with increasing concentration; hence, there are two options to calculate molar refractivities in asphaltenes: 1) account for self-association using the specific molecular weight at each concentration, or; 2) use the monomer molecular weight assuming that molar refraction is independent of self-association. Figures 3-16a and 3-16b show the cross-plots comparing the regular extrapolations in toluene and dichlorobenzene using the average nanoaggregate molecular weight and an average monomer molecular weight of 700 g/mol, respectively. The average nanoaggregate molecular weight (and therefore Rm) is usually lower in dichlorobenzene than in toluene. Hence, the regular extrapolations taking association into account significantly differ between the two solvents, Figure 3-16a. If an average monomer molecular weight is used to calculate molar refractivities, the regular extrapolations in toluene and dichlorobenzene are in excellent agreement, Figure 3.16b.

The *FRI* calculated from the monomer based Rm extrapolations in toluene and dichlorobenzene are also in excellent agreement (see Figure 3-17). The good agreement suggests that the issue is not excess properties but rather the choice of mixing rule. However, these results are not conclusive and more research should be performed to concretely define the most appropriate mixing rule for

asphaltene solutions. Hence, the FRI from regular FRI extrapolations is used in this thesis to avoid the introduction of additional errors or calculation artefacts.

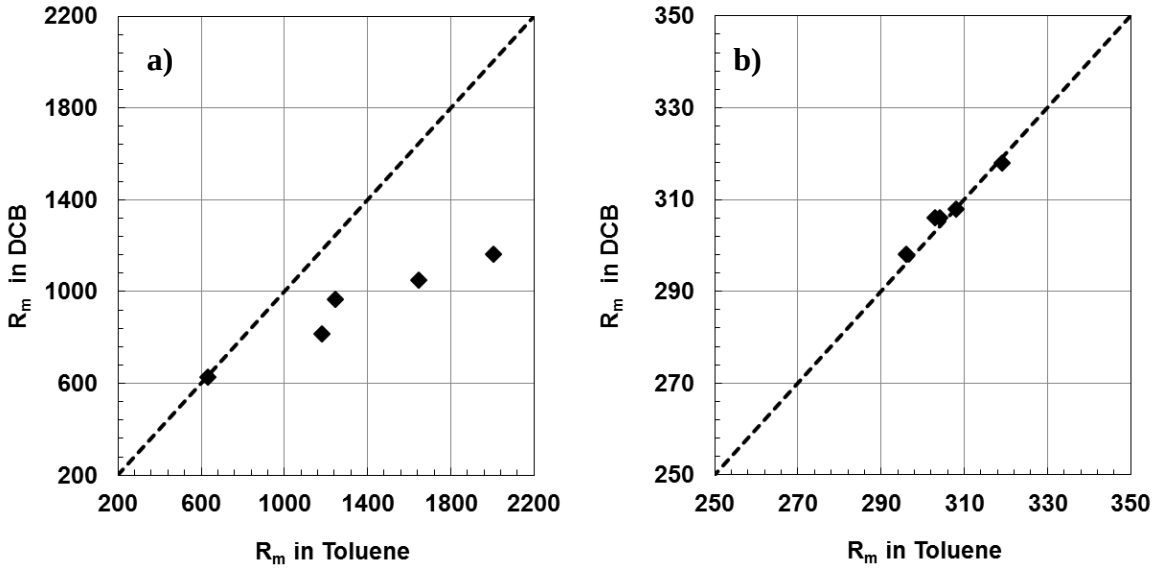

Figure 3-16. Comparison of the molar refractivity of asphaltenes in toluene and DCB solutions at 20°C and atmospheric pressure using: a) associated molecular weight; b) average monomer molecular weight.

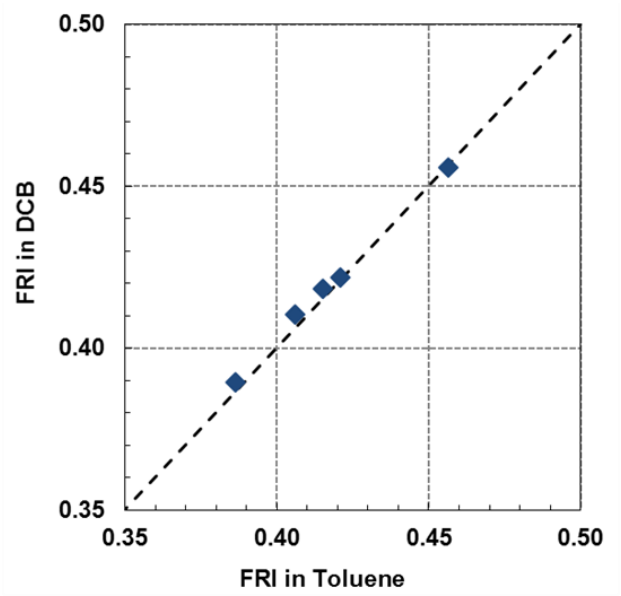

Figure 3-17. Comparison of *FRI* of Asphaltenes calculated from Rm from toluene and DCB solutions at 20°C and atmospheric pressure using average monomer molecular weight.

3.6.4 Elemental Analysis: CHNS

The elemental analysis for carbon, hydrogen, nitrogen and sulfur content was conducted at Shell Technology Center Calgary.

3.7 Solubility Measurements

3.7.1 Asphaltene Solubility

The asphaltene solubility curve is a plot of the yield of precipitated asphaltenes versus the mass fraction of the poor solvent, which is the solvent that promotes asphaltene precipitation (e.g. *n*-alkanes), see Figure 3-18. Asphaltene precipitation (solubility) measurements were performed in solutions of 10 g/L of asphaltenes in *n*-heptane-toluene (heptol) solvent mixture at 20ºC and atmospheric pressure. Asphaltenes were initially dissolved in a "good" solvent, in this case toluene, sonicating for 20 minutes. Then, a specific volume of the "poor" solvent, in this case, *n*-heptane, was added to the toluene-asphaltene mixture. The total volume of heptol mixture was usually 10 mL. The mixture was sonicated for at least 20 minutes and settled for 24 hours. Then, the vial containing the mixture was centrifuged at 4000 rpm (1800 RCF) for 6 minutes. The supernatant was decanted and the precipitated asphaltenes at the bottom of the vial were washed with the same solvent or heptol mixture. The vial was centrifuged again and the supernatant was removed. The washing procedure was repeated until the supernatant was colorless. The precipitated asphaltenes in the vial were dried under vacuum (70 kPa vacuum) at 60°C until there was no further change in mass. The asphaltene yields are calculated as the mass of precipitated asphaltenes divided by the initial mass of asphaltenes. The asphaltene yield are plotted as function of the corresponding heptane mass fraction (fraction of heptane in the heptol mixture). The main source of error was the consistency of the washing procedure. The repeatability for this type of experiments was previously determined to be approximately ±6% (Barrera 2012).

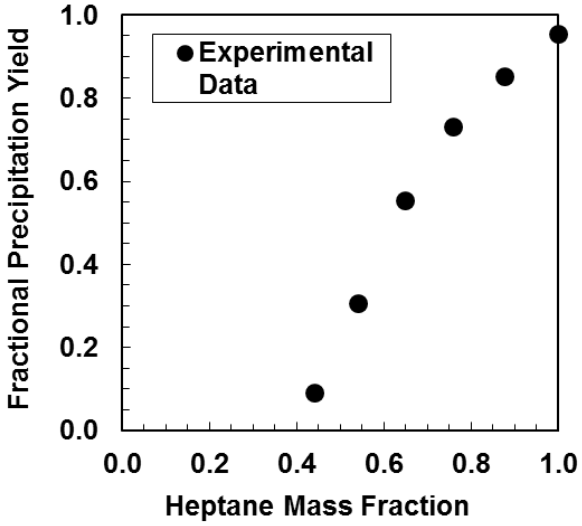

Figure 3-18. Fractional precipitation of C7 Peace River Asphaltenes from heptol mixtures at 10 g/L, 20°C and atmospheric pressure.

Asphaltene solubility plots were used to: 1) estimate solubility parameters of asphaltenes; and 2) choose the heptol (solvent mixture of heptane and toluene) ratio to fractionate asphaltenes. Fractionation of asphaltenes from the different crude oils presented this thesis (Table 3-1) was performed in two separate M.Sc. projects. The details of asphaltene fractionation procedures are explained elsewhere (Barrera 2012; Sadeghi-Yamchi 2014).

Barrera (2012) performed the fractionation and property measurements of asphaltenes from 5 native oils, 3 *in-situ* thermocracked oil and the unknown sample. Sadeghi-Yamchi (2014) performed the asphaltene fractionation and property measurements for the thermocracked and hydrocracked samples with the corresponding feedstock of the process. Data collected from the asphaltene fractionation and the property measurements were used to rebuild molecular weight and density distributions of asphaltenes.

3.7.2 Distillables, Saturates and Aromatics Solubility

Okafor *et al.,* (2014) adapted the solubility curve procedure for saturates and aromatics from reacted oil. The model solvent was saturates-toluene and *n*-heptane-aromatics rather than heptol. For the distillables solubility experiments, both distillable-*n*-heptane and distillable-toluene

solvent mixtures had to be also tested. Distillables are a combination of both aromatic and paraffinic compounds, therefore, they are an unknown mixture of poor and good solvents for asphaltenes.

Asphaltene concentration remained the same at 10 g/L for these experiments, but the total volume was adjusted to 1.5, 2 and 5 mL. In all the mixtures including saturates-toluene or distillable-toluene, the solvent used for washing the precipitated asphaltenes was *n*-heptane. Note that all the calculations and measurements in these experiments were performed on a mass basis.

Asphaltenes are not easily soluble in pure aromatics at room temperature, and therefore, the procedure was modified by Okafor (2013) to enhance dissolution for these solutions. Aromatics were initially poured into a vial of known mass; then a specific mass of asphaltenes was added. *n*-heptane was immediately added and the mixture was sonicated in a 60^{o}C water bath for at least 90 minutes. Once the asphaltenes were dissolved, the mixture was cooled to room temperature, weighed and settled for 24 hours. The vial was then weighed to determine *n*-heptane losses during the heated-mixing and settling times. The solution was centrifuged, the supernatant was decanted, and the precipitated asphaltenes were washed. The washing solvent was a solution of 90 vol% *n*-heptane and 10 vol% toluene. The precipitated asphaltenes were then dried in a 60°C oven under vacuum until no further change in mass was noted. Okafor (2013) determined the repeatability of the yields to be ±4 wt% and ±5 wt% for saturates and aromatics, respectively.

Aromatics from thermocracked and hydrocracked samples were more difficult to wash from the asphaltenes and yields higher than one were obtained, thus the washing procedure for reacted aromatic was modified to improve removal of aromatics from asphaltenes. The same washing solvent was added and sonicated for 20 minutes at 40°C. The washing procedure was repeated twice.

The solubility curves measured for distillables, saturates, and aromatics were used to determine the solubility parameters of these fractions using the modified regular solution model explained in Chapter 4.

3.7.3 Crude Oil Solubility or Stability Measurements in Terms of Asphaltene Precipitation

The crude oil solubility curve (or stability measurements) shows the asphaltene precipitation yields from a crude oil versus the mass fraction of added solvent, usually *n*-heptane. Stability of crude oil in this thesis refers to the ability of the crude oil to keep asphaltenes in solution; hence, a stable crude oil is defined as an oil which does not precipitate asphaltenes at a defined condition (temperature, pressure, amount of added solvent). Experimentally, a specific mass of crude oil (2 to 5 g) was poured into a 10 mL glass vial and diluted with *n*-heptane at a specific ratio. The mixture was sonicated for at least 60 minutes and left to settle for 24 hours at room temperature. Then, the mixture was centrifuged for 6 minutes at 4000 rpm (1800 RCF). The supernatant was decanted and the precipitated asphaltenes were washed with *n*-heptane as described earlier for the asphaltene solubility curves. When the supernatant was almost colorless, the precipitated asphaltenes were dried in an oven at 60^{o}C under vacuum (70 kPa vacuum) until no further change in mass was noted. The repeatability of the experiment was within ±6 wt% to ±12 wt% for low and high *n*-heptane mass fractions, respectively.

For highly viscous and solid-like crude oil samples, the solubility procedure was modified to include dilution and heating. To perform the experiments, the sample was left in an oven overnight at 60 or 90°C, as required, under vacuum (to prevent further oxidation). The temperature was selected based on the type of oil and its viscosity. Then, a known mass of oil was poured into a glass vial (between 0.8 and 2 g) and a specified mass of toluene was added. The mixture was sonicated in a 50^{o}C water bath for at least 60 minutes until the oil sample was dissolved. A specified mass of heptane was added and the mixture was sonicated for 20 minutes more. The mixture was left to settle for 24 hours and the same centrifuging, washing, and drying procedures were applied. This method was used for the thermocracked samples received after vacuum distillation (vacuum bottoms or short residue), which were solid at room temperature as well as for two highly viscous hydrocracked samples.

The crude oil solubility curves were used to tune the modified regular solution model in terms of the molecular weight of asphaltene in the oil (see Chapters 4 and 5).

3.8 Experimental Work Performed in this Thesis

Experimental data from several sources (Akbarzadeh et al 2005, Barrera 2012, Okafor 2013, Sadeghi-Yamchi 2014) were used in this thesis. In addition, the following experimental work was performed in this thesis:

1. Dewatering (and water content determination)
2. Distillation assays: ADC and SBD distillation
3. Characterization of the distillable fractions including solubility measurements.
4. SARA fractionations for all the samples
5. Characterization of SAR fractions from four native oils (WC-B-B2, WC-SR-A3, WC-B-C1 (preliminary), Gippsland)
6. Preliminary characterization of *in situ* converted SAR fraction: topped samples (oven procedure, not reported in this thesis because it did not allow characterization of the distillable fraction)
7. Characterization of SAR from RCH-## and X-## samples including low solubility measurements of saturates and aromatics from this samples.
8. Asphaltene fractionation and characterization of two native samples (WC-B-B2 (test sample), WC-DB-A2)
9. Asphaltene extraction (*n*-heptane) from several samples (and solids removal).
10. Molecular weight measurements (VPO) of asphaltenes at different temperatures.
11. Toluene insolubles extraction and characterization.
12. Asphaltene solubility measurements in solvents for three native asphaltenes (WC-B-A1 (test), WC-B-B2, WC-DB-A2), *in situ* asphaltenes (preliminary) and HOS asphaltenes (preliminary).
13. Crude oil solubility measurements for all the bitumens, heavy fractions and whole oils.

Chapter Four: Regular Solution Model for Asphaltene Precipitation and Self-Association Model for Asphaltene aggregation

In this chapter, a previously developed regular solution theory based model for asphaltene precipitation is described. This model has been successfully applied to model asphaltene precipitation from native/virgin oils (Alboudwarej *et al.,* 2003; Akbarzadeh *et al.*, 2005). Recent updates to the model including a new correlation of asphaltene density to molecular weight (Barrera, 2012) are presented. In this thesis, the old correlations are further updated and new correlations are developed to be applied for both native and reacted oils but these updates will be presented in later chapters.

4.1 Regular Solution Theory for Asphaltenes

Regular solution theory was first applied to asphaltene precipitation by Hirschberg *et al.,* (1984). The enthalpy contributions from the Scatchard-Hildenbrand solubility theory and the entropic contribution from the difference in molecular sizes (Flory-Huggins parameter) were included to model asphaltene precipitation. This model was later refined and extended to asphaltene precipitation from heavy oils and bitumens (Alboudwarej *et al.*, 2003; Akbarzadeh *et al*., 2005; Tharanivasan *et al.*, 2009). A liquid-liquid equilibrium is assumed to exist between the heavy liquid phase (asphaltene-rich phase including only asphaltenes and resins) and the light liquid phase (solvent-rich phase including all components). The equilibrium constant, the ratio of the mole fractions of a component in each phase, is related to the activity coefficients in each phase as follows:

$$K_i = \frac{x_i^H}{x_i^L} = \frac{\gamma_i^L f_i^{oL}}{\gamma_i^H f_i^{oH}} \exp\left[\int_0^P \frac{\Delta v_i}{RT} dP\right] \qquad \textbf{4-1}$$

where K is the equilibrium constant, x is the mole fraction, γ is the activity coefficient, f is fugacity, v is the molar volume, P is pressure, R is the universal gas constant, T is temperature in Kelvin, subscript i denotes component number, superscripts L and H refer to the light and heavy phase, respectively, and superscript o is the standard state.

For a liquid-liquid equilibrium, the term $\left(f_i^{0\,L}/f_i^{0\,H}\right)$ and $\exp\left[\int_0^P\left(\Delta\upsilon_i dP/RT\right)\right]$ are unity and Equation 4-1 reduces to the ratio between the activity coefficients, γ, of each component in the light and heavy phase. The activity coefficients are calculated using regular solution theory with the entropic contributions as follows (Prausnitz, *et al* 1999; Hildenbrand, *et al* 1970; Kontogeorgis and Folas 2010),:

$$\ln\gamma_i^L = \ln\frac{\upsilon_i^L}{\upsilon_m^L} + 1 - \frac{\upsilon_i^L}{\upsilon_m^L} + \frac{\upsilon_i^L}{RT}\sum_j^n\sum_k^n \phi_j\phi_k\left(D_{ij} - 0.5D_{jk}\right) \qquad \textbf{4-2}$$

where m is the mixture, and ϕ_i is the volume fraction defined as,

$$\phi_i = \frac{x_i\upsilon_i}{\sum x_i\upsilon_i} \qquad \textbf{4-3}$$

and

$$D_{jk} = \left(\delta_j - \delta_k\right)^2 + 2l_{jk}\delta_j\delta_k \qquad \textbf{4-4}$$

where δ is the solubility parameter and l_{jk} is the interaction parameter between the two components *j* and *k*. In the model used in this thesis, the interaction parameter is assumed to be zero; that is, $l_{jk} = 0$. Equation 4-2 then reduces to:

$$\ln\gamma_i^L = \ln\frac{\upsilon_i^L}{\upsilon_m^L} + 1 - \frac{\upsilon_i^L}{\upsilon_m^L} + \frac{\upsilon_i^L}{RT}\left(\delta_i - \delta_m\right)^2 \qquad \textbf{4-5}$$

The solubility parameter of the mixture, δ_m, is calculated as follows:

$$\delta_m = \sum_i^m \phi_i\delta_i \qquad \textbf{4-6}$$

Equation 4-5 is substituted into Equation 4-1 to obtain the following expression for the equilibrium ratio, K_i, for any given component:

$$K_i^{hl} = \frac{x_i^h}{x_i^l} = exp\left\{ \begin{array}{l} \frac{v_i^h}{v_m^h} - \frac{v_i^l}{v_m^l} + ln\left(\frac{v_i^l}{v_m^l}\right) - ln\left(\frac{v_i^h}{v_m^h}\right) + \\ \frac{v_i^l}{RT}\left(\delta_i^l - \delta_m^l\right)^2 - \frac{v_i^h}{RT}\left(\delta_i^h - \delta_m^h\right)^2 \end{array} \right\} \quad \textbf{4-7}$$

Note, it was assumed that the heavy phase contains only asphaltenes and resins. Experimental observations support this assumption (Yarranton, *et al.* 2011). Once the equilibrium ratios are known, the phase equilibrium is determined using standard techniques. To use this model, the mole fraction, molar volume, and solubility parameter of each component in the mixture must be specified.

4.2 Fluid Characterization for the Regular Solution Model

Fluid characterization involves dividing the fluid into components and pseudo-components that represent the property distributions within the fluid. The solvents used in this study are pure components or mixtures of pure components. Heavy oils and bitumens are divided into pseudo-components based on a SARA analysis. As noted above, the molar volume (molecular weight and density) and solubility parameters of each component are required.

4.2.1 Mole Fractions and Molecular Weight

The mass fraction and molecular weights of the solvent used in this thesis are known. The mass fraction (and samples for analysis) of each component in the crude oil is obtained from the SARA assay. Saturates, aromatics, and resins were treated as single uniform pseudo-components. Asphaltenes were further divided into mass fractions of different molecular weight. Once the molecular weights are determined, the mass fractions are converted to mole fractions.

4.2.1.1 Saturates, Aromatics, and Resins

When available, the measured molecular weights for the saturates, aromatics, and resins are used. If the molecular weights are not known, an average molecular weight for SAR fractions from native oils, Table 4-1, can be also used without introducing significant error in the model

(Akbarzadeh *et al*., 2005). The first set of molecular weights in Table 4-1 were based on data from SAR fractions from Western Canadian oils (Akbarzadeh *et al*., 2005). Recently, Okafor (2014), measured the molecular weights of saturates, aromatics and resins from native oils and reacted oils from a variety of sources. Okafor found that the absolute repeatability of the molecular weight measurements for saturates and aromatics was 34 g/mol and 50 g/mol, respectively. Her measurements of MW for SAR fractions from native oils are averaged with the previous measurements to determine the new average molar masses included in Table 4-1. Not surprisingly, both the old and new averages agree within the uncertainty of the measurements.

Table 4-1. Average Molecular weights (MW) of SAR fractions

Fraction	MW at 50°C (g/mol) Akbarzadeh *et al* (2005)	Molar Mass at 50°C (g/mol) including Okafor (2013)
Saturates	460	435
Aromatics	522	496
Resins	1040	1056

4.2.1.2 Asphaltenes

Asphaltenes were divided into mass fractions of different molecular weight using the Gamma probability density function given by,

$$f(MW) = \frac{(MW - MW_{mono})^{\alpha-1}}{\beta^{\alpha}\Gamma(\alpha)} \exp\left(\frac{MW_{mono} - MW}{\beta}\right) \qquad \textbf{4-1}$$

where MW_{mono} is the asphaltene monomer molecular weight, $f(MW)$ is the mass frequency of the given molecular weight, α is a parameter which determines the shape of distribution and β is given by:

$$\beta = \frac{MW_{avg} - MW_{mono}}{\alpha} \qquad \textbf{4-2}$$

where MW_{avg} is the average molecular weight of asphaltene nanoaggregates The distribution is discretized into n fractions of constant step size (ΔMW) and the mass fraction of each fraction is calculated as follows:

$$x_i = \frac{\int_{MW_i}^{MW_{i+1}} f(MW)dMW}{\int_{MW_1}^{MW_n} f(MW)dMW} \qquad \textbf{4-3}$$

In the original model, the recommended values for α are from 2 to 4. The monomer molecular weight was taken as 1500 g/mol. For asphaltenes in solvents, the input average molecular weight, MW_{avg}, is the experimental value measured for the asphaltenes in toluene at 50ºC and 10 g/L (VPO measurement) and corrected to the desired temperature as follows (Tharanivasan 2012),

$$MW_T = MW_{50^oC} \cdot \exp\left(0.0073 \cdot (50 - T)\right) \qquad \textbf{4-4}$$

where T is the temperature in ºC. For asphaltenes in crude oils, the average asphaltene molecular weight cannot be measured but is expected to be lower than the measured molecular weight in toluene due to the presence of resins. Instead, the average molecular weight of the asphaltenes in the crude oil is determined by adjusting it to fit asphaltene precipitation data.

The Gamma molecular weight distribution was experimentally tested by Barrera *et al.* (2012). They collected molecular weight data for asphaltene fractions from native oils and *in-situ* reacted oils. Molecular weight distributions were reconstructed from the experimental data by adapting a previously developed self-association model (T/P model). Details of the self-association model and the MW distributions are reported elsewhere (Barrera *et al*., 2012). Barrera *et al.* (2013) and Yarranton *et al*. (2013) found that not all the asphaltenes participate in association and defined the part of asphaltenes that does not participate in association as neutral asphaltenes. They found that the best match between the gamma distribution and the self-association model distributions was when neutrals were excluded from the gamma distribution. However, excluding neutrals is not practical because there are no straightforward techniques to determine precisely the ratio/composition of neutrals within the asphaltene fraction. Therefore, the following new guidelines are recommended for constructing a representative Gamma distribution:

1) monomer molecular weight, $M_{mono,}$ of 900 g/L.
2) average molecular weight as described for original model
3) α = 2.0 for native petroleum asphaltenes when the amount of neutrals (asphaltenes that do not associate) is unknown and they are then included in the gamma distribution
4) α = 1.8 for native petroleum asphaltenes (excluding neutrals) when the mole fraction of neutrals is known; the neutrals are included separately as a pseudo-component with monomer properties

4.2.2 Density and Molar Volume

Molar volume is the ratio of molecular weight to density as follows

$$v = \frac{MW}{\rho} * 1000 \qquad \textbf{4-5}$$

where v is the molar volume (cm^3/mol), MW is the molecular weight (g/mol) and ρ is the density (kg/m^3). Therefore, densities, along with molecular weights, are required to estimate the molar volume of each fraction.

4.2.2.1 Pure hydrocarbons (Toluene, *n*-pentane, *n*-heptane)

The molecular weight is defined by the chemical structure of each pure hydrocarbon. The densities and molar volumes of the pure components are known or can be determined using well-established Hankinson-Brobst-Thomson (HBT) method (Reid *et al.,* 1987, Perry and Green, 1997) or effective density correlations (Tharanivasan, 2012).

4.2.2.2 Saturates and Aromatics

The molecular weights are measured or with average properties. The densities of saturates or aromatics are obtained from measured values, if available; otherwise average values, shown in Table 4-2, can be used without significantly changing the model predictions. The first set of average values were reported by Akbarzadeh *et al.* (2005). Recently, Okafor (2013) measured the densities for several aromatic and saturate fractions from native and partly reacted oils. Okafor's data were averaged with the original dataset to obtain the second set of average values. The old

and new averages are within the standard deviation (20 kg/m^3) of the measurements which shows consistency of the results.

Table 4-2. Average density for Saturates, Aromatics and Resins.

Fraction	Density at 23°C (kg/m^3) Akbarzadeh et al 2005	Density at 23°C (kg/m^3) including Okafor 2013 data
Saturates	880	869
Aromatics	990	999
Resins	1044	1049

Akbarzadeh *et al.* (2005) also developed correlations to predict the change in density (and therefore molar volume) with temperature for any saturate or aromatic fraction as follows:

$$\rho_{sat} = 1069.54 - 0.6379T \qquad \textbf{4-6}$$

$$\rho_{aro} = 1164.73 - 0.5942T \qquad \textbf{4-7}$$

where ρ_{sat} and ρ_{aro} are the densities of saturates and aromatics in kg/m^3, respectively, and T is the temperature in K. Okafor (2013) studied more extensively the effect of temperature on density of saturate and aromatic fractions. She developed a new correlation to predict density at any temperature and atmospheric pressure as follows,

$$\rho_T = \rho_{20} \exp(-\alpha_{V,X}(T - 20)) \qquad \textbf{4-8}$$

where ρ_{20} is density (g/cm^3) at 20°C and $\alpha_{V,X}$ is thermal expansion coefficient for saturates or aromatics and T is temperature in °C. The thermal expansion coefficient was found to be constant over the temperature range of the dataset (20 to 60ºC) and correlated linearly to the specific volume at 20ºC as follows:

$$\alpha_{V,sat} = -0.00079116 + \frac{0.0013488}{\rho_{20}} \qquad \textbf{4-9}$$

$$\alpha_{V,aro} = -0.0004627 + \frac{0.0011372}{\rho_{20}} \qquad \textbf{4-10}$$

4.2.2.3 Asphaltenes and Resins

In a previous model Yarranton *et al.*, (1996) developed a power law correlation of asphaltene density, ρ, to molecular weight, MW, as follows:

$$\rho_A = 670\ MW^{0.0639} \qquad \textbf{4-11}$$

with the density expressed in kg/m^3 and the molecular weight (MW) in g/mol. This correlation was based on a limited set of measurements for Athabasca bitumen asphaltenes (Alboudwarej *et al* 2003). The density of resins was estimated from experimental values when available, the average value from Table 4-1 (for resins), or with Equation 4-11 if necessary.

Barrera (2012) measured the density of asphaltenes and their fractions from several other heavy oils and bitumens. The density data was plotted against the molecular weight of the asphaltenes at 10 g/L, and a revised density correlation was formulated (Barrera *et al*., 2013) as follows:

$$\rho = \rho_0 + \Delta\rho \cdot \left(1 - \exp\left(\frac{MW_0 - MW}{a}\right)\right) \qquad \textbf{4-12}$$

where ρ_0 (kg/m^3) and MW_0 (g/mol) are the density and the lowest molecular weight for an asphaltene molecule or aggregate, respectively, $\Delta\rho$ is the density difference between the lowest and highest molecular weight asphaltene, and a is a fitting parameter. Specific parameters and fitting coefficients were determined for each crude oil measured and shown elsewhere (Barrera, 2012). Average parameters were then calculated and the following correlation was proposed for the density of asphaltenes from native oils.

$$\rho_A = 1100 + 100\left(1 - \exp\left(-\frac{MW}{3850}\right)\right) \qquad \textbf{4-13}$$

Figure 4-1 compares the results from the generalized correlation with the experimental data from all the samples. The densities calculated with Equation 4-13 were within a maximum error of 40

kg/m³ and average absolute deviation of 11 kg/m³. The molar volume is then calculated using the estimated density for each subfraction of asphaltenes and its corresponding molecular weight from the Gamma distribution.

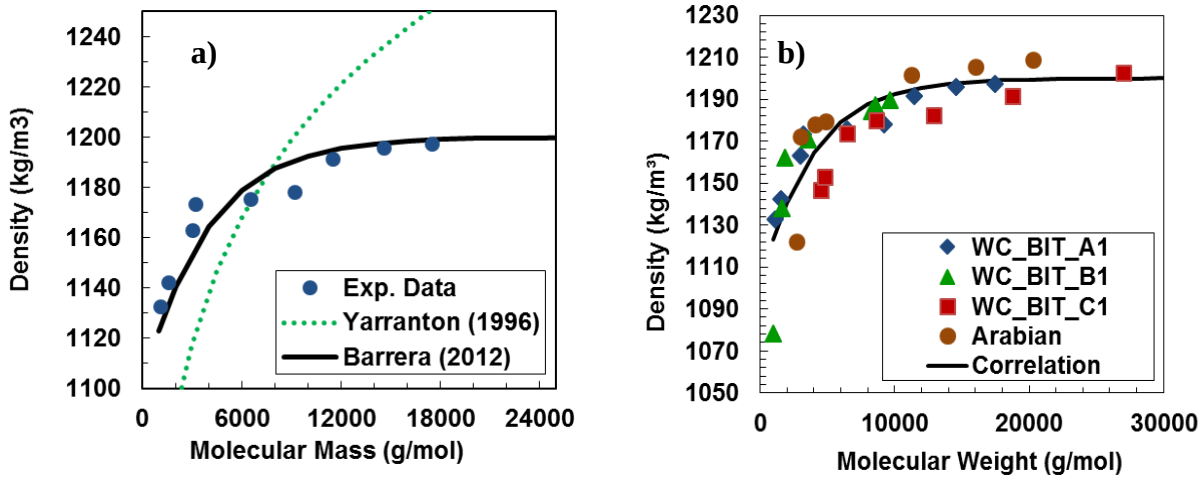

Figure 4-1. Density at 23°C as a function of molecular weight at 10 g/L for a) WC_BIT_A1 asphaltenes b) compared with density of asphaltene cuts from four samples at 23°C (Barrera *et al*. 2013).

4.2.3 Solubility Parameter

Solubilty parameters for common substances are reported in the literature but must be estimated for most of the components considered in this thesis. The solubility parameter is defined as follows,

$$\delta_T \equiv \left(\frac{\Delta U_T^{vap}}{v_T} \right)^{1/2} \equiv \left(\frac{\Delta H_T^{vap*} - RT}{v_T} \right)^{1/2} \qquad \textbf{4-14}$$

where δ is the solubility parameter in $MPa^{0.5}$, ΔU^{vap} is the internal energy of vaporization, v is the molar volume, ΔH^{vap} is the molar heat of vaporization (J/mol), R is the universal gas constant in J/mol K, T is temperature in K and v is the molar volume in cm³/mol. Equation 4-14 shows that solubility parameters can be related to heats of vaporization and molar volume. Solubility parameters are also determined by fitting the regular solution model to asphaltene precipitation data where the solubility parameter of one component is the only unknown.

4.2.3.1 Solvents

The molecular weight, density, molar volume and solubility parameter of common solvents at 23ºC are available in the literature. Table 4-4 shows the properties of two main solvents used in the model.

Table 4-3. Properties of Solvents at 23°C.

Component	Molar Mass	Density at 23°C (kg/m^3)	Solubility Parameter At 23°C (MPa$^{0.5}$)
n-heptane	100	678	15.2
Toluene	92	864	18.3

Tharanivasan (2009) adapted the model to include any *n*-alkane. The solubility parameters for *n*-alkanes were determined from Equation 4-15 with heats of vapourization correlated to molecular weight (for carbon number ≥5) as follows:

$$\Delta H_{25°C}^{vap*} = 103.65 + 368.7MW - 0.06030MW^2 \qquad \textbf{4-15}$$

Lower carbon numbers are not considered in this thesis. Note, ΔH^{vap*} is slightly different from the actual heat of vapourization because it was adjusted to fit solubility parameters at 25°C from the literature (Barton, 1991) to within 0.01 MPa$^{0.5}$.

The effects of temperature and pressure are accounted for *n*-alkane solubility parameters as follows (Akbarzadeh *et al.*, 2005):

$$\delta = \delta_{25°C}\left(\frac{v_{25°C}}{v}\right)^{1/2} - 0.0232(T - 298.15) \qquad \textbf{4-16}$$

Note that, the effect of pressure is indirectly reflected via changes in molar volume.

4.2.3.2 Saturates and Aromatics

Akbarzadeh *et al.* (2005) developed correlations for the solubility parameters of saturates and aromatics as function of temperature, which were updated by Tharanivasan (2012) as follows:

$$\delta_{sat} = 23.021 - 0.0222T \quad \textbf{4-17}$$

$$\delta_{aro} = 26.333 - 0.0204T \quad \textbf{4-18}$$

where δ_{sat} and δ_{aro} are the solubility parameters of saturates and aromatics in $MPa^{0.5}$ respectively, and T the temperature in Kelvin. Note that Equations 4-17 and 4-18 were developed by fitting a limited set of data and therefore have high uncertainties.

Okafor (2013) determined saturate and aromatic solubility parameters for a larger dataset including native oils, *in*-situ cracked oils, and a hydrocracked sample. She measured asphaltene solubility curves for several model systems of: 1) asphaltenes-saturates-toluene; 2) asphaltenes-heptane-aromatics. Solubility parameters were determined by fitting the regular solution model to the solubility data. The solubility parameters were found to be consistent for each type of oil (native, *in-situ*) and higher than the average values from Akbarzadeh (2005), Table 4-3. Note, Okafor's data was fitted using the updated density and solubility parameter correlation (Eqs. 4-13 and Eq. 4-21), an important difference from Akbarzadeh's work. The use of different correlations may partly contribute to the difference in the average solubility parameters from both studies. The solubility parameters were assumed to be independent of pressure.

Table 4-4. Average Solubility Parameter at 23°C for saturates and aromatics.

Fraction	Solubility Parameter at 23°C($MPa^{0.5}$)			
	Native Oils Akbarzadeh	Native Oils Okafor	*In-situ* Cracked Okafor	Hydrocracked Okafor
Saturates	15.9	16.7	16.3	15.8
Aromatics	20.2	20.8	20.6 to 21.0	20.8
Resins	19.6	--	--	--

4.2.3.3 Asphaltenes and Resins

Yarranton and Masliyah (1996) developed a semi-empirical correlation for the asphaltenes solubility parameter as follows:

$$\delta_A = \left(\frac{\Delta H_T^{vap*} - RT}{v_T}\right)^{1/2} = \left(\frac{r\Delta H_{M,T}^{vap*} - RT}{rMW_M/\rho_A}\right)^{1/2} = \left(\left(\frac{\Delta H_{M,T}^{vap*}}{MW_M} - \frac{RT}{rMW_M}\right) * \rho_A\right)^{1/2} \approx \left(A(T)\rho_A\right)^{1/2} \qquad \textbf{4-19}$$

where *A(T)* represents the monomer enthalpy of vaporization (kJ/g) and *r* the aggregation number. Note, the magnitude of *RT/rMW* was negligible in comparison with the magnitude of *A(T)* (Yarranton, 1996; Akbarzadeh *et al*., 2005); therefore, this term was neglected in the correlation for asphaltenes. Akbarzadeh *et al* (2005) correlated the monomer heat of vaporization to temperature as follows:

$$A(T) = 0.579 - 0.00075T \qquad \textbf{4-20}$$

where T is in K.

Barrera (2012) measured the asphaltene solubility curve for *in-situ* converted samples. It was found that the solubility parameter of asphaltenes had changed for these chemically altered samples. Barrera *et al.* (2012) modified Equation 4-19 for both native and *in situ* reacted asphaltenes for use with their new, more precise correlation for asphaltene density (Equation 4-13). The proposed solubility parameter correlation is given by,

$$\delta = \left(A(T)\rho_A\left(cMW^d\right)\right)^{1/2} \qquad \textbf{4-21}$$

where *d* is a constant, *c* is a specific parameter depending on the asphaltene source, *A(T)* is determined from Equation 4-20 and ρ_A from Equation 4-13. Parameter *d* is set to 0.0495 and *c* is tuned based on asphaltene yield data. Preliminary average *c* values of 0.643 and 0.665 were determined by Barrera (2012) for native oils and partly reacted (*in situ* cracked) oils, respectively. Testing and modification of the new density and solubility parameter correlation for the reacted oils are discussed in later chapters.

4.3 Regular Solution Model Implementation

The regular solution model is used for two applications:

a) Asphaltenes in solvents (model systems, *e,g*, mixtures of asphaltenes in toluene and *n*-heptane).

b) Heavy oil (or bitumen) with solvents (e.g. mixtures of crude oil and *n*-heptane).

The general procedure to apply the regular solution model for asphaltene precipitation for each application is described below.

a) Asphaltene in Solvents

1. Define the input conditions to the model: pressure (*e.g.* atmospheric), solvent (*e.g. n*-heptane), solvent composition (*e.g*. 0.3 toluene and 0.7 *n*-heptane mass fractions)
2. Calculate the liquid molar volumes and solubility parameters of the required solvents (toluene and *n*-alkanes).
3. Obtain Molecular weight of whole asphaltenes (the model uses the measured molecular weight of asphaltenes at 50°C and 10 g/L). For example, use equation 3-3 if the molecular weight is measured with the VPO technique.
4. Choose the shape factor for the gamma distribution (Eq. 4-1). A value of 2.0 is recommended
5. Subdivide the gamma distributions to obtain the asphaltene subfractions (Discretize in n fraction and calculate the mass fraction of each fraction with equation 4-3)
6. Calculate the molar volumes of asphaltene subfractions (Eq. 4-12 and then 4-5)
7. Calculate solubility parameter of asphaltenes (Eq. 4-21): set initial guess for c parameter with the average value for native oils or higher if the sample has been slightly processed (e.g. *in-situ* conversion).
8. Perform equilibrium calculations using the equilibrium constant from the modified regular solution theory (Eq 4-7).
9. Calculate the amount of asphaltene precipitation.
10. Check the accuracy of the model predictions: compare the model predictions with experimental data if available (less than 3% asphaltene yield difference for each solvent ratio).

11. Adjust the value of *c* and repeat the procedure to obtain a better fit if required.

b) Heavy Oil (or Bitumen) with Solvents

12. Define the input conditions to the model: pressure (*e.g.* atmospheric), solvent (*e.g. n*-heptane), solvent composition (*e.g*. crude oil diluted with 50wt% toluene)
1. Calculate the liquid molar volumes and solubility parameters of the required solvents (toluene and *n*-alkanes desired).
2. Obtain SARA analysis of the oils sample (Experimental data)
3. Determine Saturates, aromatics and resins properties (molar mass and density). Measure density and molar mass or use average values from Akbarzadeh or Okafor.
4. If modeling at different temperature is required, calculate the properties for saturates and aromatics at the desired temperature(s) (Density (eq.4-8 to 4-10) and solubility parameter (Eq. 4-17 and 4-18) temperature correction).
5. Estimate the solubility parameter of saturates and aromatics at the desired conditions.
6. Approximate/guess an initial value for the average molar mass of asphaltenes (Average molecular weight, MW_{avg}, in Eq. 4-2)
7. Choose the shape factor for the gamma distribution (Eq. 4-1 and 4-2). A value of 3.5 is recommended
8. Subdivide the gamma distributions to obtain the asphaltene subfractions
9. Calculate the mole fraction of each asphaltene subfraction
10. Calculate the molar volumes (densities and molar masses) of asphaltene subfractions (Eq. 4-12 and then 4-5)
11. Calculate solubility parameter of asphaltenes (Eq. 4-21): use *c* value determined from asphaltene model systems or average value for native oils
12. Perform equilibrium calculations using the equilibrium constant from the modified regular solution theory (Eq. 4-7).
13. Calculate the amount of asphaltene precipitation.
14. Check the accuracy of the model predictions: compare the model predictions with experimental data if available.

15. Adjust the average molar mass of asphaltenes and repeat the procedure to obtain a better fit if required.

4.4 Self-Association Model for Asphaltene Aggregation

The asphaltene self-association model originally proposed by Agrawala and Yarranton (2001) assumed asphaltene association to be analogous to a linear polymerization. Barrera (2013) and Sadeghi-Yamchi (2014) adapted the model to be applied to native and reacted asphaltenes and details can be found there. The model is briefly summarized below.

Theory

Asphaltenes (and resins) are considered to be free molecules in solutions with active sites that can interact with other molecules to form aggregates. The mixture of molecules in asphaltenes (and resins) are divided into three classes of molecules: propagators, terminators and neutrals with the following definitions:

1. Propagator: a molecule with multiple active sites which can link to form a chain, hence promote additional association.
2. Terminator: a molecule with a single active site that can link to another molecule but ends association.
3. Neutrals: a molecule with no active site which does not participate in association.

The aggregates are macromolecules of asphaltenes (and resins) which in the model are formed from multiple propagators and up to 2 terminators. The analogy in the model is an oversimplification of the aggregation phenomenon of asphaltenes; however, is sufficient to analyze the asphaltene molecular weight data and reconstruct asphaltene molecular weight distributions (Barrera 2013, Sadeghi-Yamchi 2014).

Two reaction schemes are required in the model: propagation and termination. Propagation is the linking of a monomer propagator P1 with another monomer P1 or an existing aggregate P_n (n is the number of monomers in the aggregate). The propagation reactions are assumed to be first order

with respect to both monomers and aggregates. The reactions are characterized with an association constant K which is assumed to be the same for all the reactions as follows,

$$P_1 + P_1 \overset{K}{\leftrightarrow} P_2 \longrightarrow [P_2] = K[P_1]^2 \quad \textbf{4-22}$$

$$P_1 + P_2 \overset{K}{\leftrightarrow} P_3 \longrightarrow [P_3] = K[P_1][P_2] = K^2[P_1]^3 \quad \textbf{4-23}$$

$$P_1 + P_3 \overset{K}{\leftrightarrow} P_4 \longrightarrow [P_4] = K[P_1][P_3] = K^3[P_1]^4 \quad \textbf{4-24}$$

The general equation is given by:

$$P_1 + P_n \overset{K}{\leftrightarrow} P_{n+1} \longrightarrow [P_{n+1}] = K[P_1][P_n] = K^n[P_1]^{n+1} \quad \textbf{4-25}$$

The termination reactions occurs when a terminator molecule, T, links to a monomer or an aggregate and ends association. The termination reactions are assumed to be first order with respect to both monomers and aggregates. The model assumed that both propagation and termination association constants are equal. The concentration of terminator-aggregates is described as follows,

$$P_1 + T \overset{K}{\leftrightarrow} P_1T \longrightarrow [P_1T] = KP_1T \quad \textbf{4-26}$$

$$P_2 + T \overset{K}{\leftrightarrow} P_2T \longrightarrow [P_2T] = K[P_2][T] = K^2[P_1]^2[T] \quad \textbf{4-27}$$

$$P_3 + T \overset{K}{\leftrightarrow} P_3T \longrightarrow [P_3T] = K[P_3][T] = K^3[P_1]^3[T] \quad \textbf{4-28}$$

The general termination equation is given by:

$$P_n + T \overset{K}{\leftrightarrow} P_nT \longrightarrow [P_nT] = K[P_n][T] = K^n[P_1]^n[T] \quad \textbf{4-29}$$

The set of reactions is solved simultaneously starting with the mass balance equations for propagators and terminators. $[P_1]_0$ and $[T]_0$ are defined as the initial concentration of propagator and terminator monomers.

The equilibrium concentration of propagators (monomers) is given by,

$$[P_1] = \frac{1 + K(2[P_1]_0 + [T]_0) - \sqrt{(1 + K(2[P_1]_0 + [T]_0))^2 - 4K^2[P_1]_0([P_1]_0 + [T]_0)}}{2K^2([P_1]_0 + [T]_0)} \quad \textbf{4-30}$$

and the equilibrium concentration of terminators is given by,

$$[T] = [T]_0 (1 - K[P_1]) \qquad \textbf{4-31}$$

The initial concentration of propagators and terminators and the association constant are calculated from the inputs to the model. Once the equilibrium concentration of the monomers is determined, the concentration of any aggregate can be calculated from Equations 4-22 to 4-29.

Implementation

The inputs in the model are as follows:

- Monomer T/P ratio, $(T/P)_0$
- Association constant, K
- Average molecular weight of propagators, terminators, and neutrals
- Mole fraction of neutrals.

The initial concentration of propagators and terminators in the asphaltene mixture is calculated as follows:

$$x_{T_0} = \frac{(T/P)_0}{1 + (T/P)_0} \cdot (1 - x_N) \qquad \textit{and} \qquad x_{P_0} = 1 - x_{T_0} - x_N \qquad \textbf{4-32} \text{ and } \textbf{4-33}$$

where x_{T_0}, x_{P_0} x_N are the mole fractions of terminators, propagators and neutrals in the asphaltene mixture; $(T/P)_0$ is the ratio of terminators to propagators in the whole solution. The average molecular weight MW_{mono} of the non-aggregated system is given by:

$$MW_{mono} = x_{T_0} \cdot MW_T + (1 - x_{T_0} - x_N) \cdot MW_P + x_N \cdot MW_N \qquad \textbf{4-34}$$

where MW_N is the molecular weight of neutrals, which is assumed to be the same as the molecular weight of terminator monomers.

The initial mole fractions of propagators, terminators, and neutrals in the solution depend on the mass concentration of asphaltenes C_A and the molar volume of the solvent, v_s, and are calculated as follows:

$$[P_1]_0 = \frac{1}{\left(1+\frac{MW_{mono}}{C_A \cdot \upsilon_s}\right)\left(1+(T/P)_0\right)} \cdot (1-x_N) \qquad \textbf{4-35}$$

$$[T]_0 = [P_1]_0 \cdot (T/P)_0 \qquad \textbf{4-36}$$

$$[N]_0 = \frac{x_N}{\left(1+\frac{MW_{mono}}{C_A \cdot \upsilon_s}\right)} \qquad \textbf{4-37}$$

To implement the model, the asphaltene concentration, monomer molecular weights, T/P ratio, association constant, and mole fraction of neutrals in the asphaltenes are specified. The values of $[P_1]_0$, $[T]_0$, $[N]_0$ and the equilibrium concentrations are calculated and then the equilibrium concentrations of all the aggregates can be determined. The model is usually fitted to data for the average aggregate molecular weight by adjusting the T/P ratio, association constant, mole fraction of neutrals, and the monomer molecular weights. The average molecular weight of the aggregated system at a given concentration is calculated as follows:

$$MW_{avg} = (1-x_{N,final}) \cdot \left(\sum_{n=0}^{n}\left(x_{[P_n]} \cdot MW_{[P_n]} + x_{[P_nT]} \cdot MW_{[P_nT]}\right)\right) + x_{N,final} \cdot MW_N \qquad \textbf{4-38}$$

where $x_{[X]}$ and $MW_{[X]}$ are the mole fraction and the molecular weight of aggregate *X*, and $x_{N,final}$ is the concentration of neutrals in the aggregated system and is different than x_N. The monomer molecular weights are constrained by experimental data at low asphaltene concentrations and therefore the main tuning parameters are the T/P ratio, association constant, and mole fraction of neutrals.

The output of the model is the mole or mass fraction of each aggregate at a specified concentration between 0.1 and 100 kg/m^3 of asphaltenes in the solvent and the aggregates (P-P and P-T) molecular weight and mole and mass fraction in the system. Since the aggregates are multiples of the average monomer molecular weights, the molecular weight distribution obtained is discrete. In reality there is a range of monomer molecular weights and the distribution is continuous.

Therefore, a continuous distribution is fitted of the output to the model to represent the real distribution. A continuous distribution is also more convenient for solubility modeling purposes.

The molecular weight of the aggregates are then sorted in ascending order with their corresponding mass or mole fraction and a continuous equation can be used to fit the organized molecular weight discrete distribution. For native oils, the following exponential function is used to fit the cumulative distribution,

$$\boldsymbol{f(MW) = A_1 + B_1 exp(-exp(\frac{C_1 - MW}{D_1}))} \qquad \textbf{4-39}$$

where *f(MW)* is the cumulative mass fraction function, *MW* is the molecular weight of the aggregate, A_1 and B_1 are fitting parameters controlling the upper limit of the distribution, C_1 and D_1 are fitting parameters which affect the slope and the point in which a maximum value is reached (Barrera, 2013). The fitting parameters are determined using Solver from Microsoft excel using the GRG nonlinear solving method subject to predefined constrains.

However, reacted materials can contain a significant fraction of neutrals which increase the concentration of the lower molecular weight material in the cumulative molecular weight distribution giving an initial "step" increase in the distribution. Sadeghi (2014) found that Equation 4.39 was not able to fit the "step" increase due to large amount of neutrals in highly reacted samples; hence an alternative function was proposed as follows,

$$\boldsymbol{f(MW) = \left(1 - \exp\left(-A(MW - C)\right)\right) \times B + \tanh(D(MW - C)) \times (1 - B)} \qquad \textbf{4-40}$$

where *C* is the minimum molecular weight and *A*, *B*, and *D* are fitting parameters. Solver from Microsoft Excel was also used to optimize the fitting parameters.

Chapter Five: Asphaltene Characterization

This chapter summarizes the main properties of asphaltenes required for the regular solution model: that is, molecular weight, density, and solubility parameter distributions for asphaltenes from native and reacted oils. Other properties, such as refractive index and elemental analysis, are also measured to analyze the effect of different reaction processes and because they are potential correlating properties for the effect of reaction on other properties that are more difficult to measure, such as solubility parameter.

5.1 Asphaltene Molecular Weight

Asphaltene apparent molecular weight was previously measured for asphaltene cuts from native, *in-situ* converted, thermocracked, and hydrocracked oils. Asphaltene molecular weight distributions were then reconstructed using the self-association model explained in Chapter 4. In this thesis, the molecular weight distributions are represented with a gamma distribution, excluding neutrals, to provide a consistent comparison for all the samples and to analyze the effect of the different types of reaction on the asphaltenes. A new correlation is developed to correct for the effect of temperature on the molecular weight distribution.

5.1.1 Molecular Weight Distributions: Model Distributions

The outputs of the self-association model are the molecular weights and mass fractions of each of the aggregates making up the asphaltene mixture. The distributions include the non-associating components (neutrals) which, because they are monomers, appear as a step change at the beginning of the cumulative distribution. This step change distorts the shape of the distribution plus the variation of the amount of monomers from sample to sample can cause inconsistent comparisons. The effect of the neutrals is significant for asphaltenes from highly reacted samples which have a higher proportion of neutrals (Sadeghi-Yamchi 2014). Therefore, the molecular weight distributions from the self-association model were fitted excluding the neutrals, and the neutrals were represented as a separate single component.

The cumulative mass fraction from the self-association model was plotted as function of the molecular weight. A gamma distribution was fitted to the cumulative mass fraction data excluding the neutrals and normalizing for the neutral-free composition as follows,

$$f(MW) = \frac{\frac{(MW - MW_{mono})^{\alpha-1}}{\beta^{\alpha}\Gamma(\alpha)}\exp\left(\frac{MW_{mono} - MW}{\beta}\right) + \frac{w_N}{1-w_N}}{1 + w_N/(1-w_N)} \qquad \textbf{5-1}$$

where MW_{mono} is the molecular weight of the "smallest" monomer in this case the molecular weight of the terminators, MW is the average associated molecular weight, α is a parameter that defines the shape of the distribution, w_N is the mass fraction of neutrals and β is given by:

$$\beta = \frac{MW_0 - MW_{mono}}{\alpha} \qquad \textbf{5-2}$$

where MW_0 is the apparent average molecular weight of the whole continuous asphaltene mixture. The monomer molecular weight was set by extrapolating to zero concentration the molecular weight of the lightest asphaltene fraction. MW_0 is a fitting parameter which corresponds to the average molecular weight in the normalized gamma distribution with neutrals-free based composition. MW_0 is varied to fit the output of the model. The cumulative gamma function was then discretized into 40 fractions of equal molecular weight increment.

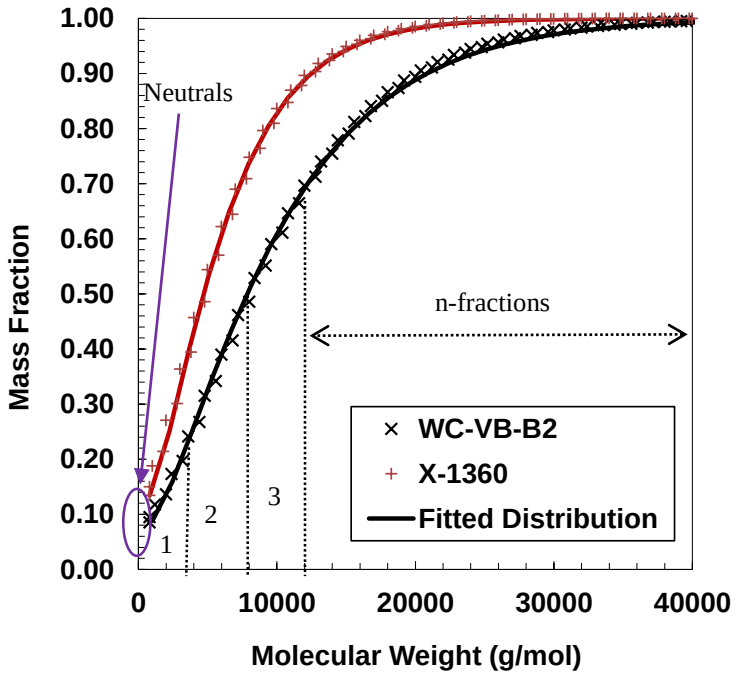

Figure 5-1. Schematic representation of the distribution discretization.

5.1.2 Molecular Weight Distributions: Native vs. Reacted Asphaltenes

Tables 5-1 to 5-3 show the mass fraction of neutrals from the self-association model and the parameters used to fit Eq. 5-1 to the mass fraction and molecular weight data obtained from the self-association model at 50ºC (the temperature of the VPO measurements). The following observations are made:

- Asphaltenes from native oils have a relatively low mass fraction of neutrals and wide molecular weight distributions, as seen in Figures 5-2a and 5-2b.
- Asphaltenes from *in-situ* converted oils are similar to the unmodified oil with similar mass fractions of neutrals, similar shapes to the molecular weight distributions, but slightly lower average molecular weights, Figure 5-3.
- Asphaltenes from thermocracked oils have major changes in comparison with the feedstock. There are more neutrals, narrower molecular weight distributions, and lower average molecular weight, Figure 5-4a.
- The trends observed for the thermocracked asphaltenes are more pronounced for asphaltenes from hydrocracked oils, Figure 5-4b. The mass fraction of neutrals is

significantly higher, the molecular weight distributions are much narrower, and the average molecular weights significantly lower. This trend is consistent with the extent of reaction such that narrower distributions are found with higher extents of reaction.

- All of the neutral excluded distributions can be fitted with an α of 1.5 except the RHC-18-37 sample. This sample has the highest conversion. The difference could be a result of the high conversion or an artefact from experimental error in the molecular weight measurements of the asphaltene solubility fractions. The fitted shape of a narrow distributions will be more sensitive to experimental error than a wide distribution.

The molecular weight distribution trends are consistent with changes expected for reacted asphaltenes. The decreased average molecular weight and narrower molecular weight distributions indicate less self-association of asphaltenes (smaller aggregates), consistent with removal of alkyl chains as well as removal of heteroatoms (e.g. sulfur and heavy metals) which may promote molecules linking with each other. The increase in the amount of neutrals with extent of reaction is also consistent with removal of side chains and elimination of associating species.

Table 5-1. Parameters used to fit Equation 5-1 for asphaltenes from native oils.

Sample	W_N	MW_0	α	MW_{mono}
WC-B-B2	0.04	8370	1.5	800
WC-B-A1	0.03	11350	1.5	800
WC-DB-A2	0.03	9420	1.5	800
WC-B-C1	0.04	14400	1.5	1280
WC-B-B1	0.04	6020	1.5	800
WC-VB-SR	0.06	10200	1.5	800
WC-VB-B2	0.08	10700	1.5	800
Arabian	0.02	7010	1.5	800

Table 5-2. Parameters used to fit Equation 5-1 for asphaltenes from *in-situ* converted oils (and the original oil).

Sample	W_N	MW_0	α	MW_{mono}
WC-B-B2 (original)	0.04	8370	1.5	800
27034-113	0.06	7890	1.5	800
27034-87	0.04	8360	1.5	800
26845	0.05	6260	1.5	800

Table 5-3. Parameters used to fit Equation 5-1 for asphaltenes from cracking processes and their feedstocks.

Sample	W_N	MW_0	α	MW_{mono}
Thermocracked				
WC-VB-B2 (Feed)	0.08	10700	1.5	800
X-1357	0.08	10740	1.5	800
X-1359	0.10	7860	1.5	800
X-1360	0.13	6720	1.5	800
Hydrocracked				
WC-VB-SR (Feed)	0.06	10200	1.5	800
RHC-18-19	0.22	3650	1.5	450
RHC-18-37	0.23	2300	1.2	420
HOS Bottoms	0.17	3500	1.5	450

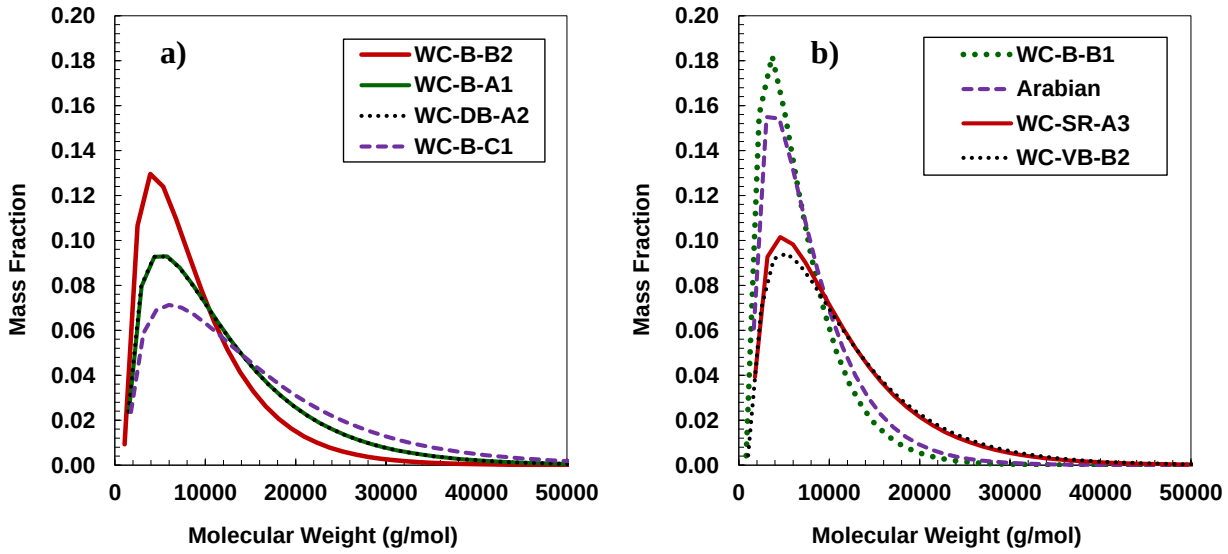

Figure 5-2. Molecular weight distribution at 50°C for asphaltenes from native oils.

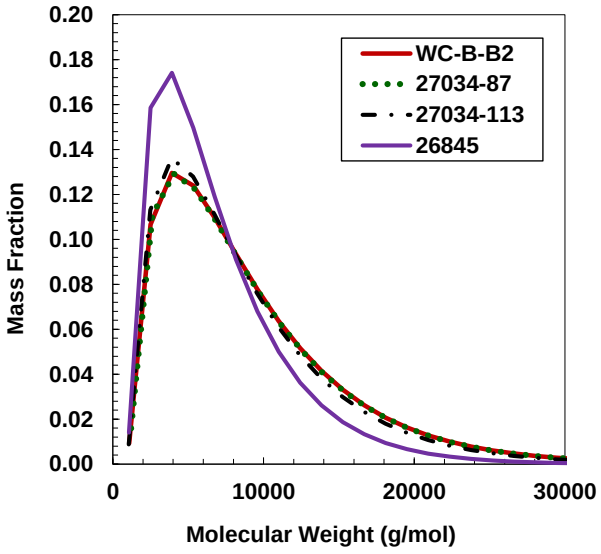

Figure 5-3. Molecular weight distribution at 50°C for asphaltenes from *in-situ* converted oils.

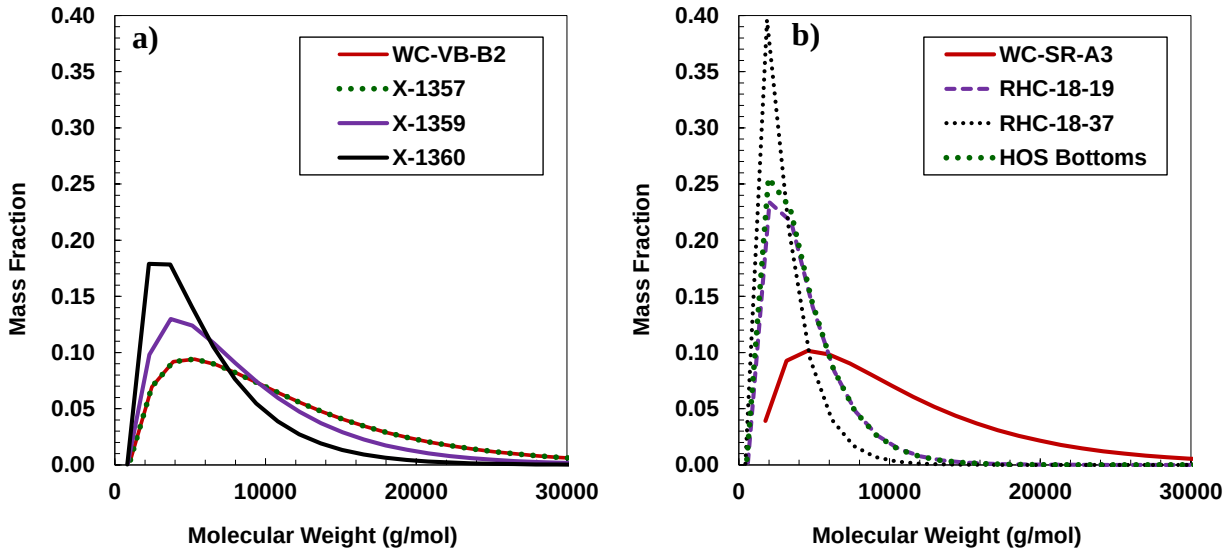

Figure 5-4. Molecular weight distribution at 50°C for asphaltenes from a) thermocracked and b) hydrocracked oils.

Excluding the neutrals from the associating asphaltenes allows for a more precise fitting of the molecular weight distribution and a more meaningful comparison of different samples. However, the mass fraction of neutrals is usually unknown and; in general, the whole asphaltene fraction must be represented/approximated with a distribution in this case, the Gamma distribution to capture the self-association behaviour and polydispersity in molecular weight of the asphaltene fraction.

5.2 Effect of Temperature on Molecular Weight

Since asphaltenes are a self-associating system, their nano-aggregate molecular weight distribution depends on temperature. The molecular weight distributions were determined at 50°C but, for modeling purposes, are required at the temperature of the asphaltene solubility data to be modeled, in this case room temperature of 20 to 23°C. Therefore, the effect of temperature in asphaltene molecular weight was evaluated in order to develop a temperature correction.

5.2.1 Previous Correlation of Average Molecular Weight to Temperature

Akbarzadeh *et al*., (2005) found that self-association decreases with increasing temperature and suggested the following correlation of average asphaltene molecular weight to temperature,

$$MW_T = MW_{23} - 10.599(T - 296.15) \quad \textbf{5-3}$$

where M_T is the average molar mass at temperature T, MW_{23} is the average molar mass at 23°C, and T is the temperature in K. The molecular weight temperature dependence was improved as follows (Tharanivasan 2012),

$$MW_T = MW_{50}\exp(0.007321 * (323.15 - T)) \quad \textbf{5-4}$$

The correlation applies between 0 and 120°C and its use is not recommended to be used outside of this temperature range.

The above temperature dependence correlation was developed by fitting the regular solution model to diluted heavy oil solubility data at different temperatures. The molecular weight of asphaltenes in the oil was adjusted for each temperature and then a trend between the fitted molecular weight and temperature was fitted. However, the equation was developed from a limited set of data from native oils. The additional data collected in this thesis allows the development of a more robust correlation.

5.2.2 Molecular Weight Measurements at Different Temperatures

The apparent molecular weight was measured at different temperatures 37, 50, 73 and 88°C in solutions of toluene in order to identify the temperature dependence in asphaltene association. The general effect of temperature was to decrease the average molecular weight of the aggregated asphaltenes with increasing temperature as seen in Figures 5-5a and 5-5b for C7 asphaltenes from WC-DB-A2 and WC-VB-B2, respectively. This trend is consistent with previous observations from Akbarzadeh *et al.,* (2005) for native oils.

The altered chemistry of asphaltenes from thermocracked or hydrocracked oils is likely to alter the temperature dependence of self-association in comparison with asphaltenes from native oils.

Figure 5-6a shows that molecular weight of aggregated asphaltenes from thermocracked oils which also decreased with temperature but to a lesser extent. The molecular weight of asphaltenes from hydrocracked oils was not affected by temperature within the scatter of the VPO data, Figure 5-6b. The same trend was observed for other thermocracked and hydrocracked samples (Appendix B). Not surprisingly, the molecular weight temperature dependence is less for less self-associated (lower molecular weight) asphaltenes; when there is little association to begin with, there is little potential for a reduction in self-association.

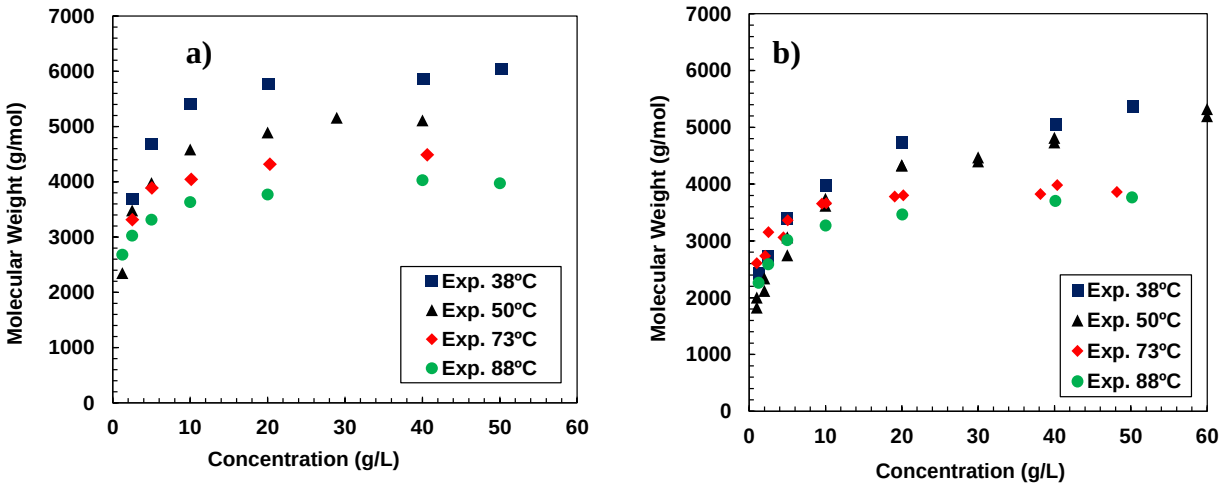

Figure 5-5. Effect of temperature in molecular weight measurements for asphaltenes from a) WC-DB-A2 and b) WC-VB-B2.

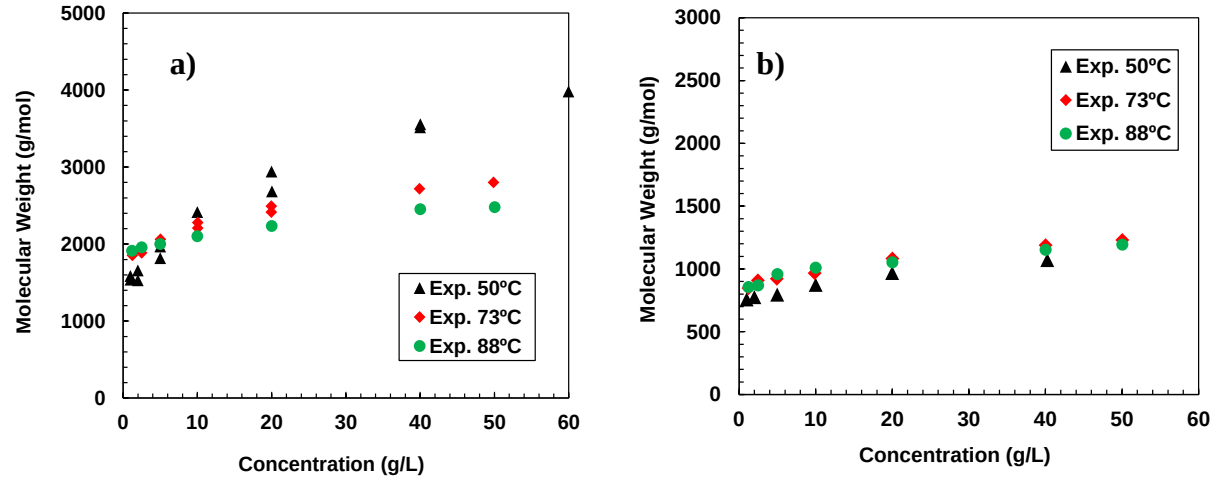

Figure 5-6. Effect of temperature in molecular weight measurements for asphaltenes from a) X-1360 and b) RHC-18-37.

In order to verify that temperature changes had negligible effect in the molecular weight of asphaltenes from hydrocracked samples, additional molecular weight measurements were performed with a light and heavy asphaltene fraction from HOS Bottoms thermocracked oil, Figure 5-7. As expected, the light fraction had a lower molecular weight than the whole asphaltenes and did not exhibit any noticeable change on the molecular weight by increasing the temperature. Interestingly, the heavy fraction, with higher apparent molecular weight (up to 5000 g/mol), also did not show much change of the molecular weight with temperature. Hence, the molecular weight of even the more associated asphaltenes from hydrocracked oils did not exhibit a significant change with temperature. The reason for the disappearance of the temperature effect is not known but one possibility is that hydrocracking eliminates the most temperature sensitive self-association mechanisms; for example, hydrogen bonding related mechanisms.

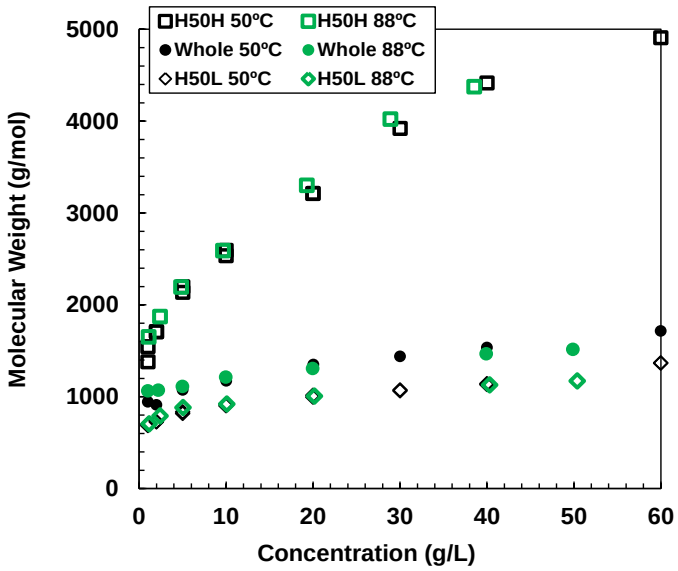

Figure 5-7. Temperature effect in molecular weight for asphaltene fractions from HOS Bottoms. H50H refers to the heavy (or precipitated) fraction from the precipitation experiment (solubility curve) with 50wt% heptol. H50L refers to the light (or soluble) fraction from the precipitation experiment (solubility curve) with 50wt% heptol.

5.2.3 Self-Association Model to Quantify the Molecular Weight Temperature Dependence

The self-association model developed explained in Chapter 4 is used with the temperature molecular weight data to quantify and compare the changes in molecular weight distributions with temperature for asphaltenes from native and thermocracked oils. Barrera and Sadeghi used the self-association model to reconstruct the molecular weight distributions of asphaltene aggregated material from native (Barrera, 2012) and reacted (Sadeghi-Yamchi, 2014) oils.

The temperature dependency can be captured by adjusting either the *T/P* ratio or the association constant and both have different effects in the model predictions. The molecular weights of the monomers (propagators, terminators and neutrals) and the mole fraction of neutrals should not change with temperature and they are assumed to be constant and equal to the optimized value found by Barrera and Sadeghi-Yamchi for asphaltenes from native and reacted oils. Figures 5-8a and 5-8b show the model predictions by adjusting the association constant (*K*) and the *T/P* ratio for asphaltenes from WC-DB-A2 at different temperatures.

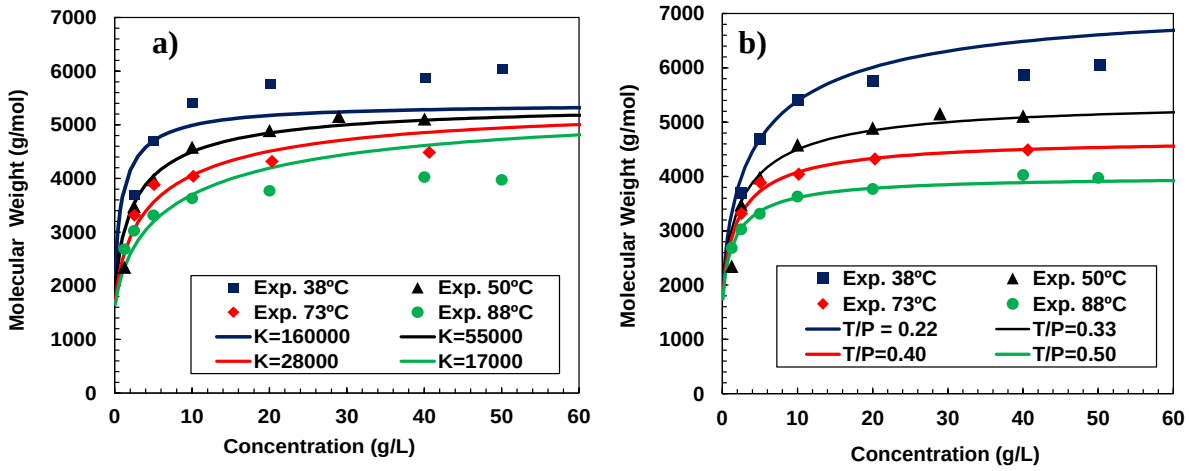

Figure 5-8. Effect of a) the association constant, K, and b) T/P ratio in the self-association model.

The association constant changes the concentration range at which the molecular weight reaches its highest value. Note that at constant *T/P* ratio, the maximum molecular weight is within a small range for all *K* values. On the other hand, the *T/P* ratio changes the maximum molecular weight, but has little effect on the inflexion concentration. It is clear that the trend obtained by changing

the *T/P* ratio at constant *K* better fits the molecular weight data. Therefore, fitting the temperature molecular weight data was performed by adjusting only the *T/P* ratio and leaving all the other parameters fixed at the values from Barrera and Sadeghi's optimization.

The molecular weight distributions at each temperature, excluding neutrals, were fitted with the Gamma function (Eq. 5-1) as described previously. The molecular weight distributions of asphaltenes from native and thermocracked samples at different temperatures are shown in Figures 5-10 to 5-13. In all cases, increasing the temperature led to narrower distributions corresponding with the lower average molecular weight. Note that, the initial spike in Figure 5-10 to 5-13 corresponds to the amount of neutrals determined for asphaltenes from each oil. Additional plots for all the samples analyzed in the temperature study are presented in Appendix B.

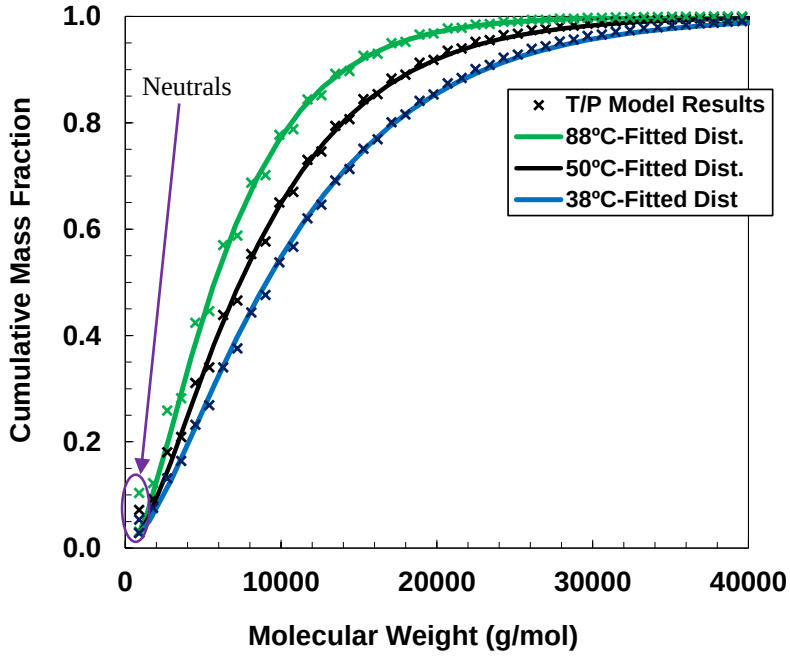

Figure 5-9. Self-association model results and fitted cumulative distribution with Eq. 5-1 for asphaltenes from WC-DB-A2.

.

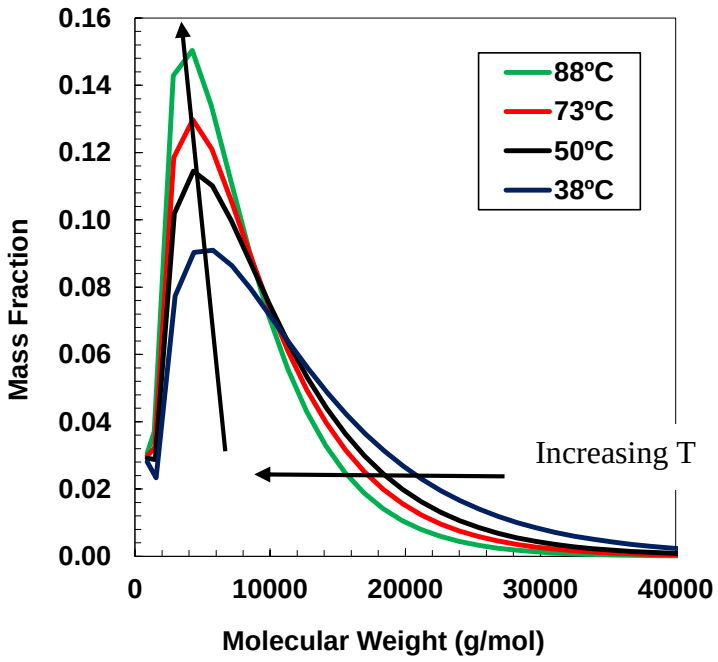

Figure 5-10. Effect of temperature in the molecular weight distribution of asphaltenes from WC-DB-A2.

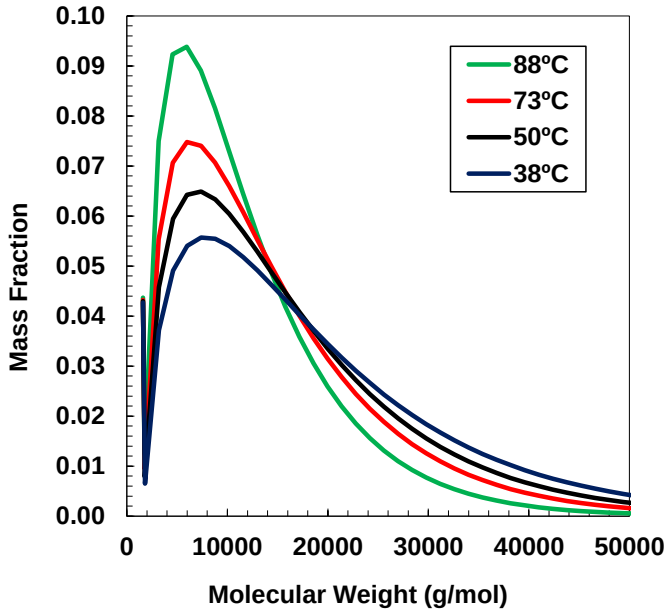

Figure 5-11. Effect of temperature in the molecular weight distribution of asphaltenes from WC-B-C1.

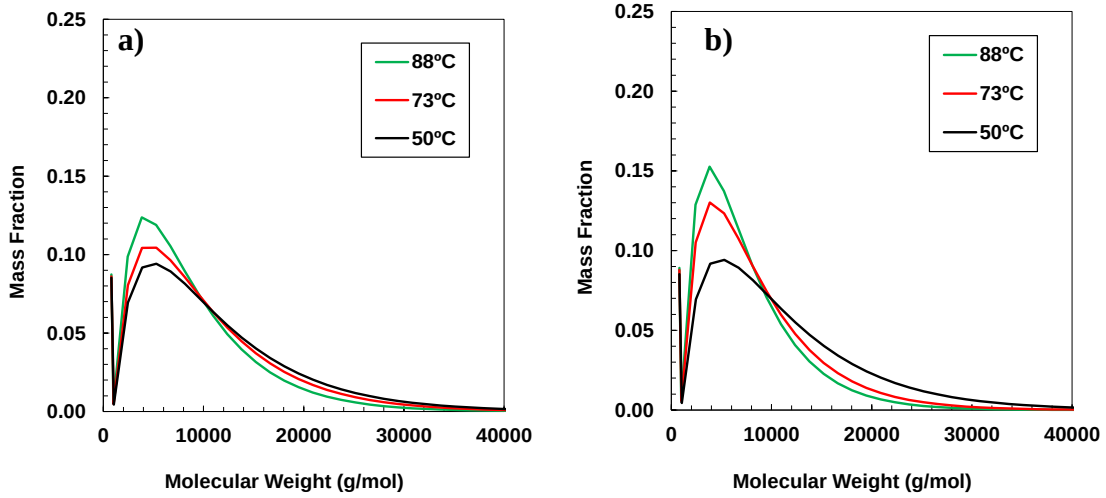

Figure 5-12. Effect of temperature in the molecular weight distribution of asphaltenes from a)WC-VB-B2 and b) X-1357 oil samples.

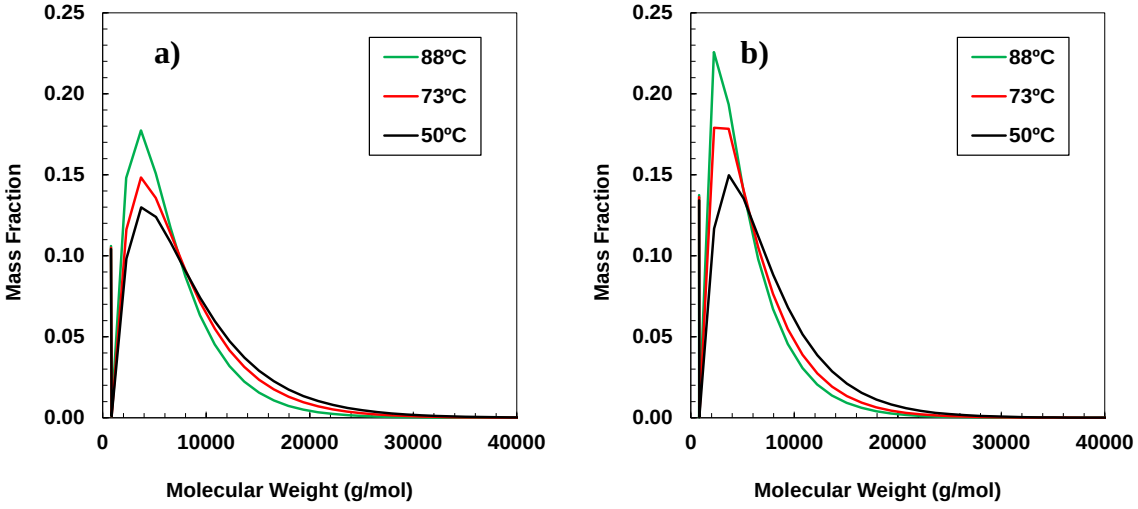

Figure 5-13. Effect of temperature in the molecular weight distribution of asphaltenes from a) X-1359 and b) X-1360 oil samples.

The next step was to develop a correlation to predict the self-association model parameters at room temperature (20ºC), which is the temperature at which most of the solubility data in this thesis was collected. Recall that the T/P ratio was the adjustable parameter to fit the temperature molecular weight data for each sample. When the T/P ratio is plotted against 1/T a clear trend is observed,

Figures 5-14a and 5-14b for native and thermocracked asphaltenes, respectively. The data were fit with the following exponential function:

$$\left(\frac{T}{P}\right)_{T(K).} = A * Exp\left(\frac{B}{T}\right) \qquad \textbf{5-5}$$

where $(T/P)_{T(K)}$ is the terminators to propagators (T/P) ratio at temperature T (in K) and A and B are fitting parameters. The fitted A and B constants for each oil are presented in Table 5-4 along with the T/P ratio predicted at 20°C.

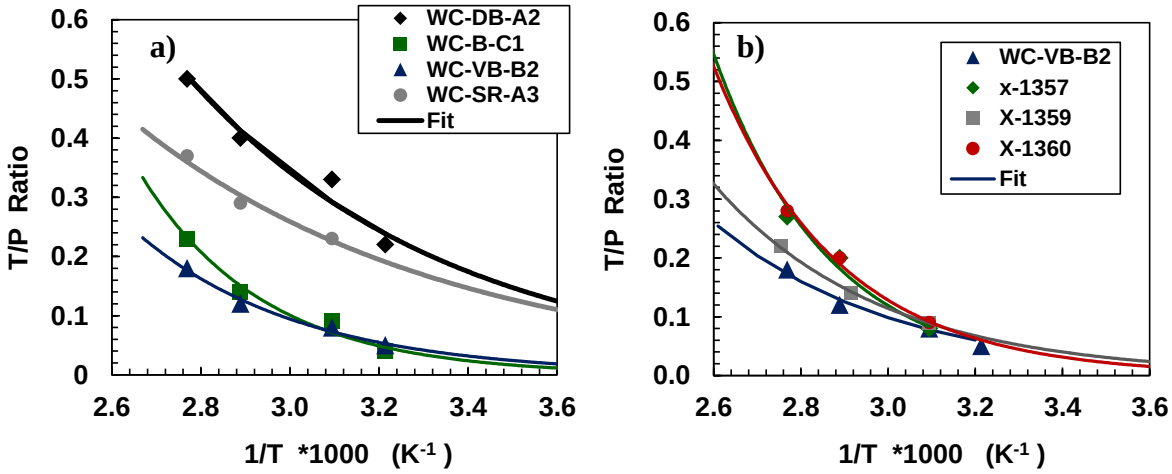

Figure 5-14. Temperature dependence of T/P ratio from the self-association model and fitted Equation. 5-5.

Table 5-4. Parameters for Equation 5-5 and T/P ratio predicted at 20°C.

Sample	A	B	T/P (20°C)
Native			
WC-B-C1	8200	-3.75	0.023
WC-DB-A2	53.6	-1.68	0.171
WC-VB-B2	145.8	-2.43	0.036
WC-SR-A3	8.62	-1.15	0.171
Thermocracked			
X-1357	11067	-3.81	0.025
X-1359	294.7	-2.62	0.039
X-1360	5073	-3.53	0.030
Hydrocracked	No Temperature Effect		

Once the T/P ratio was predicted at 20°C, the molecular weight distributions were constructed. Figures 5-15a and 5-15b show an example of the cumulative distribution and discrete molecular weight density function for C7 asphaltenes from Athabasca diluted bitumen. Similar trends were obtained for all the samples in the temperature study.

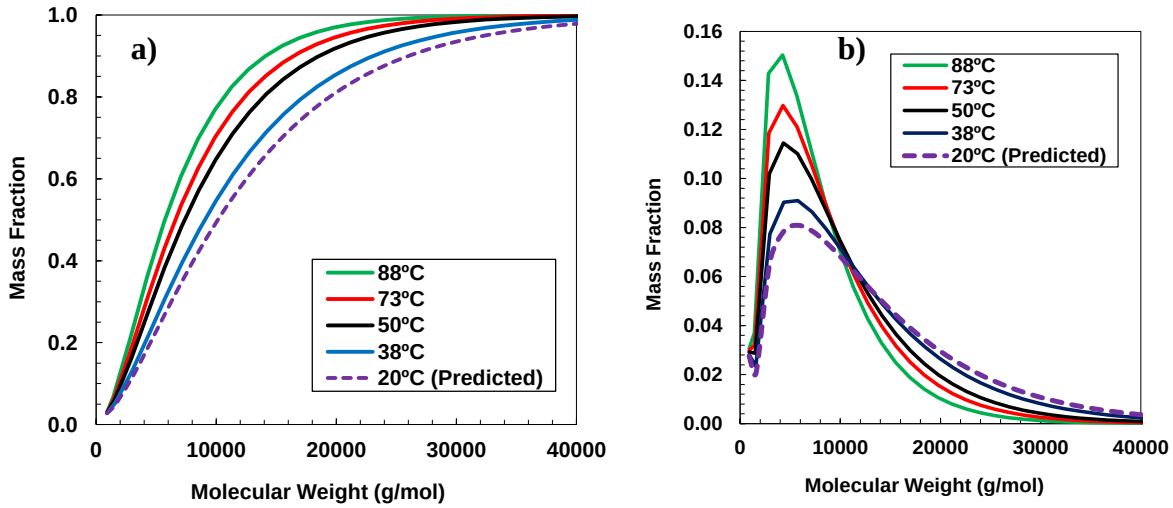

Figure 5-15. a) Cumulative and b) discrete molecular weight distribution with temperature and prediction at 20°C.

5.2.4 New Correlation of Average Molecular Weight to Temperature

The self-association model method requires a large amount of experimental data to predict the molecular weight distributions at any temperature for each sample. Therefore, a less data intensive correlation was developed based on the average apparent molecular weight at each temperature. A complete dataset of molecular weights and temperatures was obtained from the asphaltene molecular weight distributions for all the samples in the temperature study. Recall that the average apparent molecular weight is defined at an asphaltene concentration of 10 g/L because this is the concentration of the solubility experiments. Therefore, the molecular weights at 10 g/L were plotted against temperature from 20°C to 88°C. Note that the data at 20°C was predicted from the method described in previous section. Figures 5-16a and 5-16b show that the asphaltenes from both native and thermocracked oils have a linear trend although with different slopes.

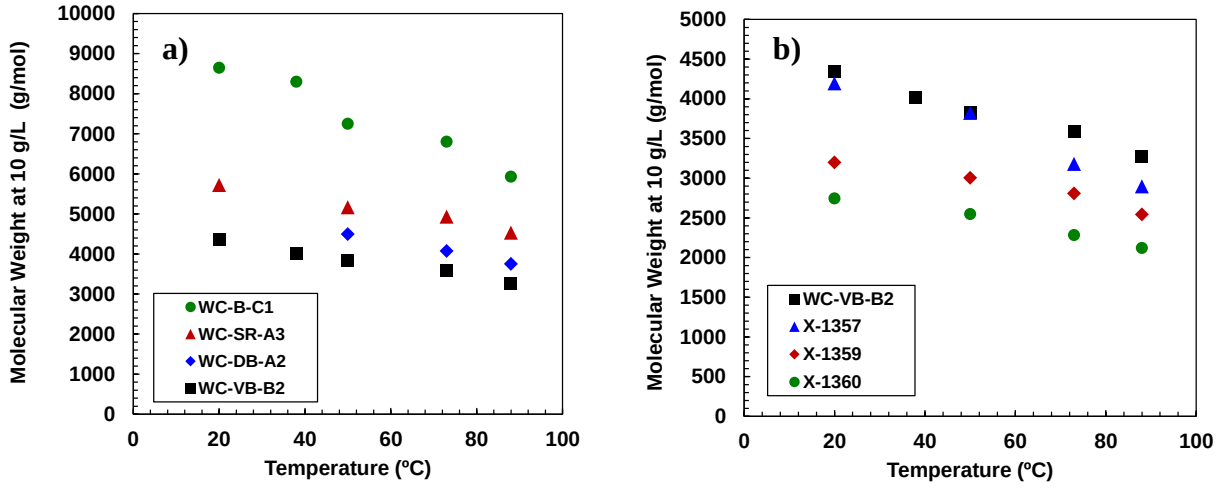

Figure 5-16. Molecular weight of asphaltenes at 10 g/L as function of temperature for asphaltenes from a) native and b) thermocracked oil samples.

The linear trends were extrapolated to higher temperatures and it was found that most of the linear trends intersect over a small range of temperatures (approximately 240 to 260°C) and low molecular weights between 600 and 900 g/mol,. Therefore, an apparent average "monomer" or "disassociation" temperature can be defined with a monomer molecular weight of 800 g/mol and a temperature of 250°C, Figure 5-17. Note, while it tempting to interpret this observation as a common dissociation temperature, the extrapolation is significant and may pass through a phase

transition in the asphaltenes (Agrawal *et al.* 2011). Hence, the observed trends should be applied with caution above 100°C because the phase behaviour of asphaltenes at higher temperature is uncertain and the extrapolation may not have a physical meaning.

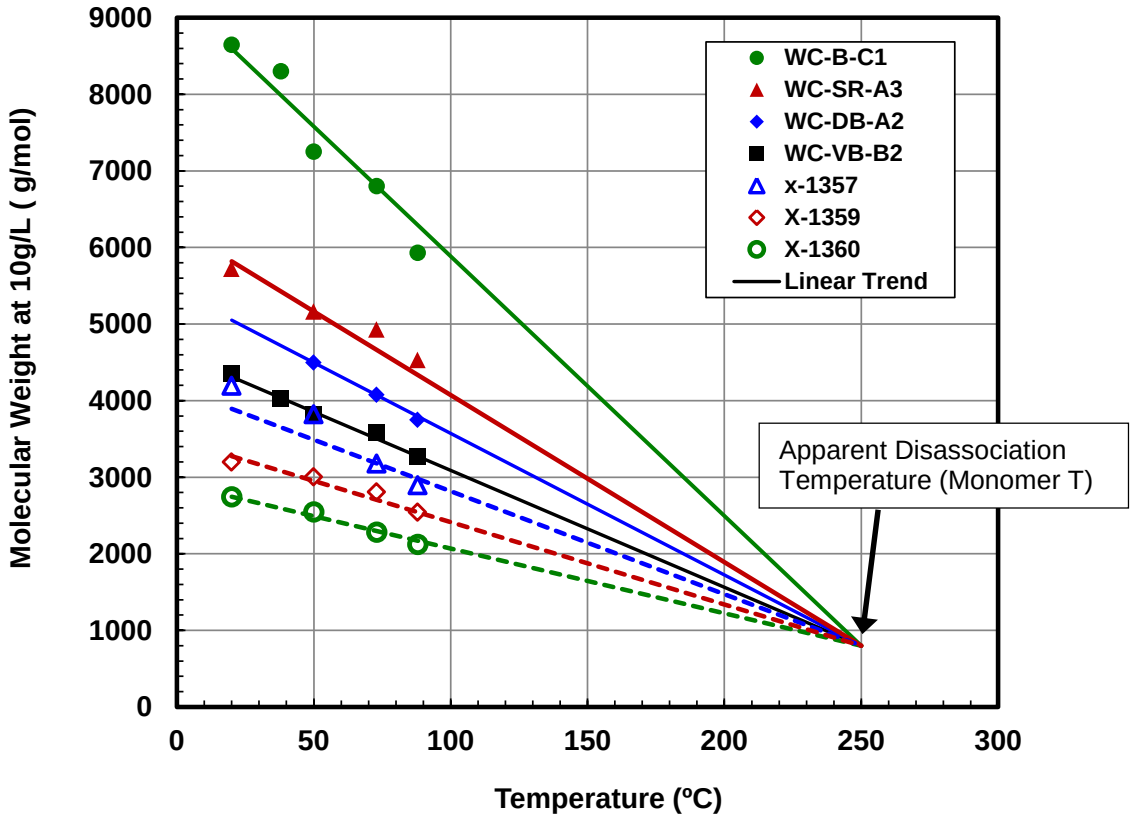

Figure 5-17. Linear temperature dependence and average apparent disassociation temperature for the molecular weight of Asphaltenes from native and reacted oils.

For each asphaltene, the data were fit with the least squares method constrained to match the common disassociation temperature, as shown in Figure 5-17. The average deviations were well within the scatter of the VPO data (±10 to 15%), Table 5-5. Therefore, as long as the average molecular weight is known at one temperature, the following correlation can be used to find the molecular weight at a desired temperature between 0 and 88ºC:

$$MW(T)_{Avg} = \frac{MW(T_1)-800}{T_1-250} * (T - T_1) + MW(T_1)_{Avg} \qquad \textbf{5-6}$$

where T is the desired temperature in ºC, $MW(T)$ is the molecular weight at T, T_1 is the available experimental temperature, $MW(T_1)$ is the molecular weight obtained at the experimental temperature T_1. Equation 5-6 can then be used with the Gamma function to predict the molecular weight distribution at any temperature, assuming that α is independent of temperature. In fact, fitting the molecular weight distributions for the data collected at different temperatures, the value of α did not change from the value of 1.5 fitted at 50°C (Tables 5-1 to 5-3).

Table 5-5. Absolute deviation and average relative error between the experimental molecular weight and the linear temperature dependence, Equation 5-6.

Sample	AAD g/mol	ARD at 50ºC %
WC-B-C1	210	4.5
WC-DB-A2	16	0.0
WC-VB-B2	33	0.8
WC-SR-A3	140	0.0
X-1357	180	8.7
X-1359	58	1.7
X-1360	29	2.2
Average	**95**	

5.3 Asphaltene Density Distribution

Barrera (2012) and Sadeghi-Yamchi (2014) determined the density distribution of asphaltenes from the density measurements of the asphaltene solubility fractions. They developed a correlation of density to molecular weight for input into the regular solution model. However, there is a flaw with this approach because the molecular weight distribution of a self-associating system is not a fixed quantity. Therefore, in this thesis, density was instead correlated to the cumulative mass fraction of the asphaltenes.

Figures 5-18 to 5-19 show the density distributions of asphaltene from native, *in-situ* converted, thermocracked and hydrocracked oils. All the samples have the same trends with a steep slope at low mass fractions followed by a plateau. Therefore, the following correlation of asphaltene density of asphaltenes (ρ_A) to mass fraction (w_A) is proposed:

$$\rho_A = \rho_{min} + (\rho_{max} - \rho_{min}) * (1 - Exp(-w_A * \tau)) \quad \textbf{5-7}$$

where ρ_A, ρ_{min} and ρ_{max} are the asphaltene densities in kg/m^3 at w_A, $w_A = 0$, and $w_A = 1$, respectively (note that the exponential of the product of w_A*τ gives values of the order of magnitude of 10^{-4}) , w_A is the cumulative mass fraction, and τ is a fitting parameter related to the neutrals content as $1/\tau$ and determines mass fraction range at which the density plateau is reached. Tables 5-6 to 5-8 show the parameter used for each sample to fit the density distribution which will be used in the regular solution model. Note that higher values of τ (*e.g.*, 9) is equivalent to small amount of neutrals (<5 wt%) characteristic of native asphaltenes. Lower values of τ correspond to larger amount of neutrals. Therefore, reacted asphaltenes have lower values of τ (τ=4) consistent with their higher proportion of neutrals.

Table 5-6. Parameters for the density distribution correlation (Equation 5-7) for asphaltenes from native oils.

Sample	ρ_{min} kg/m^3	ρ_{max} kg/m^3	τ
WC-B-B2	1050	1200	9
WC-B-A1	1050	1200	9
WC-DB-A2	1050	1200	9
WC-B-C1	1050	1200	9
WC-B-B1	1050	1200	9
WC-SR-A3	1020	1140	9
WC-VB-B2	1050	1200	9
Arabian	1050	1200	9

Table 5-7. Parameters for the density distribution correlation (Equation 5-7) for asphaltenes from *in-situ* converted oils.

Sample	ρ_{min} kg/m^3	ρ_{max} kg/m^3	τ
WC-B-B2 (original)	1050	1200	9
27034-113	1130	1250	7
27034-87	1130	1200	7
26845	1050	1230	7

Table 5-8. Parameters for the density distribution correlation (Equation 5-7) for asphaltenes from thermocracked and hydrocracked oils.

Sample	ρ_{min} kg/m^3	ρ_{max} kg/m^3	τ
Thermocracked			
WC-VB-B2 (Feed)	1050	1200	9
X-1357	1050	1250	7
X-1359	1080	1280	4
X-1360	1050	1280	4
Hydrocracked			
WC-SR-A3 (Feed)	1020	1140	9
RHC-19-03*	1050	1250	7
RHC-18-19	1050	1280	4
RCH-18-37	1050	1280	4
HOS Bottoms	1050	1300	4

* Fitted from asphaltene whole data only.

Asphaltenes from native oils have very similar density distributions with the maximum density approximately at 1200 kg/m^3, the minimum density at an average of 1050 kg/m^3, and similar inflexion points, Figures 5-18a and 5-18b. The density distribution of asphaltenes from WC-SR-A3 is the only exception for native oils with a significantly lower maximum density. This sample was taken from a partially deasphalted process stream but it is not known if the partial deasphalting would result in such a low residual asphaltene density.

Density distributions of asphaltenes from *in situ*, thermocracked, and hydrocracked samples have the type of trend, but the density "plateau" or maximum density significantly increases and the inflexion point occurs at higher mass fractions than for native oils, Figure 5-19 and 5-20.

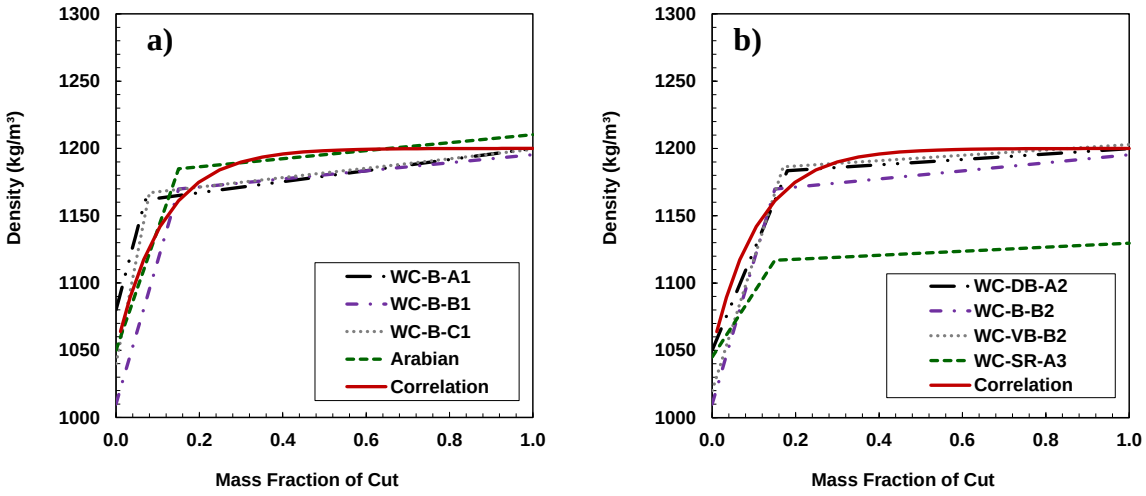

Figure 5-18. Density distribution for asphaltenes from native oils at 20^{o}C and atmospheric pressure. Lines in Figures are previous density distributions fitted by Barrera et al (2013) for asphaltene from each specific native sample. The density distribution used two linear correlations (Barrera 2012, Barrera *et al*. 2013).

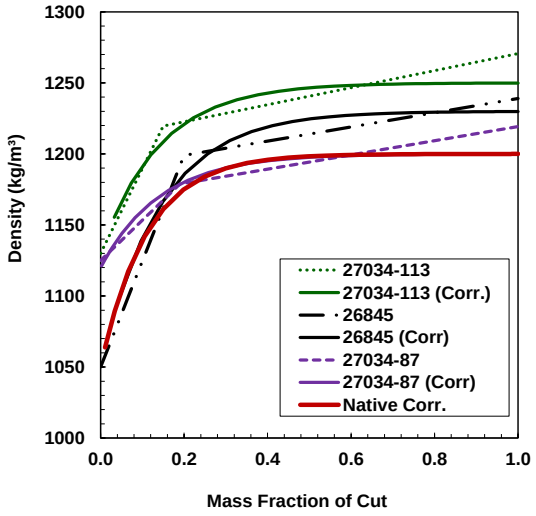

Figure 5-19. Density distribution for asphaltenes from in-situ converted oils at 20°C and atmospheric pressure.

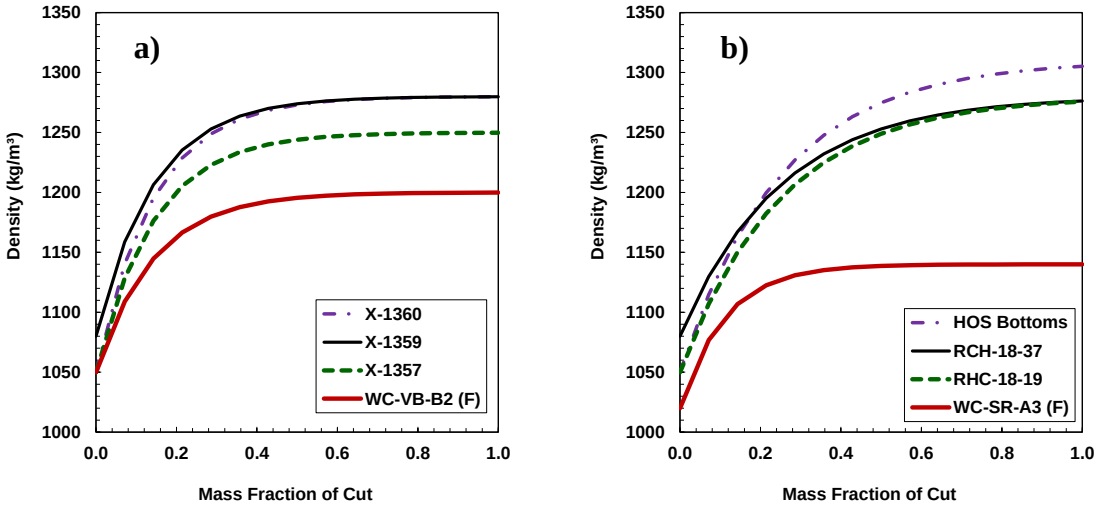

Figure 5-20. Density distribution for asphaltenes from a) thermocracked and b) hydrocracked oils.

5.4 Asphaltene Solubility Parameter

As outlined in Chapter 4, Barrera *et al*. (2012) correlated the asphaltene solubility parameter to molecular weight, Equation 4-21 which is repeated here for convenience:

$$\delta = \left(A(T)\rho_A\left(cMW^d\right)\right)^{1/2} \quad \textbf{5-8}$$

where *c* and *d* are constants specific to each asphaltene, *A(T)* is determined from Equation 4-20 and ρ_A from Equation 4-21. Barrera (2012) demonstrated that a common value for *d* of 0.0495 can be applied for asphaltenes from native and *in-situ* reacted oils and only *c* varied for each asphaltene. However, for highly reacted asphaltenes from thermocracked and hydrocracked oils, both *c* and *d* varied (Sadeghi, 2014). In this thesis, a new solubility parameter correlation is developed to reduce the number of fitting parameters.

5.4.1 New Solubility Parameter for Asphaltenes from Native and Reacted Oils.

A new solubility parameter correlation is proposed based on the solubility parameter definition, Equation 4-14, repeated here for convenience:

$$\delta_T = \left(\frac{\Delta H^T_{vap^*} - RT}{v_T}\right)^{1/2} \quad \textbf{5-9}$$

where δ is the solubility parameter in $MPa^{0.5}$, $\Delta H^T_{Vap}{}^*$ is the molar heat of vaporization (dJ/mol), *R* is the universal gas constant in dJ/molK, *T* is temperature in K, and *v* is the molar volume in cm^3/mol or the ratio of molecular weight to density. Since both molecular weight and density have already been determined, the only unknown is the heat of vaporization.

The following correlation for the enthalpy of vaporization at room temperature to molecular weight is proposed:

$$ln\Delta H^T_{vap} = a * MW^b_{Asph.} \quad \textbf{5-10}$$

where MW_A is the molecular weight of asphaltenes, *a* is a constant and *b* is a fitting parameter. Note, a dependence on molecular weight is retained because the solubility parameter is expected to depend on the size of the nano-aggregate; larger components tend to be less soluble. The

constant parameter *a* was found to be 9.72; parameter *b* varied from approximately 0.0633 to 0.0645, as is explained below. Hence, the new correlation has only one adjustable parameter. Note, when the enthalpy of vapourization correlation is extrapolated to lower molecular weights (lower than asphaltene MW_{mono}), it is consistent with the enthalpy of vaporization of pure hydrocarbons, Figure 5-21.

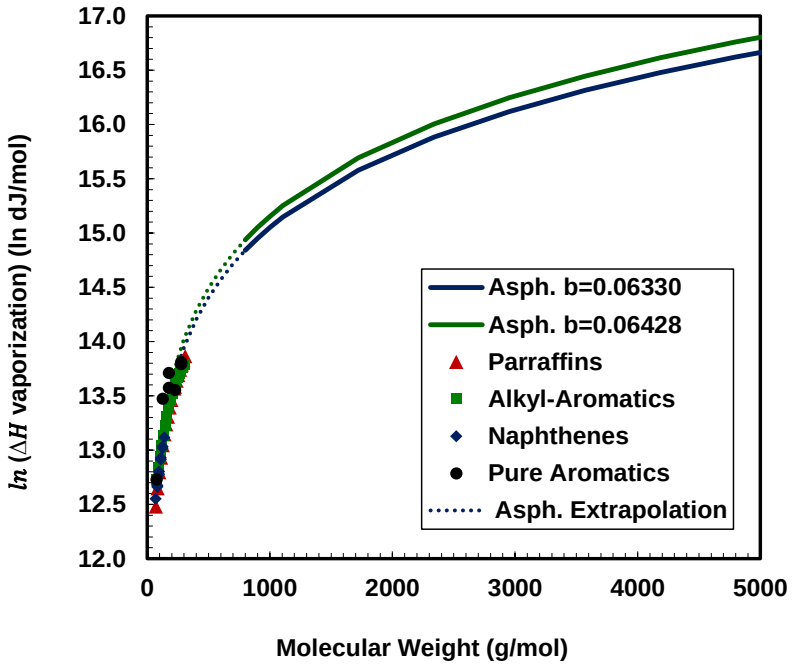

Figure 5-21. Extrapolation of the enthalpy of vapourization correlation.

As described in Chapter 4, the asphaltene solubility parameters are determined by fitting the regular solution model to asphaltene precipitation data from mixtures of heptane and toluene. The properties of heptane and toluene are provided in Table 5-9. The asphaltene input parameters are: the measured average aggregate molecular weight and α (shape factor) for the Gamma distribution (including neutrals as part of the distribution), equations 4-1 and 4-2; density distributions using Equation 5-7 with the parameter values in Tables 5-6 to 5-8, and; solubility parameters from Equations 5-9 and 5-10. The asphaltene fractional yield or solubility curves are then modeled by adjusting the parameter *b* to fit the experimental data. Additionally, the α shape factor in the Gamma distribution is adjusted to fine tune the fit.

Table 5-9. Properties of the solvents at 23°C and atmospheric pressure.

Compound	Density g/cm^3	Molecular Weight g/mol	Molar Volume cm^3/mol	Solubility Parameter MPa$^{1/2}$
Toluene	0.866	92	106.4	18.3
n-heptane	0.681	100	147.1	15.2

Figures 5-22 to 5-25 show the modeled asphaltene solubility curves for some of the respective native, *in-situ*, thermocracked, and hydrocracked asphaltene samples. Note that the reacted asphaltenes include significantly less soluble components than the native asphaltenes but retain some relatively soluble components. This wide range of solubility could not be matched with the previous model. The revised regular solution model successfully represents the solubility of asphaltenes from not only native oils, but also highly reacted oils. The revised model was also successfully tested with previous data from Akbarzadeh (2005), (Appendix C). The fitted values of *b* and α, and the average measure molecular weight of asphaltenes at 10 g/L are provided in Tables 5-10 to 5-12.

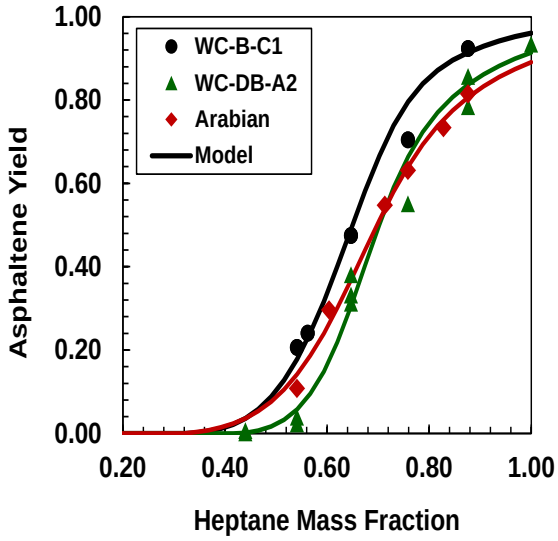

Figure 5-22. Fractional precipitation of asphaltenes in heptol solutions at 20°C for native samples.

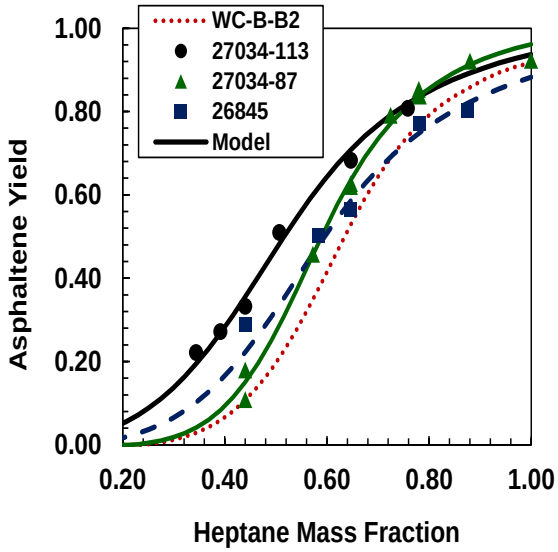

Figure 5-23. Fractional precipitation of asphaltenes in heptol solutions at 20°C for *in-situ* converted samples.

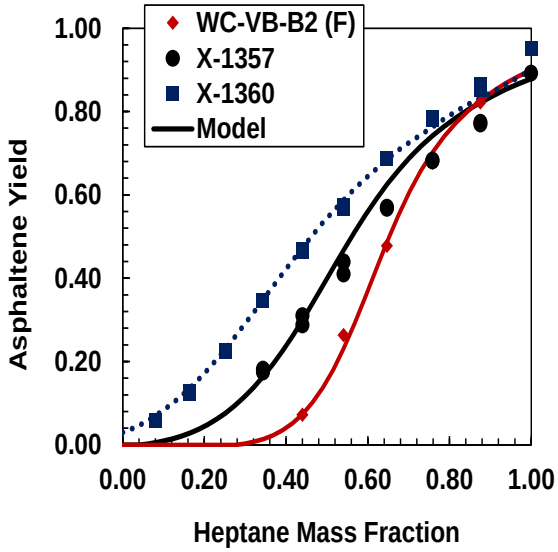

Figure 5-24. Fractional precipitation of asphaltenes in heptol solutions at 20°C for thermocracked samples and the feedstock.

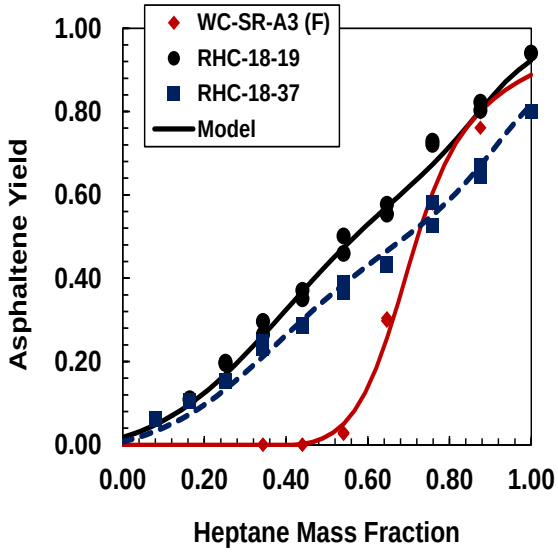

Figure 5-25. Fractional precipitation of asphaltenes in heptol solutions at 20°C for hydrocracked samples and the feedstock.

Table 5-10. Input parameters to the regular solution model for asphaltene-heptol mixtures for native samples.

Sample	b	α	$MW_{@10g/L(50^oC)}$
WC-B-B2	0.0635	2	4500
WC-DB-A2	0.0636	4	4200
WC-B-C1	0.0633	5	6980
WC-B-B1	0.0637	1.5	2900
WC-SR-A3	0.0637	4	4900
WC-VB-B2	0.0636	2	3800
Arabian	0.0635	2	3950
Cold Lake*	0.0634	10	7900
Lloydminster*	0.0635	8	6700
Venezuela 1*	0.0633	10	10000
Venezuela 2*	0.0634	10	7700
Russia*	0.0633	6	7100
Average	**0.0634**		

*Solubility and MW data from Akbarzadeh (2005)

Table 5-11. Input parameters to the regular solution model for asphaltene-heptol mixtures for *in-situ* converted samples.

Sample	b	α	$MW_{@10g/L(50^oC)}$
WC-B-B2 (original)	0.0635	2	4500
27034-113	0.0637	1	3500
27034-87	0.0637	2	3950
26845	0.0637	1	3020

Table 5-12. Input parameters to the regular solution model for asphaltene-heptol mixtures for thermocracked and hydrocracked samples.

Sample	*b*	α	$MW_{@10g/L(50^oC)}$
Thermocracked			
WC-VB-B2 (Feed)	0.0634	2	3700
X-1357	0.0637	0.7	2900
X-1359	0.0638	0.6	2800
X-1360	0.0640	0.5	2300
Hydrocracked			
WC-SR-A3 (Feed)	0.0637	4	4900
RHC-19-03	0.0642	0.5	2100
RHC-18-19	0.0642	0.3	1500
RCH-18-37	0.0644	0.2	900
HOS Bottoms	0.0644	0.3	1200

Asphaltenes from native oils have similar values of b with an average of 0.0634. The asphaltene solubility for native asphaltenes is similar and depends mostly on the molecular weight of each sample. Solubility curves for reacted samples, thermocracked and hydrocracked, are significantly different from those of native asphaltenes. Conversion decreases asphaltene solubility which is quantified by increasing values of *b*. Small increments in *b* indicate larger solubility parameters,

hence, less soluble asphaltenes. Reacted asphaltenes are smaller and less associated molecules (lower MW_{mono} and narrower MW distributions) likely to be more "abundant" in condensed aromatic rings which decreases are less soluble in solvents even making part of the asphaltenes insoluble in toluene.

5.4.2 Uncertainty of Fitted Parameters b and α

A sensitivity analysis was performed to determine the uncertainties in the fitted parameters: *b* from the solubility parameter correlation (Eq. 5-10) and α from the gamma distribution (Eq. 4-1 and 4-2).

Parameter *b*

Recall that the repeatability of the solubility measurements of asphaltenes in heptol was ±6 wt% on average. Figure 5-26 shows the solubility data with error bars (repeatability) and the results from the regular solution model for C7 asphaltenes from WC-B-B2. The solid line indicates the best fit model results with a "*b*" parameter of 0.0635 as explained in the previous section. Changing *b* to 0.0636 and 0.0634 fits the upper and lower end of the yield error bars respectively. Hence, the uncertainty in *b* for native asphaltenes is ±0.0001.

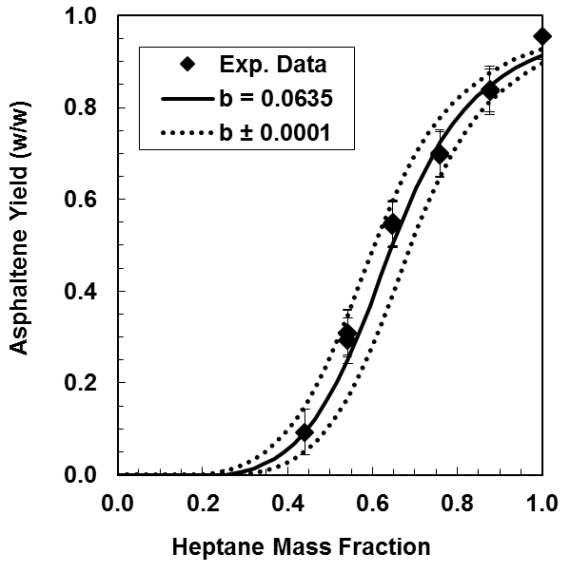

Figure 5-26. Fractional precipitation of WC-B-B2 asphaltenes in heptol solutions at 20°C and model results for $b = 0.0635 \pm 0.0001$.

Similar trends are observed for reacted asphaltenes. Figure 5-27a shows that changing b by ±0.0001 captures the uncertainty of most, but not all, of the solubility measurements. Figure 5-27b shows that changing *b* by ±0.0002 overestimates the uncertainty for most of the solubility data points. Therefore, the uncertainty of *b* for reacted oils is about ±0.00015.

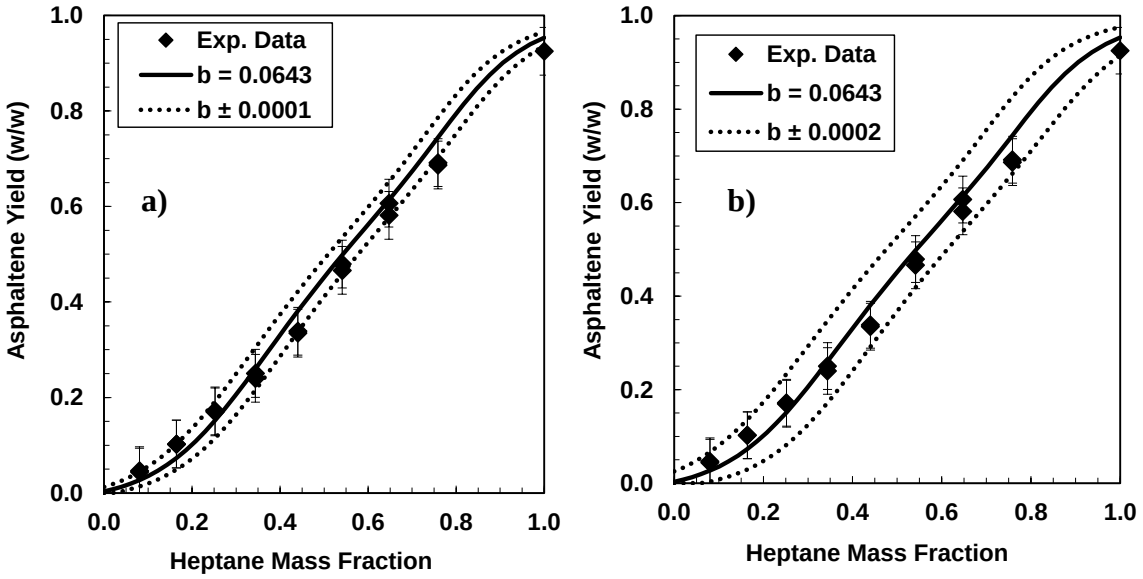

Figure 5-27. Fractional precipitation of HOS Bottoms asphaltenes in heptol solutions at 20°C and model results for a) $b = 0.0643 \pm 0.0001$ and b) $b = 0.0643 \pm 0.0002$.

Figures 5-28a and 5-28b show the solubility parameter distribution for C7 asphaltenes from WC-B-B2 and HOS Bottoms. The uncertainty in the solubility parameter for both these asphaltenes ranges between 0.1 $MPa^{0.5}$ and 0.2 $MPa^{0.5}$ for low and high solubility parameters, respectively. Therefore, the uncertainty for the solubility parameter of both native and reacted asphaltenes is 0.2 $MPa^{0.5}$.

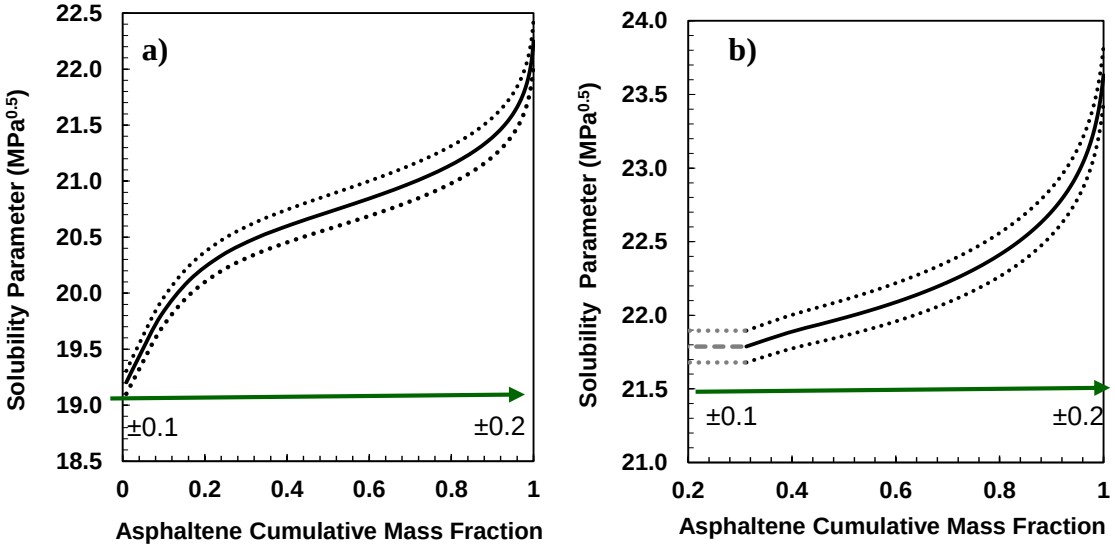

Figure 5-28. Solubility parameter trend and uncertainty for asphaltenes from a) WC-B-B2 and b) HOS bottoms.

Parameter α

As mentioned previously, α controls the shape of the molecular weight distribution. An α of unity gives an exponential distribution. Higher values of the shape factor produce less skewed distributions; for example, the shape of a Gamma distribution with α = 10 very closely resembles the shape of the standard normal (Gaussian) distribution. Figures 5-29a and 5-29b show the effect of changing α ±0.5 and ±1.0, respectively from the best fit value of 2.0. The main effect of the shape factor on the Gamma distribution is observed at low heptane mass fraction when asphaltene precipitation is dominated by the high molecular weight pseudo-components. The lowest α of 1.0 clearly over-predicts beyond the experimental error for the asphaltene yield curve. In general, for higher α (>3) the effect on the yield curve is not as large as for low shape factors. Therefore, for α =2.0 the uncertainty is 0.5 or 1/4 of α; higher values of α (α>4) have uncertainties of 1.0.

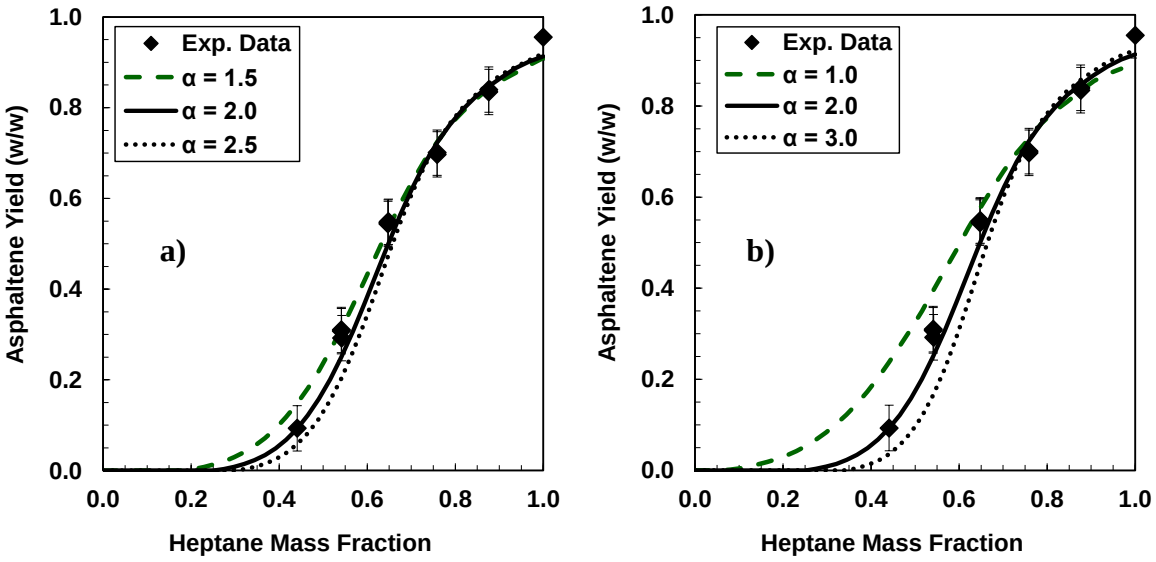

Figure 5-29. Fractional precipitation of WC-B-B2 asphaltenes in heptol solutions at 20°C and model results for a) $\alpha = 2.0 \pm 0.5$ and b) $\alpha = 2.0 \pm 1.0$.

Asphaltenes from highly reacted samples have shape factors lower than 1.0 (Table 5-12). Smaller changes for very low shapes factors significantly affect the model results. Figure 5.30 shows the model results for HOS Bottoms with shapes factors of 0.2, 0.3 (best fit with lowers AAD) and 0.4. The main difference is again at low heptane mass fractions, but there are now some small differences at high heptane mass fractions as well. If the shape factor is reduced to 0.1, the model predicted an unrealistic asphaltene yield of greater than 10 wt%. Recall that the asphaltenes used in the experiments are toluene-insoluble-free, therefore, all the material in the experiment is soluble in toluene. Hence, the uncertainty in α for highly reacted samples is ±0.1 or 1/3 of α. In general, the uncertainty of α is 1/3 to 1/4 of its value.

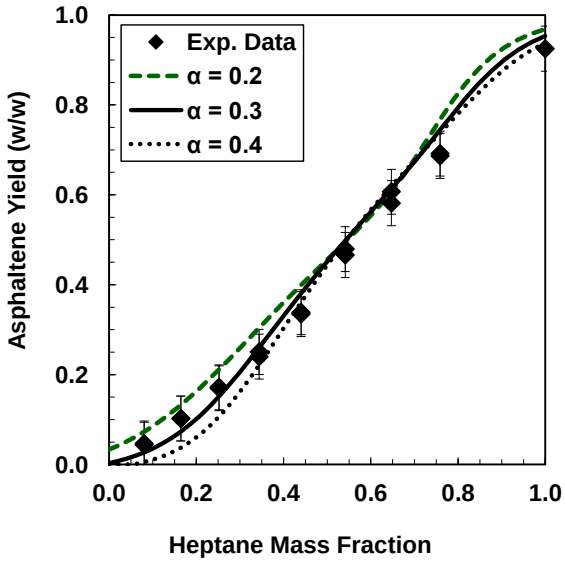

Figure 5-30. Fractional precipitation of HOS Bottoms asphaltenes in heptol solutions at 20°C and model results for $\alpha = 0.3 \pm 0.1$.

5.4.3 Sensitivity of Regular Solution Model to Asphaltene Input Parameters

A sensitivity analysis was performed to determine the effect of uncertainties in the model input parameters on the model results. The following input parameters are analysed: average asphaltene molecular weight and the fitted parameters of the density equation.

Average Aggregated Molecular Weight

Recall that the input to the regular solution model is the average aggregated molecular weight of asphaltenes measured in the VPO at 10 g/L at 50°C in toluene. The average molecular weight error of the VPO was approximately ±10 to 15%. Figures 5-31a and 5-31b shows the effect on the model predictions of a ±10% variation in the average input molecular weight from WC-B-B2 and HOS Bottoms. The deviation of ±10% in molecular weight is generally within the error of the solubility experiments.

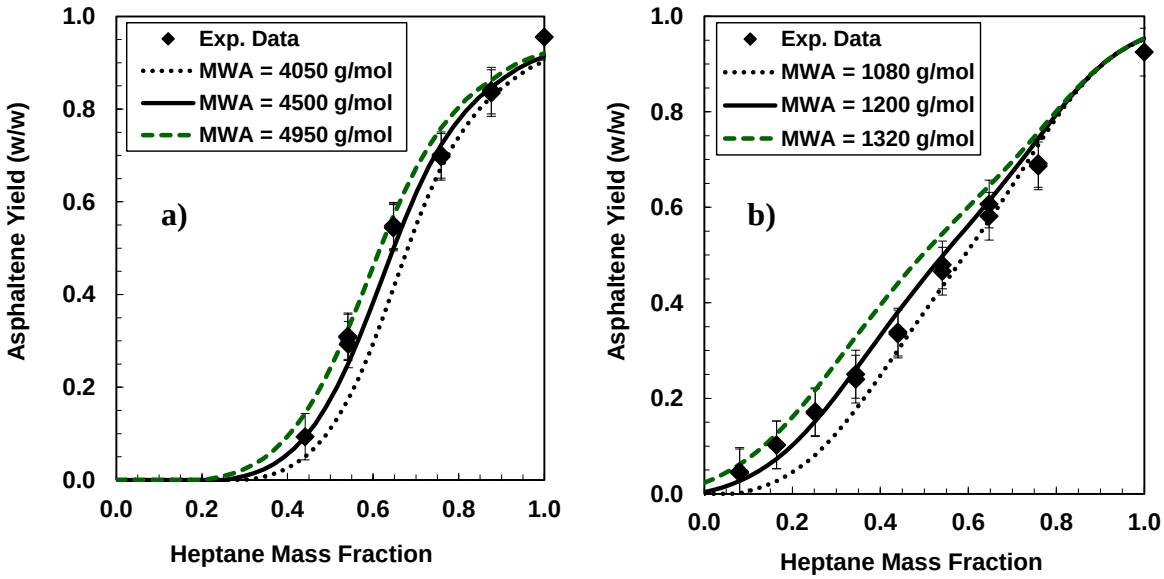

Figure 5-31. Fractional precipitation of asphaltenes in heptol solutions at 20°C and model results for a) WC-B-B2 with MW_A = 4500 g/mol ± 10% and b)HOS bottoms with MW_A = 1200 g/mol ± 10%.

Density Distribution Parameters

Recall the density distribution function which has three main parameters: ρ_{min}, ρ_{max} and τ. These parameters are set with the fitting of the density distribution equation (Eq. 5-7) to the experimental distribution from the measurements of the density of the asphaltene fractions. The experimental error in the density extrapolations for asphaltenes is ± 5 kg/m^3. Recall that the density extrapolations were performed using Eq.3-4 as explained in section 3.6.2. The uncertainty in the density fitting equation is between ±10 and ±15 kg/m^3.

The effect of ρ_{min} is first analyzed. Figures 5-32a and 5-32b show that a change in ±50 kg/m^3 does not significantly affect the results in the model; small changes are observed and only at high heptane fractions. Hence, the error in this parameter from the density distribution equation (<20 kg/m^3) will not affect the results in the model.

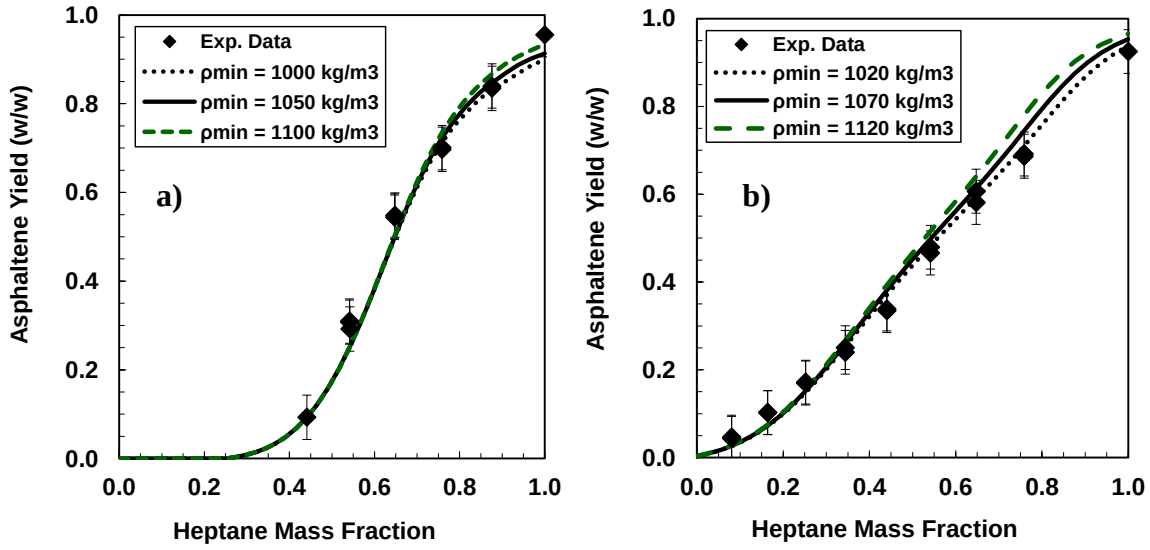

Figure 5-32. Fractional precipitation of asphaltenes in heptol solutions at 20°C and model results for a) WC-B-B2 with ρ_{min} = 1050 ± 50 kg/m^3 and b) HOS bottoms with ρ_{min} = 1070 ± 50 kg/m^3.

The next parameter in the fitted density distribution equation is the maximum density, ρ_{max} . Recall that, ρ_{max} is 1200 kg/m^3 for all native asphaltenes and increases for reacted asphaltenes depending on conversion. In general, this parameter has a larger effect than the minimum density in the model results. Figures 5.34a and 5-34b show the effect of ±20 kg/m^3 in ρ_{max} for WC-B-B2 and HOS Bottoms asphaltenes. An uncertainty of ±20 kg/m^3 is just within the error of the solubility measurements. Therefore, density errors could be compensated by adjusting the *b* parameter within its range of uncertainty, *b*±0.0001.

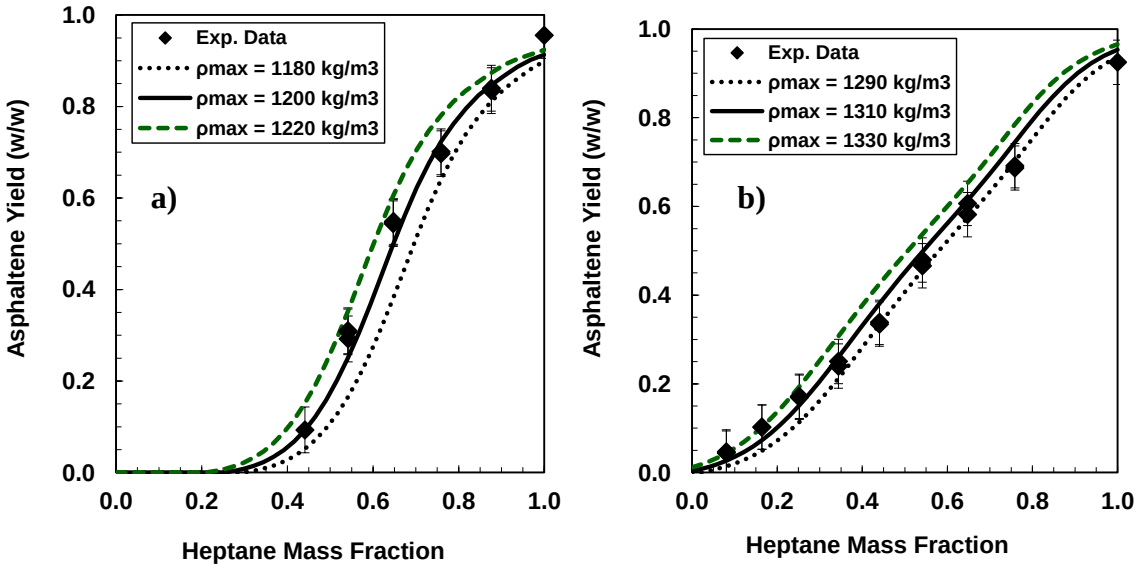

Figure 5-33. Fractional precipitation of asphaltenes in heptol solutions at 20°C and model results for a) WC-B-B2 with ρ_{max} = 1200 ± 20 kg/m^3 and b) HOS bottoms with ρ_{max} = 1310 ± 20 kg/m^3.

The last parameter in the density equation is τ which is an indicator of the amount of neutral material present within the asphaltene fraction and determines the "inflexion" in the density distribution. Figure 5-34a shows that for a large value of τ (τ=9) in the case of native asphaltenes, τ ±2 does not significantly affect the density distribution, thus does not affect the asphaltene yield model results, Figure 5-35a. In the case of reacted asphaltenes with smaller values of τ (τ=4), τ ± 1 significantly affect the density distribution, Figure 5-34b. However, the effect in the asphaltene yield model results with τ ± 1 for reacted asphaltenes is within the error in the solubility data, Figure 5-35b. Therefore, the effect of τ ± 1 for native and reacted asphaltenes is within the error of the experimental data.

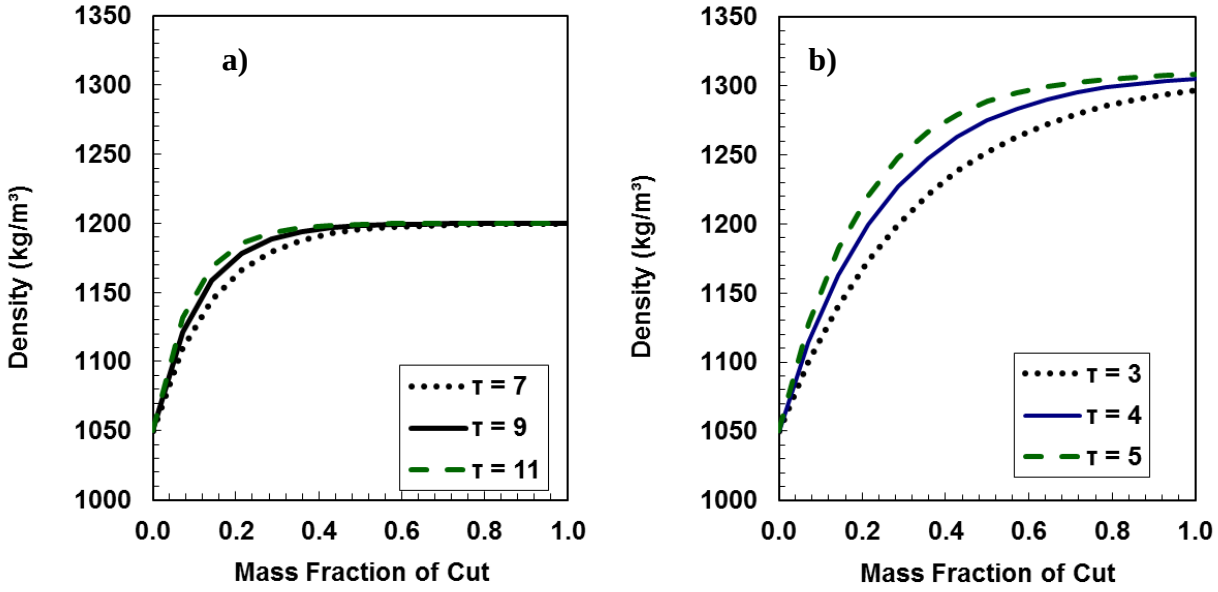

Figure 5-34. Density distribution at 20°C and atmospheric pressure for asphaltenes from a) native oils and b) HOS bottoms.

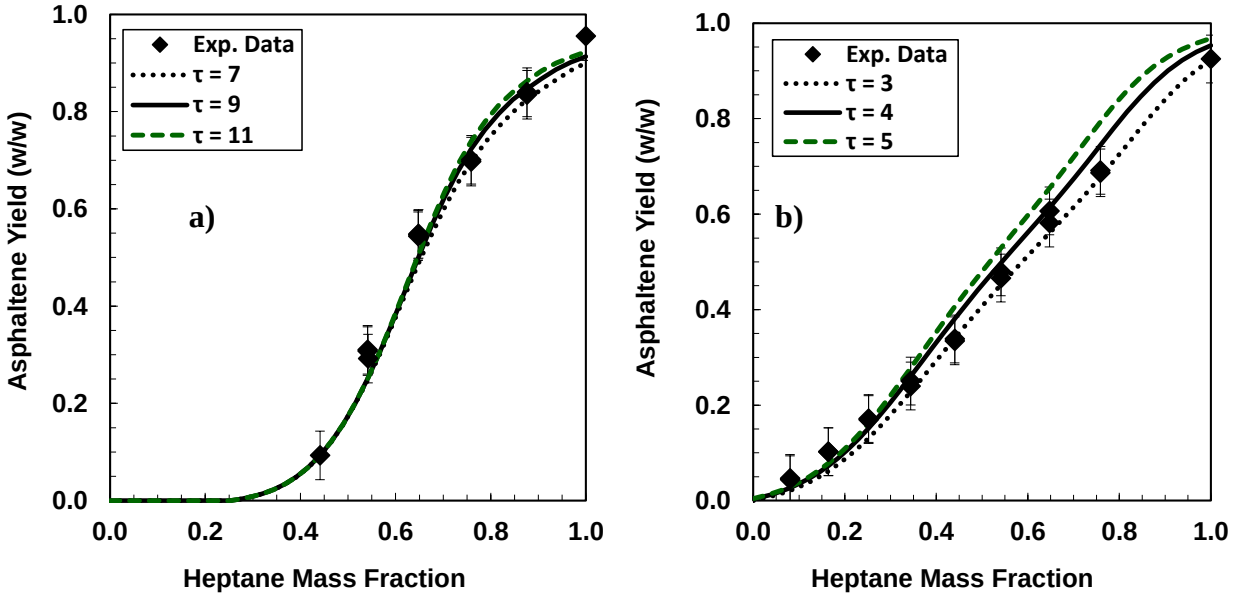

Figure 5-35. Fractional precipitation of asphaltenes in heptol solutions at 20°C and model results for a) WC-B-B2 with $\tau = 9 \pm 2$ and b) HOS bottoms with $\tau = 4 \pm 1$ kg/m^3.

5.4.4 Correlation of the Parameter b to Average Molecular Weight

When the fitted *b* values are plotted against the average aggregate molecular weight for all the samples tested, a consistent trend is observed, Figure 5-36. A change in slope is also observed between reacted samples and native oils. There may be two components to the apparent correlation: 1) changes in monomer properties due to reaction; 2) the effect of self-association. In both cases, the average molecular weight may be a proxy for changes in monomer properties.

The gradual decrease in *b* of native asphaltenes at molecular weights above 3000 g/mol suggests that part of the contribution to *b* is related to self-association. In this region, large changes in average molecular weight cause a small decrease in *b*; that is, slightly more solubility at a given molecular weight. Perhaps asphaltenes with lower solubility parameters tend to self-associate more. Another possibility is that the mathematical expression relating the heat of vaporization to molecular weight is not exact. Nonetheless, the "*b*" values for native asphaltenes fall in a small range and within the uncertainty of *b*; hence, an average value of *b*=0.0634 can be used for any native asphaltene.

Below 3000 g/mol, the parameter *b* increases significantly as the average molecular weight decreases. Only reacted asphaltenes have average molecular weights below 3000 g/mol. The trend is consistent with the lower solubility observed for reacted asphaltenes. Higher b (higher enthalpy of vaporization) gives higher solubility parameters. Note that the density of reacted asphaltenes also increased and is also a contribution to larger solubility parameters. Reacted asphaltenes have lost paraffinic side chains are more aromatic than unreacted asphaltenes. Aromatic components have higher solubility parameters than paraffins (18.25 for toluene versus 15.3 $MPa^{0.5}$ for n-heptane). Reacted asphaltenes also associate less than native asphaltenes. Hence, the increase in b is a change in the monomer properties that correlates to a change in average molecular weight. While an average value of *b* is adequate for native asphaltenes, the fitted (or correlated) values of *b* must be used for reacted asphaltenes. The *b* values obtained for asphaltenes in heptol will also be used for the crude oil modeling presented in Chapter 7.

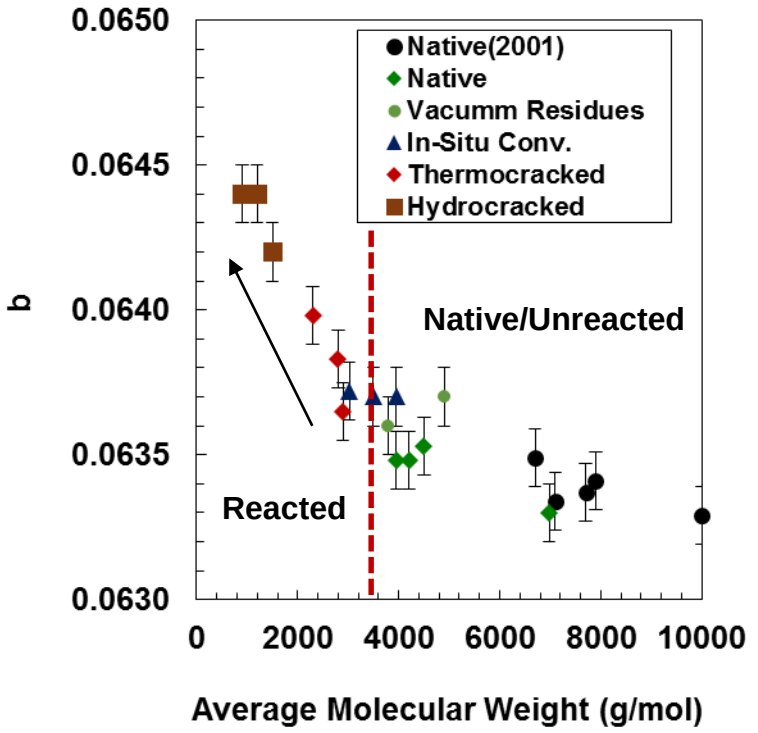

Figure 5-36. Fitted parameter b as function of the average aggregated molecular weight of asphaltenes at 50°C. Note that the error bars come from the sensitivity analysis explained in section 5.4.2.

5.5 Other Properties of Asphaltenes and the Effect of Reaction

Refractive index was also measured for most of the asphaltene samples. Although this property is not an input into the regular solution model, there is evidence that the refractive index relates to density and to the solubility parameter. One important advantage of this property is that it is very easy and fast to measure. Elemental analysis was also performed on asphaltenes from thermocracked and hydrocracked oils to identify chemical changes after reaction and to study possible relationships to other properties.

5.5.1 Refractive Index

Figure 5-37 shows the refractive index for asphaltenes from native oils. The refractive index is between 1.725 and 1.755 with the exception of WC-SR-A3 which is much lower, consistent with its lower density. Figures 5-38a and 5-38b (data from Sadeghi-Yamchi, 2014) show that the

refractive index for asphaltenes from thermocracked and hydrocracked samples significantly increased above the average refractive index of asphaltenes from native oils (horizontal line). This consistent increase of the refractive index with reaction indicates that this property, as well as density, can be a reaction indicator. In fact, Okafor (2013) and Sadeghi-Yamchi (2014) found that, in general, the refractive index is proportional to density as expected from the Lorenz-Lorentz relationship, Equations 2-11 and 2-12.

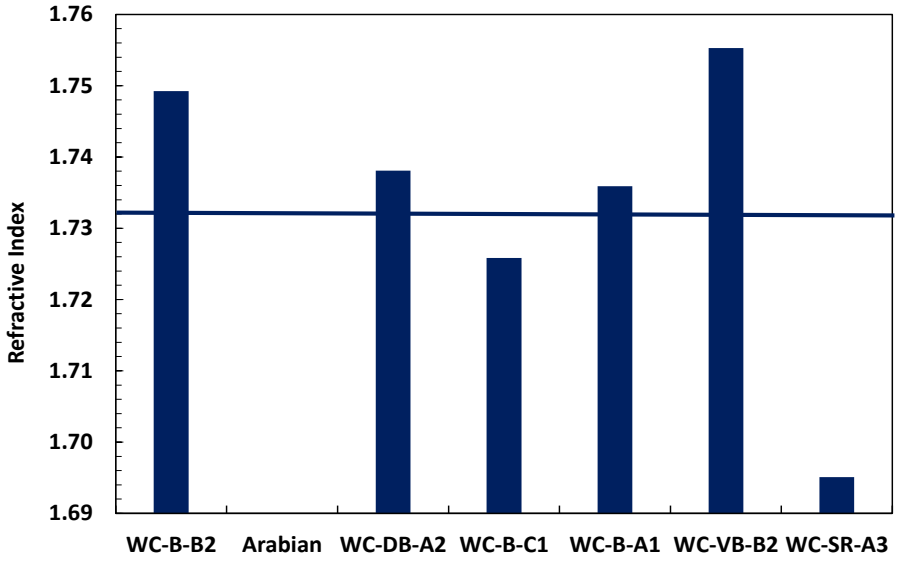

Figure 5-37. Refractive index comparison of asphaltenes from native oils at 20^{o}C and atmospheric pressure.

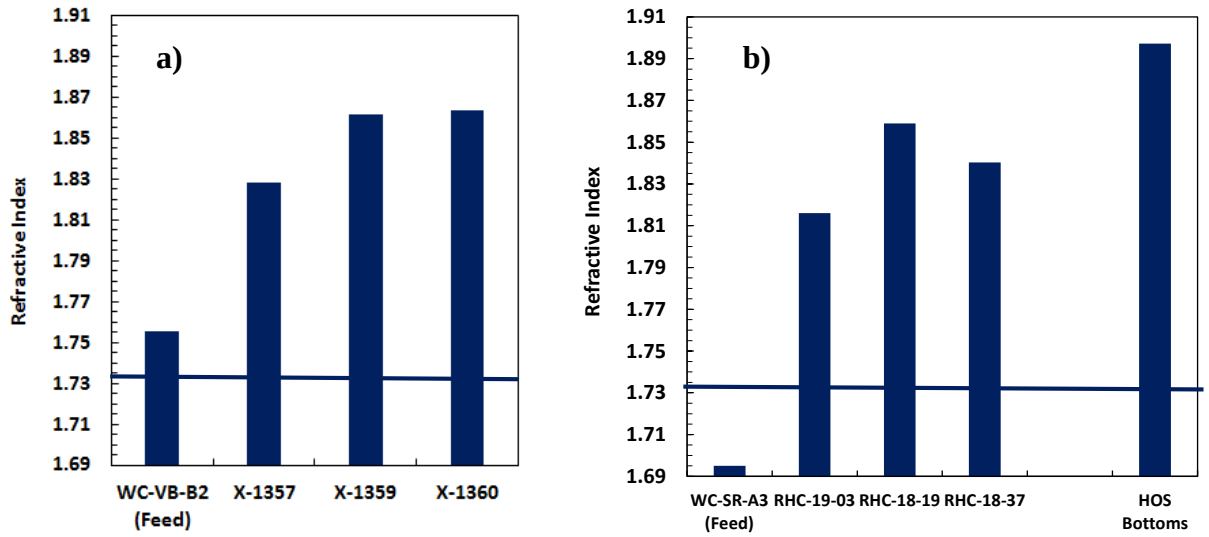

Figure 5-38. Refractive index comparison of asphaltenes from a) thermocracked and b) hydrocracked oils at 20^{o}C and atmospheric pressure.

5.5.2 Elemental Analysis

Elemental analysis, CHNS, was performed on the whole asphaltene samples. Figures 5-39a and 5-39b show the H/C atomic ratio for asphaltenes from native oils and *in-situ* converted oils, respectively. The H/C ratio for asphaltenes from native oils was between 0.9 and 1.2 consistent with previous studies (Tharanivasan, 2010). The H/C ratio of asphaltenes from *in-situ* converted oils slightly decreased in comparison with the original oil especially for 27034-113 asphaltenes. Note that 27034-113 asphaltenes were from the samples that had a lower reported extent of reaction, but the molecular weight and density results indicated that these asphaltenes were significantly reacted.

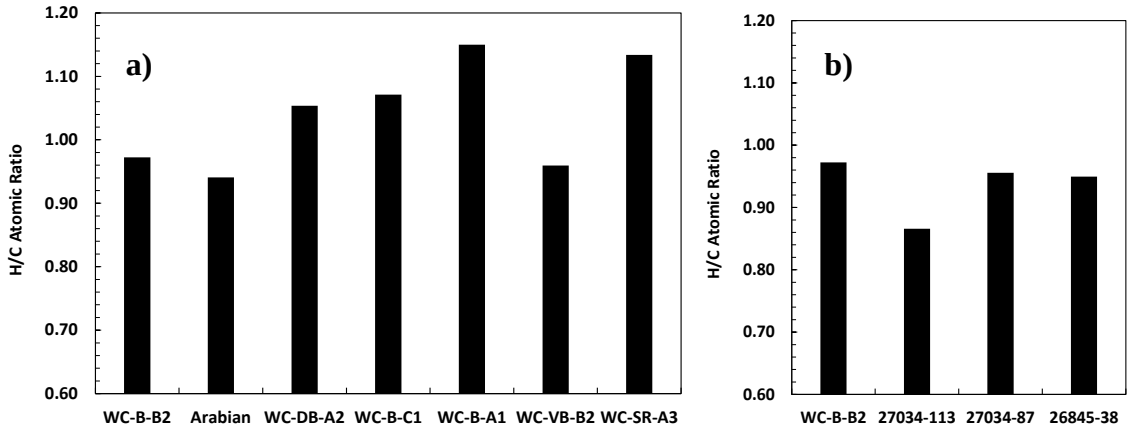

Figure 5-39. H/C atomic ratio of asphaltenes from a) native and b) *in-situ* converted oils at 20^{o}C and atmospheric pressure.

Thermocracked and hydrocracked processes significantly decreased the H/C ratio of asphaltenes, Figures 5-40a and 5-40b, and the reduction is consistent with the extent of reaction for most of the samples. A high reduction of H/C ratio is expected for thermocracking processes because paraffinic side chains are removed. Interestingly, hydrocracking also significantly reduced the H/C ratio. It is possible that removing side chains dominates any hydrogen addition in the asphaltenes. It is also possible that some the original asphaltenes were converted to lower molecular weight compounds that then reported to the resin fraction. The residual asphaltenes would then be the more stable aromatic components that are difficult to saturate and crack. This material would be very insoluble consistent with the solubility data.

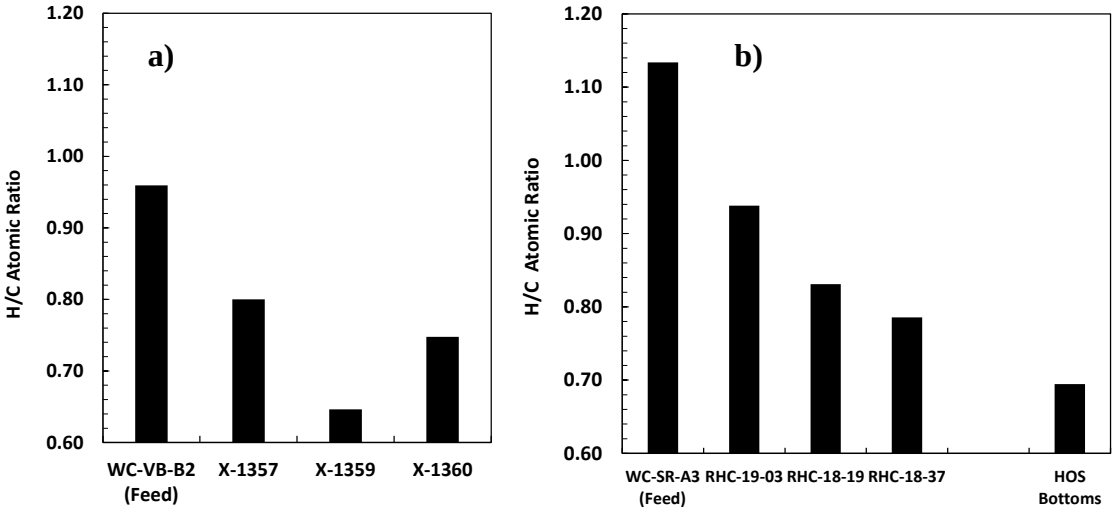

Figure 5-40. H/C atomic ratio of asphaltenes from a) thermocracked and b) hydrocracked oils.

The nitrogen content of asphaltenes from native oils was consistent from 10,000 and 12,000 ppm and no significant changes were observed for asphaltenes from *in-situ* converted oils in Figures 5-41a and 5-41b, and not even for asphaltenes from thermocracked oils (Figure 5-42a). However, hydrocracking increases the nitrogen content. It appears that the nitrogen heteroatom structures are difficult to crack and remove; hence, nitrogen is concentrated within the residual asphaltenes. It is probable that the nitrogen is largely present in heterocyclic structures. Nitrogen is more stable and less reactive when present as a heterocyclic structure with a basic nitrogen (*e.g.* pyridine) than as a heterocyclic structure with non-basic nitrogen such as pyrrole (Huc, 2011).

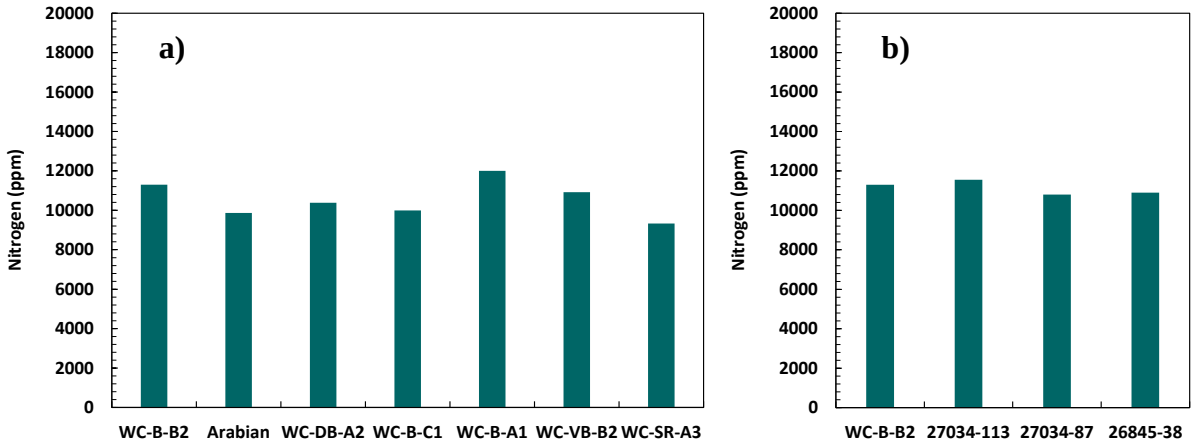

Figure 5-41. Nitrogen content of asphaltenes from a) native and b) *in-situ* converted oils.

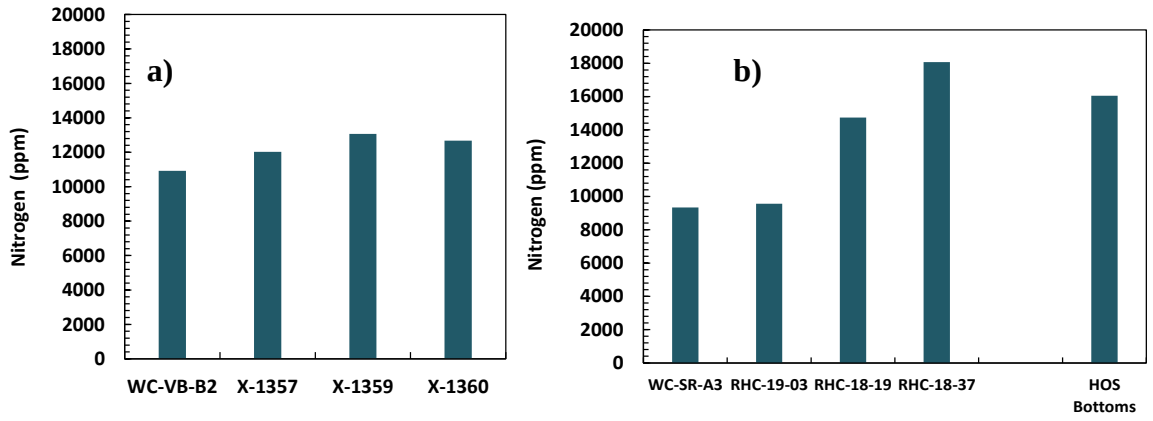

Figure 5-42. Nitrogen content of asphaltenes from a) thermocracked and b) hydrocracked oils.

The sulphur content varied from 60,000 ppm to 100,000 ppm for asphaltenes from native oils, Figure 5-43a, and slightly decreased for asphaltenes from *in-situ* converted and thermocracked oils, Figures 5-43b and 5-44a. As expected, the hydrocracking process is very efficient at removing sulphur (Huc, 2011; Raseev, 2003), Figure 5-36b, decreasing it from 30,000 to 10,000 ppm. Note that the lowest sulphur reduction was for RHC-19-03 which is also the sample with the lowest extent of reaction. However, some caution is advised in interpreting these data because the hydrocracking process for the RHC samples was a batch process using a fixed bed. Therefore, the catalyst would be very efficient at the beginning of the operation and may become poisoned with heteroatoms and coke as the process progressed.

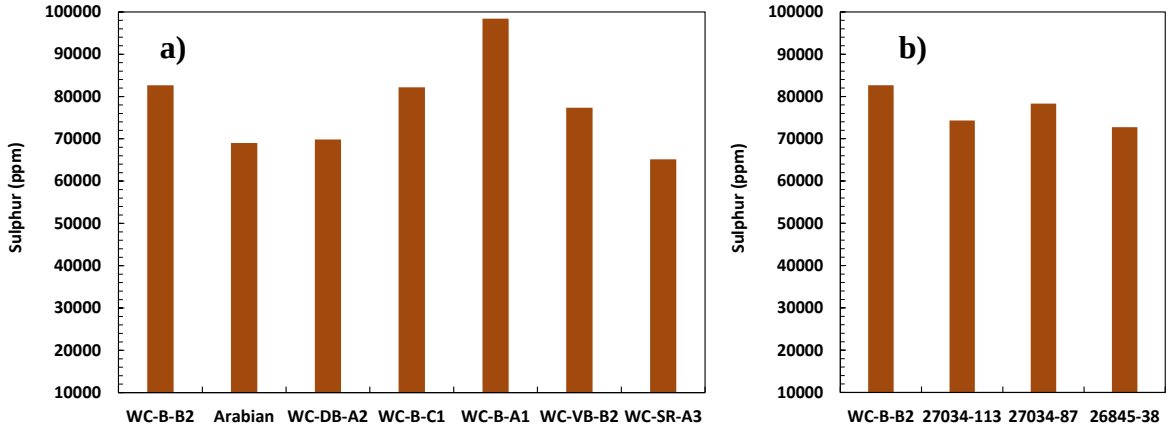

Figure 5-43. Sulphur content of asphaltenes from a) native and b) *in-situ* converted oils.

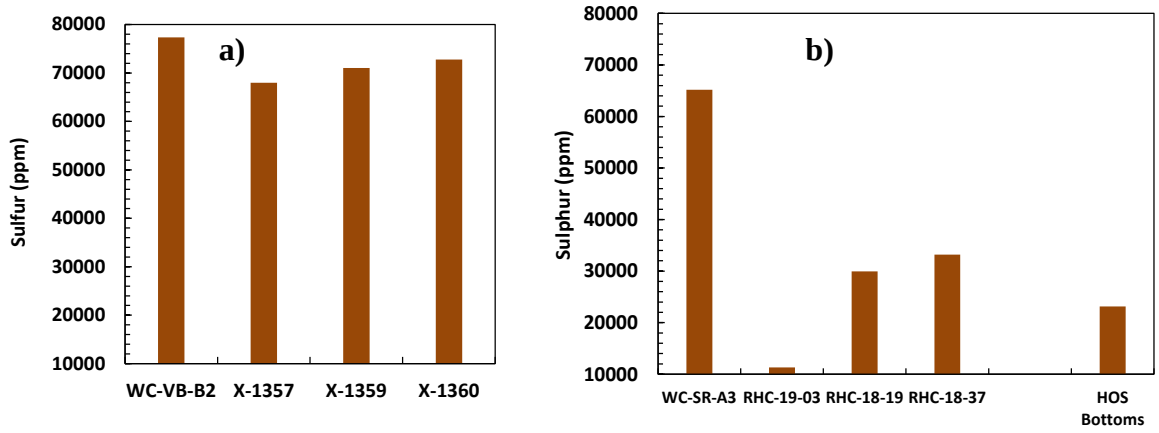

Figure 5-44. Sulphur content of asphaltenes from a) thermocracked and b) hydrocracked oils.

5.6 Toluene Insolubles Characterization

Precipitated asphaltenes from native oils usually contained relatively small amounts of toluene insoluble material, no more than 3-5 wt% of the asphaltenes. However, during reaction processes, asphaltenes undergo a series of complex reactions involving hydrogenolysis of C-S and C-N bonds, removal of metals, hydrogenation of aromatic cyclics, and heterocyclic disaggregation and cracking. These reactions create a variety of products from the asphaltenes including: 1) resin-like material produced from the less polar asphaltenes; 2) smaller asphaltene molecules or aggregates with lower molecular weight but also with a high proportion of aromatic cores; 3) coke (highly insoluble, highly aromatic core structures), and; 4) an intermediate material between asphaltenes and coke called carboids. Therefore, the precipitated asphaltenes from reacted oils include not only inorganic solids and possibly small catalytic particles, but also carboids and coke. However, these carboids and a fraction of the coke material may be soluble in stronger solvents such as dichlorobenzene (DCB), dichloromethane (DCM), methylnaphthalene (MN) and pyridine.

Sadeghi-Yamchi (2014) removed the toluene insoluble material from asphaltenes from thermocracked (X-##)) and hydrocracked (RHC-##) oil samples as described in Chapter 3. In this thesis, Toluene Insolubles (TI) from HOS Bottoms were used as a test sample because this sample had a high TI content. To characterize the TI (or a fraction of them), the TI must be soluble in some solvent to enable measurements such as density and molecular weight. Therefore, the TI

were first dissolved in three different solvents, dichlorobenzene (DCB), dichloromethane (DCM), and 1-methylnaphthalene (MN), to test which solvent dissolved the most TI. Table 5-13 shows the fraction of toluene insolubles that dissolved in each of the solvents. DCM dissolved the least while DCB and MN dissolved equal amounts. DCB was selected as the solvent to do further characterization of the toluene insoluble due to its convenience, availability, and applicability for VPO mesaurements.

Table 5-13. Percent solubility of toluene insolubles in different solvents.

Solvent	Solublility wt%
Dichlorobenzene (DCB)	53.2
Dichloromethane (DCM)	38.3
Methylnaphthalene (MN)	53.6

The DCB soluble part of the toluene insoluble (TI*) was then further characterized in terms of molecular weight and density. Solutions of low concentrations of TI* in DCB were prepared (<20 g/L) and the molecular weight was measured in the VPO at 110^{o}C. Figure 5-45 shows that the molecular weight of TI* appears to be independent of concentration with an average of 3400 g/L. The TI* molecular weight was significantly higher than the heaviest fraction of asphaltenes from HOS Bottoms (open circles) measured at the same conditions. Note that the measured molecular weight for the same HOS Bottoms fraction in toluene at 50^{o}C was significantly higher, up to 4500 g/mol (open triangles). With so little data, a number of interpretations are possible. The molecular weight may be a monomer molecular weight although this interpretation is unlikely given that the coke is believed to consist of condensed aromatic core groups fragmented from the original asphaltenes. Alternatively, the data may be scattered at low concentrations masking the changes in molecular weight with concentration expected with self-association. More likely, the self-association may arise from a different mechanism such as stacking of aromatic cores. This mechanism may reach completion at very low concentrations.

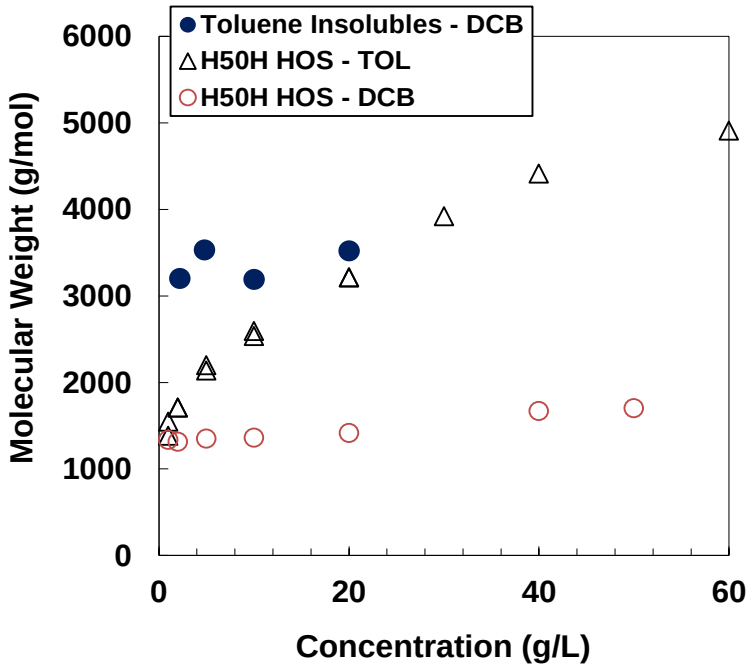

Figure 5-45. Molecular weight of toluene insolubles in dichlorobenzene at 110°C and comparison with the molecular weight of the heaviest fraction of asphaltenes from HOS Bottoms.

Density was measured from the same TI solutions prepared for the molecular weight measurements. The densities were determined assuming a regular solution with no excess volumes. Table 5-14 shows the density for TI* and asphaltenes from HOS Bottoms and its heavy fractions. There is a progressive increase in density from the HOS Bottoms through the heaviest fraction to the TI*.

The TI* could also be fractionated into solubility cuts in solutions of DCB and toluene, Figure 5-46. This progressive change in solubility along with the progression in density indicates that the TI* are part of a continuum of properties from resins to asphaltenes to TI*. The density increases and solubility decreases along this continuum. The data are not conclusive but self-association may also increase along this continuum. No further characterization was performed on the toluene insolubles due to the limited amount of sample and the challenging nature of the characterization.

Table 5-14. Density of toluene insolubles compared with the density of asphaltenes from HOS Bottoms.

Sample	Density kg/m^3
Toluene Insolubles	1380
H50H HOS Asphaltenes (Heaviest Asph. fraction)	1298
C7 HOS Asphaltenes	1250

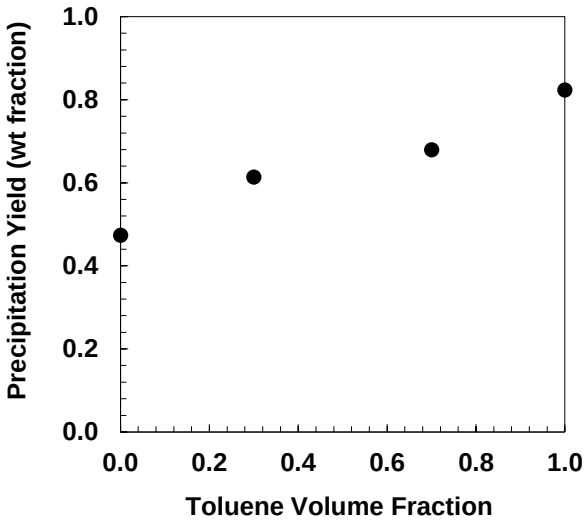

Figure 5-46. Fractional precipitation yield of toluene insoluble in a mixture of toluene and dichlorobenzene at 20^{o}C and atmospheric pressure.

5.7 Chapter Summary

In this thesis, a detailed characterization of asphaltenes was performed on asphaltenes from native and reacted oils. The characterization focused on determining molecular weight and density distributions and the solubility parameter which are inputs in the regular solution model. These distributions are part of the step 1 in the general methodology depicted in Chapter 1. In addition, refractive index and elemental analysis were measured to help in the understanding of the effect

of reaction, thermocracking and hydrocracking of asphaltenes. Note that, reacted oils have also an increased amount of toluene insolubles formed during processing. An attempt was made to characterize part of the toluene insolubles of HOS bottom sample to understand their continuum properties with respect to asphaltenes. The main results from this chapter are summarized below. Note that some of the experimental data for asphaltenes were taken from two MSc thesis but all the data analysis and modeling explained in this chapter were performed as part of this thesis.

Molecular Weight Distributions of Asphaltenes:

Asphaltenes from native oils have wide molecular weight distributions from an average monomer molecular weight of 800 g/mol to average maximum aggregate size of 20,000 to 50,000 g/mol depending on the oil source. The mass fraction of neutrals or asphaltenes that do not participate in association is lower than 4 wt% for native unprocessed oils and 8 wt% for vacuum residues. Asphaltenes from reacted thermocracked oils (in-situ and visbreaker processes) have slightly narrower distributions and increasing amount of neutrals up to 13 wt%. However, hydrocracking significantly alters the asphaltenes to much narrower molecular weight distributions with neutral contents up to 23 wt%. These changes are consistent with the removal of side chains leaving behind smaller molecules that self-associate less.

Effect of Temperature in Molecular Weight Distributions:

Increasing temperature decreased the average aggregated molecular weight of asphaltenes from native and thermocracked oils but had little effect on asphaltenes from hydrocracked oils. The molecular weight at different temperature was compared for all the samples analysed at an asphaltene concentration of 10 g/L. A linear temperature dependence was observed with a different slope for all the samples. The linear trends for all the samples were found to intersect over a small range of temperature and molecular weight defining an apparent monomer temperature at 250°C and 800 g/mol. This convergence was used to build a new temperature dependence correlation applicable for all types of asphaltenes between 20 to 90°C. The correlation is not recommended to be used outside of the temperature range because asphaltenes may undergo a phase transition before 250°C.

Density Distribution of Asphaltenes:

Density distributions showed a similar trend for native and reacted asphaltenes with an initial steep increase in density attributed to those monomers too large or polar to be soluble in *n*-pentane (and report to the resins). The densities reached a plateau interpreted to coincide with the asphaltene nano-aggregates. The small variation in density at this point suggests aggregates all have a similar average density over a wide range of size and solubility. Native asphaltenes have similar density distributions with a maximum density at 1200 kg/m^3. Reacted asphaltenes have higher densities than native oils and their density increases with extent of conversion up to 1300 kg/m^3.

Solubility Parameter of Asphaltenes:

A new correlation was developed to estimate the solubility parameter of asphaltenes from both native and reacted oils. The solubility parameter correlation has one fitting parameter, *b*, which is an indication of increasing or decreasing solubility parameter distribution of asphaltenes. An average *b* value of 0.0634 was found to apply for all native asphaltene samples. Reacted asphaltenes have higher values of *b* indicating higher solubility parameters, therefore, less soluble asphaltenes, which precipitate a lower heptane ratios than asphaltenes from native oils. The uncertainty of *b* was found to be ± 0.0001 for native oils and ± 0.0002 for reacted oils giving an uncertainty in the solubility parameter distribution between ±0.1 and ±0.2 $MPa^{0.5}$. The solubility parameter correlation and its parameters can be applied or adapted in simulation software that require asphaltene properties as part of the heavy oil characterization or used for oil companies for asphaltene precipitation models that required the solubility parameter of asphaltenes (also as part of heavy oil or bitumen characterization).

Refractive Index and Elemental Composition:

The refractive index for native oils was between 1.725 and 1.755 but significantly increased for asphaltenes from reacted oils up to 1.890. Refractive index is proportional to density and the increase in refractive index is consistent with the increasing density. The H/C ratio for asphaltenes from native oils was between 0.9 and 1.2 and significantly decreased for asphaltenes from thermocracked and hydrocracked oils which was between 0.6 and 0.9. This reduction is consistent with the removal of alkyl-chains, leaving more aromatic cores. The nitrogen contest did not

significantly change for thermocracked asphaltenes in comparison with native asphaltenes. However, it increased for hydrocracked asphaltenes, most likely because nitrogen is more difficult to remove and therefore becomes concentrated in the residual highly cracked asphaltenes.

Chapter Six: Characterization of Saturates, Aromatics, and Resins

This chapter summarizes the main properties of saturates, aromatics, and resins (SAR) required for the regular solution model: that is, molecular weight, density, and solubility parameter distributions for asphaltenes from native, *in-situ* converted (ISC), thermocracked (TC) and hydrocracked (HC) oils. Other properties, such as refractive index and elemental analysis, are also measured for a selection of the SAR cuts to analyze the effect of different reaction processes and because they are potential correlating properties for the effect of reaction on other properties that are more difficult to measure, such as the solubility parameter.

6.1 Molecular Weight of SAR Fractions

Figure 6-1 compares the molecular weights of SAR fractions from native oils. The molecular weight of saturates from native oils ranged between 360 to 450 g/mol and 400 to 500 g/mol for aromatics, both consistent with data from Akbarzadeh *et al.* (2005) for saturates and aromatics from seven different native oils from around the globe. The molecular weight for resins was also consistent with previous data with the exception of resins from WC-B-C1 bitumen which have a significantly higher molecular weight. The asphaltene extraction procedure for the WC-B-C1 bitumen was slightly different than for the other oils. The WC-B-C1 asphaltenes had to be more extensively washed (three times for the sonicated-washing stage) than any other oil due to the "gummy" nature of these asphaltenes. This extensive washing likely washed through some low molecular weight (more soluble) asphaltenes into the maltene (deasphalted oil) fraction. These washed-through asphaltenes would report to the resin fraction, have higher molecular weight than the resins, and therefore would increase the resins molecular weight. Note, the molecular weight of the WC-B-C1 asphaltenes was higher than other native asphaltenes, consistent with the washing out of lower molecular weight asphaltenes.

The molecular weight of SAR fractions from the vacuum residues (WC-VB-B2 and WC-SR-A3) was significantly higher than the average native oils. Although WC-VB-B2 and WC-SR-A3 are "non-reacted" oils, they differ from the other native oils because they are the residues of vacuum distillation. A higher fraction of low molecular weight compounds are removed during the vacuum

distillation process leaving behind a much heavier residue. Therefore, the molecular weight of SAR fractions for vacuum residues is expected to be higher than for SAR fractions from native oils.

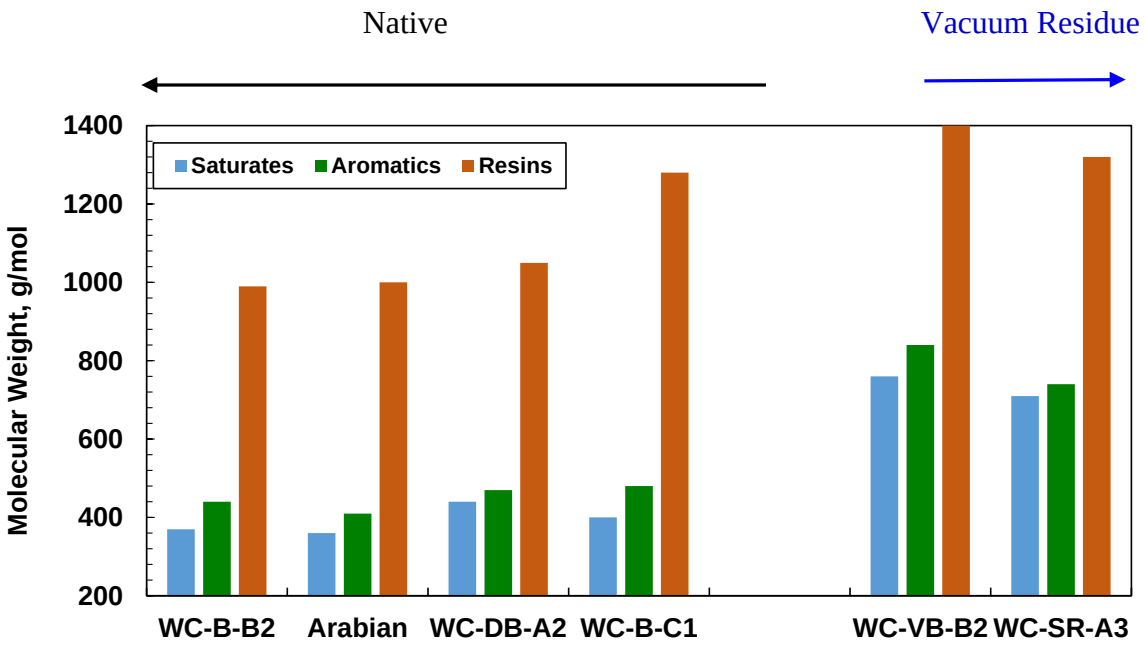

Figure 6-1. Molecular weight of SAR fractions from native oils and vacuum residues.

Figures 6-2 to 6-4 compare the molecular weights of SAR fractions from *in-situ* converted, thermocracked, and hydrocracked oils, respectively. During cracking reactions, hydrocarbon molecules are broken down through scission of carbon-carbon bounds. Hence, molecular weights are expected to be lower for the fractions of cracked oils. SAR fractions from *in-situ* converted oils had slightly lower molecular weights than the SAR fractions from the original oil but there was not a clear trend with the extent of reaction, Figure 6-2. It is likely that bitumen or heavy oil migration from other parts of the reservoir mixed with the converted oil (Zhongxin 2010) and obscured the trends with extent of reaction . The extent of reaction for in-situ converted oils was provided by Shell without providing its definition; hence, any conclusions regarding the extent of reaction of these samples are uncertain.

SAR from thermocracked oils showed some reduction in the molecular weight, but especially for aromatics and resins at higher extents of reaction (>56 wt%), Figure 6-3. SAR fractions from hydrocracked oils showed a significantly decrease in molecular weight with extent of reaction, Figure 6-4. Hydrogenolysis and hydrodemetalization are predominant reactions during the hydroconversion processes. These reactions, along with hydrogenation of aromatic rings and heterocyclic structures, promote fast cleavage of molecular bonds, increasing the yield of low molecular weight compounds.

One notable effect of both thermo- and hydrocracking was the redistribution of the molecular weight of the SAR fractions. For example, the aromatics usually have a higher molecular weight than saturates in native oils but, after reaction, have a lower molecular weight than saturates. This change in the distribution of SAR molecular weights, along with the change in the relative amount of each fraction, affects the phase behaviour of the oil, particularly the onset of asphaltene precipitation.

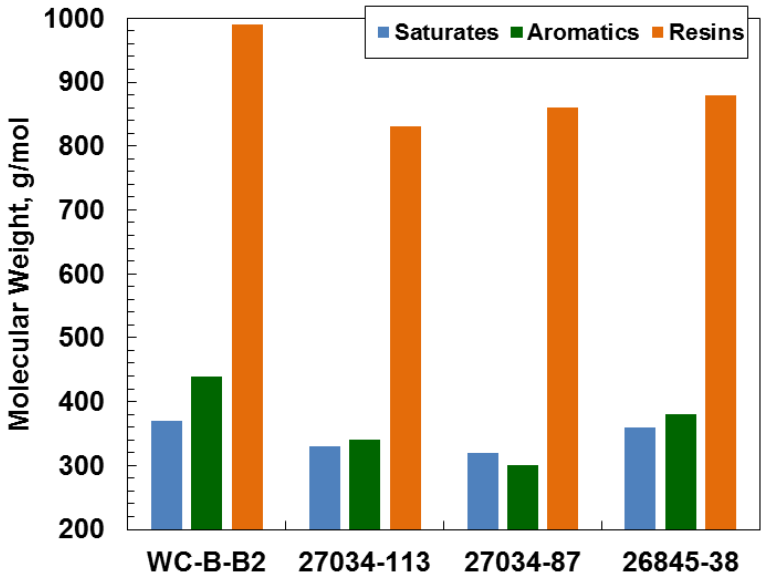

Figure 6-2. Molecular weight of SAR fractions from *in-situ* converted (ICP) oils and the "original" native oil.

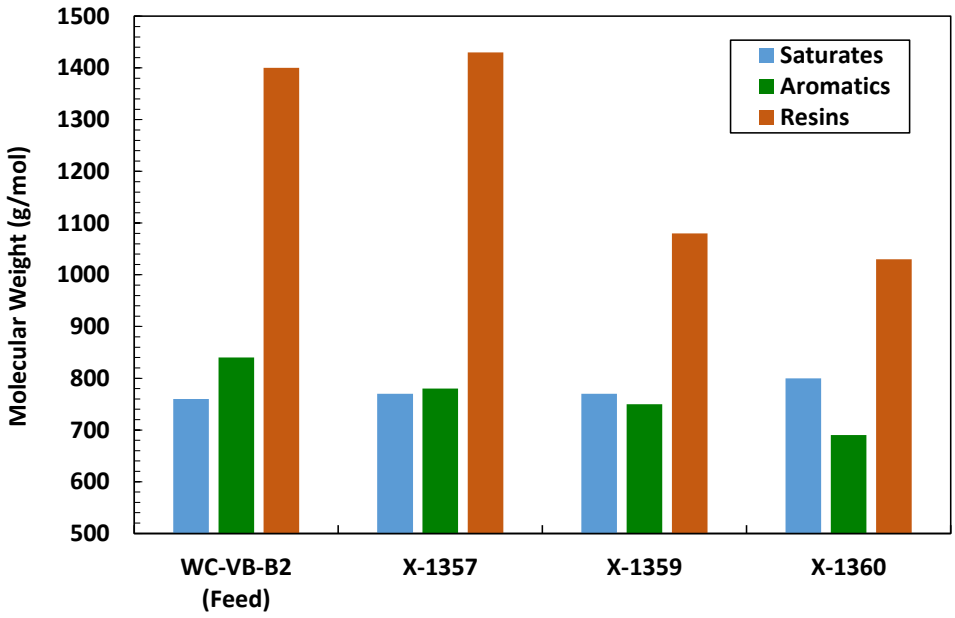

Figure 6-3. Molecular weight of SAR fractions from thermocracked oils and the feedstock.

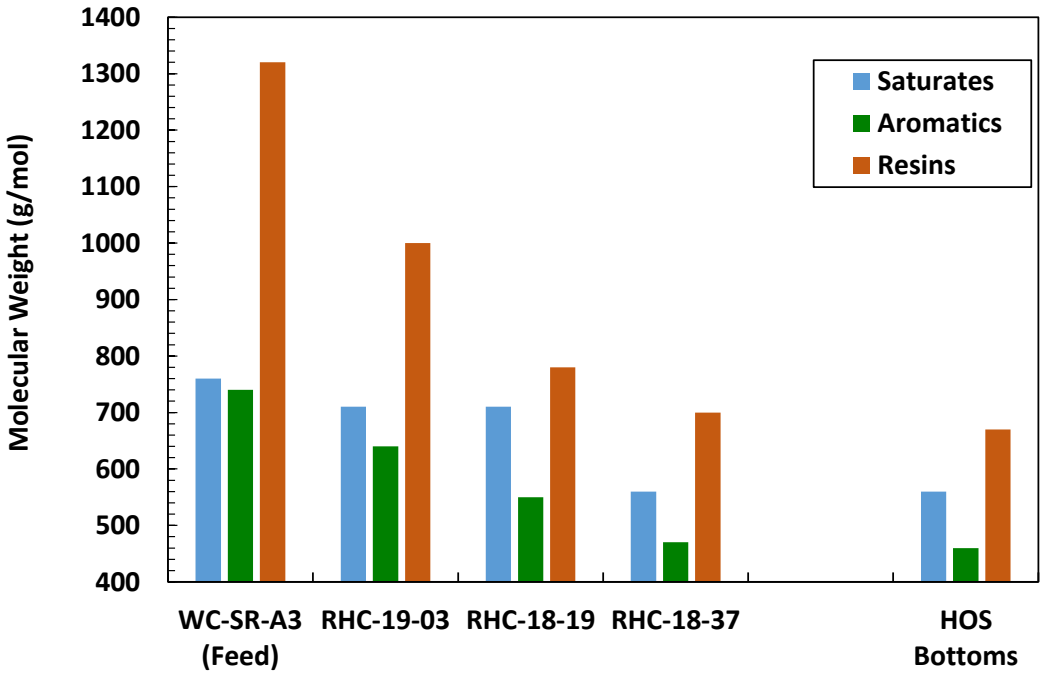

Figure 6-4. Molecular weight of SAR fractions from hydrocracked oils and the feedstock.

6.2 Density of SAR Fractions

Figures 6-5 to 6-8 compare the densities for SAR fractions from native, *in-situ* converted, thermocracked and hydrocracked oils. Densities of SAR fractions from native oils are consistent with previous data (Akbarzadeh *et al.*, 2005). Note that, unlike the molecular weight, there was no significant difference between densities of native and vacuum residues (WC-VR-B2 and WC-SR-A3).

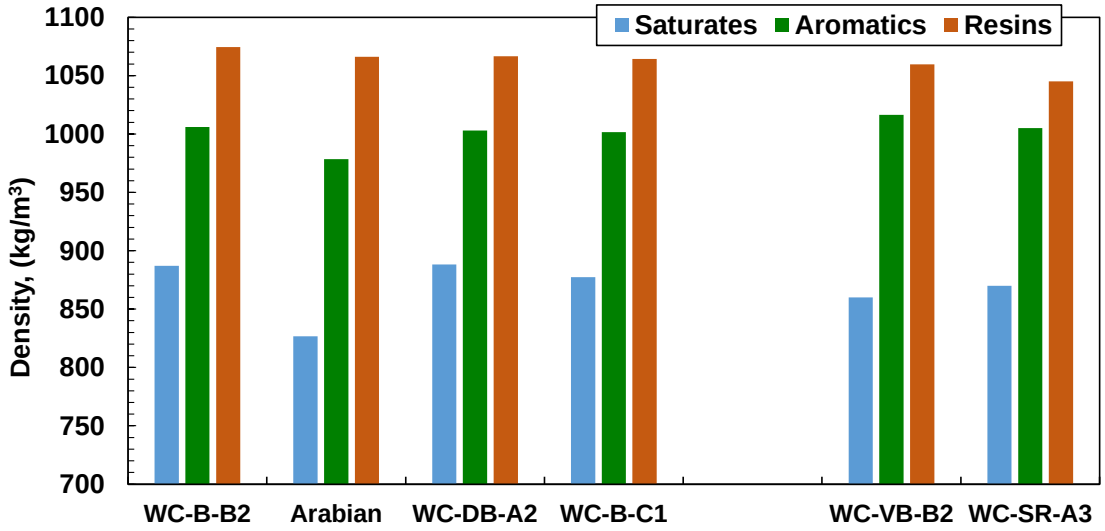

Figure 6-5. Density of SAR fractions from Native oils at 20°C and atmospheric pressure.

The densities of the SAR fractions from *in-situ* converted oils did not dramatically change with conversion. The saturate density decreased slightly and the density of aromatics and resins fell within a small range for each fraction. A similar trend in densities was observed for saturates and aromatics of thermocracked oils. Saturates had no noticeable change and aromatic density ranged between 1020 kg/m^3 and 1050 kg/m^3, a very small increase from the feedstock aromatic density (WC-VB-B2 aromatic density = 1016 kg/m^3). The small changes in density suggest that:

1) density is dictated mainly by the chemical family of each fraction. Chemical families, such as paraffins, naphthenes, and aromatics, each have densities within a small range (±50 kg/m^3), especially for the hydrocarbons with molecular weights higher than 100 g/mol. For example, alkyl-aromatic hydrocarbons have very similar densities independently of the

size of the alky-chain attached to the aromatic ring. Therefore, breaking down some alkyl-chains (C-C bounds) in an aromatic fraction would have little effect on its density.

2) thermocracking breaks down alkyl-chains but may not be very effective at breaking heterocyclics and aromatic rings or removing heteroatom compounds, The latter changes in chemistry would have a more significant effect on density.

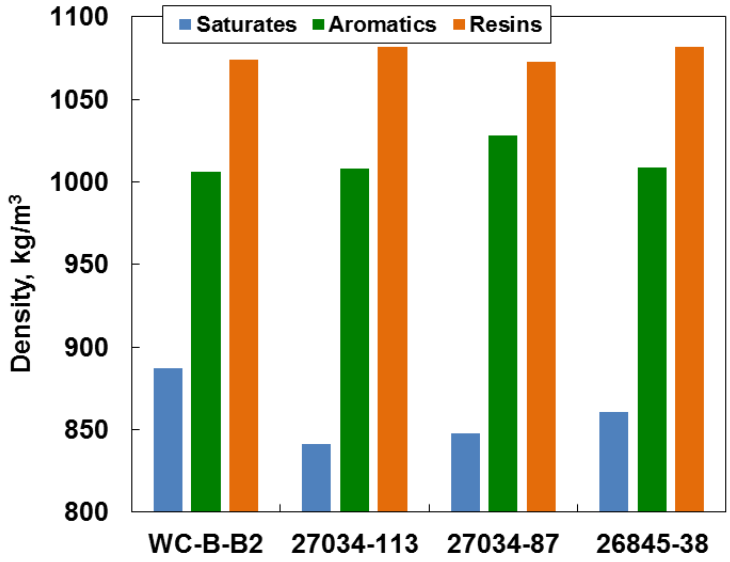

Figure 6-6. Density of SAR fractions from *in-situ* converted oils at 20°C and atmospheric pressure.

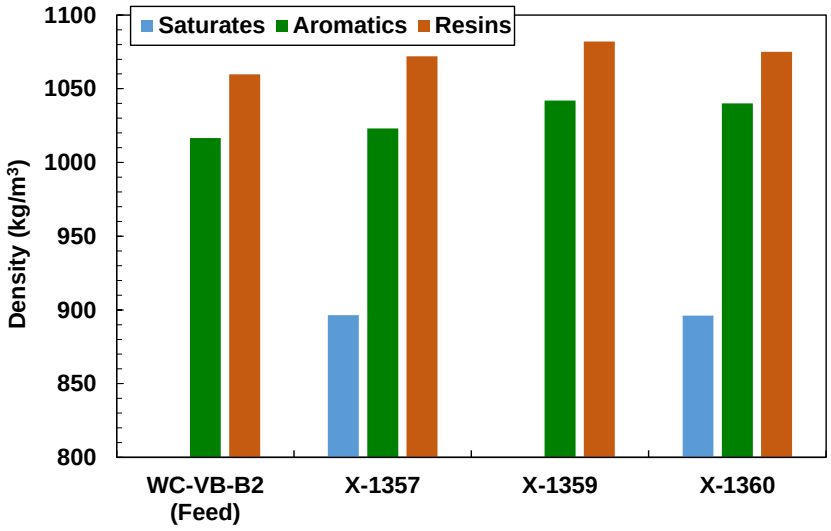

Figure 6-7. Density of SAR fractions from thermocracked oils and the feedstock at 20°C and atmospheric pressure. Note that for WC-VB-B2 and X-1359 there was not enough saturate sample to performed complete characterization.

Saturate density from hydrocracked oils did not significantly change and was within the density range for native oils. Note, the densities of *n*-alkanes with molecular weights greater than 170 g/mol do not significantly change with increasing carbon number (up to 310 g/mol) (see Figure G-5a in Appendix G). Hence, the density of saturates may not be directly affected by reaction although its molecular weight decreased.

The density of aromatics and resins from hydrocracked oils increased with extent of reaction likely indicating less aliphatic carbons and a more aromatic structure within these fractions, Figure 6-8. During catalytic cracking in the presence of hydrogen (hydrocracking), one of the most important chemical reactions is the hydrogenation (saturation) of cyclics and heterocyclics. Some of these functional groups will then report to saturates or distillables leaving the aromatics and resins enriched in aromatic structures.

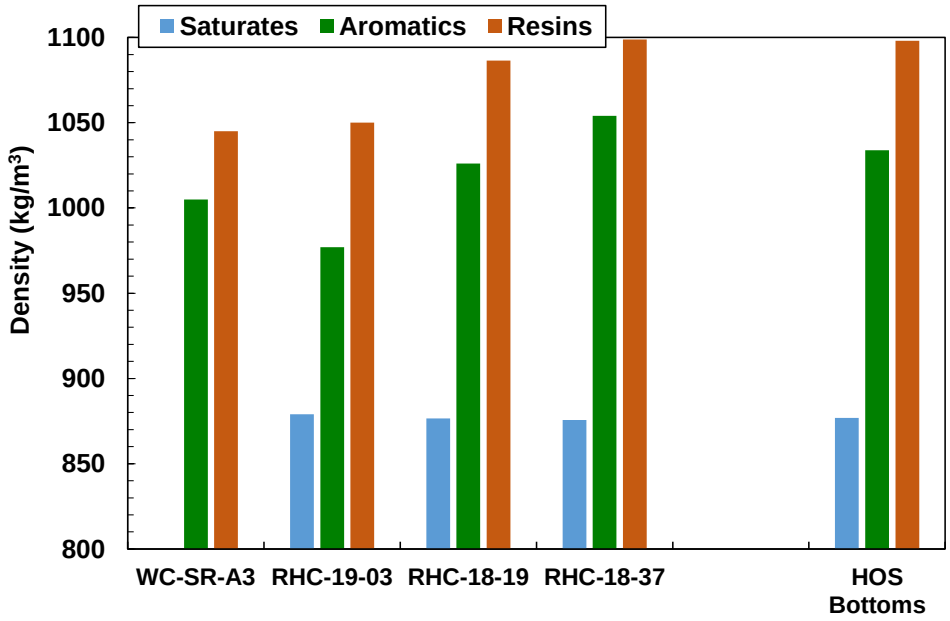

Figure 6-8. Density of SAR fractions from hydrocracked oils and the feedstock at 20°C and atmospheric pressure.

6.3 Solubility Parameter of Saturates and Aromatics

Okafor (2013) determined solubility parameters from yield measurements of saturates and aromatics from native and *in situ* converted oils. This section presents the solubility parameters for saturates and aromatics from thermocracked and hydrocracked oils and compares the results with those of native oils.

Saturates and aromatics solubility parameters were determined by fitting asphaltene precipitation data from toluene-saturates and aromatics-heptane mixtures using the regular solution model as described in Chapter 4. Recall the equilibrium constant in the modified regular solution model (Eq. 4-7) requires the molar volumes (densities and molecular weights) and solubility parameters (δ_i) of each of the components (or pseudo-components) making up the mixture. The properties of the solvents used, toluene and *n*-heptane, are known from literature and the properties of the asphaltenes used, WC-B-B2, were determined in Chapter 5. Hence, the only unknown is the solubility parameter of saturates or aromatics in the mixture. Table 6-1 provides the properties of the solvents applied in the regular solution model for asphaltenes-solvent systems. Table 6-2 list the properties of the 30 subfractions of the WC-B-B2 asphaltenes.

Table 6-1. Properties of the solvents at 21^{o}C and atmospheric pressure.

Compound	Density g/cm3	Molecular Weight g/mol	Molar Volume cm^{3}/mol	Solubility Parameter $MPa^{1/2}$
Toluene	0.866	92	106.4	18.3
n-heptane	0.681	100	147.1	15.2

Table 6-2. Properties of asphaltenes pseudo-components from WC-B-B2 bitumen at 23°C.

Asphaltene Subfraction	Mass Fraction	Molecular Weight g/mol	Density g/cm^3	Molar Volume cm^3/mol	Solubility Parameter $MPa^{0.5}$
1	0.009	1123	1.061	1058	19.23
2	0.031	1769	1.095	1614	19.47
3	0.053	2414	1.135	2127	19.84
4	0.069	3060	1.165	2626	20.15
5	0.079	3706	1.183	3133	20.38
6	0.084	4351	1.192	3651	20.54
7	0.084	4997	1.196	4177	20.65
8	0.080	5643	1.198	4710	20.75
9	0.074	6289	1.199	5245	20.85
10	0.067	6934	1.199	5781	20.93
11	0.060	7580	1.200	6318	21.02
12	0.052	8226	1.200	6856	21.10
13	0.045	8872	1.200	7394	21.18
14	0.038	9517	1.200	7932	21.25
15	0.032	10163	1.200	8470	21.33
16	0.027	10809	1.200	9008	21.40
17	0.022	11454	1.200	9546	21.48
18	0.019	12100	1.200	10084	21.55
19	0.015	12746	1.200	10622	21.62
20	0.012	13392	1.200	11160	21.69
21	0.010	14037	1.200	11698	21.75
22	0.008	14683	1.200	12236	21.82
23	0.006	15329	1.200	12774	21.88
24	0.005	15974	1.200	13312	21.95
25	0.004	16620	1.200	13850	22.01
26	0.003	17266	1.200	14389	22.07
27	0.003	17912	1.200	14927	22.13
28	0.002	18557	1.200	15465	22.19
29	0.002	19203	1.200	16003	22.25
30	0.001	19849	1.200	16541	22.31

6.3.1 Saturates Solubility Measurements and Solubility Parameters

Okafor (2013) measured the asphaltene yield for saturates in toluene solutions from native and *in-situ* converted oils. She used Barrera's (2013) regular solution model to back-calculate the solubility parameter; that is, she used the density correlation as a function of molecular weight, Eq. 4-15, and the solubility parameter correlation from Eq. 4-27. The average solubility parameter for native saturates was determined to be 16.7 $MPa^{0.5} \pm 0.1$.

In this thesis, the solubility parameters for saturates from native and *in-situ* converted oils were recalculated using the new properties and correlations of asphaltenes explained in Chapter 5, and are presented in Table 6-3. The re-calculated solubility parameters were 0.1 to 0.2 $MPa^{0.5}$ lower than Okafor's values. Note that the uncertainty of the solubility parameter of saturates and aromatics was determined as ± 0.3 $MPa^{0.5}$ using the sensitivity analysis methodology presented in Chapter 5.

Figure 6-9a shows the fitting and general trend of saturates from native oils. The saturates from the native oils all have a similar effect on asphaltene solubility and all have similar solubility parameters. Hence native saturates are used as a baseline to identify changes with reaction. Figure 6-9b shows the slight change observed for saturates from in-situ converted oils. The asphaltene yields at any given saturate concentration are higher for the converted saturates; that is, these saturates are slightly "poorer" solvents for asphaltenes (lower solubility parameter) than native saturates, Table 6-4.

Table 6-3. Solubility parameter for saturates from native oils at 23°C and atmospheric pressure.

Sample	Molecular Weight g/mol	Density g/cm^3	Molar Volume cm^3/mol	Solubility Parameter $MPa^{0.5}$
WC-B-B2	370	0.8871	417	16.5 ±0.3
WC-DB-A2	440	0.8882	495	16.5 ±0.3
WC-B-C1	400	0.8773	456	16.5 ±0.3

Table 6-4. Solubility parameter for saturates from *in-situ* converted oils at 23°C and atmospheric pressure.

Sample	Molecular Weight g/mol	Density g/cm^3	Molar Volume cm^3/mol	Solubility Parameter MPa$^{0.5}$
WC-B-B2 (F)	370	0.8871	417	16.5 ±0.3
27034-113	330	0.8415	392	16.0 ±0.3
27034-87	320	0.8478	377	16.2 ±0.3
26845	360	0.8606	418	16.3 ±0.3

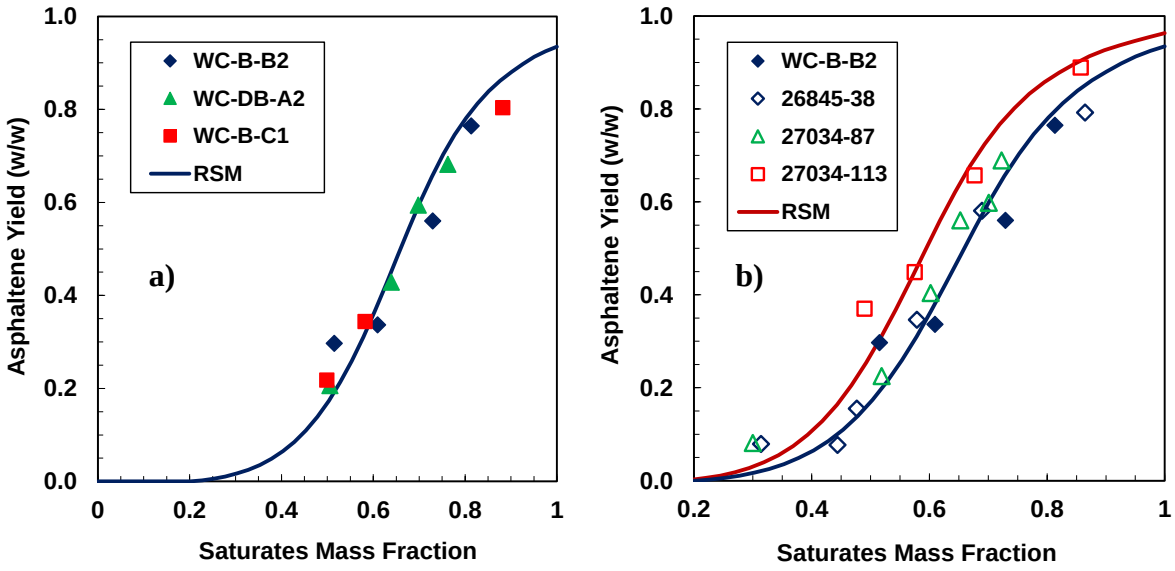

Figure 6-9. Fractional asphaltene precipitation of 10 g/L solutions of asphaltenes from WC-B-B2 bitumen in toluene and various saturates from a) native and b) *in-situ* reacted oils at 21°C and atmospheric pressure and regular solution model predictions.

Saturates from thermocracked and hydrocracked samples were clearly poorer solvents for asphaltenes than saturates from native oils, Figures 6-10a and 6-10b. The asphaltene precipitation onset occurred at a lower saturates mass fraction and a higher asphaltene yields was obtained at each saturate content, shifting the solubility curve to the left. Note, the low mass solubility experimental method was used for these tests because only a small mass of saturates was collected

during the SAR fractionations, as explained in Chapter 3. The low mass solubility experiments have a higher scatter and the data below 30 wt% saturates was not very repeatable. Therefore, the model was tuned to match the data at higher saturate content as shown in Figure 6-10. Table 6-5 presents the fitted solubility parameters for thermocracked and hydrocracked samples. Highly reacted saturates have significantly lower solubility parameters than native saturates. Reacted saturates are smaller molecules than native saturates due to thermal cracking, lower solubility parameters for smaller molecules is consistent with general of paraffinic compounds (alkanes) in which the solubility parameter decreased for lower molecular weight compounds (e.g $\delta_{n\text{-tridecane}}$ = 16.05 $MPa^{0.5}$ (MW=184.4 g/mol) and $\delta_{n\text{-hexane}}$ = 14.69 $MPa^{0.5}$ (MW=86.2 g/mol)).

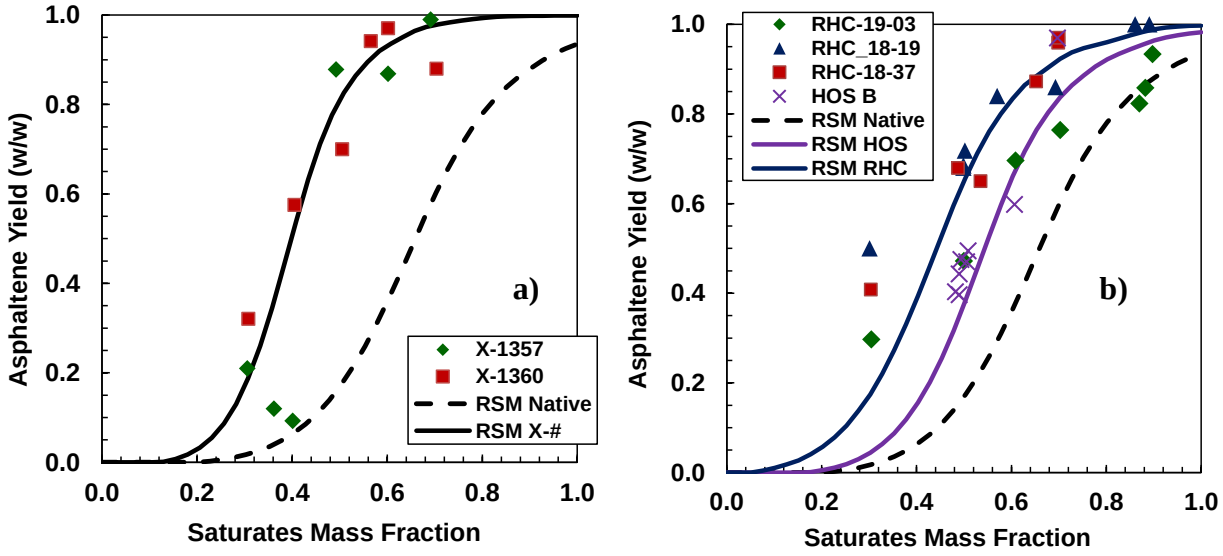

Figure 6-10. Measured and modeled fractional asphaltene precipitation of 10 g/L solutions of asphaltenes from WC-B-B2 bitumen in toluene and various saturates from a) thermocracked and b) hydrocracked oils at 21^{o}C and atmospheric pressure.

Table 6-5. Solubility parameter for saturates from thermocracked and hydrocracked oils at 23°C and atmospheric pressure.

Sample	Molecular Weight g/mol	Density g/cm^3	Molar Volume cm^3/mol	Solubility Parameter MPa$^{0.5}$
Thermocracked				
X-1357	770	0.8965	859	14.0 ±0.3
X-1359*	785	0.8964	876	14.0 ±0.3
X-1360	800	0.8962	893	14.0 ±0.3
Hydrocracked				
RHC-19-03	710	0.8790	808	16.0 ±0.3
RHC-18-19	710	0.8766	810	15.0 ±0.3
RCH-18-37	560	0.8756	640	15.0 ±0.3
HOS Bottoms	560	0.8769	639	15.8 ±0.3

* Not enough sample to measure properties, assumed to be average of X-1357 and X-1360

6.3.2 Aromatics Solubility Measurements and Solubility Parameter

Okafor (2013) observed that aromatics from native oils also showed a uniform trend and determined the solubility parameter of native aromatics to be 20.8 ± 0.2 MPa$^{0.5}$. Aromatics from *in-situ* conversion process had the same trend and similar solubility parameters.

In this thesis, the solubility parameters were recalculated with the new density and solubility parameter correlation explained in Chapter 5. The properties for aromatics from native and *in-situ* converted oils are presented in Table 6-6. With the exception of WC-VB-B2, the aromatics solubility parameters obtained were the same as Okafor's but with a better match for low heptane ratios, Figures 6-11a and 6-11b. WC-VB-B2 is a vacuum residue and its SAR fractions have higher molecular weights than the SAR fractions from native oils. The aromatics from native oils have an average solubility parameter of 20.8± 0.3 MPa$^{0.5}$. The solubility parameter for aromatics from WC-VR-B2 was 21.4 ± 0.3 MPa$^{0.5}$ even though the asphaltene yield curve followed the same

native trend. Note that the updated uncertainty determined for the aromatics solubility parameter of aromatics was ±0.3 $MPa^{0.5}$.

Table 6-6. Solubility parameter of aromatics from native oils at 21°C and atmospheric pressure.

Sample	Molecular Weight g/mol	Density g/cm^3	Molar Volume cm^3/mol	Solubility Parameter $MPa^{0.5}$
WC-B-B2	440	1.0059	437	20.8 ±0.3
WC-DB-A2	470	1.0093	469	20.8 ±0.3
WC-B-C1	480	1.0016	479	20.8 ±0.3

Table 6-7. Solubility parameter of aromatics from *in-situ* converted oils at 21°C and atmospheric pressure.

Sample	Molecular Weight g/mol	Density g/cm^3	Molar Volume cm^3/mol	Solubility Parameter $MPa^{0.5}$
WC-B-B2 (F)	440	1.0059	437	20.8 ±0.3
27034-113	340	1.0083	337	20.8 ±0.3
27034-87	300	1.0281	292	20.6 ±0.3
26845	380	1.0087	377	21.0 ±0.3

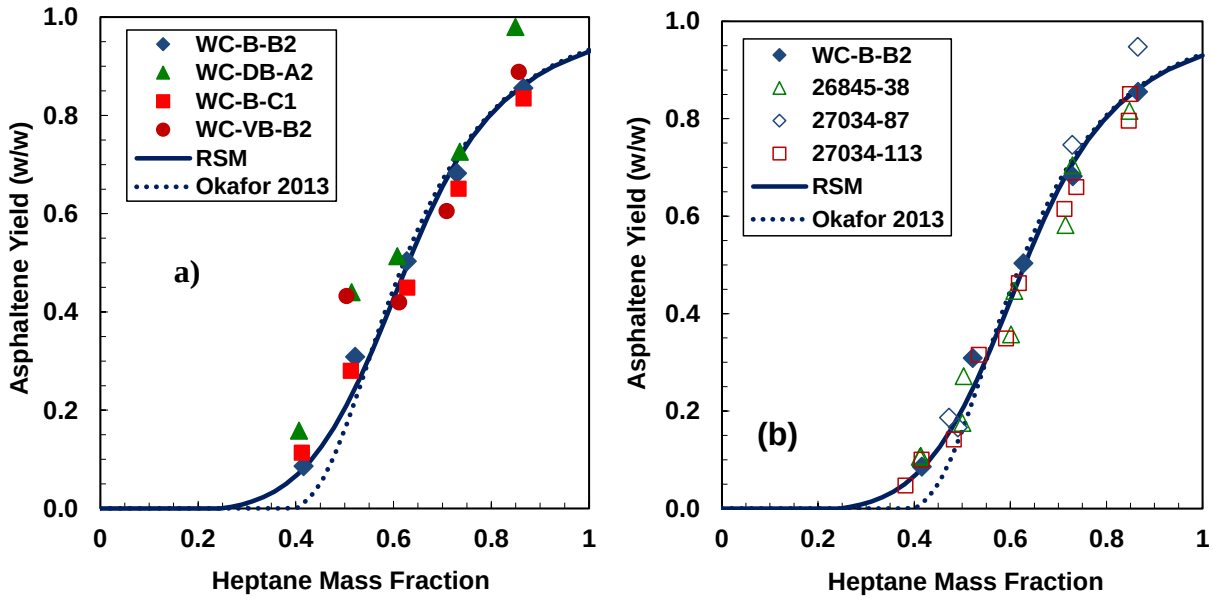

Figure 6-11. Fractional asphaltene precipitation of 10 g/L solutions of asphaltenes from WC-C-B2 bitumen in toluene and various aromatics from a) native and b) *in-situ* reacted oils at 21°C and atmospheric pressure.

Surprisingly, aromatics from thermocracked and hydrocracked oils had a similar trend as the aromatics from native oils, but with more scatter at heptane fractions lower than 0.5, Figures 6-12a and 6-12b. Recall that the scatter at heptane mass fractions lower than 0.5 for reacted aromatics was due to the strong interactions between reacted aromatics and asphaltenes which caused "washing" issues during the experiments (see Chapter 4). The molecular weight and density significantly changed for reacted aromatics and these changes in properties also impact the solubility parameter calculation. Hence, the solubility parameter for reacted aromatics was expected to change despite having similar yields as aromatics from native oils. Note that the yield data are compared against aromatics from WC-VR-B2 because the reacted samples were produced from a similar vacuum residue feedstock.

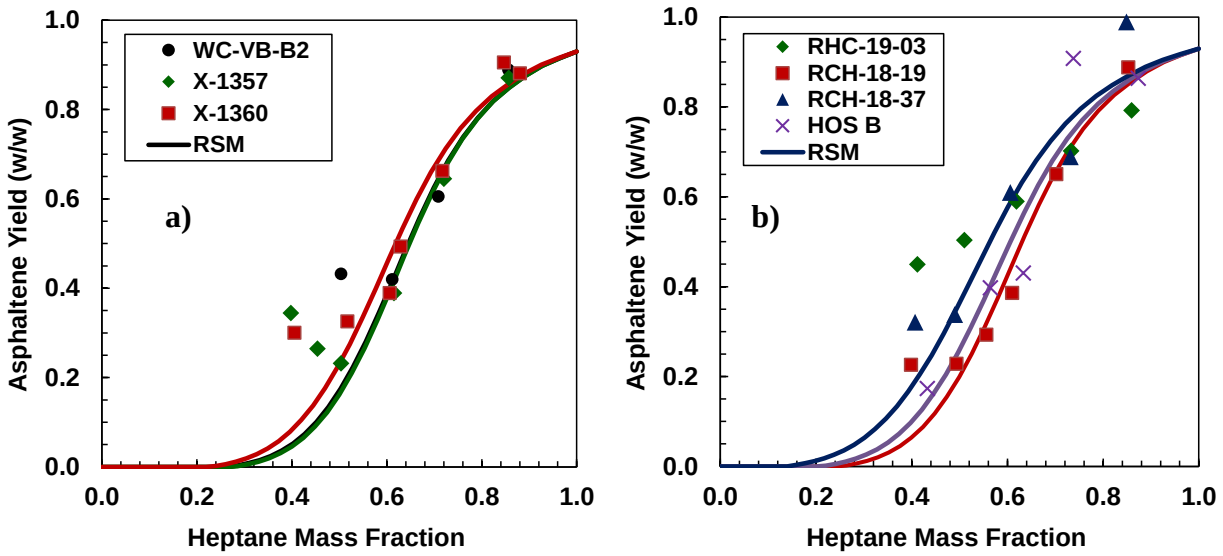

Figure 6-12. Measured and modeled fractional asphaltene precipitation of 10 g/L solutions of asphaltenes from WC-C-B2 bitumen in toluene and various aromatics from a) thermocracked and b) hydrocracked oils at 21°C and atmospheric pressure.

Solubility parameters of aromatics from thermocracked and hydrocracked oil were fitted using the regular solution model for asphaltene-solvent (aromatic-heptane) mixtures with the parameters found for WC-B-B2 (properties Table 6-2). Table 6-8 presents the fitted solubility parameters. The solubility parameter for reacted aromatics, especially from hydrocracked oils, decreased in comparison with the solubility parameter of aromatics form WC-VR-B2 (vacuum residue). However, the solubility parameter change was not as large as observed for saturates and is within the uncertainty of the fitting. The small change in solubility parameter can be attributed to two opposing effects occurring in the aromatic fraction. During thermal cracking reactions removal of some alkyl-chains attached to the aromatics may occur; the decrease in size of alky-aromatics (smaller alkyl-chains in the aromatic ring) increases the solubility parameter. However, cracking of cyclic rings (smaller naphthenes) and formation and cracking of olefins can also occur in the aromatic fraction. Formation of smaller molecules through these reactions decreases the solubility parameter.

Table 6-8. Solubility parameter of aromatics from thermocracked and hydrocracked oils at 21°C and atmospheric pressure.

Sample	Molecular Weight g/mol	Density g/cm^3	Molar Volume cm^3/mol	Solubility Parameter MPa$^{0.5}$
Thermocracked				
WC-VB-B2 (F)	840	1.016	827	21.4 ±0.3
X-1357	780	1.023	762	21.4 ±0.3
X-1359	750	1.042	720	-
X-1360	690	1.040	634	21.0 ±0.3
Hydrocracked				
WC-SR-A3 (F)	740	1.005		-
RHC-19-03	640	977	655	20.6 ±0.3
RHC-18-19	550	1.026	536	21.0 ±0.3
RCH-18-37	470	1.054	446	20.5 ±0.3
HOS Bottoms	460	1.034	445	20.6 ±0.3

6.4 Other Properties

6.4.1 Refractive Index

For native oils, the refractive index was between 1.47 and 1.48 for saturates, between 1.55 and 1.57 for aromatics, and between 1.60 and 1.63 for resins, Figure 6-13. Like density, the refractive index clearly distinguished between solubility classes in crude oils and between chemical families of hydrocarbons. The changes in the density and refractive index of SAR fractions after reaction were similar, Figure 6-14 to 6-16. The refractive index of saturates did not significantly change. The refractive index of aromatics increased with reaction for all the reacted samples, *in-situ* converted, thermocracked and hydrocracked. The refractive index of resins did not significantly change for *in-situ* converted samples, but increased with the extent of reaction for thermocracked and hydrocracked samples. The consistent trends with extent of reaction suggests that, like density, the refractive index is a potential reaction indicator property. In fact, Okafor (2013) showed that

the function of the refractive index (FRI) correlated very well with density for the saturates and aromatic fractions, the correlation was extended to all SARA fractions and it is shown in Appendix G. Hence, refractive index measurements are an alternative to density measurements using equation G-2 in Appendix G.

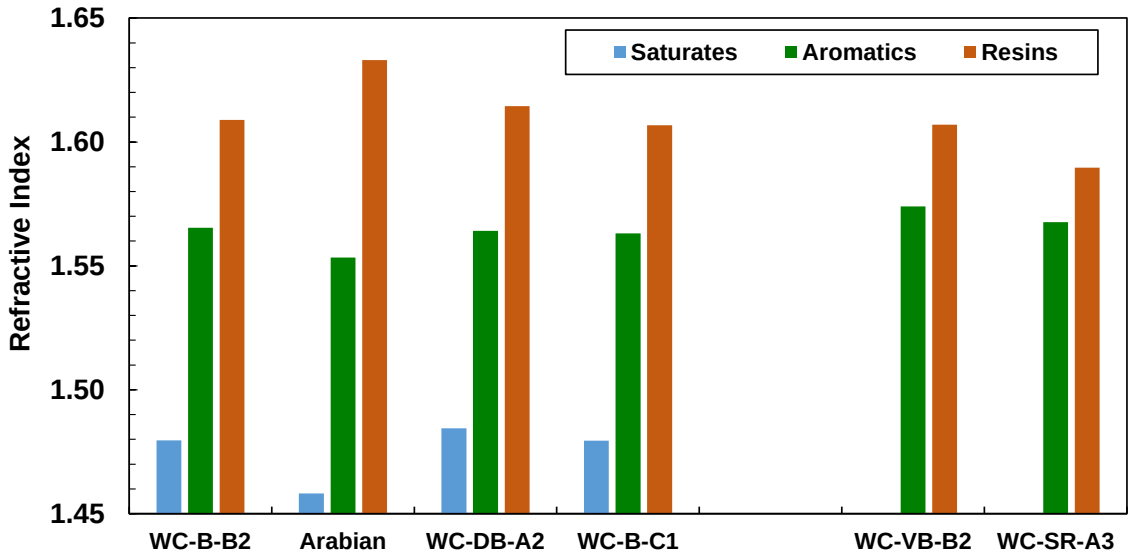

Figure 6-13. Refractive index of SAR fractions from native oils at 20°C and atmospheric pressure.

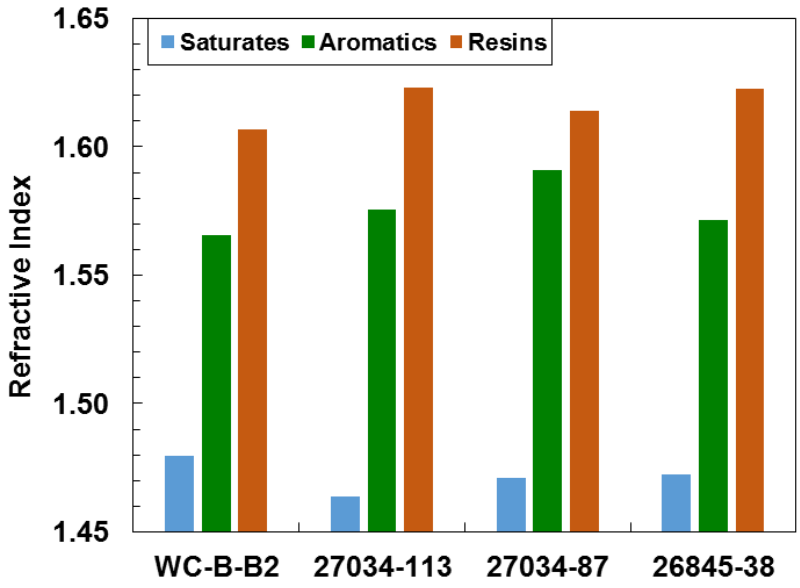

Figure 6-14. Refractive index of SAR fractions from in-situ converted oils at 20°C and atmospheric pressure.

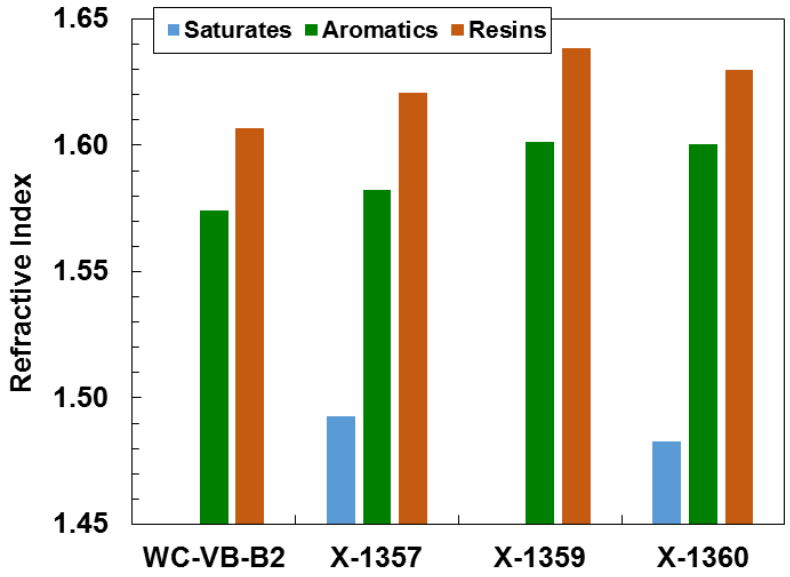

Figure 6-15. Refractive index of SAR fractions from thermocracked oils at 20°C and atmospheric pressure. Note, there was not enough samples of saturates from X-1359 for detailed characterization.

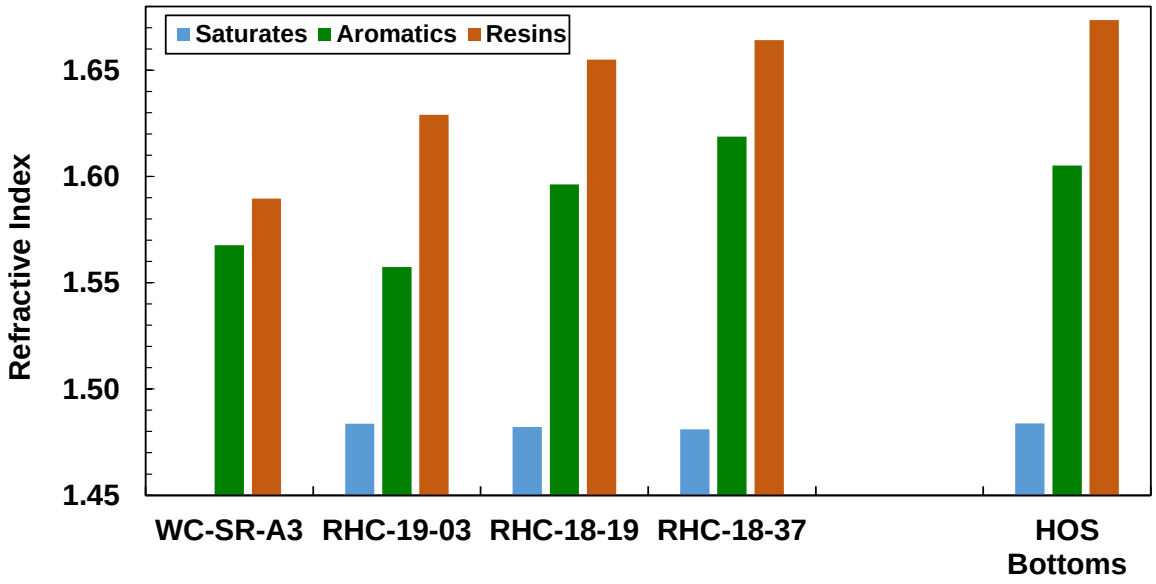

Figure 6-16. Refractive index of SAR fractions from hydrocracked oils at 20°C and atmospheric pressure.

6.4.2 Elemental Analysis

Elemental analysis is not an input in the regular solution model but it was performed on the SAR fractions to identify "chemical" changes after reaction and study its possible relationship with other properties for future work. The atomic H/C ratios of thermo- and hydrocracked SAR fractions are shown in Figures 6-17 and 6-18, respectively. The H/C ratio of saturates from thermocracked and hydrocracked oil samples slightly increased with increasing extent of reaction (from 1.80 to 1.85 for thermocracked and 1.85 to 1.90 for hydrocracked samples). Possible explanations are shorter paraffin chain lengths or a higher concentration of paraffinic structures, both of which are consistent with an accumulation of cleaved side chains reporting to saturates.

The H/C ratio of aromatic and resin fractions from thermocracked oils decreased with increasing extent of reaction, confirming that cracking created a more "aromatic" fraction. Counterintuitively, with hydrocracking, there was also a clear trend of decreasing H/C ratio with the extent of reaction for aromatics and resins. A possible explanation is that the C-C bonds from the aromatic fractions are very stable due to the electronic resonance of the aromatic rings making them less susceptible to cracking reactions and more difficult to hydrogenate. Hence, side chain cleavage may be the dominant mechanism for the changes in chemical structure. Another possibility is that the structures that were saturated and fragmented may report to saturates or distillables after reaction leaving the aromatics and resins enriched in aromatic structures. A third possibility is coke formation. Several factors including operational conditions, type of catalysis, catalyst poisons, and presence of free radicals, will affect the efficiency of hydrogenating aromatic rings sometimes promoting more condensation reactions which favour the formation of coke (Huc, 2011; Raseev, 2003). Coke and coke precursors are high carbon content material and therefore contribute to a lower H/C ratio. The high content of toluene insolubles in the hydrocracked samples is consistent with the formation of coke.

During cracking, C-C, C-S and S-S bonds are cracked first because of their lower bonding energy (Raseev 2003). As expected, the sulfur content was reduced for saturate and resin fractions as the extent of reaction increased, Figures 6-19 and 6-20. For the hydrocracked samples, the sulfur content is almost half that of the thermocracked samples due to hydrodesulphurization reactions.

However, the sulfur content in aromatic fractions did not change or even increase. The lack of change in sulfur content may suggests that the sulfur atoms that are attached to aromatic rings are less likely to be removed (due to the resonance stabilization of the aromatic rings) or that the smaller reacted resins (or asphaltenes) with sulfur atoms (desulfurized resins or asphaltenes) now report to the aromatic fraction balancing the loss of sulfur in the aromatic fraction.

Nitrogen is present in residue as both non-basic and basic heterocyclic structures. The latter are less active as the nitrogen atom is embedded in an aromatic ring. It is believed that in order to remove nitrogen, the first step in the reaction process is the transformation of the heterocylic structure (aromatic C-N bond) into an aliphatic structure through hydrogenation, which is weaker and thus susceptible to cracking. As expected, aromatics and resins from thermocracking had a slight increase in nitrogen because there was no hydrogen present to make weaker aliphatic structures, Figures 6-21 and 6-22. Aromatics and resins from the hydrocracked samples had a significant increase in nitrogen content and no increase in the H/C ratio. The increase in nitrogen content suggests that nitrogen is present mostly in a basic form embedded in the aromatic rings and making the C-N bond very stable. Other components are removed through the hydrocracking process leaving the remaining material enriched in nitrogen. Kekäläinen *et al*. (2013) also found that nitrogen is one of the most abundant heteroatoms before and after processing residues. The authors reported that the number of N species was almost unaltered after processing (Kekalainen *et al*., 2013).

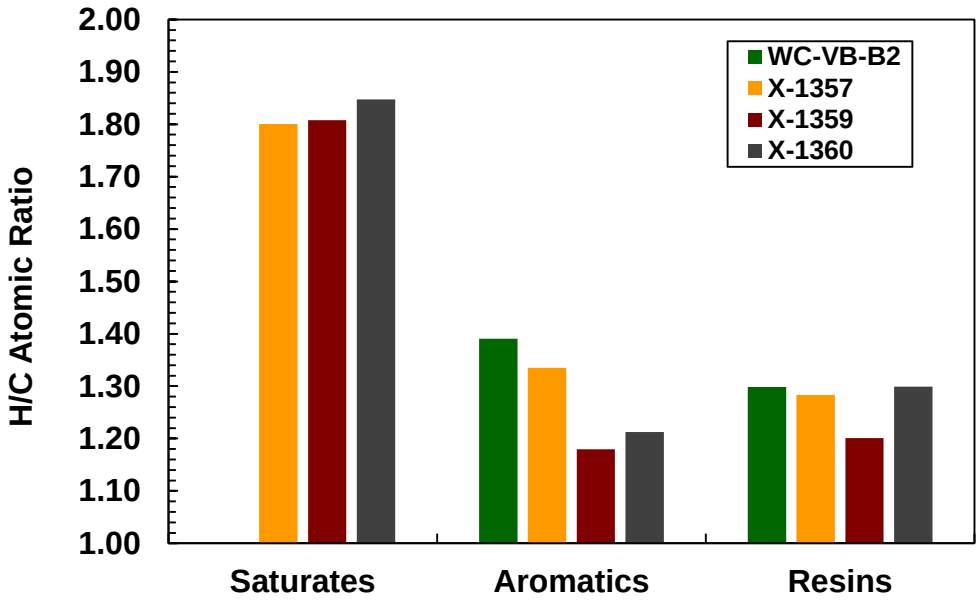

Figure 6-17. H/C atomic ratio for SAR fractions from thermocracked oils and the feedstock.

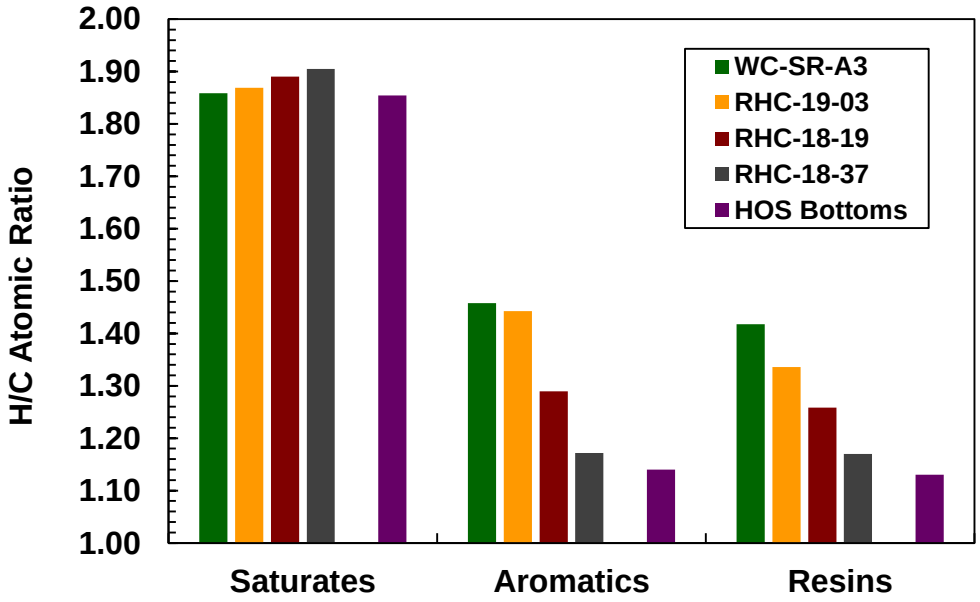

Figure 6-18. H/C atomic ratio for SAR fractions from hydrocracked oils and the feedstock.

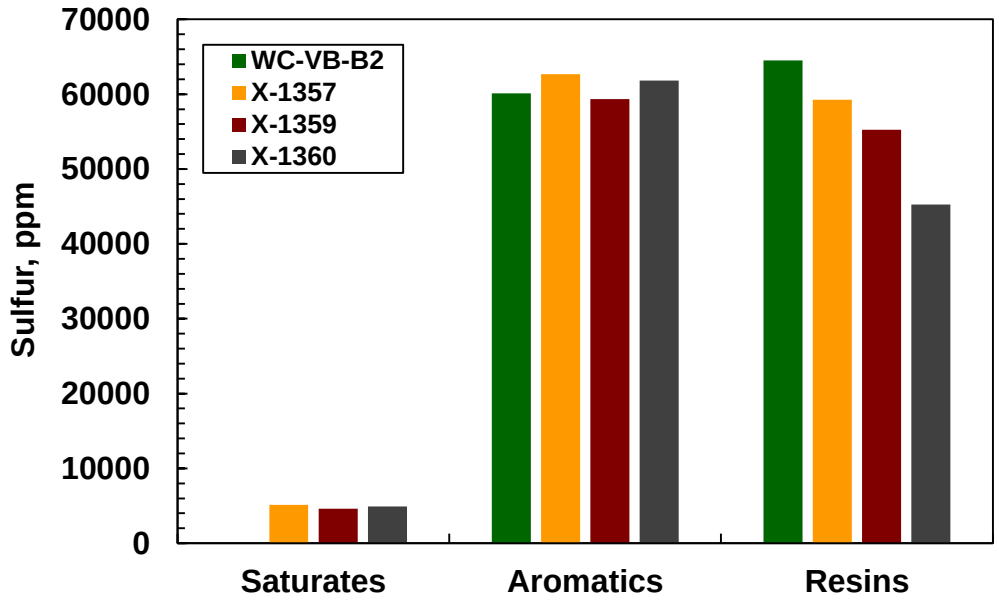

Figure 6-19. Sulfur content in SAR fractions from thermocracked oils and the feedstock.

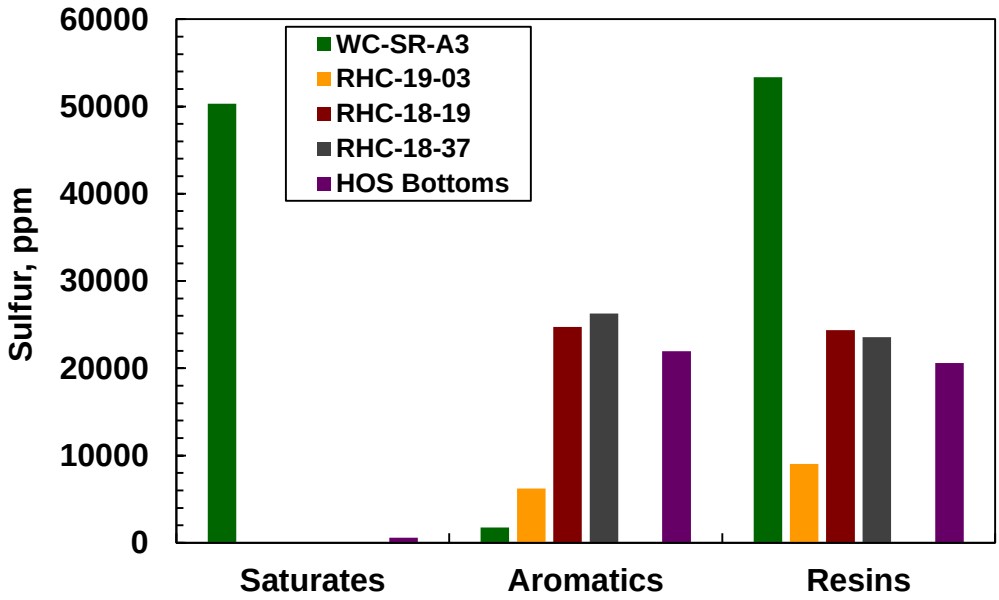

Figure 6-20. Sulfur content of SAR fractions from hydrocracked oils and the feedstock.

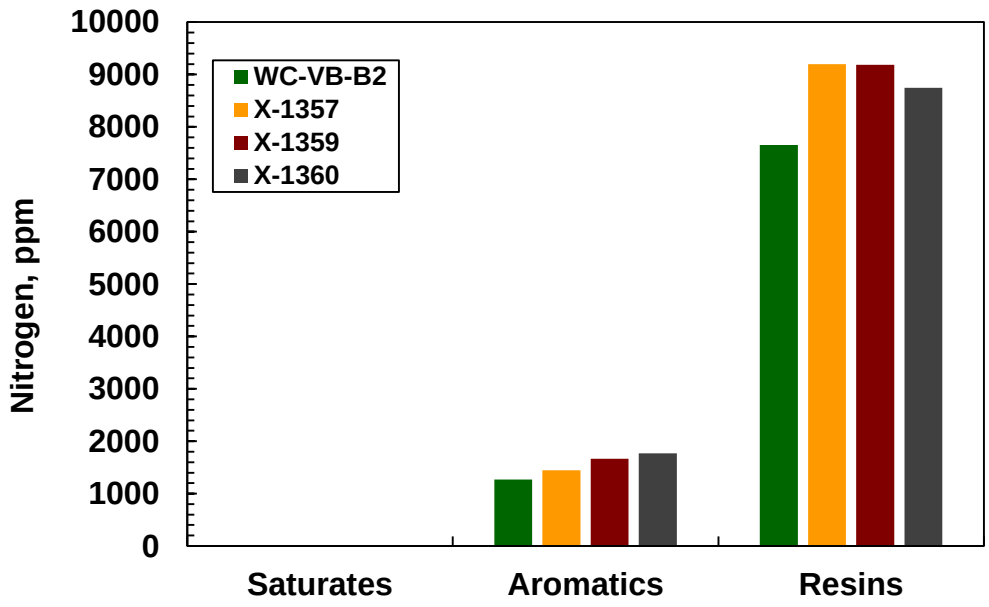

Figure 6-21. Nitrogen content in SAR fractions from thermocracked oils and the feedstock.

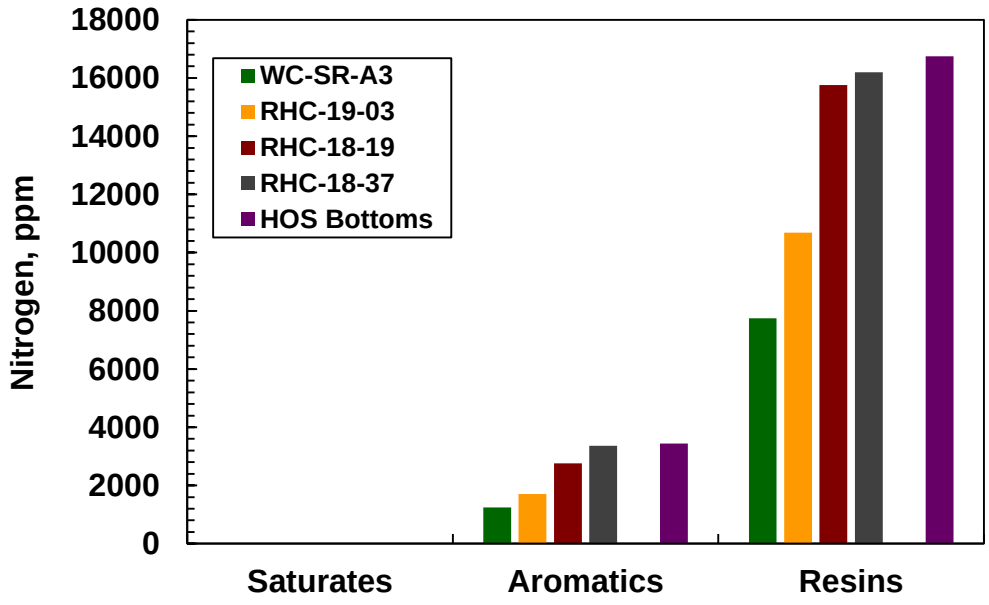

Figure 6-22. Nitrogen content in SAR fractions from hydrocracked oils and the feedstock.

6.5 Summary: Properties of Native versus Reacted SAR

The molecular weight of the SAR fractions of native oils was consistent within a small range for each SAR fraction. Hence, these values can be averaged to estimate the molecular weights of unknown native SAR fractions. The molecular weight of SAR fractions from vacuum residues was higher due to the removal of lighter compounds of each fraction during the vacuum distillation. SAR molecular weight from reacted samples showed some reduction as expected due to cracking reactions. Additionally, thermo- and hydrocracking redistributed the molecular weight of the SAR fractions which can affect the phase behaviour of the oil.

The density of the SAR fraction from native oils was within a small range for each fraction and consistent with previous data. Thermocracking reactions did not significantly change the density of the SAR fractions suggesting that density is mainly dominated by the chemical families and stays within a small range for a span of molecular sizes in the same chemical family. Hydrocracking slightly increases the density of the aromatic and resin fractions indicating some change in the chemical structure such as hydrogenation and then cracking of the cyclic and heterocyclic compounds leaving behind a more aromatic structure.

The solubility parameter of saturates and aromatics was indirectly estimated using the regular solution model. Saturates and aromatics from native oils had the same average solubility parameters. Saturates from thermo and hydrocracked oils had lower solubility parameter, therefore reaction make poorer saturates for asphaltenes. The solubility parameter of aromatics from reacted samples also decreased but to a lesser extent than saturate solubility parameter. In general, reaction makes maltenes poorer solvents for asphaltenes with lower solubility parameters.

Refractive index and elemental analysis was also measured to study the effect of reaction on the chemistry of the SAR fractions. The refractive index results had the same trend as density consistent with the proportionality between density and refractive index. The H/C ratio decreased for reacted aromatics and resins but it did not change significantly for saturates. The sulfur content was reduced for reacted saturates and resins and it did not change (and even increased) for

aromatics. The nitrogen content increased for reacted aromatics and resins, indicating that nitrogen is a difficult heteroatom to remove from the SAR fractions.

Chapter Seven: Regular Solution Model for the Heavy Fraction of Native and Reacted Oils

The regular solution approach presented in Chapter 4, and modified as described in Chapter 5, was used to model asphaltene solubility in the heavy fraction of crude oils (distillables excluded). The heavy fractions are characterized from SARA assays. The dataset included seven native oils, three in-situ converted oils and their original oil, three thermocracked oils from a visbreaker and their feedstock, and four hydrocracked samples and their feedstock. The samples are described in more detail in Chapter 3.

The inputs required for the model are: the SARA composition of each oil; the molecular weight, molar volume (density), and solubility parameter of the saturates and aromatics; the molecular weight and density of the resins; the asphaltene density distribution, the shape factor of the gamma distribution, and the *b* parameter in the asphaltene and resin solubility parameter correlation (Equation 5-10). The SARA compositions are presented in this chapter. Saturate, aromatic, and resin properties were presented in Chapter 6. Asphaltene properties were presented in Chapter 5. The only unknown for the dead native and thermocracked crude oils is the average molecular weight of the asphaltene nano-aggregates in the crude oil. The average molecular weight was determined from asphaltene solubility data for n-heptane diluted oil samples. For hydrocracked oils, it was also necessary to re-examine the value of the *a* parameter in the asphaltene enthalpy of vaporization correlation (Equation 5-10).

7.1 Crude Oils Compositions

SARA fractionation, including distillables separation and toluene insolubles (TI) determination, was performed on the heavy fractions as described in Chapter 3. Tables 7-1 to 7-4 show the SARA composition obtained for the native, in-situ converted, thermocracked and hydrocracked samples, respectively.

Table 7-1. SARA Composition for Native oils and Vacuum Residues.

Sample	Distillables wt%	Saturates wt%	Aromatics wt%	Resins wt%	C5-Asphaltenes wt%	TI* (wt% of Asph.)
Native Crudes						
WC-B-B2	<5	17	44	19	20	3.8
Arabian	33	24	28	11	5	0.5
WC-DB-A2	20	17	36	19	8	2.3
WC-B-C1	15	13	38	18	16	1.8
Vac. Bottoms						
WC-VB-B2	--	5	37	20	37	6.6
WC-SR-A3	--	8	38	27	28	1.3
Unknown						
27-168-179	35	30	21	11	3	0.9

* Toluene insoluble in native samples are mostly inorganic solids present in the crude oil.

Table 7-2. SARA composition for atmospheric residue of i*n-situ* converted oil.

Sample	Distillables wt%	Saturates wt%	Aromatics wt%	Resins wt%	C5-Asphaltenes wt%	TI* (wt% of Asph.)
27034-113	61	11	15	8	4	1.8
27034-87	71	6	15	4	3	1.3
26845-38	34	12	31	14	10	1.8

Table 7-3. SARA Composition for Short Residues of Thermocracked Samples.

Sample	Saturates wt%	Aromatics wt%	Resins wt%	C5-Asphaltenes wt%	TI* (wt% of Asph.)
WC-VB-B2(Feed)	5	37	20	37	2.4
X-1357	5	34	19	43	3.2
X-1359	4	31	13	51	8.1
X-1360	4	24	11	61	11.5

Table 7-4. SARA Composition for Short Residues of Hydrocracked Samples**.**

Sample	Saturates wt%	Aromatics wt%	Resins wt%	C5-Asphaltenes wt%	TI* (wt% of Asph.)
WC-SR-A3 (Feed)	8	38	27	28	0.2
RHC-19-03	33	49	15	3	0.9
RHC-18-19	21	48	18	14	1.1
RHC-18-37	15	45	15	25	4.0
HOS Bottoms	20	47	18	15	2.4

SARA composition for the native oils varies according to the origin of the oils, Table 7-1. Note that WC-DB-A2 is a diluted bitumen, therefore, the distillable fraction corresponds to the amount of diluent which is usually between 15 and 20 vol% depending on the oil properties such as density and viscosity. Vacuum residues contain very little saturates due to the deeper distillation which removes intermediate boiling point compounds. These are the lowest molecular weight fractions of the bitumen.

Table 7-2 shows that the *in-situ* sample 27034-87 has a higher amount of distillables than 27034-113, which is in agreement with the greater extent of reaction. Additionally, saturates, aromatics and resins content decrease indicating that part of these fractions were converted to smaller size molecules reporting now to the distillable fraction. It is also possible that some asphaltenes became unstable and precipitated in the reservoir decreasing the overall asphaltene content. On the other hand, the distillables content in Sample 26845 decreases and SARA fraction contents increase even though this sample has the highest reported extent of reaction. This composition change suggests that Sample 26845 is a mixture of converted bitumen from within the treatment area and unconverted bitumen that could have migrated into the treatment area.

The thermocracked samples composition, Table 7.3, changes with the extent of reaction. The saturate content decreases slightly and the aromatic and resin contents decrease as expected with conversion. Interestingly, the asphaltene content increases with greater extent of reaction. One would expect the asphaltene content to decrease as asphaltenes are converted to

distillables/saturates (removed side chains), aromatics, resins, and toluene insolubles. However, if the other fractions (saturates, aromatics, and resins) are converted to distillables faster than asphaltenes are converted, then asphaltenes will become more concentrated in the reacted product. Hence, the increasing asphaltene content with the extent of reaction does not mean that asphaltenes did not react; in fact, their properties do change with reaction. As expected, the TI content also increases with reaction because there is more coke formation with increasing temperature and extent of reaction.

At first glance, the compositional trends for the hydrocracked samples, Table 7-4, seem inconsistent. For the lowest conversion sample, RHC-19-03, the saturate and aromatic contents increase relative to the feed and the resin and aromatic contents decrease. However, increasing conversion decreases the saturate and aromatic contents, has little effect on the resins content, and increases the asphaltene content. This trend reversal may be an artefact arising from the nature of the batch experiments performed on a reactor with a fixed catalytic bed. At the beginning of the operation the catalytic bed is highly efficient for all the SARA fractions and it may also filter out asphaltenes and coke. As time passes and conversion increases, the catalytic bed becomes saturated with coke, metals, and asphaltenes and loses efficiency and filtering capacity. The composition changes appear to have been affected by the asphaltene filtering effect. The initial decrease in asphaltene content suggests effective filtering while the later increases in asphaltene content may arise from less effective filtering. All of the other compositions will be skewed from the asphaltene content changes. Note that, the conversion is calculated using distillation assays and therefore is maltenes conversion and it is calculated as follows (Shell-Canada 2014),

$$Conversion = \frac{[(flow\ rate{*}524°C\ Content)_{FEED} - (flow\ rate{*}524°C\ Content)_{PRODUCT}]}{(flow\ rate{*}524°C\ Content)_{FEED}} \quad \textbf{7.1}$$

The asphaltene conversion is calculated with the same equation but replacing the 524°C content with the asphaltene content from the feed, Table 7-5.

Table 7-5. Maltenes and asphaltenes conversion for RHC samples.

Sample	Maltenes Conversion (vol%)	C7 Asphaltenes Conversion (wt%)
RHC-19-03	57	96
RHC-18-19	67	69
RHC-18-37	81	60

7.2 Crude Oil Stability and Model Results for Native Oils.

Crude oil stability measurements, in terms of asphaltene precipitation, are used to tune the regular solution model. Typically, crude oil stability is assessed by the amount of a poor solvent (in this case heptane) required to precipitate asphaltenes. In this case, the entire yield curve is used not just the onset condition (solvent content at which precipitation first occurs).

7.2.1 Asphaltene Solubility in Heavy Fractions from Native Crude Oils

For native oils diluted with *n*-heptane, the onset of asphaltene precipitation occurs in a relatively narrow range, between 40 and 60 wt% *n*-heptane, Figure 7-1a. There is more difference in the asphaltene yields from different oils because the yield is proportional to the asphaltene content of the oil sample and each sample has a different asphaltene content.

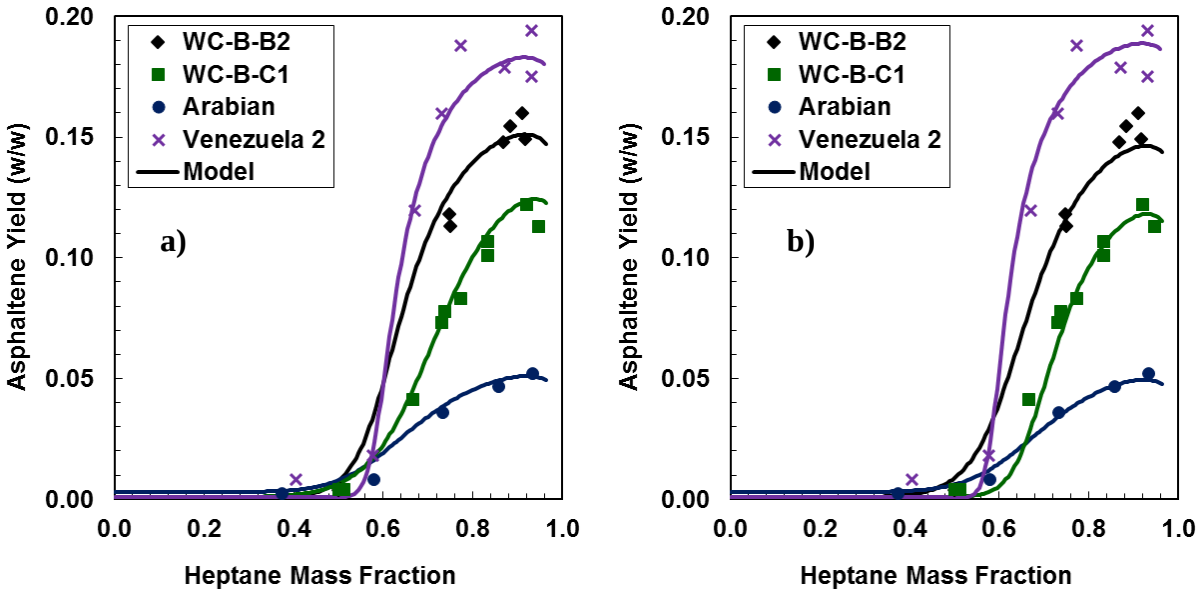

Figure 7-1. Asphaltene yield for crude oils diluted with n-heptane at 20°C: a) solubility parameter calculated with tuned *b* for each crude oil asphaltenes; b) solubility parameter calculated with average *b* for native oils (b=0.0634).

The modified regular solution model was tested on native samples from this work and from Akbarzadeh *et al.* (2005). *n*-Heptane parameters were provided in Table 5-9. The input properties for each oil are summarized in Table 7-6. Additional model results for other native oils are presented in Appendix E. The model was run with: 1) tuned *b* values found by fitting asphaltene-solvent model systems, and; 2) average *b* determined for native oils. In both cases, the average aggregated molecular weight of asphaltenes was adjusted to fit the data, Table 7-7 and Figures 7-1a and 7-1b. Interestingly, when the average *b* is used the fitted molecular weight increases monotonically with the asphaltene content. The success of modeling with an average *b* means that the average value can be assumed for new native oils, eliminating the necessity of measuring asphaltene solubility in solvents to determine the value of *b* for each new oil. Fine tuning of the shape factor of the gamma distribution to improve the fit to the crude oil solubility data is still recommended.

The predictive capability of the model was tested on asphaltene solubility data for native oils diluted in *n*-pentane from Akbarzadeh *et al.*, (2005). Figures 7-2a and 7-2b show that the model

tuned to *n*-heptane dilution data was able to predict asphaltene stability in *n*-pentane without any further adjustment.

Table 7-6. Properties of the SARA fractions for native oils used in the RSM.

Sample	Density[(1)] kg/m^3 at 20°C	Molecular Weight[(2)] g/mol	Solubility Parameter MPa$^{0.5}$	*b* (Eq. 5-10)	Tuned α (Eq. 4-2)
WC-B-B2					
Saturates	887	370	16.6	-	-
Aromatic	1006	440	20.8	-	-
Resins	1054	990	19.26	0.0635	-
Asphaltenes[(3)]	1200	4500	19.20-21.35	0.0635	2
Arabian					
Saturates	827	360	16.6	-	-
Aromatic	978	440	20.8	-	-
Resins	1048	990	19.18	0.0635	-
Asphaltenes[(3)]	1200	3950	19.28-21.17	0.0635	2
WC-B-C1					
Saturates	877	400	16.7	-	-
Aromatic	1002	480	20.8	-	-
Resins	1045	1280	19.09	0.0633	-
Asphaltenes[(3)]	1190	6980	19.10-20.98	0.0633	5
Venezuela 2 [(4)]					
Saturates	882	400	16.6	-	-
Aromatic	997	508	20.8	-	-
Resins	1052	1090	19.67	0.0634	-
Asphaltenes	1200	7700	19.09-20.77	0.0634	10
Venezuela 1 [(4)]					
Saturates	885	447	16.6	-	-
Aromatic	1001	542	20.8	-	-
Resins	1056	1240	19.50	0.0633	-
Asphaltenes[(3)]	1200	10000	18.93-20.75	0.0633	10

1 Reported density of asphaltenes is the maximum density in the density distribution. The minimum density is 1050 kg/m^3 for all native samples

2 Average MW of asphaltenes measured at 50°C at 10 g/L, used for asphaltenes in solvents. See Table 7-2 for fitted MW of asphaltenes in the oil.

3 Minimum and maximum solubility parameter of asphaltenes from Equations 5-9 and 5-10 and reported *b*.

4 MW and density data from Akbarzadeh *et al.* (2005), average solubility parameters from this work.

Table 7-7. Fitted asphaltene molecular weight in oil and average absolute deviation, AAD, of the fractional yield for native oils.

Sample	MW in oil (tuned *b*) g/mol	MW in oil (average *b*) g/mol	AAD (tuned *b*) wt fr	AAD (average *b*) wt fr%
WC-B-B2	2400	2800	0.005	0.006
Arabian	2300	2400	0.002	0.003
WC-B-C1	3200	2500	0.003	0.007
Venezuela 2	3000	3300	0.008	0.009
Venezuela 1	--	3600	--	0.004

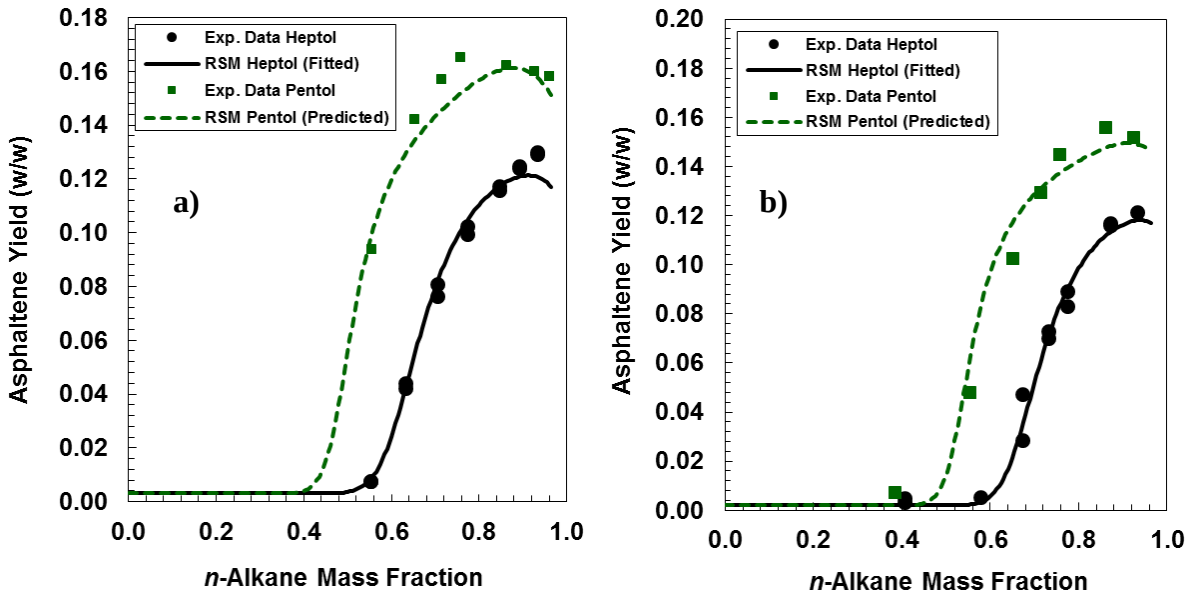

Figure 7-2. Asphaltene yield and model results and predictions for Cold Lake (a) and Venezuela 1 (b) crude oils diluted with *n*-heptane (black dots) and *n*-pentane (green squares) at 20°C. Solubility parameter calculated with average *b* for native oils.

7.2.2 Asphaltene Solubility in Heavy Fractions from In-Situ Converted Oils

The asphaltene solubility curves from in-situ converted samples show that asphaltenes have become less soluble than in the original oil with onsets of precipitation as low as 20 wt% *n*-heptane, Figure 7-3. Since the asphaltene content varied for the in-situ converted samples in comparison with the original oil (WC-B-B2), Table 7-2, the asphaltene yields will vary both from the change in solubility and the difference in asphaltene content.

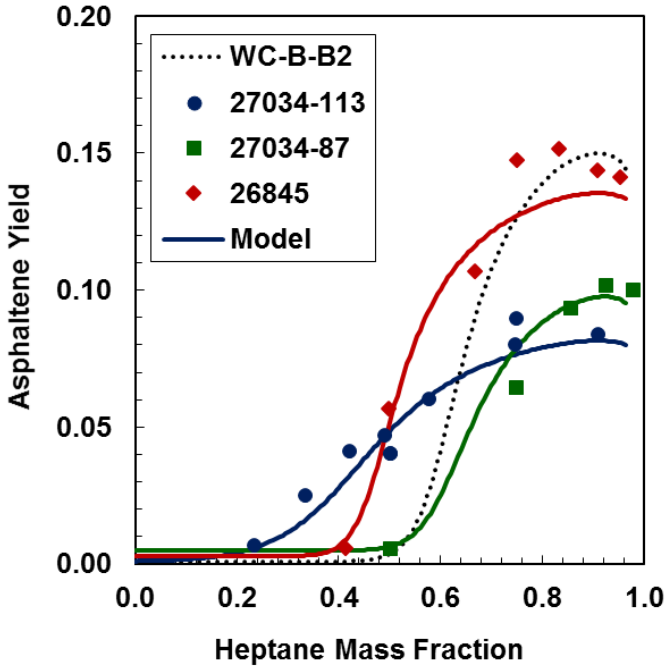

Figure 7-3. Asphaltene yield for in-situ converted oils diluted with *n*-heptane at 20°C.

The input properties to the modified regular solution model are summarized in Table 7-8 and 7-9. The model was fit to the data by adjusting the average aggregated molecular weight of asphaltenes, for all the three in-situ converted samples, Figure 7-3. The fitted average molecular weights are provided in Table 7-9. The AAD of the fitted asphaltene yields are less than 1 wt% in all cases.

Table 7-8. Properties of SARA fractions from in-situ converted oils.

Sample	Density[(1)] at 20°C kg/m^3	Molecular Weight[(2)] g/mol	Solubility Parameter MPa$^{0.5}$	*b* (Eq. 5-10)	Tuned α (Eq. 4-2)
27034-113					
Saturates	841	330	16.1	-	-
Aromatic	1008	340	20.8	-	-
Resins	1059	830	19.44	0.0636	-
Asphaltenes[(3)]	1250	3500	20.67-22.41	0.0636	0.7
27034-87					
Saturates	848	320	16.3	-	-
Aromatic	1028	300	20.6	-	-
Resins	1054	860	19.72	0.0638	-
Asphaltenes[(3)]	1200	3950	20.15-21.08	0.0638	3
26845					
Saturates	861	360	16.5	-	-
Aromatic	1009	380	21.0	-	-
Resins	1063	880	19.88	0.0639	-
Asphaltenes[(3)]	1230	3020	19.80-21.57	0.0639	2

1 Reported density of asphaltenes is the maximum density in the density distribution. The minimum density is 1050 kg/m^3 for all *in situ* samples
2 Average MW of asphaltenes measured at 50°C at 10 g/L. See Table 7-4 for fitted MW of asphaltenes in the oil.
3 Minimum and maximum solubility parameter of asphaltenes from Equations 5-9 and 5-10 and reported *b*.

Table 7-9. Fitted asphaltene molecular weight in oil and average absolute deviation of the fractional yield for in-situ converted samples.

Sample	MW in oil g/mol	AAD wt fr
27034-113	2000	0.0050
27034-87	1700	0.0050
26845	1600	0.0098

7.2.3 Asphaltene Solubility in Heavy Fractions from Thermocracked (Visbroken) Oils

Thermocracked oils were received from Shell as vacuum residues. They have a very high asphaltene content (>40 wt%) and were solid at room temperature. As noted in Chapter 3, to perform the solubility experiments on the whole oil sample, the samples were heated and then diluted in toluene with a 2.3 toluene to oil ratio (70 wt% toluene). *n*-heptane was added to the oil-toluene mixture at different ratios.

Figures 7-4 shows that thermocracking generates less soluble asphaltenes and less stable oils with lower asphaltene precipitation onsets as conversion increases. As noted in Section 7-1, the asphaltene content increases with conversion and the amount of toluene insolubles also increased with conversion; although this is not noticeable at high toluene dilutions. Overall, the thermocracked product contains more asphaltenes than the feed and those asphaltenes are less soluble.

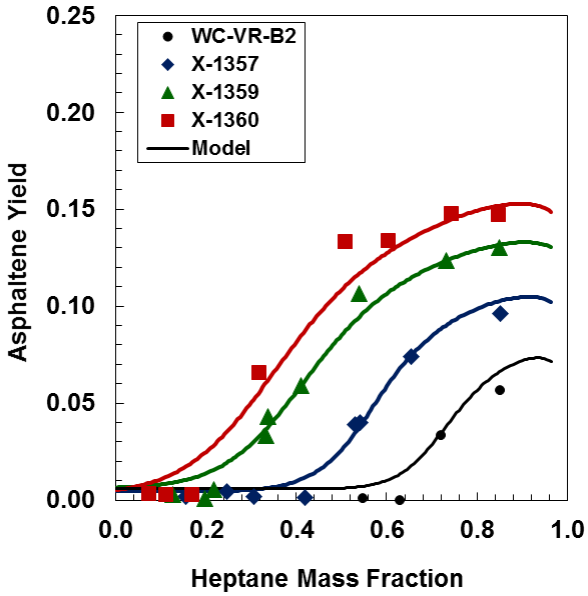

Figure 7-4. Asphaltene yield for toluene-diluted-thermocracked oils (2.3 g tol/g oil) diluted with *n*-heptane at 20°C.

Table 7-10 and 7-11 presents the properties used in the regular solution model for the diluted thermocracked oils. Toluene properties were provided in Table 5-9. The regular solution model was fitted to the stability data from the toluene diluted oils by adjusting the average aggregated

molecular weight of asphaltenes. The fitted molecular weight was then used to predict the asphaltene precipitation yield of the oil with no toluene. Figures 7-5 to 7-7 show the model fitted to the toluene diluted data (black solid line) and the predictions for the oil with no toluene (dashed blue line). The model fitted the experimental data in all cases to within 1 wt%. The predictions for the oil with no toluene are consistent with the C7-asphaltene content determined by Sadeghi – Yamchi (2014).

Table 7-10. Properties of SARA fractions from thermocracked oils.

Sample	Density[(1)] at 20°C kg/m^3	Molecular Weight[(2)] g/mol	Solubility Parameter MPa$^{0.5}$	*b* (Eq. 5-10)	Tuned α (Eq.4-2)
X-1357					
Saturates	896	770	14.0	-	-
Aromatic	1023	780	20.8	-	-
Resins	1072	1430	19.46	0.0637	-
Asphaltenes[(3)]	1250	2900	20.74-22.35	0.0637	0.7
X-1359					
Saturates		770	14.0	-	-
Aromatic	1042	750	21.0	-	-
Resins	1082	1080	19.92	0.0640	-
Asphaltenes[(3)]	1280	2800	20.80-23.07	0.0640	0.6
X-1360					
Saturates	896	800	14.0	-	-
Aromatic	1040	690	21.0	-	-
Resins	1075	1030	19.77	0.0640	-
Asphaltenes[(3)]	1280	2300	20.73-23.97	0.0640	0.5

1 Reported density of asphaltenes is the maximum density in the density distribution. The minimum densities are 1050, 1080, and 1050 kg/m³, respectively.
2 Average MW of asphaltenes measured at 50°C at 10 g/L. See Table 7-6 for fitted MW of asphaltenes in the oil.
3 Minimum and maximum solubility parameter of asphaltenes from Equations 5-9 and 5-10 and reported *b*.

Table 7-11. Fitted asphaltene molecular weight in oil and average absolute deviation of the fractional yield for in-situ converted samples.

Sample	**MW in oil g/mol**	**AAD wt fr**
X-1357	1700	0.0038
X-1359	1800	0.0056
X-1360	1700	0.0098

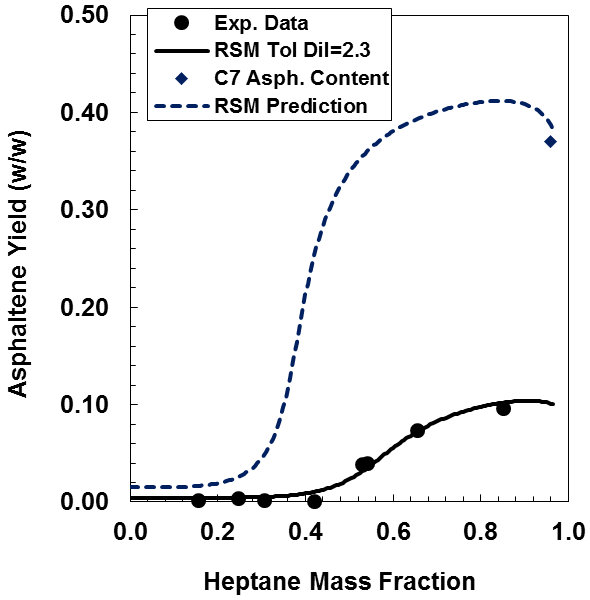

Figure 7-5. Asphaltene yield and model results for X-1357 (diamond) and toluene diluted X-1357 (circle) both diluted with *n*-heptane at 20°C.

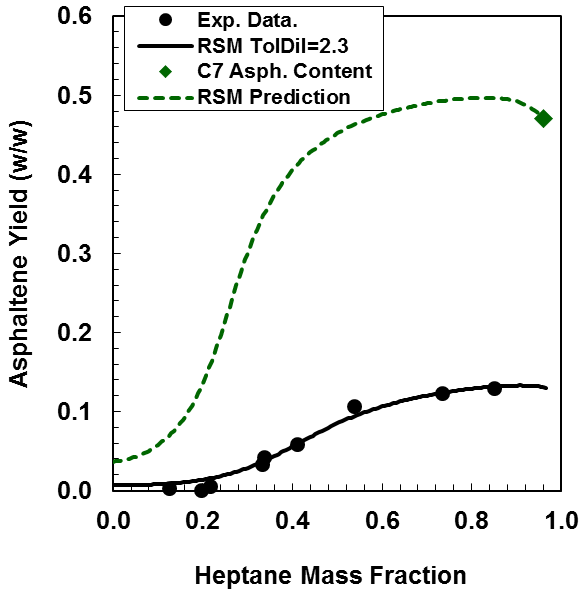

Figure 7-6. Asphaltene yield and model results for X-1359 (diamond) and toluene diluted X-1359 (circle) both diluted with *n*-heptane at 20°C.

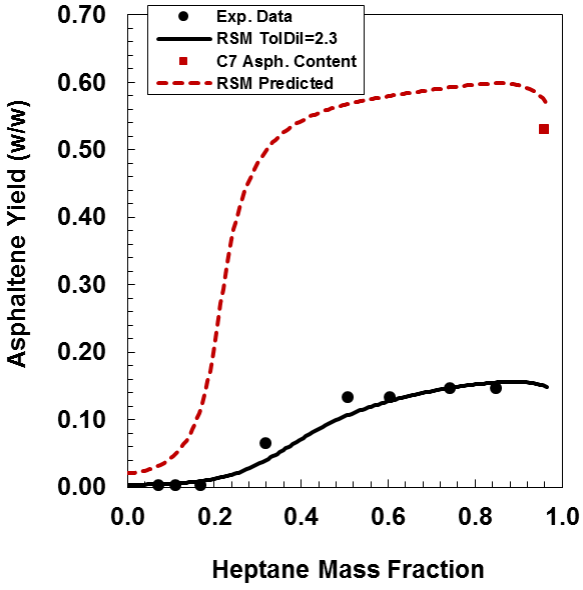

Figure 7-7. Asphaltene yield and model results for X-1360 (diamond) and toluene diluted X-1360 (circle) both diluted with *n*-heptane at 20°C.

Figure 7-8 compares the predicted results for the thermocracked samples with no toluene. Three important observations come from this plot. First, there is a noticeable increase of toluene insolubles with conversion which was measured by Sadeghi and is predicted with the model. Second, as the extent of reaction increases, the onset of asphaltene precipitation occurs at lower *n*-heptane content, consistent with less soluble asphaltenes (higher solubility parameter) and a poorer media (maltenes) for asphaltenes (lower solubility parameters). Third, as the extent of reaction increases, there is an increase in asphaltene content. All three observations are consistent with the previous results for crude oil stability with toluene dilutions.

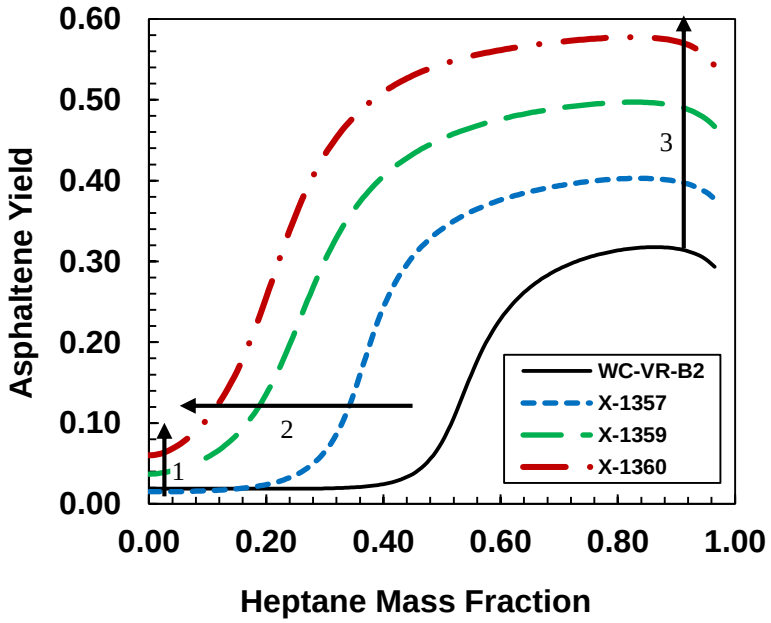

Figure 7-8. Asphaltene precipitation model predictions for thermocracked oils at 20°C. With higher conversion, the amount of TI increases (1), the onset shifts to lower concentrations (2), and the yield increases (3).

7.2.4 Asphaltene Solubility in Heavy Fractions from Hydrocracked Oils

Figure 7-9a shows that hydrocracking generates less soluble asphaltenes and less stable oils with lower asphaltene precipitation onsets and higher toluene insoluble content as conversion increases. As noted in Section 7-1, the changes in asphaltene yield with conversion are related to both the conversion of asphaltenes and the effectiveness of the catalyst during the batch experiment. Figure

7-9b shows that HOS bottoms results are consistent with observations for the RHC samples. Thermocracking and hydrocracking processes both shift the onset of asphaltene precipitation to lower *n*-heptane content; that is, thermal reaction of crude oils with or without hydrogen makes less soluble asphaltenes.

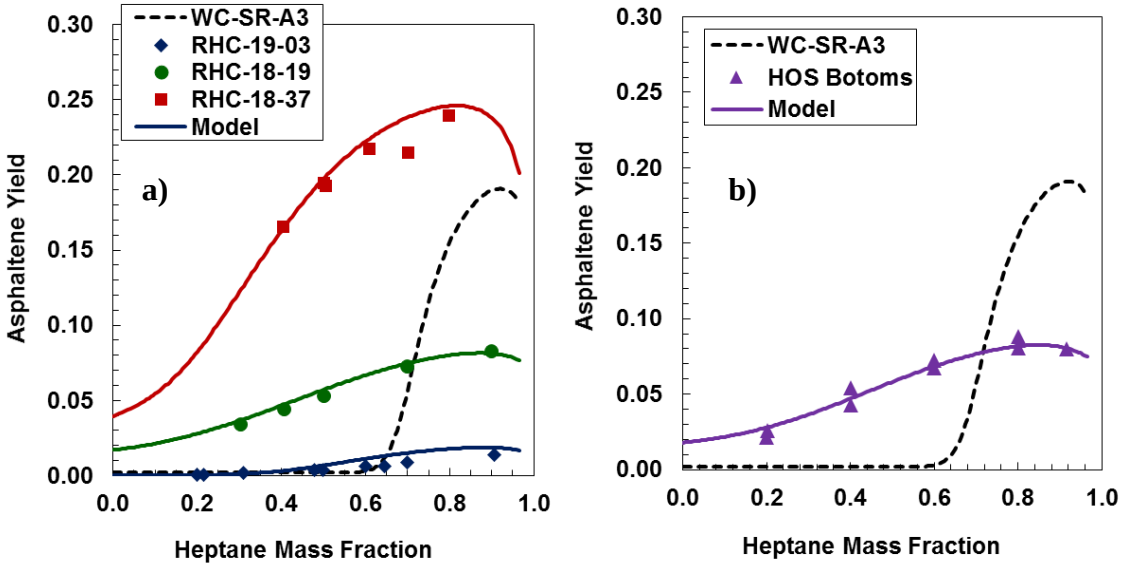

Figure 7-9. Asphaltene yield for hydrocracked oils diluted with n-heptane at 20°C a) RHC samples b) HOS bottoms.

The input properties for the SARA fractions from the hydrocracked samples are presented in Tables 7-12 and 7-13. The fitted α parameter for the gamma distribution is also provided. The molecular weight of hydrocracked asphaltenes in toluene is very low (e.g. 900 and 1500 g/mol for RHC-18-37 and RCH-18-19) and close to the monomer molecular weight. The solubility data could not be fitted by adjusting the average asphaltene molecular weight within this narrow range. Therefore, for the hydrocracked samples with measured asphaltene molecular weight lower than 1500 g/mol, the aggregated molecular weight was set to the measured value in toluene at 50°C and the *a* parameter in the enthalpy of vaporization equation was instead used as the fitting parameter. The rationale for adjusting *a* is that hydrocracking significantly alters the chemistry of the asphaltenes and therefore their heat of vaporization is expected to change. Note, a similar but lesser effect likely occurs in the thermocracked oils but the effect could not be distinguished from the

effect of the reduced association. Figures 7-14a and 7-14b show the model results for the RHCs and HOS Bottoms samples. The model fit the yield data with an ARD less than 1 wt% in all cases.

Table 7-12. Properties of SARA fractions from hydrocracked samples.

Sample	Density[(1)] at 20°C kg/m^3	Molecular Weight[(2)] g/mol	Solubility Parameter MPa$^{0.5}$	*b* Eq. 5-10	Tuned *a* Eq. 5-10	Tuned α Eq. 4–2
RHC-19-03						
Saturates	879	710	16.0	-	-	-
Aromatic	977	740	21.0	-	-	-
Resins	1050	1320	19.89	0.0642	-	-
Asphaltenes	1250	2100	19.86-22.25	0.0642	9.63	0.5
RHC-18-19						
Saturates	877	710	15.22	-	-	-
Aromatic	1026	550	21.3	-	-	-
Resins	1086	780	19.22	0.0642	-	-
Asphaltenes[(3)]	1280	1500	20.46-23.24	0.0642	9.66	0.3
RHC-18-37						
Saturates	876	560	15.22	-	-	-
Aromatic	1054	470	21.6	-	-	-
Resins	1099	700	20.24	0.0644	-	-
Asphaltenes[(3)]	1280	900	21.63-24.03	0.0644	9.70	0.15
HOS						
Bottoms						
Saturates	877	560	15.8	-	-	-
Aromatic	1034	460	20.8	-	-	-
Resins	1098	670	19.39	0.0644	-	-
Asphaltenes[(3)]	1300	1200	20.64-23.01	0.0644	9.65	0.3

1 Reported density of asphaltenes is the maximum density in the density distribution. The minimum density was 1050 kg/m^3 for all the hydrocracked samples.
2 Average MW of asphaltenes measured at 50°C at 10 g/L. See Table 7-8 for fitted MW of asphaltenes in the oil.
3 Minimum and maximum solubility parameter of asphaltenes from Equations 5-9 and 5-10 and reported *b*.

Table 7-13. Fitted average aggregated molecular weight of asphaltenes in the oil or *a* parameter and average absolute deviations.

Sample	MW in oil (g/mol)	a	AAD wt fr
WC-SR-A3	2400	-	0.0034
RHC-19-03*	1000	9.63	0.005-0.002
RHC-18-19	-	9.66	0.0037
RHC-18-37	-	9.70	0.0019
HOS Bottoms	-	9.65	0.0037

* fitted either by adjusting MW or *a* parameter.

7.3 Sensitivity of the Regular Solution Model to the SAR Solubility Parameters

The obvious difference between modeling asphaltene solubility in crude oil versus solvents is the introduction of saturates, aromatics, and resins. The most uncertain and sensitive property of these components is the solubility parameter. Therefore, a straightforward sensitivity analysis for the solubility parameter of the SARA fractions was performed to analyze their effect on the results in the regular solution model. Two cases studies are presented, one for a native sample and one for a reacted (visbreaker) sample.

Saturate Solubility Parameter

As explained in Chapter 6, the uncertainty of the saturate solubility parameter, ± 0.3 $MPa^{0.5}$ (Chapter 6), has insignificant effect on the model results, Figures 7-10 and 7-11a. Note that, the saturate content in sample X-1360 is very low and even lower with the toluene dilution; hence, the effect of a deviation as high as ± 1.0 $MPa^{0.5}$ is insignificant even for the predictions with no dilutions, Figure 7-11b.

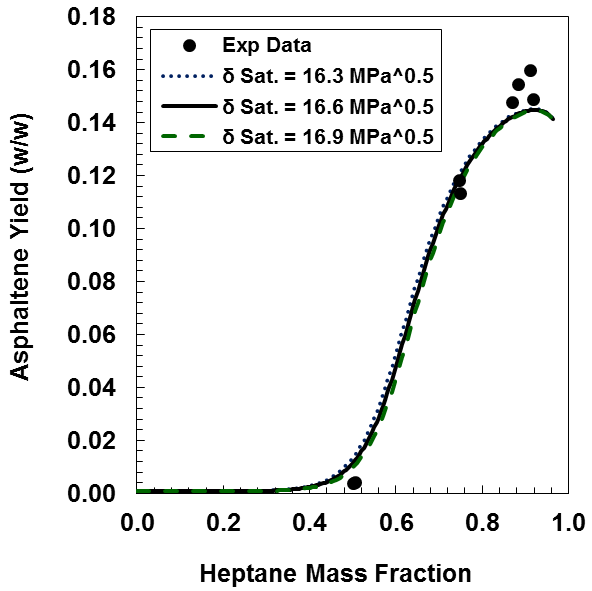

Figure 7-10. Asphaltene yield for WC-B-B2 with heptane at 20°C and effect of saturates solubility parameter in the RSM results.

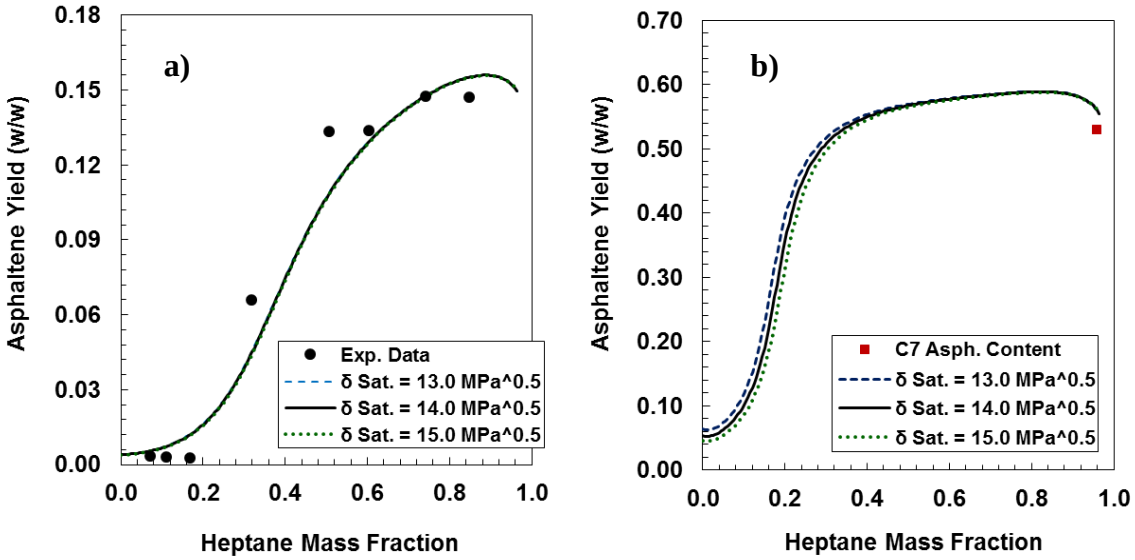

Figure 7-11. Asphaltene yield for X-1360 diluted with *n*-heptane a 20°C and effect of the saturates solubility parameter on the RSM results for: a) 2.3 w/w tol/oil dilution; b) predictions with no toluene dilution.

Aromatic Solubility Parameter

The uncertainty of $\delta \pm 0.3$ MPa$^{0.5}$ in the aromatic solubility parameter gives a maximum deviation in the asphaltene yield from the native oil of 1.6%. The maximum deviation occurs between 60 and 65 wt% *n*-heptane; that is, in the steeper part of the solubility curve, Figure 7-12. This difference is within the uncertainty of the solubility measurements.

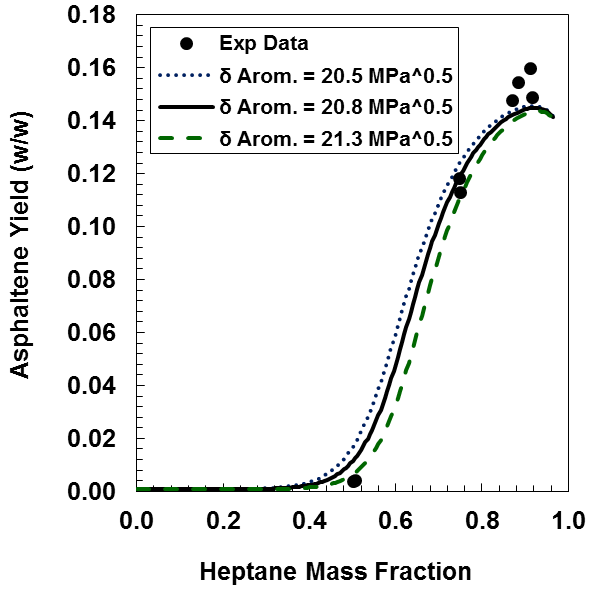

Figure 7-12. Asphaltene yield for WC-B-B2 with *n*-heptane at 20°C and effect of the aromatics solubility parameter on the RSM results.

The uncertainty of the solubility parameter of aromatics for reacted oils ($\delta \pm 0.3$ MPa$^{0.5}$) has no effect on the yield predictions for toluene diluted x-1360, Figure 7-13a; however, it does affect the yield predictions for the thermocracked oils without toluene, Figure 7-13b. The sensitivity is again highest in the steepest part of the solubility curve reaching a maximum deviation of 10 wt% yield at an *n*-heptane content of approximately 15 wt%. The yield measurements also have their maximum error in the steepest part of the curve and therefore the uncertainty in the model prediction is still within the uncertainty of the solubility measurements.

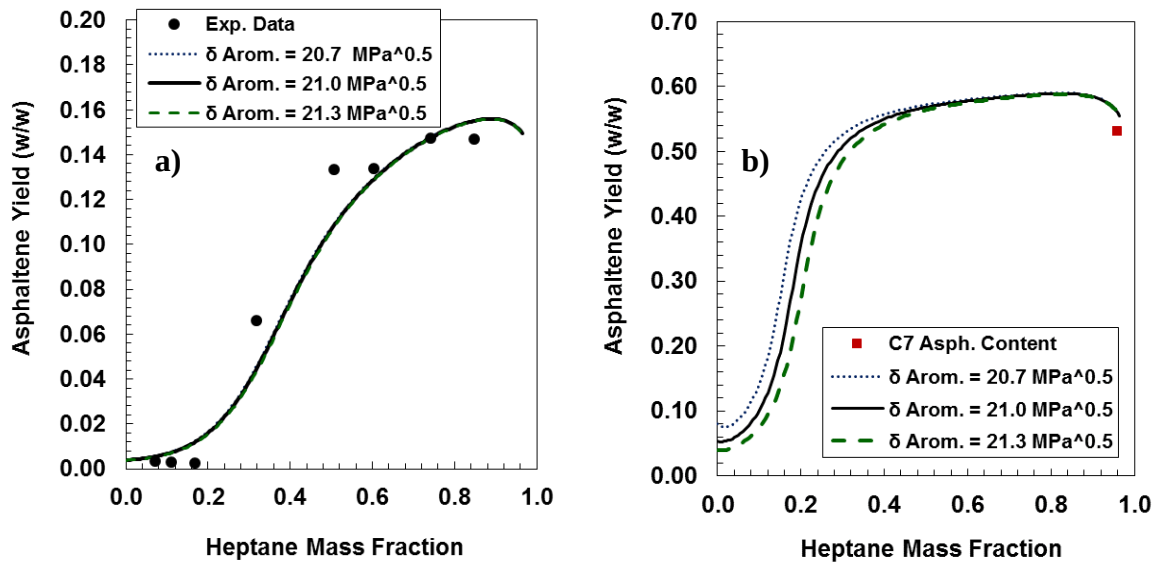

Figure 7-13. Asphaltene yield for X-1360 diluted with *n*-heptane a 20°C and effect of the aromatics solubility parameter on the RSM results for: a) 2.3 w/w tol/oil dilution; b) predictions with no toluene dilution.

Resin Solubility Parameter

Recall that the solubility parameter of resins is estimated with the same correlation used for asphaltenes with the same fitted *b* value. They are assumed to be a monomer fraction of asphaltenes. This raises the question of what is the best solubility parameter to use for resins: the lowest solubility parameter in the asphaltene distribution, the solubility parameter given by the correlation, or an average?

The solubility parameter given by correlation with the resin properties (measured density and molecular weight) as it was used in the previous section was selected as the reference value for the sensitivity analysis. The uncertainty of the resin parameter based on the uncertainty of the molecular weight of resins (± 15%) used in the correlation is from ±0.01 to ± 0.02 $MPa^{0.5}$. Table 7-14 shows the solubility parameter for resins and asphaltenes obtained from the correlation based on the measured resin molecular weight (δ resins) and the lowest and highest molecular weight of asphaltene (δ minimum and δ maximum). The lower values and higher values of the solubility parameter were tested.

Table 7-14. Solubility parameters of resins and asphaltenes at 20°C.

Sample	δ Resins $MPa^{0.5}$	δ min Asphaltenes $Mpa^{0.5}$	δ max Asphaltenes $MPa^{0.5}$
WC-B-B2	19.3	19.2	21.3
X-1360	19.9	21.0	23.7

Figure 7-14a shows that decreasing the solubility parameters by 1.0 $MPa^{0.5}$ gives a slightly higher asphaltene yield; however, this increase is not significant, no more than 1.6 wt% yield. Figure 7-14b shows that an increase in 0.6 $MPa^{0.5}$ does not affect significantly the results; however, a larger increase in the resin solubility parameter (within the average of minimum and maximum solubility parameter of asphaltenes) causes the model to predict resins precipitation which leads to significant error.

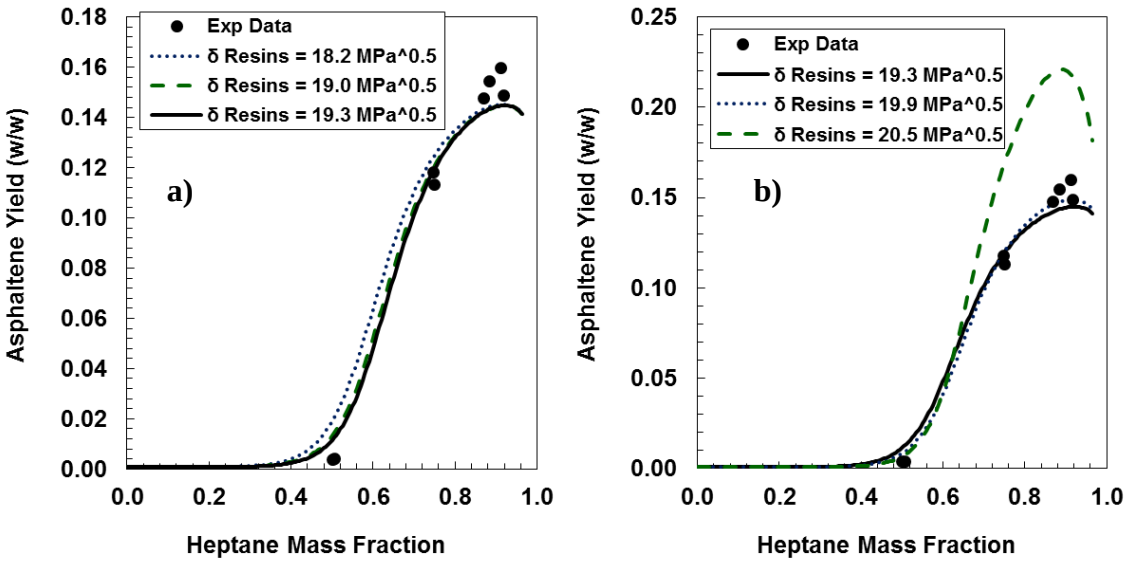

Figure 7-14. Asphaltene yield for WC-B-B2 diluted with *n*-heptane at 20°C and effect of uncertainty in the solubility parameter of resins on the model results for: a) lower values; b) higher values of the solubility parameter than given by the correlation for native oils.

Figure 7-15a shows that the effect of lowering the solubility parameter of resins for the toluene diluted X-1360 sample is insignificant. However, as observed with the solubility parameter of aromatics, lowering the solubility parameter of resins will strongly affect the yield predictions for dilutions with no toluene, becoming unrealistic at low *n*-heptane contents, Figure 7-15b. Increasing the solubility parameter of resins for X-1360 toluene diluted oils does not affect the asphaltene yield at low heptane content but does predict precipitation of resins at higher *n*-heptane contents, Figure 7-16a. The increase becomes larger for the predictions with no toluene dilution, Figure 7-16b, giving inconsistent results when compared with the C7 asphaltene content. In general, applying the correlation developed for asphaltene solubility parameter seems to provide the best results in the model and is closer to solubility experimental data.

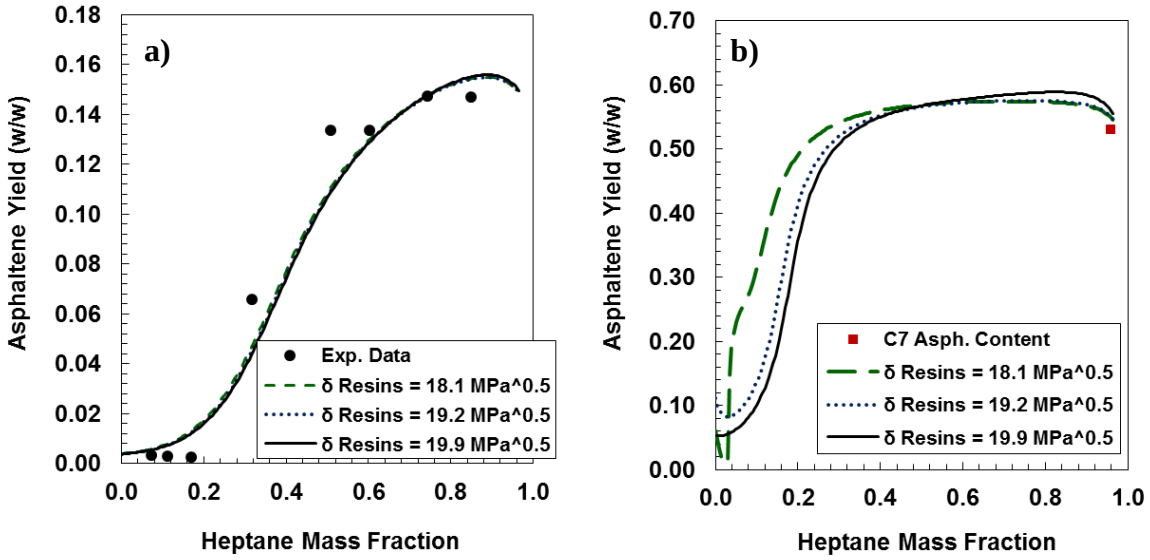

Figure 7-15. Asphaltene yield of X-1360 diluted with *n*-heptane at 20°C and effect of lower solubility parameter of resins on the model results for: a) toluene diluted sample; b) no toluene dilution.

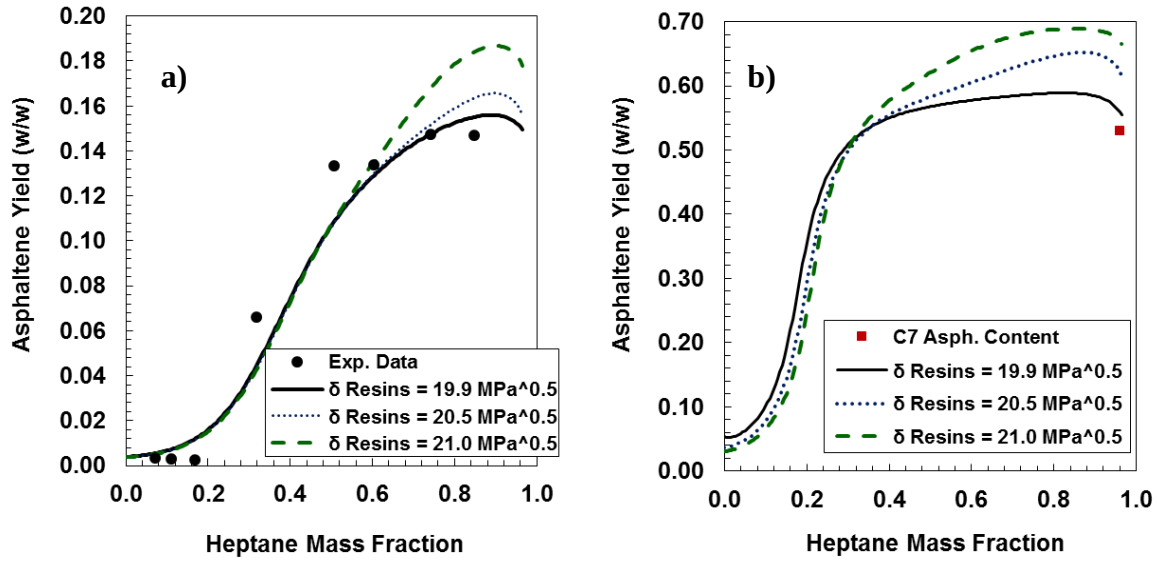

Figure 7-16. Asphaltene yield of X-1360 diluted with *n*-heptane at 20°C and effect of higher solubility parameter of resins on the model results for: a) toluene diluted sample; b) no toluene dilution.

7.4 Correlation of Parameter *b* to Average Molecular Weight of Asphaltenes in the Oil

Recall that the solubility parameter of asphaltenes was tuned by adjusting the value of *b* in the enthalpy of vaporization correlation (Eq. 5-10). An average *b* of 0.0634 was found to be appropriate for native oils. For reacted oils, the *b* value depended on the type and extent of reaction and was determined by fitting asphaltene-solvent solubility data for each sample. Hence, at this point, data from asphaltene-solvent systems are required in order to model crude oil stability for reacted oils.

In order eliminate the need for this time-intensive experimental data, a correlation of the *b* parameter to a more easily measured property is needed. A correlation would allow to model asphaltene precipitation data directly for crude oils without the need of applying step 1 (asphaltene characterization and modeling of asphaltene model systems) in the general methodology (Chapter 1). Correlations were sought with a variety of properties including density, H/C atomic ratio, and molecular weight, Appendix G. Some trends were observed only for a specific type of processes, for example, b vs conversion or b vs H/C atomic ratio for asphaltenes (one trend for HC samples

and another trend of TC samples), see Appendix G. The only consistent correlation, which applies to all the samples from different sources and processes, was observed between *b* value and the average molecular weight of asphaltenes, Figure 7-17. The average aggregated molecular weight of asphaltenes, MW_A, was correlated to *b* as follows,

$$b = 0.0634 + (1 - \varphi)(0.0645 - 0.0634) \quad \textbf{7-1}$$

where

$$\varphi = \frac{1}{2}\left[1 + erf\left(\frac{MW_A - 1025}{\sqrt{2(375)^2}}\right)\right] \quad \textbf{7-2}$$

Figure 7-17 shows that all the data follows in the correlation within the uncertainty of the fitted parameters with the exception of only two data points. Note, the error bars for the data are ±0.0001 for *b* and ±10% for the molecular weight. WC-SR-A3, the green closed circle outlier, is a native oil, with an asphaltene average density significantly lower than any of the other native oils. Therefore, as explained in the sensitivity analysis in Chapter 5, the value of *b* was higher to compensate for the lower density. The closed circle outlier is a native oil from Akbarzadeh *et al.* (2005) and the uncertainty and repeatability of the experimental data used to tune the model is unknown. Therefore, it is not possible to determine if the deviation comes from experimental data or something different about the sample.

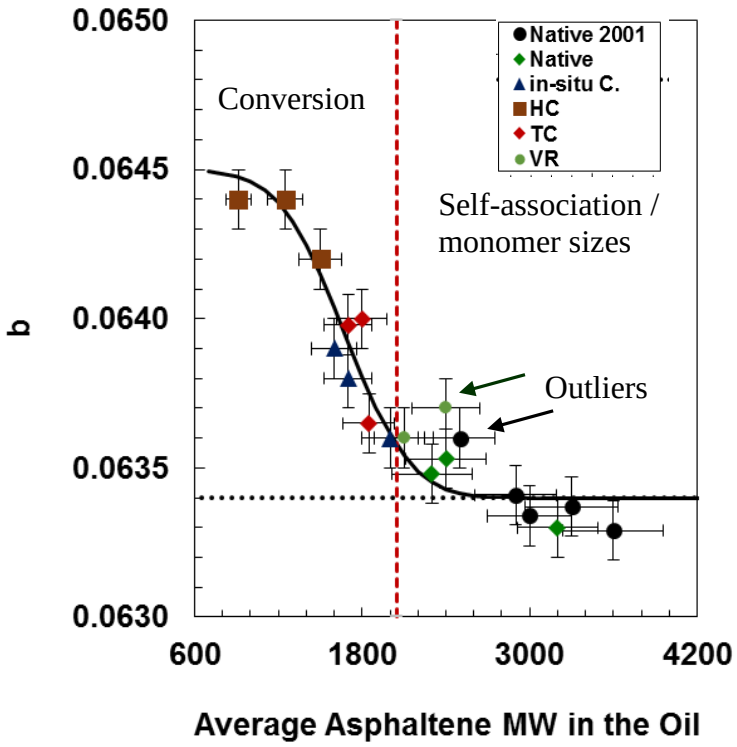

Figure 7-17. Average aggregated molecular weight fitted for all the oil samples as function of the fitted b value from asphaltene-solvent systems and its correlation.

It is not obvious why the asphaltene apparent heat of vaporization (*b* parameter) would correlate to the average aggregate molecular weight. Rather, it is likely that the average molecular weight is a proxy for differences in monomer properties for reacted asphaltenes. For example, cracked asphaltenes are likely more aromatic (higher heat of vaporization) and less soluble in heptane (larger *b* for higher solubility parameter). These cracked components coincidentally self-associate less than the original asphaltenes; hence, a negative correlation arises between *b* and average aggregate molecular weight.

The weakness of the proxy relationship becomes obvious when the correlation for asphaltenes in crude oil is compared with the correlation for asphaltenes in solvents, Figure 7-18. The two correlations do not match. It is known that asphaltenes self-associate less in the presence of resins (Yarranton, *et al.*, 2003) and therefore the average molecular weights in the crude oil are less than in the solvent even though the monomers are the same. The proxy correlation cannot account for

a difference in self-association caused by the medium rather than by the monomer properties. Nonetheless, the correlation appears to provide consistent results for asphaltenes in native and reacted crude oils.

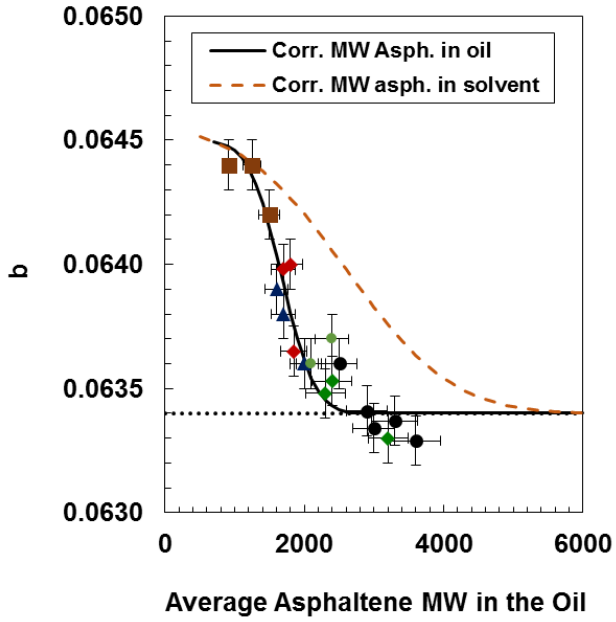

Figure 7-18. Comparison of the molecular weight of asphaltenes in solvent (toluene) and the b value.

7.5 Chapter Summary

The regular solution model was successfully used to model asphaltene precipitation from bitumen and heavy fractions of native oils and mildly and highly reacted oils from in-situ conversion, visbreaking and hydrocraking processes. The inputs into the model are SARA composition, molecular weight, density and solubility parameters of the SAR fractions, the density distribution of asphaltenes, and the *b* parameter for the solubility parameter correlation. The fitting parameters are the molecular weight of nano-aggregated asphaltenes and the shape factor in the gamma distribution for fine tuning.

SARA composition was measured for all the samples. The SARA composition of native oils varied depending on the origin of the oils. The SARA composition of the reacted samples was altered by

reaction but no consistent trend was observed with conversion alone except that the asphaltene content consistently increased with the extent of reaction.

Crude oil stability was modeled for native and reacted oils. Native oils have similar onset of asphaltene precipitation, which was captured when fitting the model. An average value of *b* of 0.0634 in the solubility parameter correlation gave similar results to those of the individually tuned *b* values and therefore is recommend for use with any native oil. Additionally, the model was able to predict the asphaltene yield data in *n*-pentane without any further adjustment, confirming its predictive capability.

Asphaltene precipitation from reacted oils was also successfully modeled with deviations (ARD) lower than 1%. In general, reaction decreased asphaltene solubility by making less soluble asphaltenes with lower onsets and maltenes with poorer solvency power, that is, lower solubility parameters. Additionally, oils from thermo- and hydrocracked processes had a significant amount of toluene insolubles which was captured in the model. Hydrocracked oils with average asphaltene molecular weights lower than 1500 g/mol, close to the monomer molecular weight, could not be modeled by fitting the average molecular weight. Hence, the value of *a* in the solubility parameter correlation was used as a fitting parameter instead.

A sensitivity analysis was performed to study the effect of the main additional input variables in the model: solubility parameter of saturates, aromatics and resins. The solubility parameter of saturates have very little effect in the model results and the ±0.3 $MPa^{0.5}$ uncertainty in its value will not affect the model results. The uncertainty of the aromatics solubility parameter was ±0.3 $MPa^{0.5}$ and had little effect on the model results for heavy fractions and diluted mixtures. The greatest impact, 10% error, was at the low heptane mass fraction range for non-diluted thermocracked samples. The solubility parameter of resins was not estimated with experimental data but instead was calculated using the asphaltene solubility parameter correlation applied to the measured density and molecular weight of resins. The correlation provided better results than setting the resin solubility parameter to the lowest or average solubility parameter of asphaltenes.

A correlation was found for the *b* value in the solubility parameter correlation as a function of the average molecular weight of asphaltenes in the oil. The correlation can be used to reduce the amount of data collection required to tune the model for asphaltene-solvent and heavy crude oil/solvent systems.

Chapter Eight: Regular Solution Modeling for Whole Native and Reacted Crude Oils

In Chapter 7, the modified regular solution approach was applied to model asphaltene precipitation data from native and reacted heavy fractions characterized based on SARA assays. SARA characterization is only applicable to heavy oils or residues from distillation which have a negligible amount of distillables. In this chapter, the regular solution model is applied to oils with non-negligible amounts of distillables. A characterization methodology is developed for the distillables based on a distillation assay. Solubility curves are measured for the "whole" oils, including both the heavy (SARA characterized) fraction and the distillables. The solubility data are then modeled using the combined characterization: distillation assays for the distillable fraction and the SARA assay for the non-distillable residue.

8.1 Characterization of the Distillable Fraction

Characterization of the distillable fraction is required to estimate the input properties for the regular solution model. In refinery operations, distillable components are commonly characterized for phase behavior modeling using distillation assays (Riazi 2005) and, therefore, the characterization for regular solution modeling was also based on distillation assays. The distillation (true boiling point or TBP) curve is pseudoized (divided in a specific number of pseudo-components) using a standard methodology.

As discussed in Chapter 3, two distillation experiments were used in this work:

1) the ADC distillation to remove all the material that distills below 300°C as measured in the boiling pot. In other words, the residue is a 300+°C residue. The ADC residue was used for the SARA fractionation. The ADC distillables are the material to be characterized here.
2) the spinning band distillation (SBD) to determine the TBP curve. This TBP is used for the pseudoization method.

8.1.1 Distillation Curves and Pseudoization

The first step is to fit a Gaussian distribution to the TBP distillation data measured for the whole oil, Figure 8-1. The temperature ($T_{b\ max}$) corresponding to the volume fraction distilled with the

ADC (V_{max}) is identified. The TBP curve for the distillable fraction is then the TBP curve of the whole oil truncated to Tb_{max}. The truncated TBP curve is divided in 5 pseudo-components of equal temperature range. Note, the extrapolation of the Gaussian distribution data above the maximum volume distilled is not used.

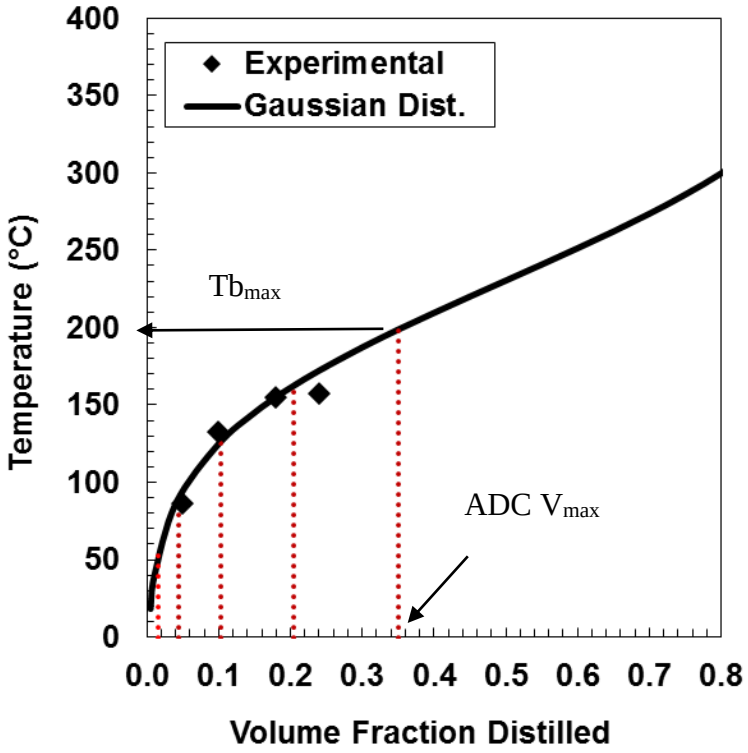

Figure 8-1. TBP distillation curve at atmospheric pressure obtained from the SBD and pseudoization in 5 pseudo-components with equal temperature range for in-situ converted oil 26845.

8.1.2 Distillate Properties Estimation

The following properties of each of the defined pseudo-components must be estimated: density, molecular weight, and solubility parameter. Density is determined with a Gaussian distribution constrained with an average set to the measured density of the crude oil and the measured density of the distillate. The molecular weight is estimated using Riazi-Daubert correlation (Eq. 2-1)

A method is required to determine the solubility parameter. One approach is to correlate the solubility parameter directly to a commonly measured property, in this case the boiling point. Figure 8-2 shows that the solubility parameter as a function of the boiling point has different trends for different chemical families. Since distillables are a mixture of components from different chemical families, a generalized correlation for the solubility parameter of a distillable cut cannot be constructed based on boiling point data alone. Data on the proportion of each chemical family would also be required or other properties, sensitive to the chemical family, would have to be included in the correlation. While such an approach is possible, a more straightforward alternative was investigated.

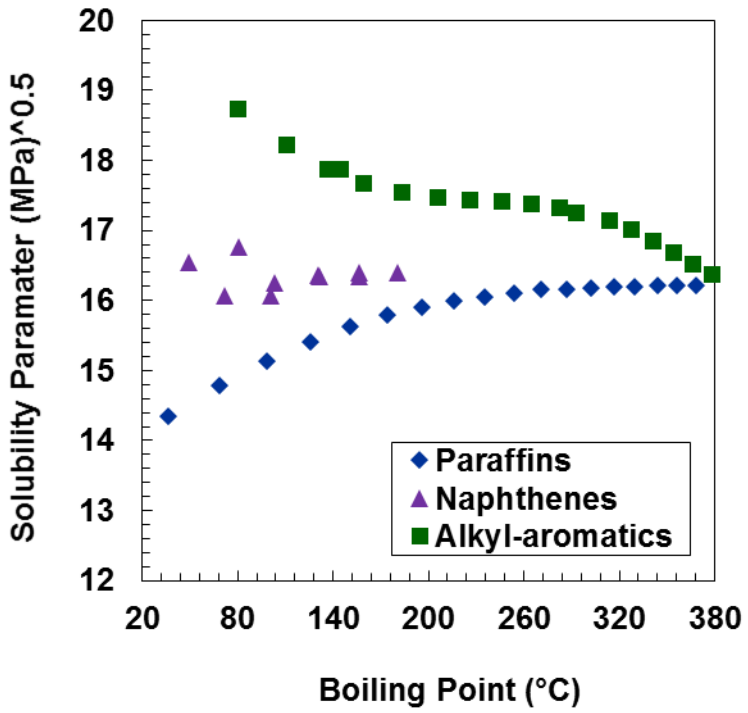

Figure 8-2. Solubility parameter at 25°C as function of the boiling point of different chemical families.

This alternative is to start from the definition of the solubility parameter, (Eq. 4-23), repeated here for convenience:

$$\delta_i = \left(\frac{\Delta H_i^{vap*} - RT}{v_i} \right)^{1/2} \qquad \textbf{8-1}$$

Once the density and molecular weights of the pseudo-component are known, the molar volume is easily calculated. Recall that ΔH_i^{vap*} is the enthalpy of vaporization of component *i* modified slightly to match a known solubility parameter. The challenge is to develop a correlation for this modified enthalpy of vaporization that can be applied to distillable pseudo-components.

The modified enthalpy of vaporization was determined for a number of pure components using their solubility parameters as reported in the literature (NIST 2014; Riazi, 2005). Interestingly, the modified enthalpies of vaporization for all the chemical families appear to follow the same trend with boiling temperature at temperatures below 300°C, Figure 8-3. Additionally, the modified enthalpies of vaporization match closely the experimental data for the actual enthalpies of vaporization available in the literature. Therefore, instead of correlating solubility parameter to boiling point, the modified enthalpy of vaporization was correlated to boiling point.

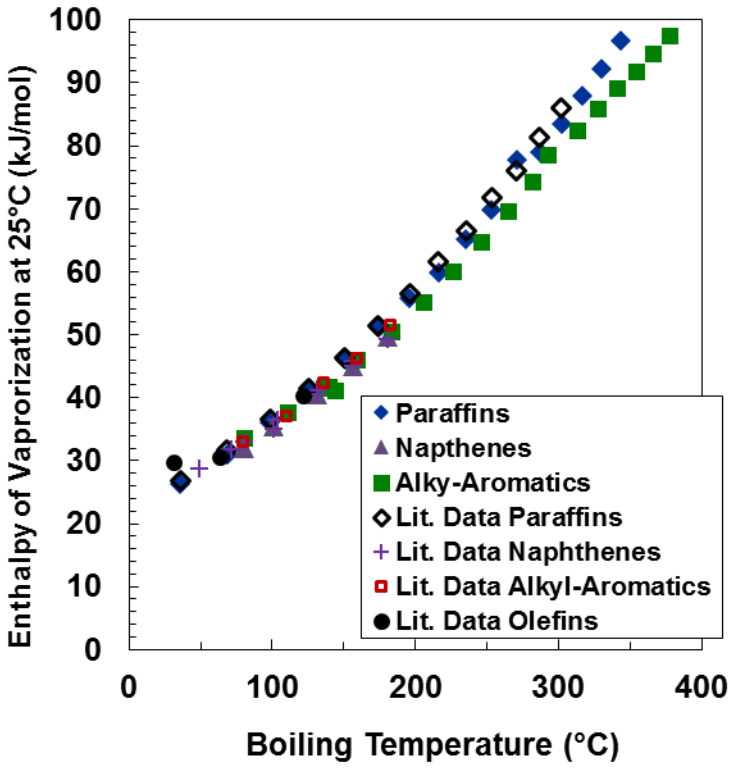

Figure 8-3. Apparent enthalpy of vaporization (solid symbols) and actual enthalpy of vaporization data from the literature at standard conditions (open symbols) versus boiling point for different chemical families.

Table 8-1 lists five correlations, usually applied for hydrocarbons, which were tested for correlating the modified enthalpy of vaporization at 25°C. Two of the correlations require the critical properties and these were estimated using Riazi-Daubert method (Riazi 2005). Most of the correlations give the enthalpy of vaporization at the boiling point and the Watson correlation (see Chapter 2) was used to convert the enthalpy of vaporization at 25°C. Figure 8-4 shows that these correlations do not match the trend of the modified enthalpy of vaporization (nor the literature data) and have large deviations at temperatures larger than 100°C.

Table 8-1. Correlations used to predict properties of the distillable pseudo-components.

Correlation	**Dependent Variables**	**Eq. #**
Enthalpy of Vaporization*		
Vetere 1	Tb, Tc, Pc	Eq.2-5
Vetere 2	Tb, MW	Eq. 2-6
Chen	Tb, Tc, Pc	Eq. 2-4
Trouton's rule	Tb	Eq. 2-7
Temperature Correction*		
Watson	Tb, Tc	Eq. 2-9
Critical Properties**		
Critical pressure – Riazi		Eq. 2-3
Critical temperature - Riazi		Eq. 2-2

*Riazi (2005) ** Poling *et al*. (2001)

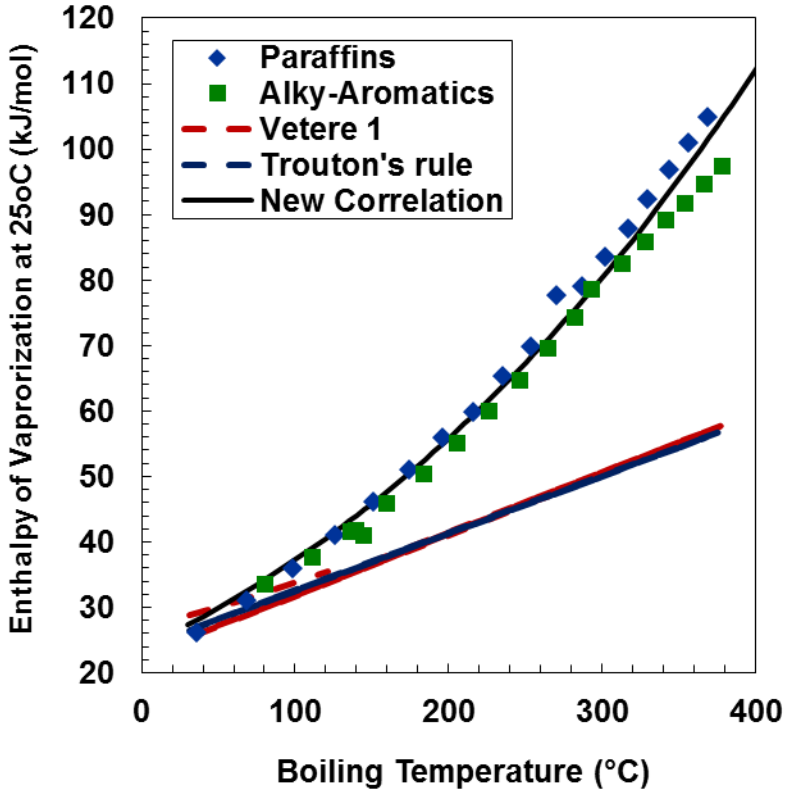

Figure 8-4. Fitted and correlated apparent enthalpy of vaporization for light hydrocarbons.

Since the available correlations for enthalpy of vaporization proved unsuccessful, the following empirical equation was fitted to the modified enthalpies of vaporization,

$$ln\Delta H^{25,vap*} = 12.38 + 4.62 * \left(1 - \exp\left(\frac{-T_b}{980}\right)\right) \qquad \textbf{8-2}$$

where $\Delta H^{25,vap*}$ is the modified enthalpy of vaporization at 25°C and T_b is the boiling point in °C. The only input to Equation 8-2 is the boiling point of the component or pseudo-component. Figure 8-4 shows the fit of the correlation to the modified enthalpies of vaporization of pure components. The average and maximum deviation below a boiling point of 300°C are 1.6 kJ/mol and 5.1 kJ/mol, respectively.

8.1.3 Validation of Distillables Solubility Parameter

To verify the average solubility parameter of the distillable fraction, asphaltene solubility experiments were performed on 27034-087 asphaltenes in mixtures of:

- toluene and distillable fraction
- heptane and distillable fraction

Note that the distillable fraction is a mixture of paraffinic, naphthenic, and aromatic compounds; hence, mixtures in both toluene and *n*-heptane were tested.

The average properties of the 27034-087 distillate, Table 8-2, were calculated from the properties of five pseudo-components and input into the asphaltene-solvent model. "High" and "Low" solubility parameter values (based on the sensitivity study presented later) were also determined. Figures 8-5a and 8-5b compare the model predictions with solubility data for asphaltenes in distillate and heptane and in distillate and toluene, respectively. The unmodified correlation for the enthalpy of vaporization gives the most consistent results for the modeling. Note, these results are model predictions with no adjustments to any parameters.

Table 8-2. Average properties for the ADC distillable fraction from 27034-87 in-situ converted oil.

Property	**Value**
MW, g/mol	124
Density, kg/m³	767
Solubility Parameter, $MPa^{0.5}$: Base	16.62
Solubility Parameter, $MPa^{0.5}$: High	16.90
Solubility Parameter, $MPa^{0.5}$: Low	16.11

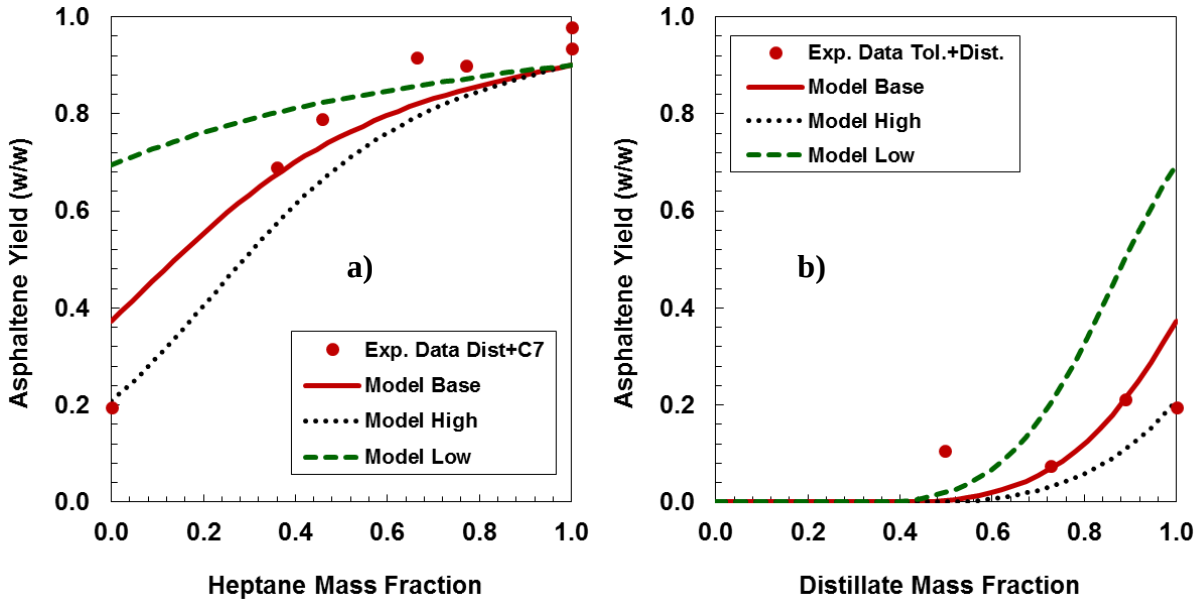

Figure 8-5. Measured and modeled asphaltene yield from mixtures of asphaltenes in: a) distillate+heptane; b) toluene+distillate; destillate from 27034-87 *in situ* converted oil and WC-B-B2 C7 asphaltenes.

The main deviation in the modeling is the asphaltene yield at low *n*-heptane mass fraction in solutions of distillates and *n*-heptane. The model with the unmodified distillate solubility parameter overpredicts the initial amount of insoluble asphaltenes in the distillate by 20 wt%. A possible explanation is that when asphaltenes are re-dissolved in the distillates (rather than toluene as was done for the asphaltene characterization), they self-associate differently (into a different molecular weight distribution). To test this idea, the model was rerun with a new value for α (the parameter which changes the shape of the gamma molecular weight distribution). Figure 8-6 shows that when α is changed from 2 (previously fitted for this asphaltenes, Chapter 4) to 5, the model now fits the initial amount of insoluble asphaltenes in the distillates.

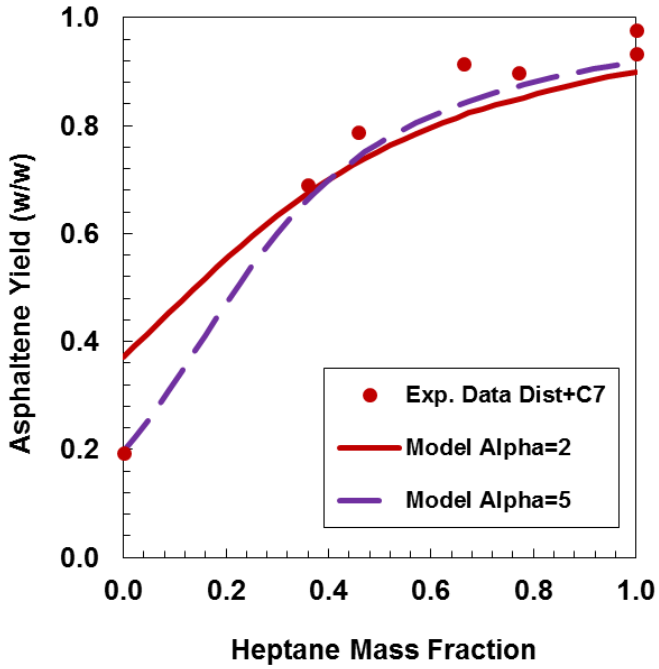

Figure 8-6. Measured and modeled asphaltene yield from mixtures of asphaltenes, distillables, and *n*-heptane at 22°C and atmospheric pressure; distillables from 27034-87 in-situ converted oil.

8.2 Modeling Crude Oils with Distillables

Two native, three in-situ converted, and the unknown 27-168-179 crude oil samples had a sufficient amount of distillables (>20 vol%) to evaluate the distillable characterization for regular solution modeling. The regular solution model was applied to these "whole" oils (crude oil before distillation) in three steps:

1) Model the heavy fraction characterized based on SARA fractionation (Chapter 7) to determine the molecular weight of the asphaltenes in the oil.
2) Fit a Gaussian distribution to the distillation assay, divide the distribution into 5 pseudo-components, and estimate properties for each pseudo-component.
3) Model the whole oil with the SARA based pseudo-components for the heavy fraction (Chapter 7), the 5 pseudo-components from Step 2, and the MW of the asphaltenes in the oil from Step 1.

Native Oils

The Arabian medium oil is a native oil with large amount of distillables and it is presented in this section. Results for a native and 27-168-179 samples are presented in Appendix F. Table 8-3 shows the properties of each pseudo-component. The complete asphaltene characterization was presented in Chapter 7. Figure 8-7 shows the model fit for the heavy fraction (black dashed line) and the model prediction for the "whole" oil (red solid line). The prediction is within the error of the yield measurement, confirming the validity of the distillable characterization.

Table 8-3. Composition and properties of Arabian Medium oil pseudo-components.

Component	**Content wt%**	**Average T_b °C**	**Density kg/m³**	**MW g/mol**	**Solubility Parameter $MPa^{0.5}$**
Pseudo-1	1.3	33	514	57	15.08
Pseudo-2	2.2	67	582	78	14.90
Pseudo-3	4.8	101	650	100	15.09
Pseudo-4	8.7	136	718	121	15.58
Pseudo-5	13	170	786	140	16.31
Saturates	24	-	827	360	16.6
Aromatics	28	-	978	440	20.8
Resins	11	-	1048	990	19.18
Asphaltenes*	5	-	1180	2400	19.17-21.02

* average properties

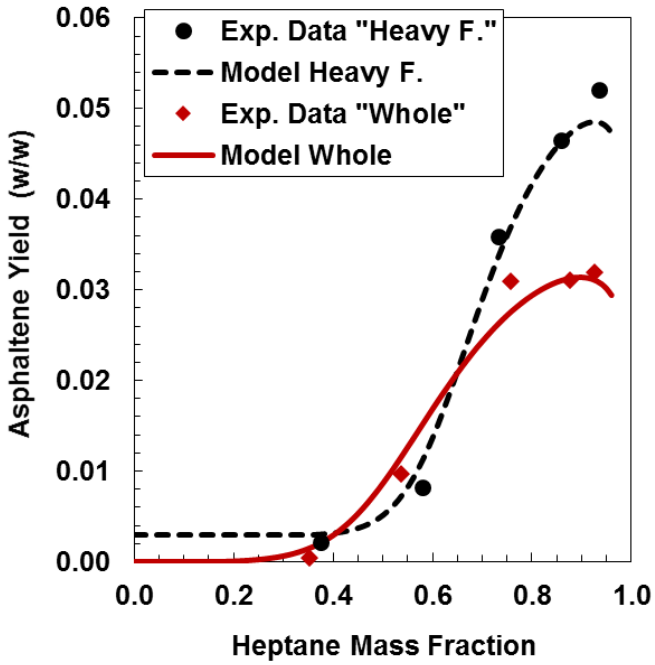

Figure 8-7. Asphaltene yield for heavy fraction and whole oil from Arabian medium oil diluted with *n*-heptane at 20°C and atmospheric pressure. Note, the whole oil contains 0.3 wt% toluene insolubles.

In-Situ Converted Oils

The in-situ converted oils had from 20 up to 60 vol% distillables. Table 8-4 shows the estimated properties for each pseudo-component for the in-situ converted samples. Figure 8-8 shows the model fitting and model predictions for the 27034-113 heavy fraction and the whole oil sample, respectively. Figure 8-9a and 8-9b shows the model predictions for the whole 27034-87 and 26845 in-situ converted samples. The model predictions for all the whole samples are very close to the experimental data with deviations lower than 0.5% for asphaltene contents lower than 5 wt% and deviations lower than 1% for higher asphaltene contents.

Table 8-4. Properties of the in-situ coverted oil pseudo-components.

Component	Content wt%	Average T_b °C	Density kg/m^3	MW g/mol	Solubility Parameter MPa$^{0.5}$
27034-113					
Pseudo-1	8.1	44	675	75	15.52
Pseudo-2	7.3	87	726	95	15.87
Pseudo-3	11.0	130	777	116	16.36
Pseudo-4	14.0	173	828	138	16.97
Pseudo-5	15.4	216	879	160	17.68
Saturates	11	-	841	330	16.1
Aromatics	15	-	1008	340	20.8
Resins	8	-	1059	830	19.44
Asphaltenes*	4	-		2000	20.67-22.41
27034-87					
Pseudo-1	7.7	48	590	72	14.97
Pseudo-2	8.2	97	669	99	15.25
Pseudo-3	12.8	145	749	126	15.91
Pseudo-4	16.3	193	828	151	16.88
Pseudo-5	17.0	242	908	174	18.11
Saturates	6	-	848	320	16.3
Aromatics	15	-	1028	300	20.6
Resins	4	-	1054	860	19.72
Asphaltenes*	3	-		1700	20.15-21.08
26845					
Pseudo-1	1.3	36	667	72	15.48
Pseudo-2	2.3	72	700	88	15.64
Pseudo-3	5.1	108	733	105	15.86
Pseudo-4	9.2	145	767	125	16.15
Pseudo-5	13.7	181	800	145	16.48
Saturates	12	-	861	360	16.5
Aromatics	31	-	1009	380	21.0
Resins	14	-	1063	880	19.88
Asphaltenes*	10	-		1600	19.80-21.57

* average properties

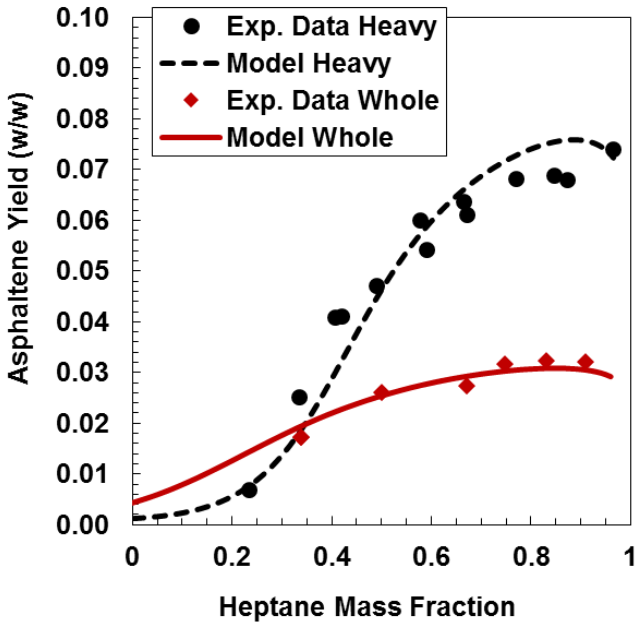

Figure 8-8. Asphaltene yield for heavy fraction and whole oil from in-situ converted oil 27034-113 diluted with *n*-heptane at 20°C and atmospheric pressure.

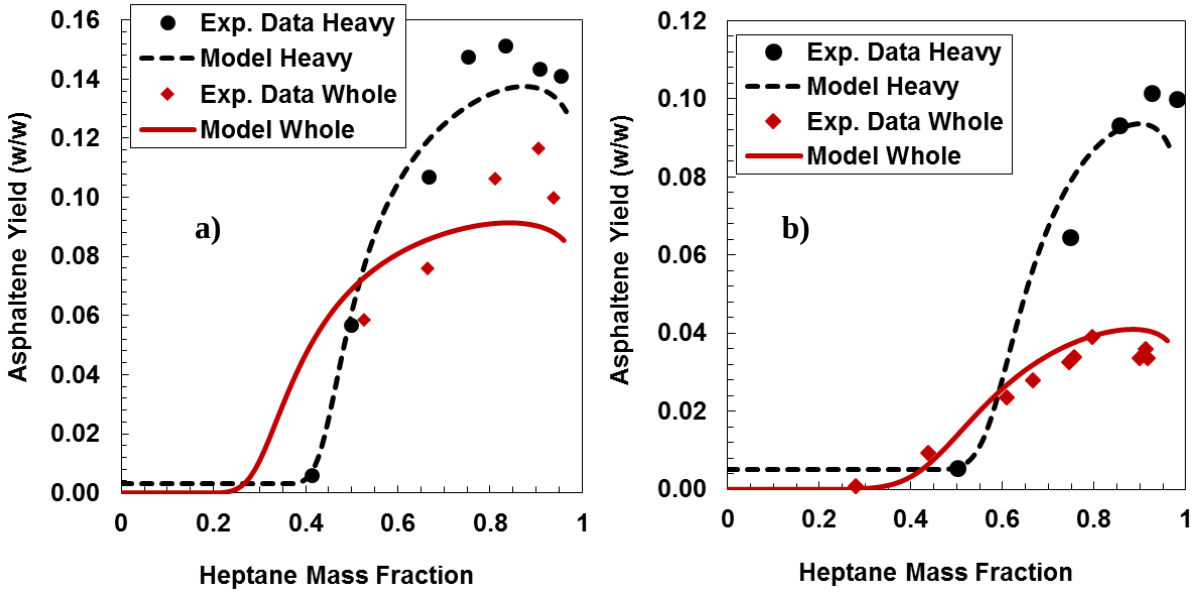

Figure 8-9. Asphaltene yield for heavy fraction and whole oil from in-situ converted oils 26845 (a) and 27034-87 (b) diluted with *n*-heptane at 20°C and atmospheric pressure.

8.3 Sensitivity Analysis.

This section analyses the effect on the model results due to small changes in the enthalpy of vaporization correlation for the solubility parameters of the pseudo-components from the distillation assays. The modified enthalpy of vaporization correlation (Eq. 8-2) was adjusted as follows:

High (trend1): more paraffinic (shift to the left in Figure 8-10):

$$ln\Delta H^{25,vap*} = 12.4 + 4.62 * \left(1 - \exp\left(\frac{-T_b}{960}\right)\right) \quad \textbf{8-3}$$

Low (trend 2): more alkyl-aromatic (shift to the right in Figure 8-10):

$$ln\Delta H^{25,vap*} = 12.3 + 4.62 * \left(1 - \exp\left(\frac{-T_b}{945}\right)\right) \quad \textbf{8-4}$$

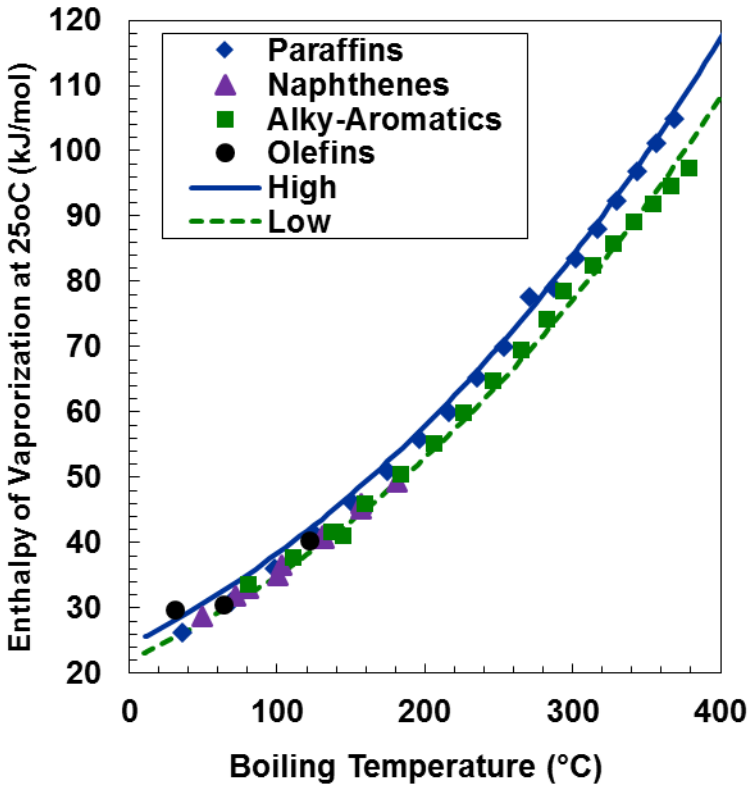

Figure 8-10. Enthalpy of vaporization correlation trends at 25°C and atmospheric pressure for hydrocarbon compounds.

Tables 8-5 and 8-6 show the solubility parameters for the five pseudo-components for the original correlation, high and low for the 27034-87 and Arabian oils, respectively. The lowest solubility parameters are obtained from low, making the distillable fraction a poorer solvent; hence, the model with parameters from low over predicts asphaltene precipitation, Figure 8-11 (dashed green line). The opposite effect was observed for the model with parameters from high, Figure 8-11 (dotted black line).

Table 8-5. Composition and properties of the distillable pseudo-components for 27031-113 in-situ converted sample.

	Volume fraction	Base	High	Low
1	0.105	15.52	15.72	14.92
2	0.089	15.87	16.11	15.31
3	0.124	16.36	16.63	15.85
4	0.149	16.97	17.28	16.49
5	0.154	17.68	18.02	17.22
Average δ		**16.62**	**16.90**	**16.11**

Table 8-6. Composition and properties of the distillable pseudo-components for Arabian oil.

	Volume fraction	Base	High	Low
1	0.022	15.08	15.27	13.70
2	0.033	14.90	15.11	13.60
3	0.065	15.09	15.32	13.82
4	0.106	15.58	15.84	14.31
5	0.144	16.31	16.61	15.03
Average δ		**15.69**	**15.95**	**14.40**

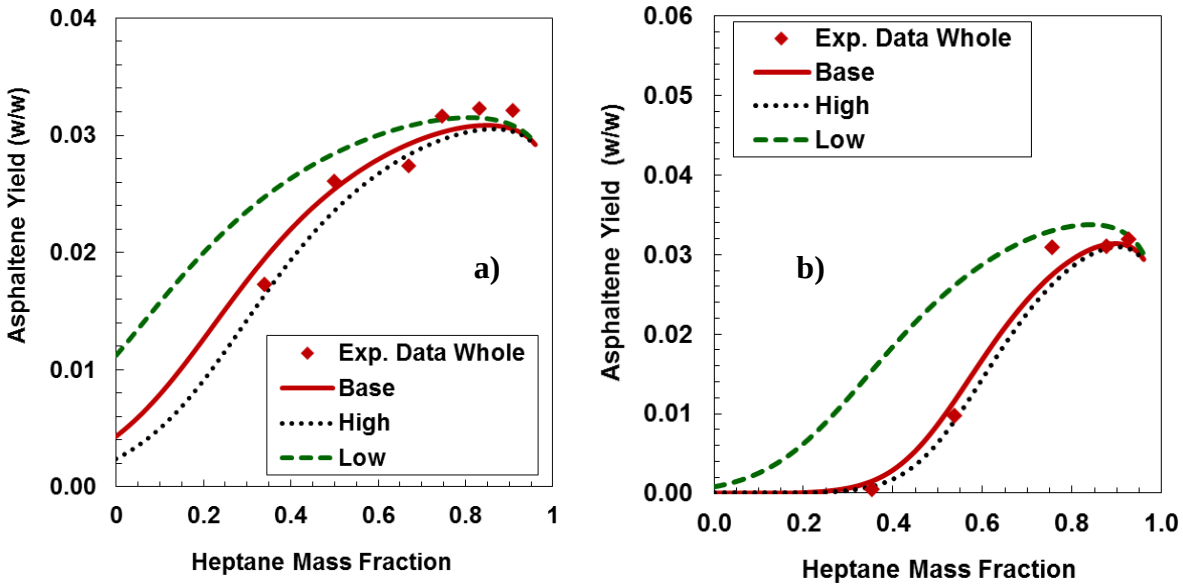

Figure 8-11. Asphaltene yield for whole crude oils diluted with n-heptane at 20°C: a) 27034-113 in-situ converted oil and b) Arabian medium oil at 20°C and atmospheric pressure using different enthalpy of vaporization correlations.

8.4 Generalized Model for Native and Reacted Crude Oils

The adapted regular solution approach has successfully modeled asphaltene precipitation from bitumens and heavy fractions from native and reacted oils as well as whole oils with distillables. The model was implemented with the proposed correlations presented in previous chapters for asphaltene densities and solubility parameters and with the measured properties (molecular weight, density and solubilities) for the SARA fractions (and distillable fraction). However, an important question arises: what is the minimum amount of experimental data set required to model the crude oil stability in terms of asphaltene precipitation?

At this point, the data requirements are:

- Atmospheric distillation assays (if the sample has >5 vol% distillables).
- SARA assay of non-distillable residue.
- Density, molecular weight, and solubility curves to calculate solubility parameter of saturates and aromatics

- Density and molecular weight of resins
- Density of asphaltenes
- One set of crude oil solubility data in a solvent (n-heptane is recommended) for tuning the model

These data requirements are onerous for many practical applications and it is desirable to find average properties or correlations to reduce the amount of data required. The distillation and SARA assays are essential to define the composition. Hence, the greatest potential to reduce data requirements is in the SARA fraction properties.

SAR Properties

Table 8-7 shows the average properties of the SAR fractions from the oils examined in this thesis. The ARD and AAD for molecular weight, density and solubility parameter of each crude oil samples are presented in Appendix A. Within each class of oil, the average absolute relative deviation, AARD, for the molecular weight was 6, 8 and 9% for saturates, aromatics and resins, respectively, all of which are within the uncertainty of the molecular weight data (~15%). The average absolute deviation, AAD, for density was 9, 13, and 7 kg/m^3 for the same respective fractions, all within the uncertainty of the density data (~15 kg/m^3). The AAD of the solubility parameter was 0.2 $MPa^{0.5}$ for both saturates and aromatics, both within the uncertainty of solubility parameters for saturates and aromatics (0.3 $MPa^{0.5}$). Since most of the deviation for the SAR fraction of the oils are within the previously defined uncertainty for each property, average properties can be used for each class of oil without the introduction of significant errors.

Table 8-7. Average properties from experimental data for the SAR fractions for each "type" of oil.

"Type" Of oil	Fraction	Molecular Weight g/mol	Density at 20°C kg/cm^3	Solubility Parameter MPa$^{0.5}$
Native	Saturates	393	870	16.5
	Aromatics	450	997	20.8
	Resins	1080	1068	-
Vacuum Residues	Saturates	735	865	16.5*
(from native oils)	Aromatics	790	1011	21.4
	Resins	1360	1052	-
In Situ Converted	Saturates	337	850	16.3
	Aromatics	340	1015	20.8
	Resins	857	1079	-
Thermocracked	Saturates	780	896	14.0
	Aromatics	740	1035	21.2
	Resins	1180	1076	-
Hydrocracked	Saturates	635	877	15.6
	Aromatics	530	1023	20.7
	Resins	788	1083	-

* Not enough sample to do solubility experiments. Value assumed equal to native oils.

Asphaltene Density Distribution

The asphaltene density distribution is defined by three parameters: the minimum density, ρ_{min}, the maximum density, ρ_{max}, and the exponential decay constant, τ. The minimum density is generalized for all the oils to a value of 1050 kg/m^3. The following guidelines are recommended for τ:

- native oils: τ =9,
- in situ: τ = 7,
- low conversion thermocracked and hydrocracked: τ= 7,
- high conversion thermocracked and hydrocracked: τ= 4.

Note high conversion is here defined as >30wt% for thermocracking and >60vol% for hydrocracking. The maximum density is generalized for native oils to 1200 kg/m³. It could not be generalized for reacted oils and must be determined from experimental data for these fluids.

Asphaltene Molecular Weight Distribution

The Gamma distribution used to represent the asphaltene molecular weight distribution is defined by three parameters: the monomer molecular weight, the average molecular weight, and the shape parameter, α. Recommended monomer molecular weights are 800 g/mol for native and *in situ* oils and 700 g/mol for highly reacted oils. Note, the error introduced by using 800 g/mol for highly reacted oils is negligible. The shape factor of native and thermocracked oils must be tuned but a value of 2.0 is recommended as a starting point. For thermo- and hydrocracked fluids, the shape factor correlates to the extent of conversion as shown in Figure 8-12 and can be closely approximated with the following correlations:

Thermocracked: $$\alpha = -0.0059(wt\%Conversion) + 0.7942$$ **8-5**

Hydrocracked: $$\alpha = -0.0156(vol\%Conversion) + 1.3869$$ **8-6**

The average molecular weight must still be determined by fitting solubility data for one solvent.

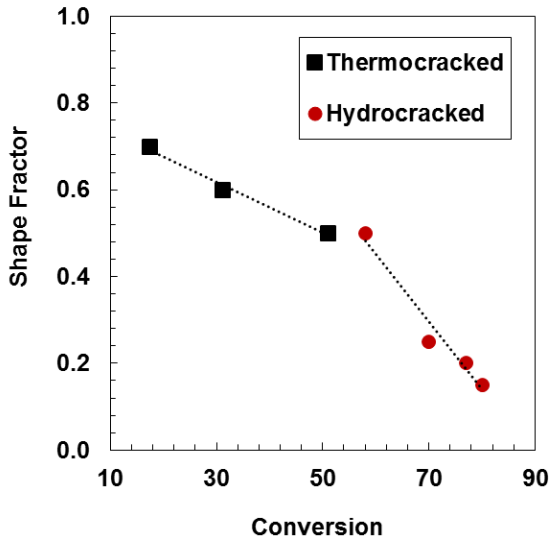

Figure 8-12. Shape factor in the gamma distribution as a function of the extent of reaction or conversion for thermocracked and hydrocracked oils.

Asphaltene Solubility Parameter

Once the asphaltene molecular weight and density distributions are defined, the only remaining parameters are the constants (*a* and *b*) in the enthalpy of vaporization correlation. The following guidelines for these parameters are recommended:

- *a* parameter = 9.72 for native, in situ and thermocracked oils.
- *b* parameter is determined as a function of the average molecular weight from Equation 7-1.
- If the average molecular weight <1500 g/mol, this value can be fixed and the parameter *a* will instead be the fitting parameter. This alternative is required for highly converted hydrocracked oils.

In summary, the minimum experimental data required to model asphaltene precipitation using the adapted regular solution model are:

- Distillation assay
- SARA assay
- Solubility curve with a solvent
- Asphaltene density

It is also helpful to know the processing history of the fluid (visbreaker or hydrocracker) and the extent of conversion. These are usually conditions known by the oil producer.

8.5 Chapter Summary

A combined characterization methodology (SARA + distillation assay) was successfully applied with the regular solution model to predict asphaltene precipitation for mildly reacted samples without adding any fitting parameter into the regular solution model. The distillable fraction was characterized with a distillation assay (or distillation curve); the distillation curve was fit with a Gaussian distribution and truncated at the maximum volume distilled with the ADC. The truncated curve was divided into five pseudo-components. The density of the pseudo-components was determined with a Gaussian distribution constrained with experimental density data. The molecular weight was estimated using the Riazi correlation. The solubility parameter was

correlated to the enthalpy of vaporization. The updated model fit solubility data for asphaltene-distillable-solvent model systems and successfully predicted crude oil stability. Using average properties and correlations, the data requirements for the model were reduced to: a distillation assay, a SARA assay, solubility data with one solvent, asphaltene density, and some knowledge of the processing history of the sample.

Chapter Nine: Conclusions and Recommendations

The main contribution of this thesis is an updated regular solution model, validated with experimental data, able to fit and predict asphaltene precipitation from both native and reacted crude oils. For tuning, the model requires measurements of asphaltene density and asphaltene yields in one solvent, such as *n*-heptane, at one temperature and pressure. The updated model also accounts for the distillable components. The characterization methodology allows for the prediction of the stability of separated oil fractions and of blends and therefore is ideally suited for refinery applications. More detailed conclusions and recommendations for future research are provided below.

9.1 Conclusions

Characterization of Asphaltenes:

Molecular weight distributions of asphaltenes were reconstructed based on experimental data using the self-association model. The asphaltenes were best represented as a mixture of neutral (non-associating species) and associating species. For convenience, the model distribution (including both neutrals and associating species) was fitted with a single Gamma distribution.

Asphaltenes from native oils had molecular weight distributions from an average monomer molecular weight of 800 g/mol to maximum aggregate sizes ranging from 20,000 to 50,000 g/mol depending on the oil source. The amount of neutrals was less than 4 wt%. Asphaltenes from reacted thermocracked oils (in-situ and visbreaker processes) had slightly narrower distributions and an amount of neutrals up to 13 wt%. Asphaltenes from hydrocracked oils had much narrower molecular weight distributions and neutrals up to 23wt%.

The effect of temperature on molecular weight and molecular weight distributions was also studied for asphaltenes from native and reacted oils. In general, the average aggregated molecular weight of asphaltenes from native and thermocracked oils (in-situ and visbreaker) decreased as temperature increased. Temperature did not have a detectable effect on the molecular weight of

asphaltenes from hydrocracked oils probably because these asphaltenes were already largely dissociated.

The temperature dependence for asphaltenes from native and thermocracked oils followed a linear trend with a different slope for each sample. The linear trends were extrapolated to higher temperatures for all the samples and, interestingly, all intersected over a small range of temperature and molecular weight defining an apparent universal monomer condition at 250°C and 800 g/mol. This common apparent monomer temperature was used to construct a temperature dependence correlation applicable for all type of asphaltenes. The correlation is valid between the measured conditions of 20 to 90°C.

Density distributions showed an initial steep increase in density versus cumulative mass fraction, reaching a plateau at a relatively low mass fraction interpreted as the mass fraction of neutrals. Native asphaltenes had almost identical density distributions with a maximum density of 1200 kg/m³. Reacted asphaltenes had higher densities than native oils and the maximum density increased with extent of conversion up to 1300 kg/m³.

Solubility parameters of asphaltenes were determined by fitting the regular solution model to asphaltene solubility data. The solubility parameters were then fitted with an updated correlation proposed in this thesis which applied to both native and reacted oils. The new solubility parameter correlation was based on the defined relationship between solubility parameter and the enthalpy of vaporization. An empirical correlation was proposed for the "apparent" enthalpy of vaporization of asphaltenes at standard conditions. The correlation has one fitting parameter, *b*, which had an average value of 0.0634 for native oils and increased for reacted asphaltenes. Increasing b values indicated higher solubility parameters, thus, less soluble asphaltenes.

The refractive index and elemental composition were also measured for asphaltenes to study the effect of reaction and to aid in future work on property correlations. The refractive index for native oils was between 1.725 and 1.755 but significantly increased for asphaltenes from reacted oils up to 1.890. Consistently to previous founding for pure hydrocarbon compounds (*n*-alkanes and alkyl-

aromatics), the refractive index had been found to be proportional to density for all SARA fractions and the trends were consistent with the density data. The H/C ratio for asphaltenes from native oils was between 0.9 and 1.2, consistent with literature data. The H/C ratio significantly decreased for asphaltenes from thermocracked and hydrocracked oils indicating more aromatic asphaltenes. The nitrogen content did not significantly change for thermocracked asphaltenes in comparison with native asphaltenes; however, it increased for hydrocracked asphaltenes. Sulfur content was significantly reduced for hydrocracked asphaltenes.

Characterization of SAR Fractions

The molecular weight of SAR fractions of native oils was consistent with previous literature data within a small range of variation. The molecular weight of SAR fractions from vacuum residues was higher due to the removal of lighter compounds of each fraction during the vacuum distillation. The density of SAR fraction from native oils were also consistent with previous literature data.

The molecular weight of SAR fractions from reacted samples showed a slight reduction. Additional conversion seemed to redistribute the molecular weight of the SAR fractions rather than reducing it. For example, the aromatics molecular weight was lower than the saturates molecular weight the opposite trend is observed for native fractions. Thermocracking reactions did not significantly change the density of the SAR fractions. Hydrocracking slightly increased the density of the aromatic and resin fractions. Small changes in density indicated that this property is mostly related to chemical families, that is, each chemical family, independent of its size (molecular weight), has a density that is within a small range.

The solubility parameters of saturates and aromatics were indirectly estimated using the regular solution model. Saturates and aromatics from different native oils had the same average solubility parameters for each type of fraction. Saturates from thermo- and hydrocracked oils had lower solubility parameters than native saturates; that is, reacted saturates were poorer solvents for asphaltenes. The solubility parameters of aromatics from reacted samples also decreased but to a lesser extent than the saturate solubility parameters. Overall, reaction made maltenes poorer solvents for asphaltenes with lower solubility parameters.

Refractive index and elemental analysis was also measured to study the effect of reaction the chemistry of the SAR fractions. The H/C ratio decreased for reacted aromatics and resins but it did not have a significant change for saturates. The sulfur content was reduced for reacted saturates and resins but did not change significantly for aromatics. Nitrogen content increased for reacted aromatics and resins.

Heavy Fraction Modeling

The regular solution model was successfully applied to model asphaltene precipitation from bitumen and heavy fractions of native and reacted oils from in-situ conversion, visbreaking and hydrocracking processes. The measured and estimated properties and distributions for the SARA fractions were used as inputs into the model. The model initially had two main fitting parameters: 1) the *b* parameter in the asphaltene solubility parameter correlation; 2) the average molecular weight of nano-aggregated asphaltenes, except for hydrocracked oils. For hydrocracked oils, the value of *a* in the apparent enthalpy of vaporization of asphaltenes was used as the fitting parameter because the average nano-aggregate molecular weight of asphaltenes was very low (<1500 g/mol) and close to the average monomer molecular weight of 800 g/mol. The shape factor in the gamma distribution was taken from fitted asphaltene-solvent data or used as a secondary fitting parameter for fine tuning the model.

Native oils had similar onset of asphaltene precipitation but their yields differed depending on the asphaltene content of the oil. In general, reaction decreased asphaltene solubility by making less soluble asphaltenes with lower onsets. After fitting precipitation data from *n*-heptane diluted oils, the model was able to predict the asphaltene onset and yield data in *n*-pentane without any further adjustment. Asphaltene precipitation from reacted oils was also successfully modeled with deviations (ARD) lower than 1%.

A correlation was found for the *b* value in the solubility parameter correlation as a function of the average molecular weight of asphaltenes in the oil. The correlation reduces the number of fitting parameters to two: 1) the average molecular weight of the asphaltenes (or *a* parameter in solubility

parameter correlation for hydrocracked asphaltenes) for major tuning; the α parameter in the Gamma distribution for fine tuning.

Whole Oil Modeling

A combined characterization methodology (SARA + distillation assay) was successfully applied to predict asphaltene precipitation for native and in-situ converted samples without adding any fitting parameters. The Spinning Band distillation curve was fit with a Gaussian distribution and truncated at the maximum volume distilled with the ADC distillation. The truncated curve was divided into five pseudo-components. Density was determined with a Gaussian distribution constrained with the measured average density. The molecular weight was estimated using the Riazi method. The solubility parameter was determined based on the defined relationship between solubility parameter and the enthalpy of vaporization. A correlation for the enthalpy of vaporization was developed based on data for pure hydrocarbon compounds.

9.2 Recommendations

It is recommended to test the new correlations and updated modeling approach on blends of native-native and native-reacted oils using the characterization data of the individual oils. Mixing rules should be tested and/or developed; for example, for the *b* parameter in the solubility parameter correlation.

A large database of experimental data was generated for several different crude oil fractions from native and highly reacted oils. The database includes compositions, molecular weights, densities, solubility parameters, refractive indexes, and elemental compositions. It is recommended to analyse the data base for property relationships and correlations that can be used to predict physical properties based on other "easy-to-measure" properties. Such correlations could be used to reduce data requirements saving time and cost in industrial applications. For example, the density of reacted asphaltenes must be measured for the current modeling approach because it changes with reaction and has not yet been correlated to a reaction indicator. It is recommended to explore correlations to estimate the whole or the maximum density of reacted asphaltenes with the extent of reaction to eliminate the density measurement requirement.

The correlation for the apparent enthalpy of vaporization of asphaltenes can be adapted/modified to be applied at different temperatures and pressures for applications such as live oils. Correlations have already been developed for properties of solvents as function of temperature and pressure (Saryazdi, et al. 2013) that can be implemented in the regular solution model approach.

9.3 Main Contributions of the Thesis.

The main contribution from the thesis is the successful updating of the regular solution approach to model asphaltene precipitation from both native and reacted oils. The author is not aware of any other model approach capable of modeling asphaltene precipitation from highly reacted oils. Specific contributions are:

1. the quantification of the changes in the property distributions of asphaltenes with reaction for input into the regular solution model of asphaltene precipitation.
2. the detailed characterization of native and reacted saturates, aromatics and resins fractions for input into the regular solution model. Until now, there were limited characterization data for these fraction from native oils and even less for reacted SAR fractions.
3. the development of a methodology to incorporate a combined characterization of distillable fractions based on a standard distillation assay and the residue based on a SARA assay.
4. a working implementation of the regular solution model including the combined characterization which predicts crude oil stability in terms of asphaltene precipitation for both native and reacted oils. The model can be used or adapted for use in production and refining process simulation.

References

Agrawal, P, F F Schoeggl, M A Satyro, and H W Yarranton. 2011. "Case Study : Modeling the Phase Behavior of Solvent Diluted Bitumen." *Canadian Society for Unconventional Gas. SPE International*, no. 2: 1–17.

Agrawala, M., and Yarranton, H.W. 2001. "An Asphaltene Association Model Analogous to Linear Polymerization." *Industrial & Engineering Chemistry Research* 40 (21): 4664–72.

Akbarzadeh, K., Alboudwarej, H., Svrcek, W., and Yarranton, H.W., 2005. "A Generalized Regular Solution Model for Asphaltene Precipitation from N-Alkane Diluted Heavy Oils and Bitumens." *Fluid Phase Equilibria* 232 (1-2): 159–70.

Akbarzadeh, K ., Dhillon, A., Svrcek, W., Yarranton H.W. 2004. "Methodology for the Characterization and Modeling of Asphaltene Precipitation from Heavy Oils Diluted with N -Alkanes." *Energy & Fuels* 18 (9): 1434–41.

Akbarzadeh, K., Hammami, H., Kharrat, A., Zhang, D., Allenson, S.,Creek, J., Kabir, S.. 2007. "Asphaltenes: Problematic but Rich in Potential." *Oildfield Review*.

Alboudwarej, H., Akbarzadeh, K., Beck, J., Svrcek, W., Yarranton H. 2003. "Regular Solution Model for Asphaltene Precipitation from Bitumens and Solvents." *AIChE Journal* 49 (11): 2948–56.

Alshareef, A. H., Scherer, A., Tan, X., Azyat, K., Stryker, J., Tykwinski,r., Gray, M.. 2011. "Formation of Archipelago Structures during Thermal Cracking Implicates a Chemical Mechanism for the Formation of Petroleum Asphaltenes." *Energy & Fuels* 25 (5): 2130–36.

Altgelt, K. H., and Boduszynski, M. 1994. *Composition and Analysis of Heavy Petroleum Fractions*. New York: Marcel Dekker.

Ancheyta, J, Centeno, J.G, Trejo, F., Marroquın, G. 2003. "Changes in Asphaltene Properties during Hydrotreating of Heavy Crudes." *Energy & Fuels* 17 (6): 1233–38.

Ancheyta, J., Trejo, F., Rana, M. 2010. *Asphaltenes: Chemical Transformations During Hydroprocessing of Heavy Oils.* Chemical I. Boca Raton, Florida. USA: Taylor & Francis Group.

Andersen, S. I., Birdi, K. 1991. "Aggregation of Asphaltenes as Determined by Calorimetry" *Journal of Colloids and Interface Science*. 142 (2): 497–502.

Andersen, S. I., Speight, j. 1999. "Thermodynamic Models for Asphaltene Solubility and Precipitation." *Journal of Petroleum Science and Engineering* 22 (1-3): 53–66.

ASTM D1160. 2006. “Test Method for Distillation of Petroleum Products at Reduced Pressure.”

ASTM D86. 2009. “Test Methdos for Distillation of Petroleum Products at Atmospheric Pressure”, no. April: 1–27.

ASTM Standard D2892. 2009. “Test Method for Distillation of Crude Petroleum (15-Theoretical Plate Column).” *Fuel Processing Technology*. ASTM.

ASTM Standard D5236. 2007. “Test Method for Distillation of Heavy Hydrocarbon Mixtures (Vacuum Potstill Method).”

Bandurski, E. 1982. “Structural Similarities Between Oil-Generating Kerogens and Petroleum Asphaltenes.” *Energy Sources* 6 (1): 19.

Barré, L., J.,Morisset, J., Palermo, T, Simon, S. 2009. “Relation between Nanoscale Structure of Asphaltene Aggregates and Their Macroscopic Solution Properties.” *Oil & Gas Science and Technology* 64 (5): 617–28.

Barrera, D. M., Ortiz, D.P., Yarranton, H.W. 2013. “Molecular Weight and Density Distributions of Asphaltenes from Crude Oils.” *Energy and Fuels* 27: 14.

Barrera, D. M. 2012. “Determination and Application of Asphaltene Property Distributions for Native and Refined Crude Oils”. University of Calgary.

Bartholdy, J., Andersen, S. 2000. “Changes in Asphaltene Stability during Hydrotreating.” *Energy & Fuels* 14 (1): 52–55.

Barton, A.F. M. 1991. *CRC Handbook of Solubility Parameters and Other Cohesion Parameters*. Second. Boca Raton, Florida. US: CRC Press.

Becker, C., Qian, K., Russell, D. 2008. “Molecular Weight Distributions of Asphaltenes and Deasphaltened Oils Studied by Laser Desorption Ionization and Ion Mobility Mass Spectrometry.” *Analytical Chemistry* 80 (22): 8592–97.

Brocos, P., Piñeiro, Bravo, R., Amigo, A. 2003. “Refractive Indices, Molar Volumes and Molar Refractions of Binary Liquid Mixtures: Concepts and Correlations.” *Physical Chemistry* 5 (3): 550–57.

Bruno, T. J. 1987. “Laboratory Applications of the Vortex Tube” 64 (11): 987–88.

Bruno, T. J.. 2006. “Improvements in the Measurement of Distillation Curves. 1. A Composition-Explicit Approach.” *Industrial & Engineering Chemistry Research* 45 (12): 4371–80.

Bruno, T. J., Ott, L, Lovestead, T., Huber, M. 2010. "Relating Complex Fluid Composition and Thermophysical Properties with the Advanced Distillation Curve Approach." *Chemical Engineering & Technology* 33 (3): 363–76.

Bruno, T., J., Ott, L. Smith, B., Lovestead, T. 2010. "Complex Fluid Analysis with the Advanced Distillation Curve Approach." *Analytical Chemistry* 82 (3): 777–83.

Buch, L, Groenzin, H., Buenrostro-Gonzales, E., Andersen, S., Lira-Galeana, C., Mullins, O.. 2003. "Molecular Size of Asphaltene Fractions Obtained from Residuum Hydrotreatment. *Energy & Fuel,* 82 (9): 1075–84.

Buckley, J.S, Hirasaki, G.J., Liu Y., Von Drasek, S., Wang, J-X., Gill, B.S. 1998. "Asphaltene Precipitation and Solvent Propoerties of Crude Oils" *Petroleum Sicence and Technology*. 16 (3): 251–285.

Castanier, L.M., Brigham, W.E.. 2003. "Upgrading of Crude Oil via in Situ Combustion." *Journal of Petroleum Science and Engineering* 39 (1-2): 125–36.

Castellanos-Díaz, O., J. Modaresghazani, Satyro, M., Yarranton, H.W. 2011. "Modeling the Phase Behavior of Heavy Oil and Solvent Mixtures." *Fluid Phase Equilibria* 304 (1-2). Elsevier B.V. 74–85.

Castellanos-Diaz, O., Sanchez-Lemus, M.C, Schoegg, F., Satyro, M.A. Taylor, S., Yarranton, H. 2014. "Deep-Vacuum Fractionation of Heavy Oil and Bitumen, Part I: Apparatus and Standardized Procedure." *Energy and Fuels* 28 (2857-2865): 9.

Chartier, G. 2005. *Introduction to Optics*. New York: Springer.

Chung, Ting-Horng. 1992. "Thermodynamic Modeling for Organic Solid Precipitation." In *SPE Annual Technical Conference and Exhibition*. Society of Petroleum Engineers.

Corma,. Wojciechowski. 1985. "The Chemistry of Catalytic Cracking." *Catalysis Reviews* 27 (1): 29–150.

Creek, J., Wang, J., Buckley, J.. 2009. "Verification of Asphaltene-Instability-Trend (ASIST) Predictions for Low-Molecular-Weight Alkanes." *SPE Production & Operations* 24 (2).

Ting, P., Hirasaki, Chapman, W.. 2003. "Modeling of Asphaltene Phase Behavior with the SAFT Equation of State." *Petroleum Science and Technology* 21 (3-4). Taylor & Francis: 647–61.

Dickie, J. P, and Yen, T. 1967. "Macroesctures of the Asphaltic Fractions by Various Lnstrumental Methods." *Analytical Chemistry* 5213 (14): 1963–68.

Galimov, R.A., L.B. Krivonozhkina, V.V. Abushayeva, and G.V. Romanov. 1993. “Extraction of Vanadyl Class porphyrins from Petroleum asphaltenes. *Petroleum Chemistry* v 33, n 6: 539 – 543.

Gawrys, K. L, Blankenship, G.A., Kilpatrick, P. 2006. “On the Distribution of Chemical Properties and Aggregation of Solubility Fractions in Asphaltenes.” *Energy & Fuels* 20 (19): 705–14.

Gray, M. R. 1994. *Upgrading Petroleum Residues and Heavy Oils*. Edited by Heinz Heinemann. Chemical I. New York: Marcel Dekker.

Gray, M. R., Mccaffrey, W. 2002. “Role of Chain Reactions and Olefin Formation in Cracking, Hydroconversion, and Coking of Petroleum and Bitumen Fractions.” *Energy & Fuels* 16 (3). American Chemical Society: 756–66.

Gray, M. R., Tykwinski, R., Stryker, J., Tan, A. 2011. “Supramolecular Assembly Model for Aggregation of Petroleum Asphaltenes.” *Energy & Fuels* 25 (7): 3125–34.

Groenzin, H., Mullins, O. 1999. “Asphaltene Molecular Size and Structure.” *The Journal of Physical Chemistry* 103 (50): 11237–45.

Gupta, A.. 1986. “A Model for Asphaltene Flocculation Using an Equation of State”. Chemical and Petroleum Engineering, University of Calgary.

Hansen, C. M. 2007. *Hansen’s Solubility Parameters: A User's Handbook.* Boca Raton, Florida. US: CRC Press.

Hay, G., Loria, H., Satyro, M. 2013. “Thermodynamic Modeling and Process Simulation through PIONA Characterization.” *Energy & Fuels* 27 (6): 3578–84.

Hildenbrand, J., Prausnitz, J., Scott, R. 1970. *Regular and Related Solutions. The Solubility of Gases, Liquids and Solids*. New York: Van Nostrand Reinhold Company.

Hildenbrand, J., Scott, R. 1964. *The Solubility of Nonelectrolytes.* Thrid. New York: Dover Publications, Inc.

Hirschberg, A, L.N.J., DeJong, Schipper, B.A., Meijer, J.G.. 1984. “Influence of Temperature and Pressure on Asphaltene Flocculation.” *Society of Petroleum Engineers Journal*, 11.

Huc, Alain-Yves. 2011. *Heavy Crude Oils. From Geology to Upgrading and Overview*. First Edition. Paris, France: Editions TECHNIP.

Jia, N., R,. Moore, G., Mehta, R., Ursenbach, M., Hancock, M. 2013. “Kinetic Modelling of Thermal Cracking and Low Temperature Oxidation Reactions.” *Canadian International Petroleum Conference*, April. Petroleum Society of Canada, 1–12.

Kaes, G. 2000. *Refinary Process Modeling: A Practical Guide to Steady State Modeling of Petroleum Processes*. Athens, Georgia: Athens Printing Company.

Kawanaka, S., Mansoori, G.A. 1991. "Organic Deposition From Reservoir Fluids: A Thermodynamic Predictive Technique." *SPE Reservoir Engineering*, 8.

Kekäläinen, T., Pakarinen, J., Wickström, K., Lobodin, V., McKenna, A.,Jänis, J. 2013. "Compositional Analysis of Oil Residues by Ultrahigh-Resolution Fourier Transform Ion Cyclotron Resonance Mass Spectrometry." *Energy & Fuels* 27 (4): 2002–9.

Kelemen, S.R, George, G.N., Gorbaty, M L. 1990. "Direct Determination and Quantification of Sulphur Forms in Heavy Petroleum and Coals." *Fuels* 69 (6): 939–44.

Kontogeorgis, G, Folas, G. 2010. *Thermodynamic Models for Industrial Applications*. First. The Atrium, UK: John Wiley & Sons Ltd.

Kuznicki, T., Masliyah, J., Bhattacharjee, S. 2009. "Aggregation and Partitioning of Model Asphaltenes at Toluene−Water Interfaces: Molecular Dynamics Simulations." *Energy & Fuels* 23 (10): 5027–35.

Lababidi, M.S., Sabti, H. M, AlHumaidan, F. 2014. "Changes in Asphaltenes during Thermal Cracking of Residual Oils. *Energy & Fuel* 117 (01). 59–67.

Laštovka, V, Sallamie, N., Shaw, J.. 2008. "A Similarity Variable for Estimating the Heat Capacity of Solid Organic Compounds." *Fluid Phase Equilibria* 268 (1-2): 51–60.

Leontaritis, J. 1989. "Asphaltene Deposition : A Comprehensive Description of Problem Manifestations and Modeling Approaches." *Society of Petroleum Engineers Journal* 18892: 15.

Li, Zhidong, Firoozabadi, A. 2010. "Modeling Asphaltene Precipitation by N -Alkanes from Heavy Oils and Bitumens Using Cubic-Plus-Association Equation of State." *Energy & Fuels* 24 (2): 1106–13.

Lian, H, J., Yen, T. 1994. "Peptization Studies of Asphaltene and Solubility Parameter Spectra. *Energy & Fuel* 73 (3): 423–28.

Macchietto, S., G. F. Coletti, H.F., Crittenden,B.D., Dugwell, D.R., Jackson, et al. 2011. "Fouling in Crude Oil Preheat Trains: A Systematic Solution to an Old Problem." *Heat Transfer Engineering* 32 (3-4): 197–215.

Maruska, P, Bhaskara M.L. Rao. 1987. "The Role of Polar Species in Aggregation of Asphaltenes." *Fuel Science and Technology International* 5 (2). Taylor & Francis: 119–68.

McKenna, A. M.,. Donald, L., Fitzsimmons, J., Juyal, P., Spicer, V., Standing, G., Marshall, A., Rodgers, R. 2013. "Heavy Petroleum Composition. 3. Asphaltene Aggregation." *Energy and Fuels* 27 (3): 1246–56.

Minderhoud, J.K., van Veen., J.R. 1993. "First-Stage Hydrocracking: Process and Catalytic Aspects." *Fuel Processing Technology* 35 (1-2): 87–110. J.

Mitra-kirtley, S., Mullins, O., Branthaver, J., Cramerl, S. 1993. "Nitrogen Chemistry of Kerogens and Bitumens from X-Ray Absorption Near-Edge Structure Spectroscopy." *Energy & Fuels* 7 (4): 1128–34.

Moschopedis, S, Fryer, J., Speight, J. 1976. "Investigation of Asphaltene Molecular Weights. *Energy & Fuel* 55 (3): 227–32.

Mullins, O. 2008. "Review of the Molecular Structure and Aggregation of Asphaltenes and Petroleomics." *SPE Journal,*. October 2007: 9–12.

Mullins, O., Sabbah, H., Pomerantz, A., Andrews, B., Ruiz-morales, Y., Mostow, F., Mcfarlane, R. 2012. "Advances in Asphaltene Science and the Yen − Mullins Model." *Energy & Fuels* 26: 3986–4003.

Murgich, J.. 2003. "Molecular Simulation and the Aggregation of the Heavy Fractions in Crude Oils." *Molecular Simulation* 29 (6-7). Taylor & Francis: 451–61.

Murgich, J., Abanero, J., Strausz, O. 1999. "Molecular Recognition in Aggregates Formed by Asphaltene and Resin Molecules from the Athabasca Oil Sand." *Energy & Fuels* 13 (2): 278–86.

NIST. 2014. "NIST Chemistry WebBook." *NIST Standard Reference Database Number 69.* http://webbook.nist.gov/chemistry/.

Okafor, J.. 2013. "Characterization of Non-Distillable Crude and Refined Oil Fractions for Asphaltene Precipitation Modeling". University of Calgary.

Ortiz, D.P., Satyro, M., Yarranton, H.W. 2013. "Thermodynamics and Fluid Characterization Using Trajectory Optimization." *Fluid Phase Equilibria* 351 (August). Elsevier B.V. 34–42.

Pan, H., Firoozabadi, A. 1998. "Thermodynamic Micellization Model for Asphaltene Aggregation and Precipitation in Petroleum Fluids." *SPE Production & Facilities*,

Parkash, S., Moschopedis, S., Speight, J. 1979. "Physical Properties of Asphaltenes and Surface Characteristics. *Energy* & *Fuel* 58: 877–82.

Payzant, J D,. Lown, E. M., Strausz, O.. 1991. "Structural Units of Athabasca Asphaltene : The Aromatics with a Linear Carbon Framework." *Energy & Fuels* 5 (8): 445–53.

Peramanu, S., Pruden, B., Rahimi, P. 1999. “Molecular Weight and Specific Gravity Distributions for Athabasca and Cold Lake Bitumens and Their Saturate, Aromatic, Resin, and Asphaltene Fractions.” *Industrial & Engineering Chemistry Research* 38 (8): 3121–30.

Poling, B. E.,. Prausnitz, J.,O’Conell John P. 2001. *The Properties of Gases and Liquids.* Fifth. New York: McGraw-Hill.

Prausnitz, J., Lichtenthaler R., Gomez de Acevelo, E.. 1999. *Molecular Thermodynamics of Fluid-Phase Equilibria*. Third Edition. New Jersey: Prentice Hall.

Qian, K., E., Mennito, K., Walters, A., , Kushnerick, C. 2010. “Enrichment, Resolution, and Identification of Nickel Porphyrins in Petroleum Asphaltene by Cyclograph Separation and Atmospheric Pressure Photoionization Fourier Transform Ion Cyclotron Resonance Mass Spectrometry.” *Analytical Chemistry* 82 (1): 413–19.

Rana, M. S., Ancheyta, J. Maity, S. K,. Rayo, P. 2007. “Hydrotreating of Maya Crude Oil: I. Effect of Support Composition and Its Pore-Diameter on Asphaltene Conversion.” *Petroleum Science and Technology* 25 (1-2): 187–99.

Raseev, S.. 2003. *Thermal and Catalytic Processes in Petroleum Refining*. New York: Marcel Dekker.

Rastegari, K., Svrcek, W., Yarranton, H. 2004. “Kinetics of Asphaltene Flocculation.” *Industrial & Engineering Chemistry Research* 43 (21): 6861–70.

Riazi, M.R. 2005. *Characterization and Properties of Petroleum Fractions.* 1st ed. ASTM Manual Series.

Roes, Augustinus-Wilhelmus, Vijay, Munsterman, E., Van Bergen, F.P., s Van Den Berg, F.G.A. 2009. “Patent US7604052”. Hoston, TX. (US).

Rogel, E, Carbognani, L. 2003. “Density Estimation of Asphaltenes Using Molecular Dynamics Simulations”, no. 11: 378–86.

Rogel, E., Ovalles, C., Moir, M. 2012. “Asphaltene Chemical Characterization as a Function of Solubility: Effects on Stability and Aggregation.” *Energy & Fuels* 26 (5): 2655–62.

Rogel, E., Cesar Ovalles, Michael E. Moir, and John F. Schabron. 2009. “Determination of Asphaltenes in Crude Oil and Petroleum Products by the on Column Precipitation Method.” *Energy & Fuels* 23 (9). American Chemical Society: 4515–21.

Kenneth D., M. A. Francisco. 1988. “A Two-Step Chemistry for Highlighting Heteroatom Species in Petroleum Materials Using Carbon-13 NMR Spectroscopy.” *Journal of the American Chemical Society* 110 (2). American Chemical Society: 637–38.

Sadeghi-Yamchi, H. 2014a. “Effect of Refining on Asphaltene Property Distributions”. University of Calgary.

Sánchez-Lemus, M. C., Schoeggl, F. Taylor, S. D. Růžička, K. Fulem, M, Yarranton, H. W. 2014. “Deep-Vacuum Fractionation of Heavy Oil and Bitumen, Part II: Interconversion Method.” *Energy & Fuels* 28 (5): 2866–73.

Saryazdi, F., Motahhari, H., Schoeggl, F, Taylor, S. D., . Yarranton, H. W. 2013. “Density of Hydrocarbon Mixtures and Bitumen Diluted with Solvents and Dissolved Gases.” *Energy & Fuels* 27 (7): 3666–78.

Schabron, J. F., Rovani, J.F.. 2008. “On-Column Precipitation and Re-Dissolution of Asphaltenes in Petroleum Residua.” *Fuel* 87 (2): 165–76.

Shell-Canada. 2014. “Personal Communication”. Calgary, AB. Canada.

Sheremata, J. M, Gray, M., Dettman, H. D., Mccaffrey, W. 2004. “Quantitative Molecular Representation and Sequential Optimization of Athabasca Asphaltenes.” *Energy & Fuels* 13 (12): 1377–84.

Sirota, E. B. 2005. “Physical Structure of Asphaltenes”. *Energy & Fuels* 19 (4): 1290–96.

Speight, J.G., Moschopedis, S.E.. 1979. “Influence of Crude Oil Compostion on the Nature of the Upgrading Process: Athabasca Bitumen.” *1st International Conference on the Future of Heavy Crude and Tar Sands*. Edmonton, AB.

Speight, J. G. 1998. *Chemistry and Technology of Petroleum*. New York: Marcel Dekker.

Speight, J. G. 2001. *Handbook of Petroleum Analysis*. Chemical A. New York: Wiley-Interscience.

Strausz, O. P., Mojelsky, T., Lown, E. M.. 1992. “The Molecular Structure Unfolding Story of Asphaltene : An Unfolding Story.” *Energy & Fuel* 71: 1355–63.

Strausz, O. P., Peng, P., Murgich, J. 2002. “About the Colloidal Nature of Asphaltenes and the MW of Covalent Monomeric Units.” *Energy & Fuels* 16 (4). American Chemical Society: 809–22.

Sztukowski, D. M, Jafari, M., Alboudwarej, H., Yarranton, H.. 2003. “Asphaltene Self-Association and Water-in-Hydrocarbon Emulsions.” *Journal of Colloid and Interface Science* 265 (1): 179–86.

Tharanivasan, A. K. 2012. “Asphaltene Precipitation from Crude Oil Blends, Conventional Oils, and Oils with Emulsified Water.” University of Calgary.

Tharanivasan, A. K., Svrcek, W., Yarranton, H., Taylor, S., Merino-Garcia D., Rahimi, P. 2009. "Measurement and Modeling of Asphaltene Precipitation from Crude Oil Blends." *Energy & Fuels* 23 (8): 3971–80.

Tharanivasan, A. K.,, Yarranton, H., Taylor, S.. 2011. "Application of a Regular Solution-Based Model to Asphaltene Precipitation from Live Oils †." *Energy & Fuels* 25 (2). American Chemical Society: 528–38.

Toralf, S. 2007. *Polarized Light in Liquid Crystals and Polymers*. Hoboken, N.J.: Wiley-Interscience.

Trejo, F, J. Ancheyta, Morgan, A, Herod, A., Kandiyoti, R. 2007. "Characterization of Asphaltenes from Hydrotreated Products by SEC , LDMS , MALDI , NMR , and XRD." *Energy & Fuels* 21 (10): 2121–28.

Trejo, F., J. Ancheyta, Centeno, G. Marroquín, G. 2005. "Effect of Hydrotreating Conditions on Maya Asphaltenes Composition and Structural Parameters." *Catalysis Today* 109 (1-4): 178–84.

Trejo, F., Centeno, G., Ancheyta, J. 2004. "Precipitation, Fractionation and Characterization of Asphaltenes from Heavy and Light Crude Oils." *Energy & Fuel* 83 (16): 2169–75.

Trejo, F., Ancheyta, J. 2007. "Characterization of Asphaltene Fractions from Hydrotreated Maya Crude Oil." *Industrial & Engineering Chemistry Research* 46: 7571–79.

Trejo, F., Ancheyta, J., Rana, M. 2009. "Structural Characterization of Asphaltenes Obtained from Hydroprocessed Crude Oils by SEM and TEM." *Energy & Fuels*, no. 5: 429–39.

Tsonopoulos, C.,. Heidman, J. L., Hwang, S.. 1986. *Thermodynamic and Transport Properties of Coal Liquids.* New York: Wiley-Interscience.

Vargas, F.M., Chapman, W.G., 2010. .Application of the One-Third Rule in Hydrocarbon and Crude Oil Systems, *Fluid Phase Equilibria* 290, 103-108,

Velásquez Rueda, R. 2013. "Characterization of Asphaltene Molecular Structures by Cracking under Hydrogenation Conditions and Prediction of the Viscosity Reduction from." University of Alberta

Vezirov, R. R. 2011. "Visbreaking – Technologies Tested by Practice and Time." *Chemistry and Technology of Fuels and Oils* 46 (6): 367–74.

Viswanath, D.S.,. Kullor, N. R. 1965. "1 . Theorem of Corresponding States." *Journal of Scientific and Industrial Research* 24: 2014.

Wang, J X, Buckley, J S, Prrc N M. 2001. “An Experimental Approach to Prediction of Asphaltene Flocculation.” *Society of Petroleum Engineers Journal*, 1–9.

Wang, J. X., Buckley, J. S.. 2001. “A Two-Component Solubility Model of the Onset of Asphaltene Flocculation in Crude Oils.” *Energy & Fuels* 15 (5): 1004–12.

Weissberger, A. 1959. *Technique of Organic Chemistry*. New York: Interscience Publishers.

Wiehe, I. A. 2008. *Process Chemistry of Petroleum Macromolecules*. Edited by Heinz Heinemann and James G. Speight. Chemical I. Boca Raton, Florida. US: CRC Press.

Wiehe, I. A, and K.S. Liang. 1996. “Asphaltenes, Resins and Other Petroelume Macromolecules.” *Fluid Phase Equilibria* 117: 201–10.

Windom, B., Bruno, T. 2011. “Improvements in the Measurement of Distillation Curves . 5 . Reduced Pressure Advanced Distillation Curve Method”, 1115–26.

Xu, H., Xu, Z., Sun, X., Xu, C., Chung, K., Zhao, S.. 2013. “Antisolvent Separation of Thermally Cracked Vacuum Resid.” *Energy & Fuels* 27 (12): 7885–95.

Xu, Y, Koga, Y., Strausz, O. 1995. “Characterization of Athabasca Asphaltenes by Small-Angle X-Ray Scattering.” *Energy & Fuel* 74 (7): 960–64. d

Yarranton, H W, Ortiz, D P., Barrera, D M., Baydak, E N., Barre, L., Frot, D., Eyssautier, J. 2013. “On the Size Distribution of Self-Associated Asphaltenes.” *Energy & Fuels* 27: 5083–5106.

Yarranton, H. W, Fox, W., Svrcek, W.. 2003. “Effect of Resins on Asphaltene Self-Association and Solubility.” *The Candian Journal of Chemical Engineering*, no. 1996: 635–42.

Yarranton, H. W. 2005. “Asphaltene Self-Association.” *Journal of Dispersion Science and Technology* 26 (1): 5–8.

Yarranton, H. W., Alboudwarej, H., Jakher, R. 2000. “Investigation of Asphaltene Association with Vapor Pressure Osmometry and Interfacial Tension Measurements.” *Industrial & Engineering Chemistry Research* 39 (8): 2916–24.

Yarranton, H.W., Masliyah, J. 1996. “Molar Mass Distribution and Solubility Modeling of Asphaltenes.” *AIChE Journal* 42 (12): 3533–43.

Yarranton, H. W., Schoeggl, F., George, S., Taylor, S. 2011. “Asphaltene-Rich Phase Compositions and Sediment Volumes from Drying Experiments.” *Energy & Fuels* 25: 10.

Yen, T, Chilingarian G.V. 2000. *Asphaltenes and Asphalts*. Amsterdam: Elsevier Science B.V.

Yen, T. F, Wu, W., Chilingar, G. 1984. *A Study of the Structure of Petroleum Asphaltenes and Related Substances by Infrared Spectroscopy*. *Energy Sources*. Vol. 7.

Zhang, L Y., Breen, P. Xu, Z., Masliyah, J. 2007. "Asphaltene Films at a Toluene/Water Interface." *Energy & Fuels* 21 (1). American Chemical Society: 274–85.

Zhao, B., Shaw, J. 2007. "Composition and Size Distribution of Coherent Nanostructures in Athabasca Bitumen and Maya Crude Oil." *Energy & Fuels* 21 (5). American Chemical Society: 2795–2804.

Zhongxin, Huo. 2010. "Personal Communication." Calgary, AB. Canada.

Zhou, X., Thomas, F.B., Moore, R.G. 1996. "Modelling of Solid Precipitation From Reservoir Fluid." *Journal of Canadian Petroleum Technology* 35 (10). Petroleum Society of Canada.

Appendix A. Error Analysis

The sample mean $\bar{y}$ of a set of measurements is defined as,

$$\bar{y} = \frac{\sum_{i=1}^{n} y_i}{n} \qquad \text{A.1}$$

where y_i is each measured data in the sample and n is the number of measurements or repeats. The variability of scatter in the data is described by the sample standard deviation, *s*, defined by,

$$s = \sqrt{\frac{\sum_{i=1}^{n}\left(y_i - \bar{y}\right)^2}{n-1}} \qquad \text{A.2}$$

and the sample variance is defined as s^2. For each set of measurements, the sample mean and the sample standard deviation can be calculated, thus they are assumed to be known, hence, t-distribution can be employed to determine the confidence interval as follows,

$$\bar{y} - t_{(\alpha/2,\nu)}\frac{s}{\sqrt{n}} \le \mu \le \bar{y} + t_{(\alpha/2,\nu)}\frac{s}{\sqrt{n}} \qquad \text{A.3}$$

where $\nu = n - 1$ and $\alpha = 1 - (\%\text{significance}/100)$. In the current work, a significance (or confidence level) of 95% was utilized in all the error analyses. Hence, $\alpha = 0.05$. This approach is mostly used when there are 3 or more repeats (e.g. SARA compositions). Note that the confidence interval is a general definition and depending on the experimental data, any other distribution can be used to estimate the confidence interval by replacing the value form the t-distribution (*t*) to the value from the most appropriate distribution.

In some other cases, there are only two repeats for a set of measurements, hence it is more appropriate to calculate the population variance of the property measurements using a Chi-square distribution as follows:

$$\sigma = \sqrt{\frac{\lambda^2 s^2}{(n-1)}} \qquad \text{A.4}$$

where λ^2 is the Chi-square variable and σ is the population standard deviation. Taking a confidence level of 95%, the confidence interval (*CI*) can be estimated as $1.645\sigma/\sqrt{n}$ (assuming that the population mean has a normal distribution). Tables A.1 to A.40 shows the repeatability analysis for the experimental data.

Deviations between the predicted value, y_i^* and the experimentally measured value are defined as:

$$dev = \left| y_i^* - y_i \right| \tag{A.5}$$

The Average Absolute Deviation (AAD) of the fits or predictions to the experimental data is given by:

$$AAD = \frac{1}{n}\sum_{1}^{n}\left| y_i^* - y_i \right| \tag{A.6}$$

and the Absolute Average Relative Deviation percentage is given by:

$$AARD = \frac{1}{n}\sum_{1}^{n}\left| \frac{y_i^* - y_i}{y_i} \right| *100 \tag{A.7}$$

A.1. Confidence intervals (*CI*) in SARA composition: Repeatability analysis.

Table A.1. Repeatability analysis for SARA fractionation of Arabian heavy fraction

	N	μ Mass Fraction	s^2	$\pm CI$ Mass Fraction
Saturates	3	0.384	0.000157	0.031
Aromatics	3	0.384	0.000148	0.030
Resins	3	0.154	0.000067	0.020
C5-Asphaltenes	2	0.079	0.000001	0.006

Table A.2 . Repeatability analysis for SARA fractionation of WC-DB-A2 heavy fraction

	N	μ Mass Fraction	s^2	$\pm CI$ Mass Fraction
Saturates	5	0.214	0.0096	0.012
Aromatics	5	0.444	0.0134	0.017
Resins	5	0.236	0.0164	0.020
C5-Asphaltenes	3	0.106	0.0035	0.009

Table A.3. Repeatability analysis for SARA fractionation of WC-B-C1

	N	μ Mass Fraction	s^2	$\pm CI$ Mass Fraction
Saturates	4	0.147	0.000033	0.009
Aromatics	4	0.450	0.000116	0.017
Resins	4	0.212	0.000134	0.018
C5-Asphaltenes	4	0.178	0.000251	0.025

Table A.4. Repeatability analysis for SARA fractionation of WC-B-B2

	N	μ Mass Fraction	s^2	$\pm CI$ Mass Fraction
Saturates	12	0.162	0.000128	0.007
Aromatics	12	0.434	0.000824	0.018
Resins	12	0.206	0.001006	0.020
C5-Asphaltenes	6	0.196	0.000023	0.005

Table A.5. Repeatability analysis for SARA fractionation of WC-VR-B2

	N	μ Mass Fraction	s^2	$\pm CI$ Mass Fraction
Saturates	5	0.053	0.000013	0.0044
Aromatics	5	0.374	0.000013	0.0044
Resins	5	0.201	0.000016	0.0050
C5-Asphaltenes	4	0.372	0.000063	0.0126

Table A.6. Repeatability analysis for SARA fractionation of WC-SR-A3

	N	μ Mass Fraction	s^2	$\pm CI$ Mass Fraction
Saturates	4	0.078	0.000011	0.005
Aromatics	4	0.375	0.000026	0.008
Resins	4	0.270	0.000017	0.007
C5-Asphaltenes	3	0.277	0.000004	0.005

Table A.7. Repeatability analysis for SARA fractionation of Heavy Atmospheric

	N	μ Mass Fraction	s^2	$\pm CI$ Mass Fraction
Saturates	4	0.243	0.000013	0.006
Aromatics	4	0.501	0.000028	0.008
Resins	4	0.136	0.000051	0.011
C5-Asphaltenes	2	0.121	0.000000	--

Table A.8. Repeatability analysis for SARA fractionation of 26845 heavy fraction

	N	μ Mass Fraction	s^2	$\pm CI$ Mass Fraction
Saturates	3	0.176	0.0086	0.021
Aromatics	3	0.461	0.0060	0.015
Resins	3	0.205	0.0081	0.020
C5-Asphaltenes	3	0.164	0.0104	0.026

Table A.9. Repeatability analysis for SARA fractionation of 27034-87 heavy fraction

	N	*μ* Mass Fraction	s^2	± *CI* Mass Fraction
Saturates	4	0.204	0.000101	0.016
Aromatics	4	0.515	0.000121	0.017
Resins	4	0.163	0.000266	0.026
C5-Asphaltenes	3	0.112	0.000013	0.009

Table A.10. Repeatability analysis for SARA fractionation of 27034-113 heavy fraction

	N	*μ* Mass Fraction	s^2	± *CI* Mass Fraction
Saturates	3	0.230	0.000201	0.035
Aromatics	3	0.473	0.000142	0.030
Resins	3	0.204	0.000044	0.017
C5-Asphaltenes	2	0.092		--

Table A.11. Repeatability analysis for SARA fractionation of 27-168-179 heavy fraction

	N	*μ* Mass Fraction	s^2	± *CI* Mass Fraction
Saturates	4	0.477	0.000272	0.026
Aromatics	4	0.315	0.000104	0.016
Resins	4	0.161	0.000197	0.022
C5-Asphaltenes	2	0.047	0.000000	--

Table A.12. Repeatability analysis for SARA fractionation of X-1357

	N	*μ* Mass Fraction	s^2	± *CI* Mass Fraction
Saturates	6	0.045	0.000002	0.001
Aromatics	6	0.340	0.000190	0.014
Resins	6	0.190	0.000189	0.014
C5-Asphaltenes	4	0.436	0.000179	0.021

Table A.13. Repeatability analysis for SARA fractionation of X-1359

	N	μ Mass Fraction	s^2	$\pm CI$ Mass Fraction
Saturates	4	0.040	0.000006	0.004
Aromatics	4	0.314	0.000409	0.032
Resins	4	0.134	0.000386	0.031
C5-Asphaltenes	4	0.518	0.000060	0.012

Table A.14. Repeatability analysis for SARA fractionation of X-1360

	N	μ Mass Fraction	s^2	$\pm CI$ Mass Fraction
Saturates	6	0.037	0.000011	0.003
Aromatics	6	0.261	0.000250	0.017
Resins	6	0.121	0.000180	0.014
C5-Asphaltenes	8	0.584	0.000433	0.017

Table A.15. Repeatability analysis for SARA fractionation of RHC-18-37

	N	μ Mass Fraction	s^2	$\pm CI$ Mass Fraction
Saturates	4	0.153	0.000344	0.030
Aromatics	4	0.451	0.000623	0.040
Resins	4	0.145	0.000050	0.011
C5-Asphaltenes	3	0.251	0.000004	0.005

Table A.16. Repeatability analysis for SARA fractionation of RHC-18-19

	N	μ Mass Fraction	s^2	$\pm CI$ Mass Fraction
Saturates	3	0.207	0.000011	0.030
Aromatics	3	0.484	0.000366	0.040
Resins	3	0.175	0.000381	0.011
C5-Asphaltenes	3	0.135	0.000004	0.005

Table A.17. Repeatability analysis for SARA fractionation of RHC-19-03

	N	μ Mass Fraction	s^2	$\pm CI$ Mass Fraction
Saturates	4	0.328	0.000093	0.015
Aromatics	4	0.493	0.000052	0.011
Resins	4	0.151	0.000024	0.008
C5-Asphaltenes	6	0.029	0.000003	0.002

Table A.18. Repeatability analysis for SARA fractionation of HOS Bottoms

	N	μ Mass Fraction	s^2	$\pm CI$ Mass Fraction
Saturates	6	0.201	0.000088	0.010
Aromatics	6	0.475	0.000117	0.011
Resins	6	0.175	0.000637	0.026
C5-Asphaltenes	6	0.151	0.000549	0.025

Table A.19. Overall repeatability of the SARA fractionation.

Fraction	n	*Average** $\sigma^2 = s^2$	s	$\pm CI$ Mass Fraction
Saturates	19	0.000083	0.012	0.019
Aromatics	19	0.000210	0.018	0.030
Resins	19	0.000183	0.017	0.028
C5-Asphaltenes	16	0.000095	0.012	0.020

* Sample Average $\sigma^2 = S^2$ from tables A.1 to A.18 for the overall SARA fraction.

A.2. Confidence Intervals for crude oil solubility measurements: Repeatability Analysis.

Table A.20. Repeatability analysis for crude oil solubility of WC-B-B2

Heptane Mass Fraction	*N*	μ Mass Fraction	σ^2
0.51	2	0.0042	1.17E-07
0.75	2	0.1157	1.25E-05
0.87	2	0.1513	2.23E-05
0.92	2	0.1544	5.74E-05
		Average (s^2)	2.31E-05
		CI	0.0074

Table A.21. Repeatability analysis for crude oil solubility of WC-B-C1

Heptane Mass Fraction	*N*	μ Mass Fraction	σ^2
0.51	2	0.004003	5.95E-08
0.67	2	0.047786	8.42E-05
0.74	2	0.075508	1.18E-05
0.83	2	0.10396	1.70E-05
		Average (s^2)	2.83E-05
		CI	0.0082

Table A.22. Repeatability analysis for crude oil solubility of Arabian heavy fraction

Heptane Mass Fraction	*N*	μ Mass Fraction	σ^2
0.51	2	0.0034	2.13E-06
0.84	3	0.0426	3.03E-05
0.91	2	0.0427	1.10E-08
0.95	3	0.0502	1.62E-05
		Average (s^2)	1.22E-05
		CI	0.0160

Table A.23. Repeatability analysis for crude oil solubility of WC-DB-A2 heavy fraction

Heptane Mass Fraction	N	μ Mass Fraction	σ^2
0.50	2	0.0008	4.74E-10
0.81	2	0.0287	1.79E-04
0.91	2	0.0476	2.56E-05
		Average (s^2)	6.82E-05
		CI	0.0142

Table A.24. Repeatability analysis for crude oil solubility of 26845 heavy fraction

Heptane Mass Fraction	N	μ Mass Fraction	σ^2
0.51	3	0.0553	0.0004
0.79	3	0.1057	0.0001
0.90	3	0.1243	0.0001
		Average (s^2)	0.0002
		CI	0.0289

Table A.25 Repeatability analysis for crude oil solubility of 27034-113 topped oil

Heptane Mass Fraction	N	μ Mass Fraction	σ^2
0.41	2	0.0411	1.39E-08
0.58	2	0.0572	1.78E-05
0.67	2	0.0624	3.14E-06
		Average (s^2)	6.98E-06
		CI	0.0053

Table A.26. Repeatability analysis for crude oil solubility of RHC-18-19

Heptane Mass Fraction	N	μ Mass Fraction	σ^2
0.30	2	0.0325	3.74E-06
0.50	2	0.0522	1.31E-06
0.70	2	0.0718	8.29E-07
0.90	2	0.0851	1.28E-05
		Average (s^2)	4.67E-06
		CI	0.0033

Table A.27. Repeatability analysis for crude oil solubility of RHC-18-37

Heptane Mass Fraction	*N*	μ Mass Fraction	σ^2
0.50	2	0.1940	1.81E-06
0.70	2	0.2290	3.86E-04
0.83	2	0.2490	8.60E-04
		Average (s^2)	4.16E-04
		CI	0.0377

Table A.28. Repeatability analysis for crude oil solubility of RHC-19-03

Heptane Mass Fraction	*N*	μ Mass Fraction	σ^2
0.21	2	0.0006	4.91E-09
0.49	2	0.0039	1.65E-09
0.62	2	0.0063	3.88E-08
0.69	2	0.0077	1.54E-06
		Average (s^2)	3.95E-07
		CI	0.0010

A.3. Average absolute deviations between experimental data and the model results for crude oil solubility

Table A.29. Average absolute deviation between measured and model results for asphaltene yield from WC-SR-A3

Heptane Mass fraction	*Measured Asph. Yield*	*RSM Asph.Yield*	*AAD*
0.822	0.0305	0.0611	0.0306
0.664	0.0005	0.0010	0.0005
0.681	0.0006	0.0011	0.0004
0.742	0.0037	0.0048	0.0011
0.529	0.0003	0.0010	0.0007
0.553	0.0003	0.0010	0.0007
		Average	0.0057

Table A.30. Average absolute deviation between measured and model results for asphaltene yield from HOS Bottoms

Heptane Mass fraction	*Measured Asph. Yield*	*RSM Asph.Yield*	*AAD*
0.202	0.0237	0.0250	0.0013
0.401	0.0487	0.0456	0.0031
0.600	0.0699	0.0710	0.0011
0.800	0.0841	0.0886	0.0045
0.916	0.0797	0.0881	0.0085
		Average	0.0037

Table A.31. Average absolute deviation between measured and model results for asphaltene yield from RHC-18-19

Heptane Mass fraction	*Measured Asph. Yield*	*RSM Asph.Yield*	*AAD*
0.303	0.0338	0.0352	0.0014
0.407	0.0439	0.0459	0.0020
0.502	0.0530	0.0561	0.0031
0.699	0.0724	0.0739	0.0015
0.900	0.0826	0.0810	0.0016
		Average	0.0019

Table A.32. Average absolute deviation between measured and model results for asphaltene yield from RCH-19-37

Heptane Mass fraction	*Measured Asph. Yield*	*RSM Asph.Yield*	*AAD*
0.403	0.1661	0.1638	0.0023
0.506	0.1940	0.1989	0.0049
0.608	0.2176	0.2238	0.0062
0.700	0.2151	0.2361	0.0210
0.797	0.2400	0.2445	0.0045
		Average	0.0078

Table A.33. Average absolute deviation between measured and model results for asphaltene yield from WC-VR-B2

Heptane Mass fraction	*Measured Asph. Yield*	*RSM Asph.Yield*	*AAD*
0.307	0.0013	0.0058	0.0045
0.420	0.0007	0.0058	0.0050
0.548	0.0006	0.0058	0.0051
0.722	0.0334	0.0246	0.0088
0.853	0.0566	0.0649	0.0083
		Average	0.0063

Table A.34. Average absolute deviation between measured and model results for asphaltene yield from x-1357

Heptane Mass fraction	*Measured Asph. Yield*	*RSM Asph.Yield*	*AAD*
0.155	0.0017	0.0045	0.0028
0.245	0.0046	0.0047	0.0001
0.306	0.0020	0.0055	0.0035
0.420	0.0012	0.0117	0.0105
0.530	0.0390	0.0347	0.0044
0.654	0.0740	0.0748	0.0008
0.852	0.0963	0.1028	0.0065
		Average	0.0038

Table A.35. Average absolute deviation between measured and model results for asphaltene yield from x-1359

Heptane Mass fraction	*Measured Asph. Yield*	*RSM Asph.Yield*	*AAD*
0.125	0.0027	0.0090	0.0062
0.197	0.0007	0.0136	0.0129
0.216	0.0054	0.0154	0.0100
0.331	0.0381	0.0360	0.0022
0.409	0.0591	0.0590	0.0002
0.538	0.1064	0.0941	0.0123

0.733	0.1238	0.1238	0.0000
0.851	0.1303	0.1317	0.0013
		Average	0.0056

Table A.36. Average absolute deviation between measured and model results for asphaltene yield from x-1360

Heptane Mass fraction	*Measured Asph. Yield*	*RSM Asph.Yield*	*AAD*
0.072	0.0034	0.0086	0.0052
0.111	0.0029	0.0119	0.0090
0.169	0.0028	0.0196	0.0169
0.317	0.0660	0.0557	0.0103
0.507	0.1335	0.1101	0.0234
0.603	0.1338	0.1277	0.0060
0.743	0.1475	0.1447	0.0028
0.848	0.1470	0.1516	0.0046
		Average	0.0098

Table A.37. Average absolute deviation between measured and model results for asphaltene yield from 27034-113 heavy fraction

Heptane Mass fraction	*Measured Asph. Yield*	*RSM Asph.Yield*	*AAD*
0.233	0.007004	0.005848	0.001156
0.335	0.025135	0.016224	0.008911
0.421	0.041194	0.031979	0.009215
0.490	0.047201	0.046654	0.000548
0.501	0.04022	0.048595	0.008375
0.577	0.060138	0.061244	0.001106
0.747	0.084794	0.076471	0.008322
0.909	0.083914	0.081543	0.002371
		Average	0.0050

Table A.39. Average absolute deviation between measured and model results for asphaltene yield from 27034-87 heavy fraction

Heptane Mass fraction	*Measured Asph. Yield*	*RSM Asph.Yield*	*AAD*
0.502	0.0054	0.0064	0.0009
0.748	0.0645	0.0783	0.0138
0.856	0.0933	0.0945	0.0012
0.926	0.1015	0.0976	0.0039
		Average	0.0050

Table A.40. Average absolute deviation between measured and model results for asphaltene yield from 26845 heavy fraction

Heptane Mass fraction	*Measured Asph. Yield*	*RSM Asph.Yield*	*AAD*
0.412	0.0060	0.0110	0.0050
0.499	0.0569	0.0580	0.0011
0.667	0.1070	0.1175	0.0105
0.751	0.1475	0.1278	0.0197
0.834	0.1514	0.1337	0.0177
0.908	0.1437	0.1356	0.0081
0.952	0.1411	0.1342	0.0070
		Average	0.0099

Appendix B. Additional Data on the Effect of Temperature on Asphaltene Molecular Weight

B.1. Effect of Temperature on Average Molecular Weight

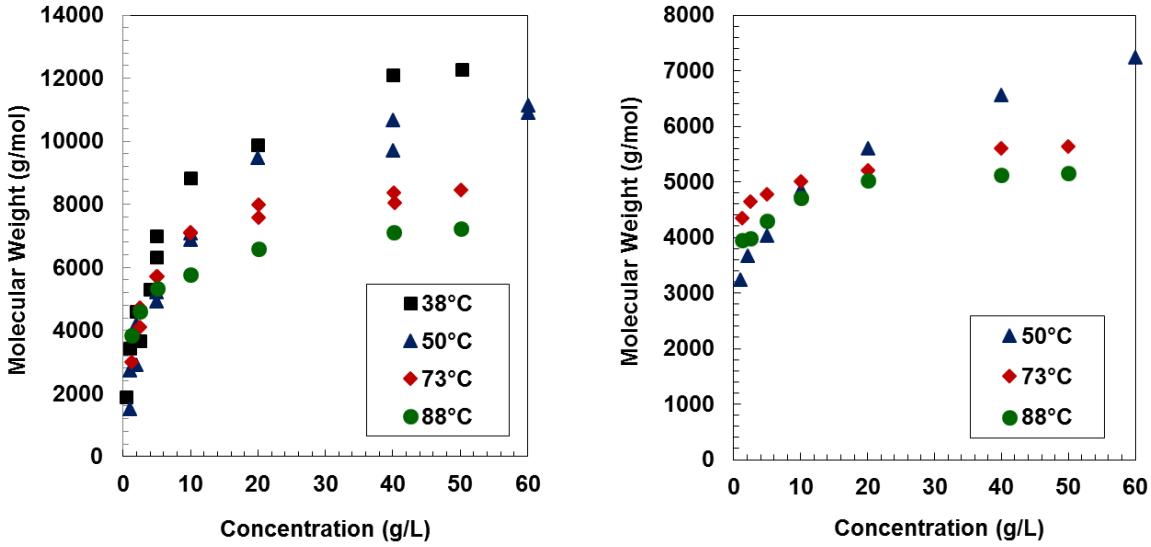

Figure B.1. Effect of temperature on molecular weight measurements for C7-asphaltenes from: a) WC-B-C1; b) WC-SR-A3.

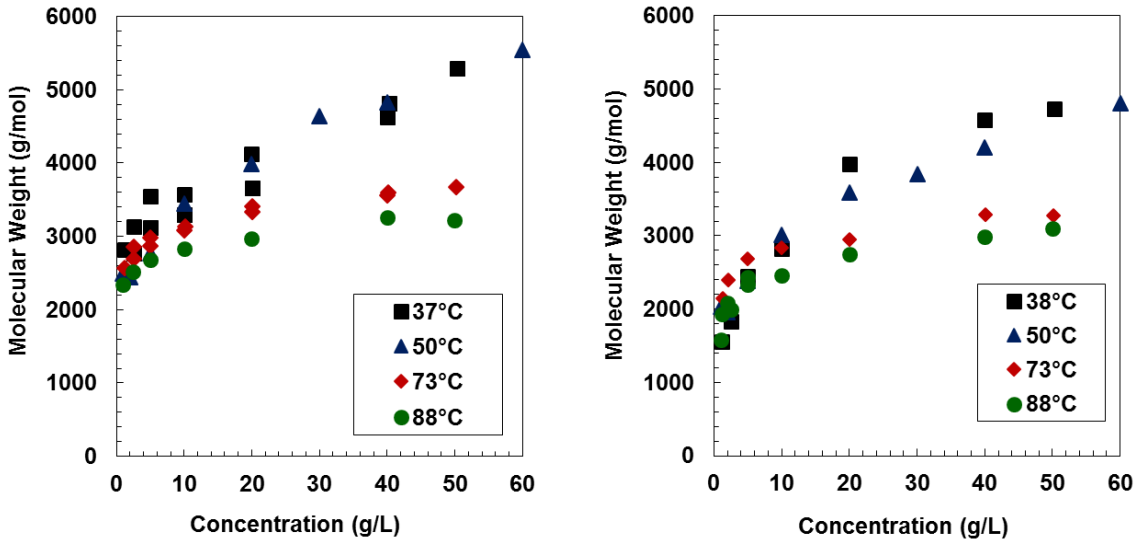

Figure B.2. Effect of temperature on molecular weight measurements for C7-asphaltenes from: a) X-1357; b) X-1359.

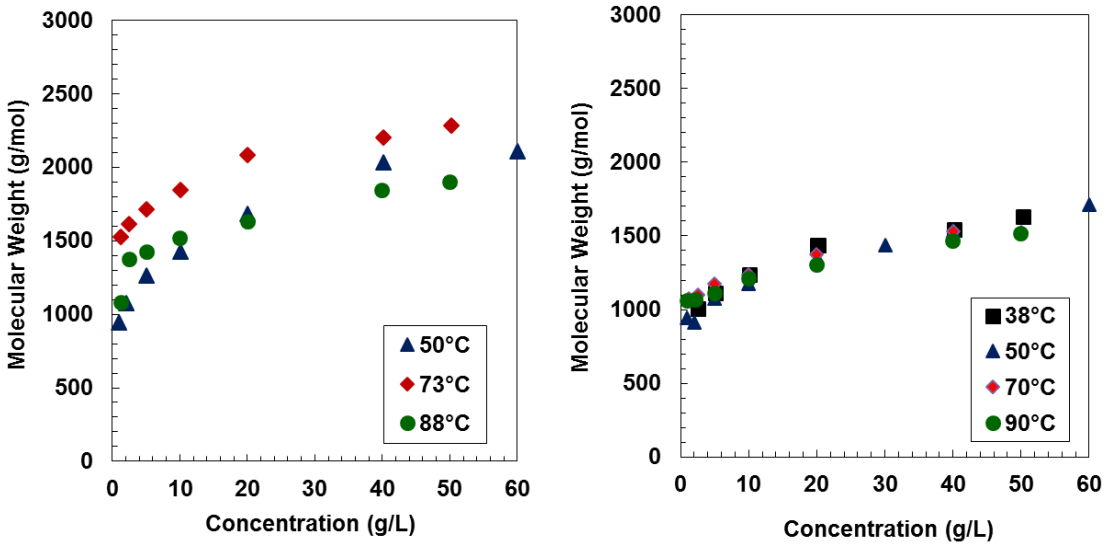

Figure B.3. Effect of temperature on molecular weight measurements for C7-asphaltenes from: a) RHC-18-19; b) HOS Bottoms.

B.2.Effect of Temperature on Molecular Weight Distributions

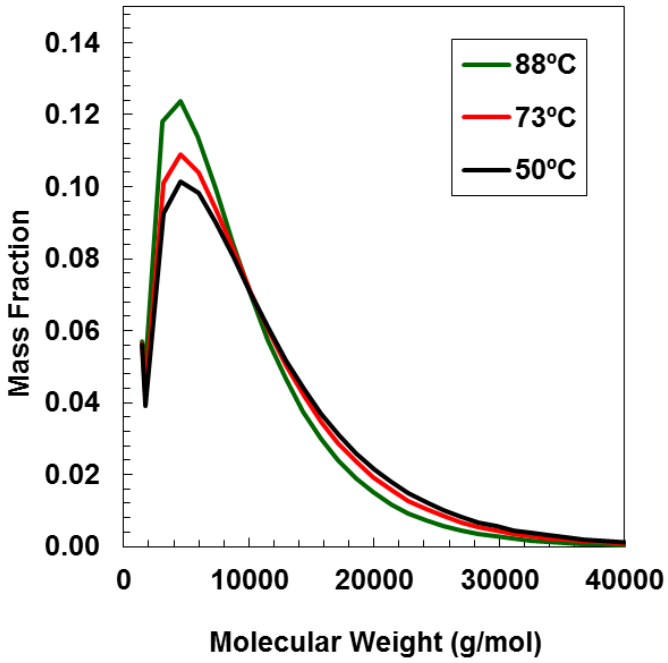

Figure B.4. Effect of temperature on the molecular weight distribution of C7-asphaltenes from WC-SR-A.

Appendix C. Additional Solubility Data and Model Results for Asphaltenes in Heptol Mixtures

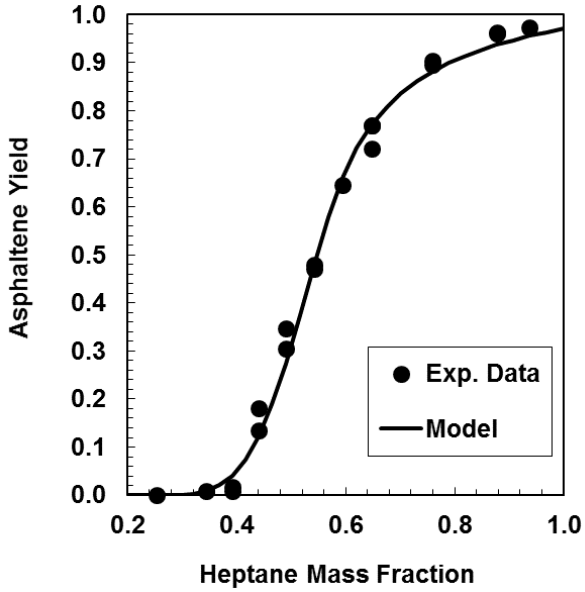

Figure C.1. Fractional precipitation of Cold Lake asphaltenes in heptol solutions at 20°C and atmospheric pressure (Exp. Data from Akbarzadeh *et al*. (2005))

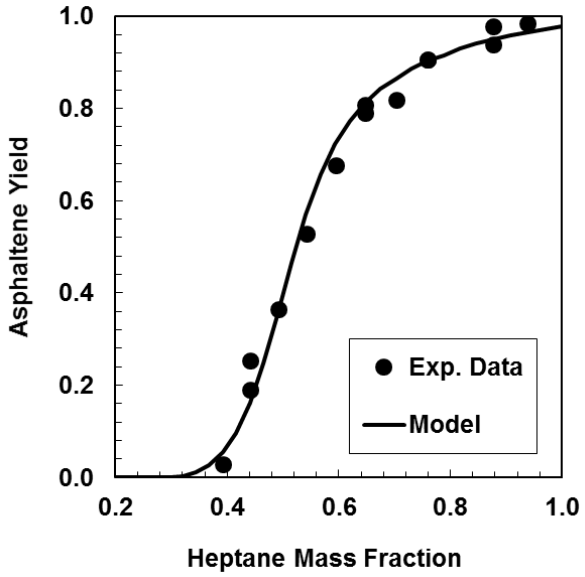

Figure C.2. Fractional precipitation of Lloydminster asphaltenes in heptol solutions at 20°C and atmospheric pressure (Exp. Data from Akbarzadeh *et al*. (2005)).

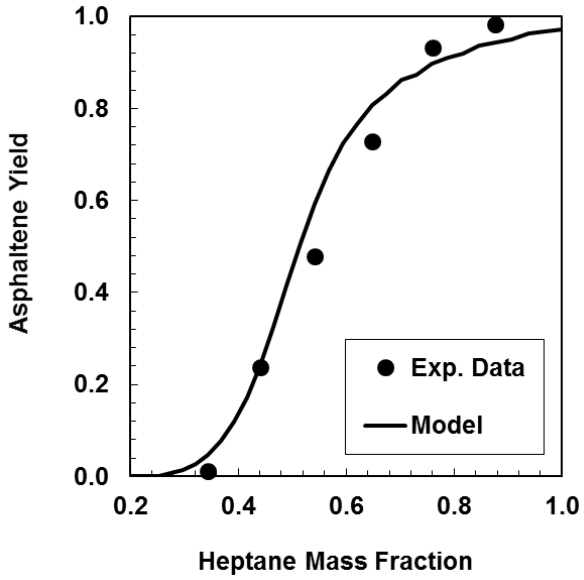

Figure C.3. Fractional precipitation of C7 Venezuela 1 asphaltenes in heptol solutions at 20°C and atmospheric pressure (Exp. Data from Akbarzadeh *et al*. (2005)).

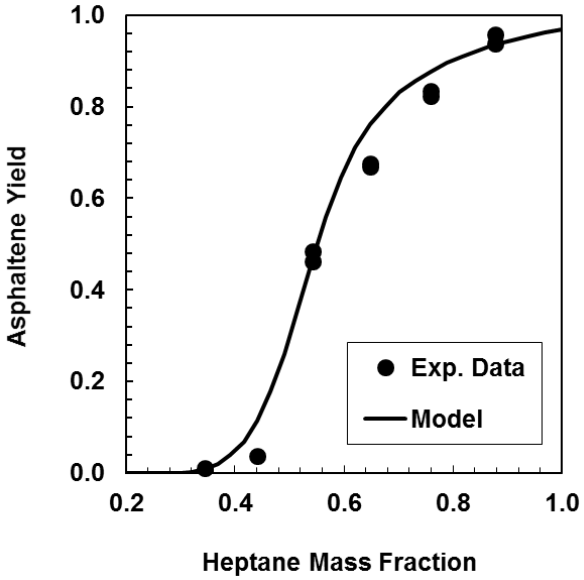

Figure C.4. Fractional precipitation of C7 Venezuela 2 asphaltenes in heptol solutions at 20°C and atmospheric pressure (Exp. Data from Akbarzadeh *et al*. (2005)).

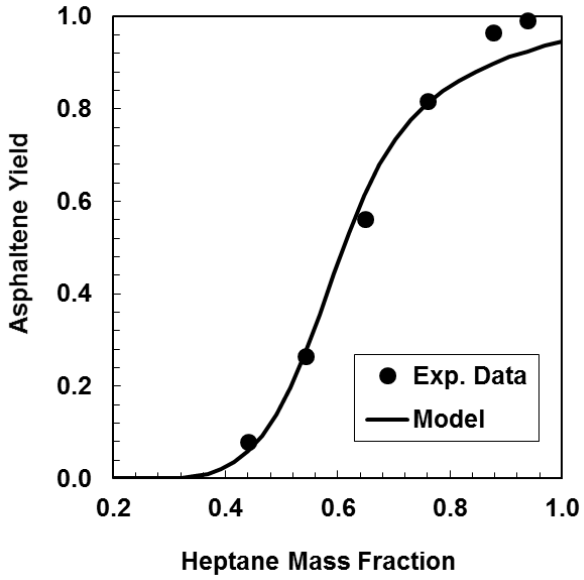

Figure C.5. Fractional precipitation of C7 Russia asphaltenes in heptol solutions at 20°C and atmospheric pressure (Exp. Data from Akbarzadeh *et al*. (2005)).

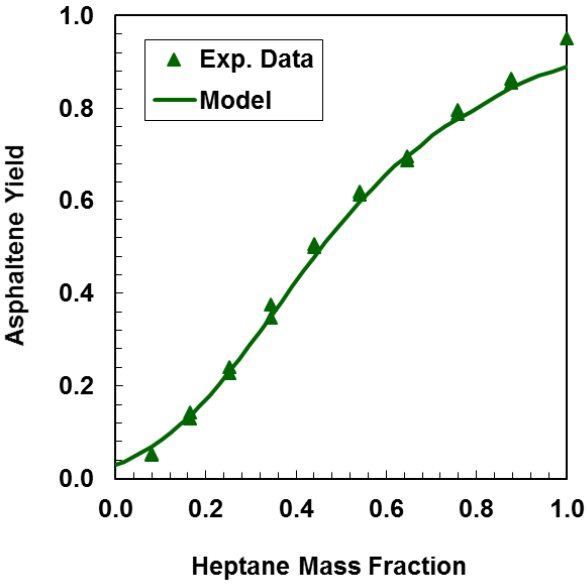

Figure C.6. Fractional precipitation of C7 X-1359 asphaltenes in heptol solutions at 20°C and atmospheric pressure.

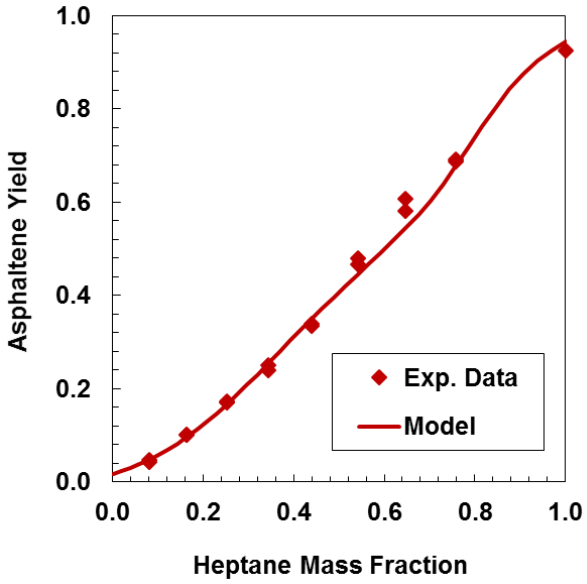

Figure C.7. Fractional precipitation of C7 RHC-19-03 asphaltenes in heptol solutions at 20°C and atmospheric pressure.

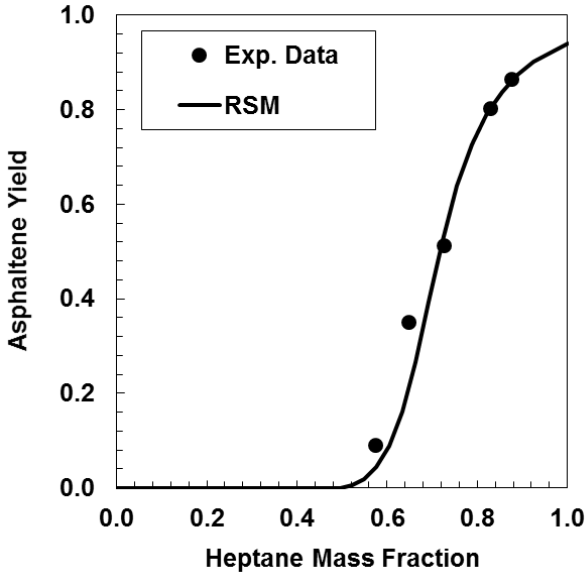

Figure C.8. Fractional precipitation of C7 27-168-179 asphaltenes in heptol solutions at 20°C and atmospheric pressure.

Appendix D. Additional Sensitivity Analysis Plots for the Uncertainty of Solubility Parameter of Saturates and Aromatics

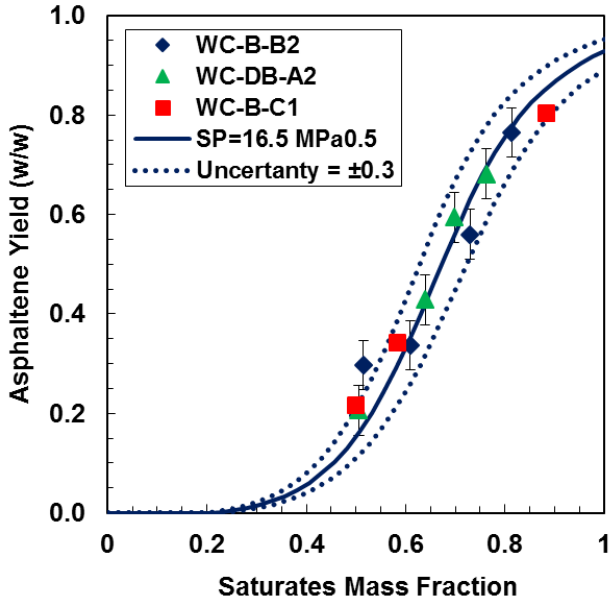

Figure D.1. Fractional asphaltene precipitation of 10 g/L solutions of asphaltenes from WC-C-B2 bitumen in toluene and various saturates from native at 21°C and atmospheric pressure and regular solution model predictions.

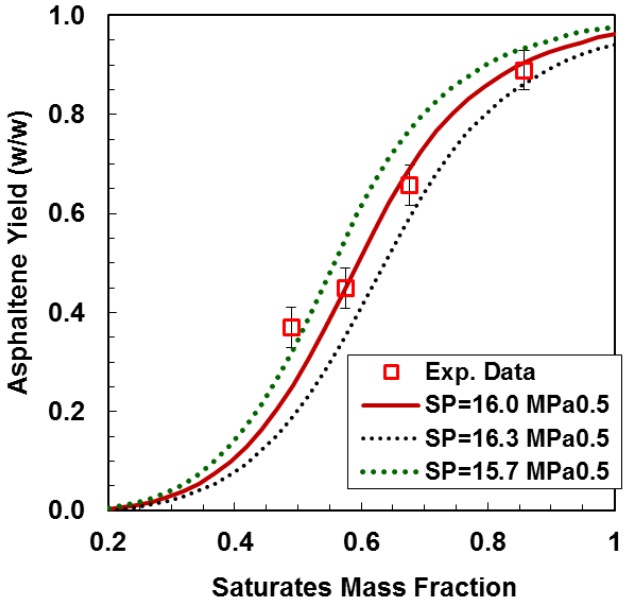

Figure D.2. Fractional asphaltene precipitation of 10 g/L solutions of asphaltenes from WC-C-B2 bitumen in toluene and saturates from 27034-113 at 21°C and atmospheric pressure and regular solution model predictions.

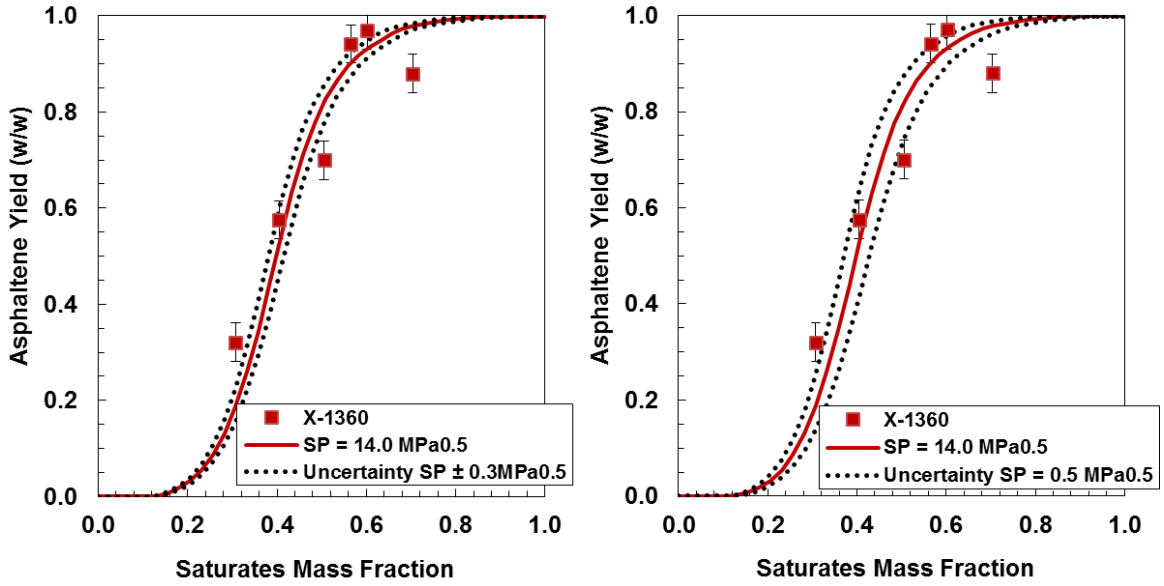

Figure D.3. Fractional asphaltene precipitation of 10 g/L solutions of asphaltenes from WC-C-B2 bitumen in toluene and saturates from X-1360 at 21°C and atmospheric pressure and regular solution model predictions with uncertainty of a) ±0.3MPa$^{0.5}$ and b)0.5MPa$^{0.5}$.

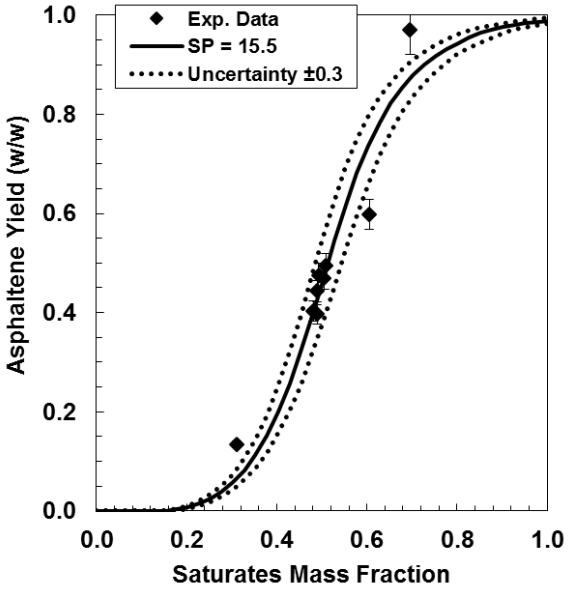

Figure D.4. Fractional asphaltene precipitation of 10 g/L solutions of asphaltenes from WC-C-B2 bitumen in toluene and saturates from HOS Bottoms at 21°C and atmospheric pressure and regular solution model predictions.

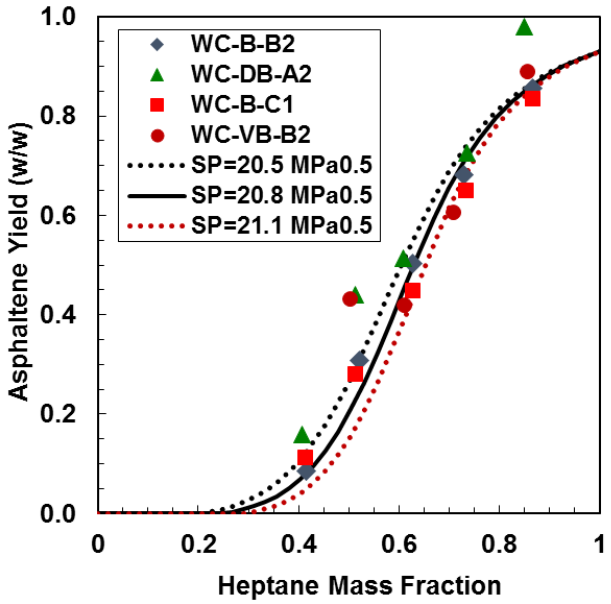

Figure D.5. Fractional asphaltene precipitation of 10 g/L solutions of asphaltenes from WC-C-B2 bitumen in toluene and various aromatics from native at 21°C and atmospheric pressure and regular solution model predictions.

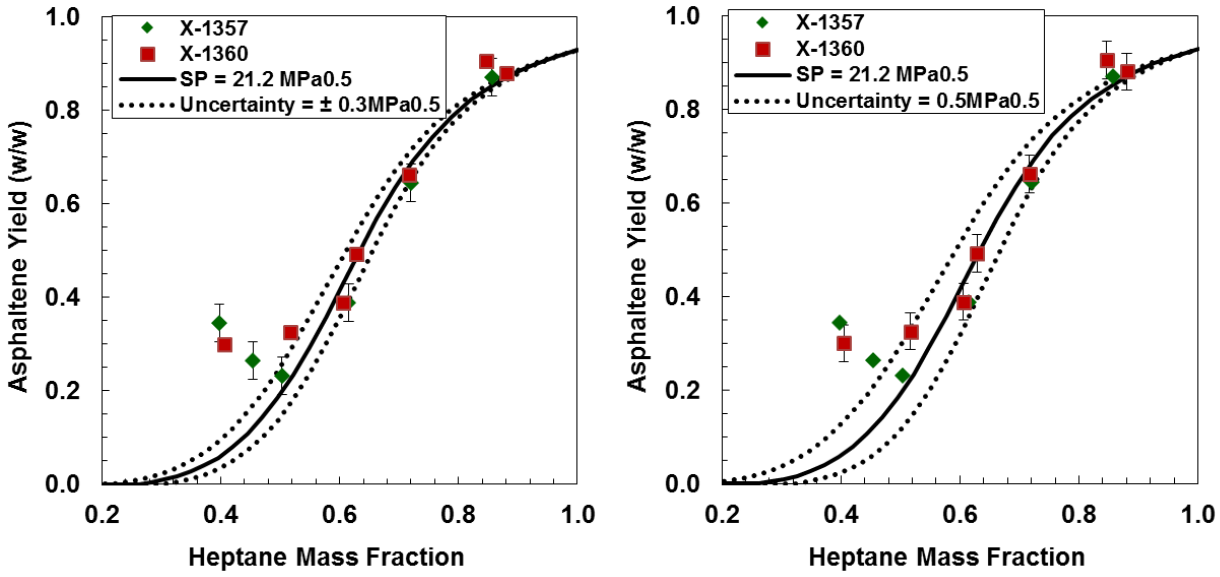

Figure D.6. Fractional asphaltene precipitation of 10 g/L solutions of asphaltenes from WC-C-B2 bitumen in toluene and aromatics from X-1357 and X-1360 at 21°C and atmospheric pressure and regular solution model predictions with uncertainty of a) ±0.3MPa$^{0.5}$ and b)0.5MPa$^{0.5}$.

Appendix E. Additional Solubility Data and Model Results for Native Oils with Heptane.

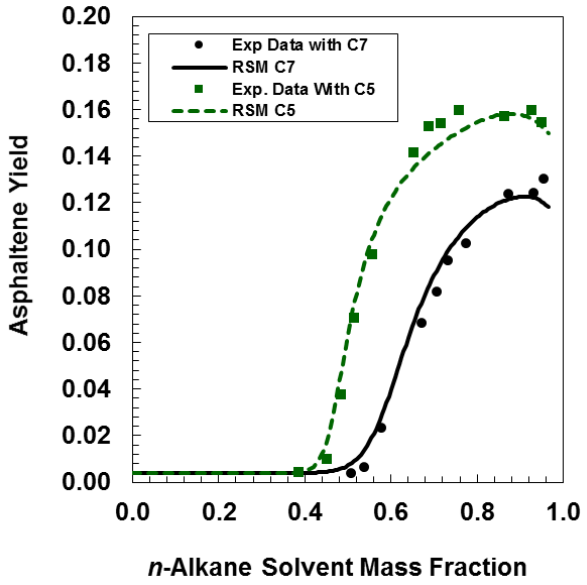

Figure E.1. Asphaltene yield and model results and predictions for Lloydminster crude oil diluted with *n*-heptane (black dots) and n-pentane and *n*-pentane (green squares) at 20°C. (Exp. Data from Akbarzadeh *et al*. (2005)).

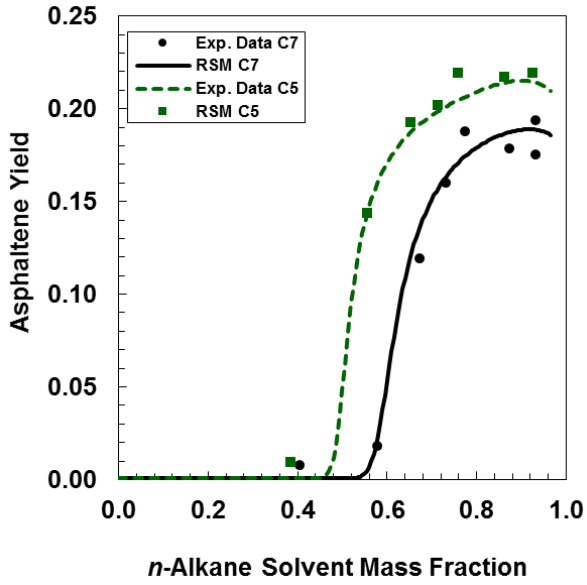

Figure E.2. Asphaltene yield and model results and predictions for Venezuela 2 crude oil diluted with *n*-heptane (black dots) and n-pentane and *n*-pentane (green squares) at 20°C. (Exp. Data from Akbarzadeh *et al*. (2005)).

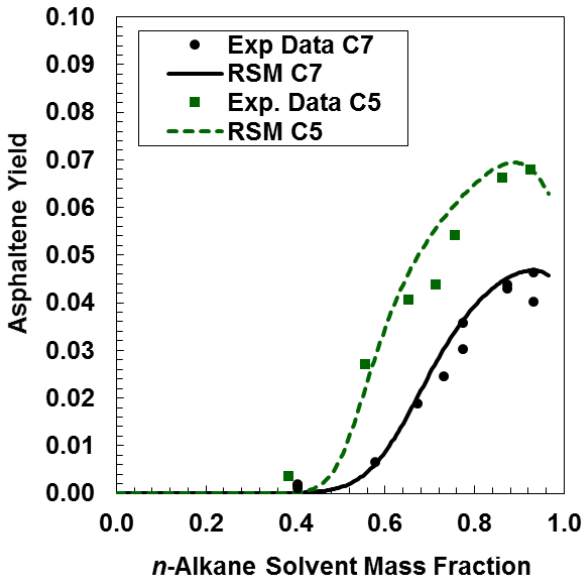

Figure E.3. Asphaltene yield and model results and predictions for Russia crude oil diluted with *n*-heptane (black dots) and n-pentane and *n*-pentane (green squares) at 20°C. (Exp. Data from Akbarzadeh *et al*. (2005)).

Appendix F. Additional Solubility Data and Model Results for Whole Crude Oils with Distillables

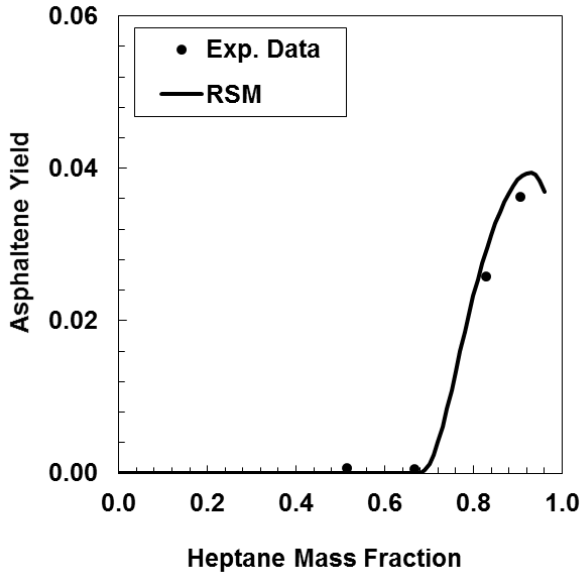

Figure F.1. Asphaltene yield for WC-DB-A3 whole crude oil diluted with n-heptane at 20°C: l at 20°C and atmospheric.

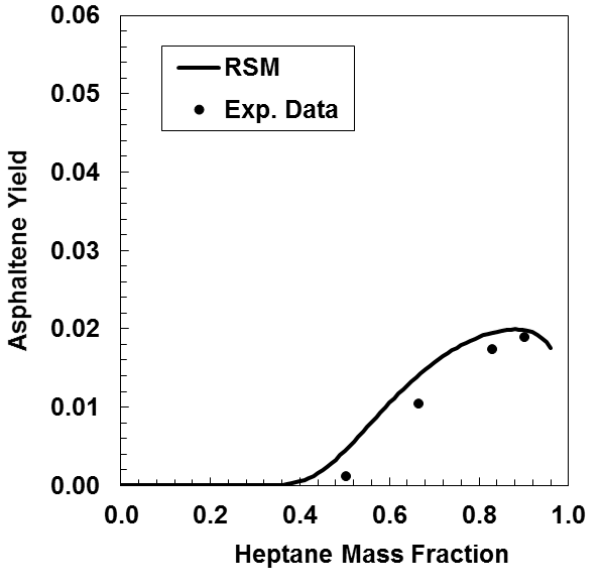

Figure F.2. Asphaltene yield for 27-168-179 whole crude oil diluted with n-heptane at 20°C: l at 20°C and atmospheric.

Appendix G. Relationships between SARA Properties

G.1 Correlations between Refractive Index, Density, and Molecular Weight

Refractive index, density and molecular weight are related thought the Lorentz-Lorenz equation (Eq. 2-12). Vargas *et al.* (2010) plotted the molar refraction of alkanes, alkylbenzenes, alkylnapthalenes and some polyaroamtic hydrocarbons with respect to their molecular weights; they observed a clear linear trend with a slope of about 1/3. Interestingly, when the molar refraction of saturates, aromatics and resins from this work are added to this plot, these fractions approximately followed the same linear trend, Figure G-1. Vargas refers to this linear trend as the one-third rule. Figure G-2 includes asphaltenes in the same plot of molar refractivity as a function of molecular weight. Figure G-2a and b show the molar refractivity calculated using an associated molecular weight (MW at 60 g/L) and using the monomer molecular weight respectively. It seems that the monomer molecular weight is more appropriate to calculate the molar refractivity; this observation suggests that the refractive index may not be affected by self-association.

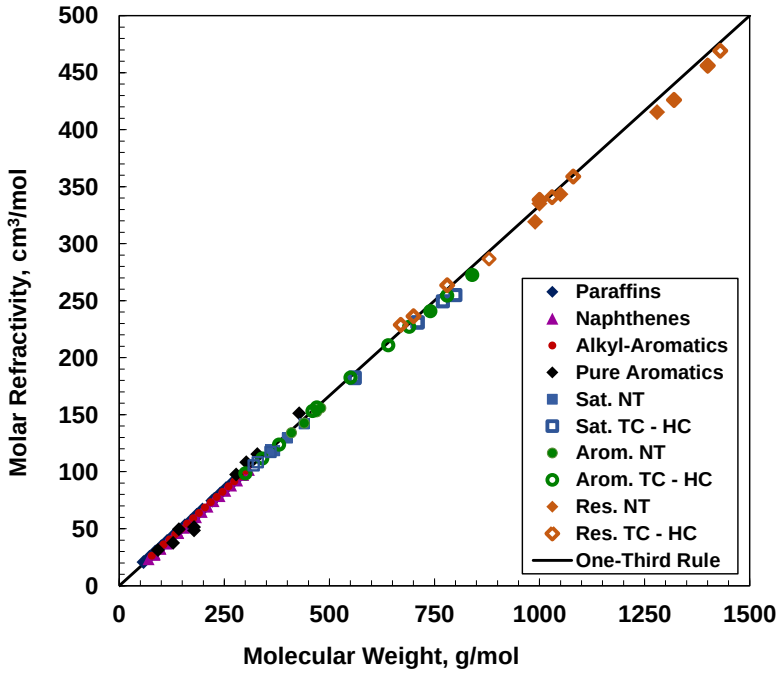

Figure G-1. Molar refraction of hydrocarbon fractions as function of molecular weight.

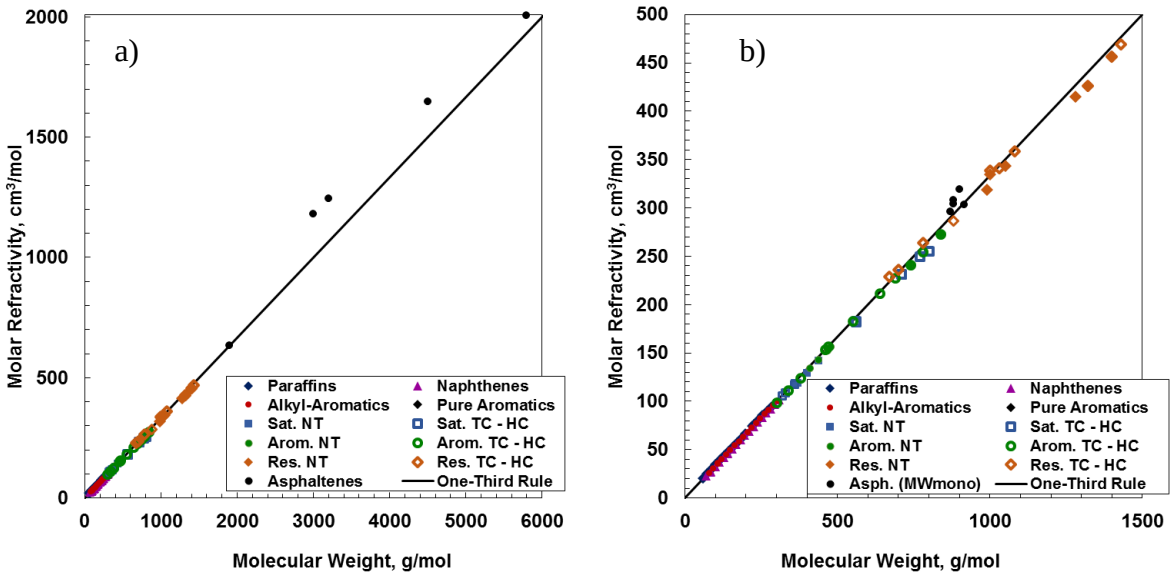

Figure G-2. Molar refraction of hydrocarbon fractions including asphaltenes using: a) associated molecular weight; b) monomer molecular weight.

Note, the one-third rule implies that the ratio of FRI to density is a constant equal to 1/3; if either FRI or density is known, the other can be calculated. Vargas *et al*. (2010) found that this rule applies to several crude oil samples. Figure G-3 shows that the FRI to density ratio for pure hydrocarbons and the SAR fractions has some scatter in comparison with the one-third rule (FRI/ρ =0.333, black line in Figures G-3). When the one third rule is used to predict the refractive index using density, the absolute average deviations (AAD) in refractive index (n_D) predictions are 0.0143, 0.0124, and 0.0152 for saturates, aromatics, and resins respectively. The refractive index for the SAR fractions were over-predicted for native and thermocracked fractions and underpredicted for all the hydrocracked and 27-168-179 resins. Note that the latter sample is suspected to be a hydrotreated sample due to its low sulphur content. Despite the one-third rule allows having close predictions of refractive indexes, the error in the second and third significant figure of the predictions are significant, particularly when the RI values are used to calculate other properties such as solubility parameters.

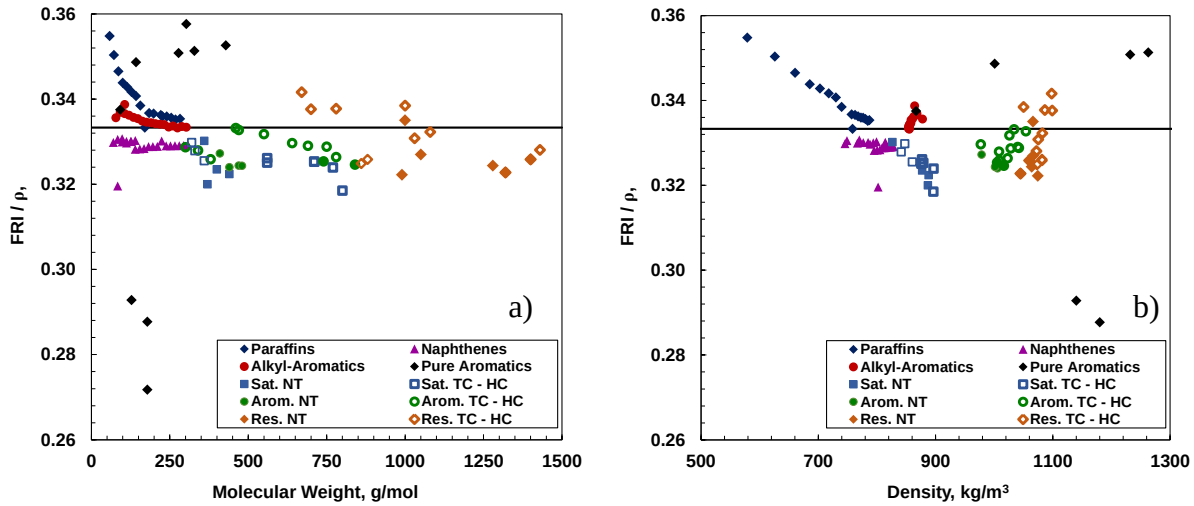

Figure G-3. FRI to density ratio for pure hydrocarbons and SAR fractions. Line indicates the "one-third-rule".

Okafor (2013) showed that FRI and density at 20°C for SAR fractions from native oils correlate very well and proposed a preliminary correlation as follows,

$$FRI_{20} = 0.5141 - 0.7745\rho + 0.5843\rho^2 \qquad \textbf{G-1}$$

The database has been updated including the data for the SAR fractions from reacted oils (thermocracked and hydrocracked) as well as asphaltenes and a few distillation cuts (Sanchez-Lemus 2014). There is a close correlation between FRI and density for all of these fractions, Figure G-4, and a new expression is proposed as follows,

$$\boldsymbol{\rho_{20^oC} = -6800 FRI^2_{20^oC} + 7270 FRI_{20^oC} - 650} \qquad \textbf{G-2}$$

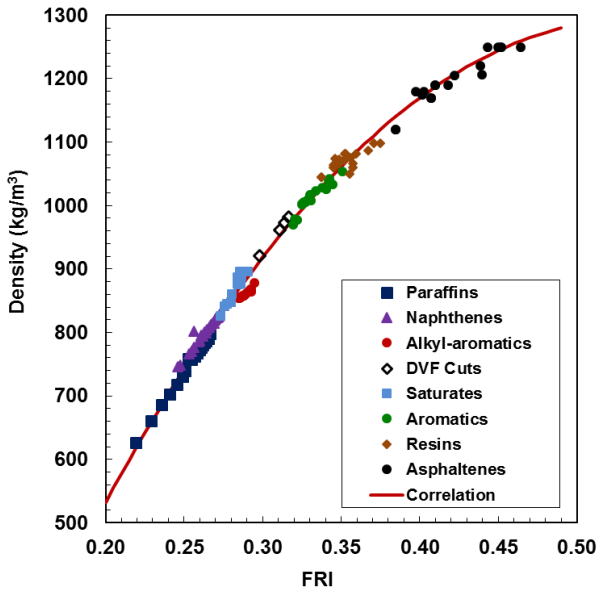

Figure G-4. Density as function of FRI at 20°C for different hydrocarbon fractions.

Table G-1 shows the deviations between experimental data and the predictions from Equation G-2 for the different hydrocarbon chemical families. The correlation predicts densities with an overall AAD less than 20 kg/m³ or RI with an AAD less than 0.0050. Equation G-2 provides a better correlation between density and RI than the one-third rule.

Table G-1. Average relative deviation and average absolute deviations for predictions of density and refractive index respectively using Equation 9-2.

Compounds	**AARD % Density**	**AAD RI**
Paraffins	0.96	0.0023
Olefins	1.96	0.0044
Alkyl-aromatics	2.3	0.0075
Naphthenes	1.1	0.0030
Saturates	1.0	0.0036
Aromatics	0.6	0.0030
Resins	1.3	0.0075
Asphaltenes	0.8	0.0091
DVF Cuts	1.0	0.0043

G.2. Density, RI, Molecular Weight, and Elemental Analysis of Chemical Families

When plotting density or FRI as function of molecular weight, a hydrocarbon "chemical map" is identified, Figures G-5a and G-5b. As expected, both density and FRI properties follow very similar trends for each chemical family. One difference is that saturates deviate from the paraffin/naphthene density trends, Figure 9-5a, but follow the paraffin/naphthene RI trend, Figure G-5b. Saturates are known to be mixtures of naphthenes and paraffins and it is not clear why the density trend deviates.

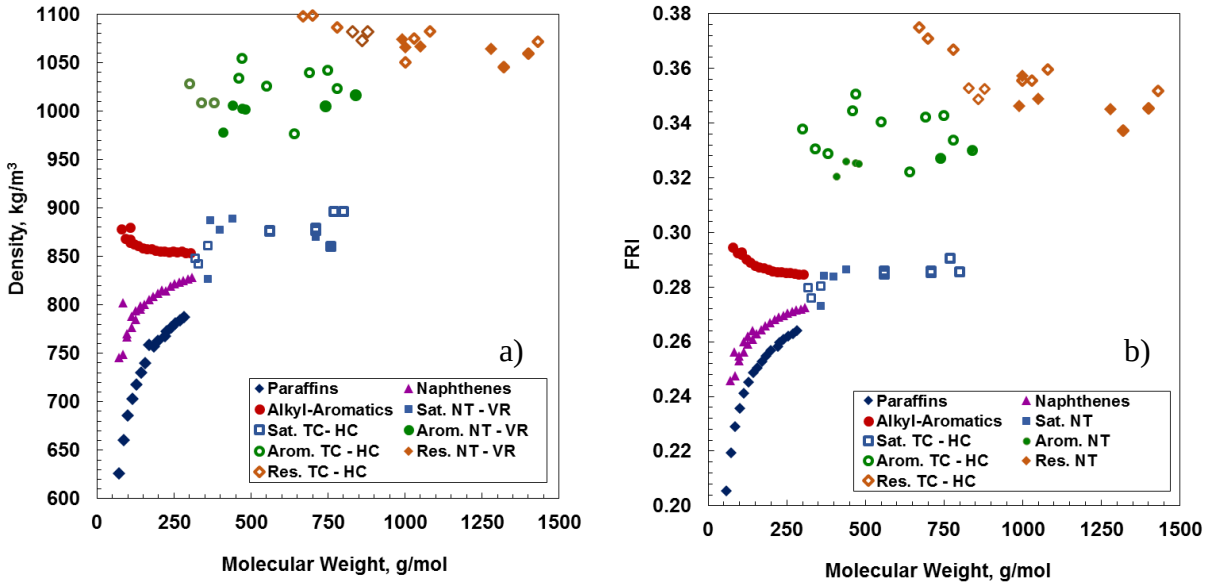

Figure G-5. a) Density at 20°C and b) refractive index at 20°C as function of molecular weight of different hydrocarbon families/fractions.

The same cross plots are shown for asphaltenes from native and reacted oils, Figures G-6a and G-7b. As expected, in both cases, the asphaltenes plot above the resins (higher density and FRI) and to the right of condensed aromatics (higher molecular weight), consistent with the large, aromatic structures. The high molecular weight shows the effect of self-association of asphaltenes. When asphaltenes are converted, their molecular weight decreases and density and FRI increases toward the trend of pure aromatic compounds. In other words, reaction tends to leave behind more condensed aromatic structures and to decrease the extent of asphaltene self-association.

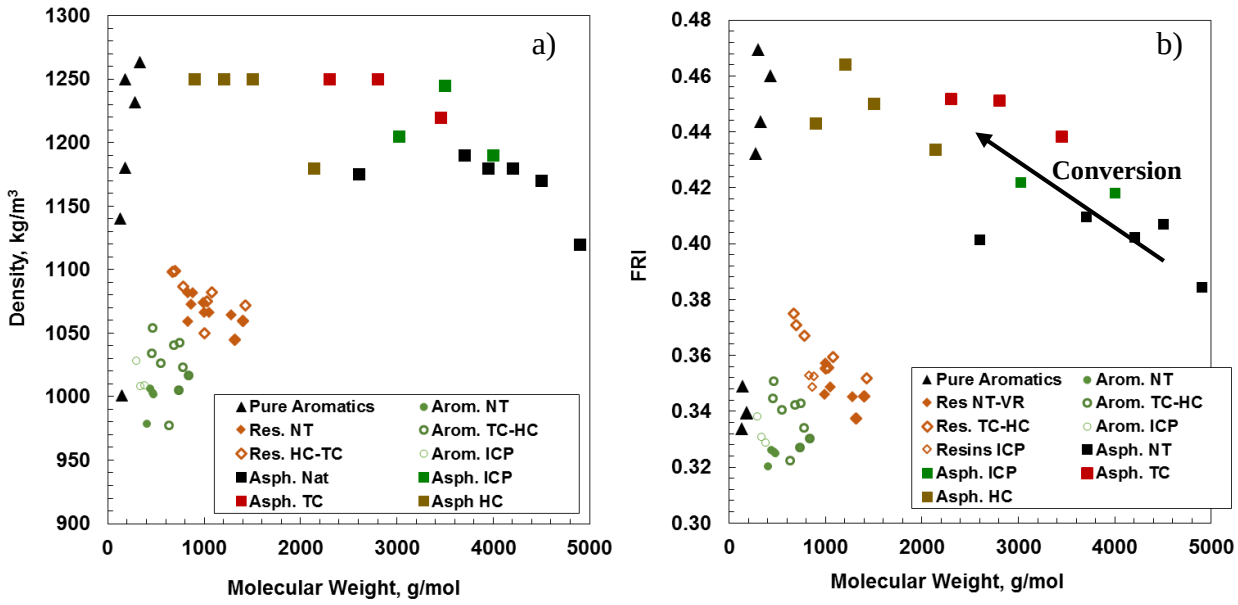

Figure G-6. a) Density at 20°C and b)FRI at 20°C as function of molecular weight for aromatics, resins and asphaltenes.

One way of distinguishing chemical families is the atomic H/C ratio. Figure G-7 shows that in general for the SARA fractions, the H/C ratio decreases linearly with density and FRI. The correlation with FRI, Figure G-7b, is better than with density, Figure G-7a. Figure G-8 shows that the FRI increases with conversion while the H/C ratio decreases with conversion for thermocracked and hydrocracked asphaltenes. In other words, the inverse relationship between FRI and H/C ratio also applies to reacted components (as can also be seen in Figure G-7b). A combination of properties should be tested to verify what the best combination of properties would be proper to use as indicators of reaction and further prediction of properties. Note, no correlatable relationship was observed between H/C ratio and molecular weight, Figure G-9.

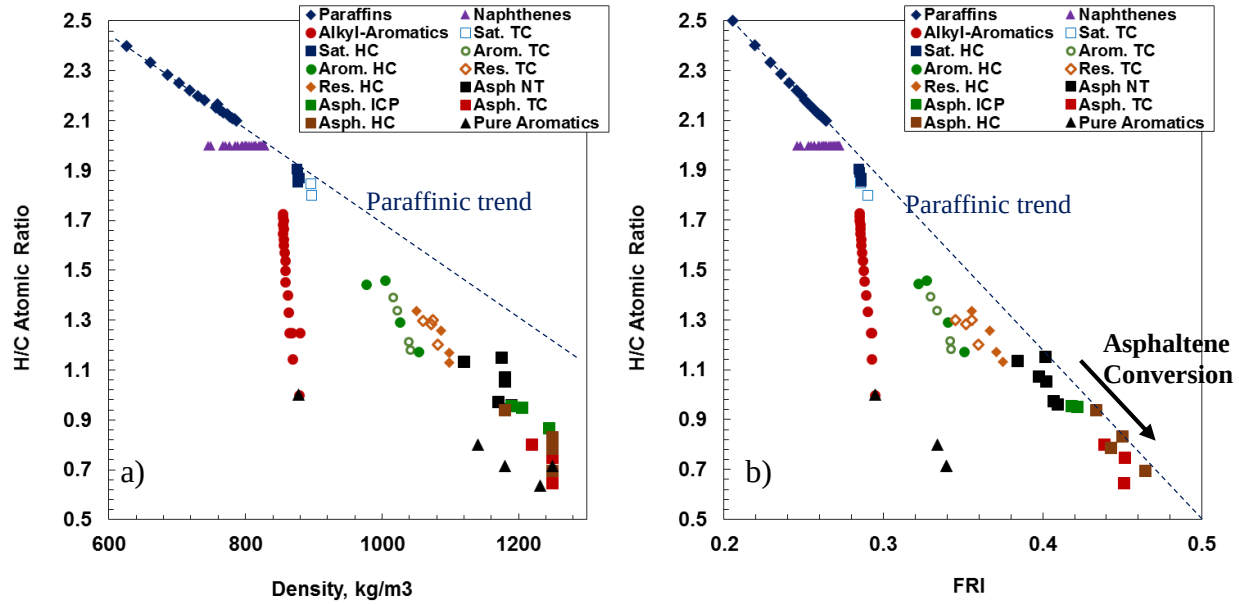

Figure G-7. H/C Atomic ratio as a function of density (a) and FRI (b) of hydrocarbon families and fractions.

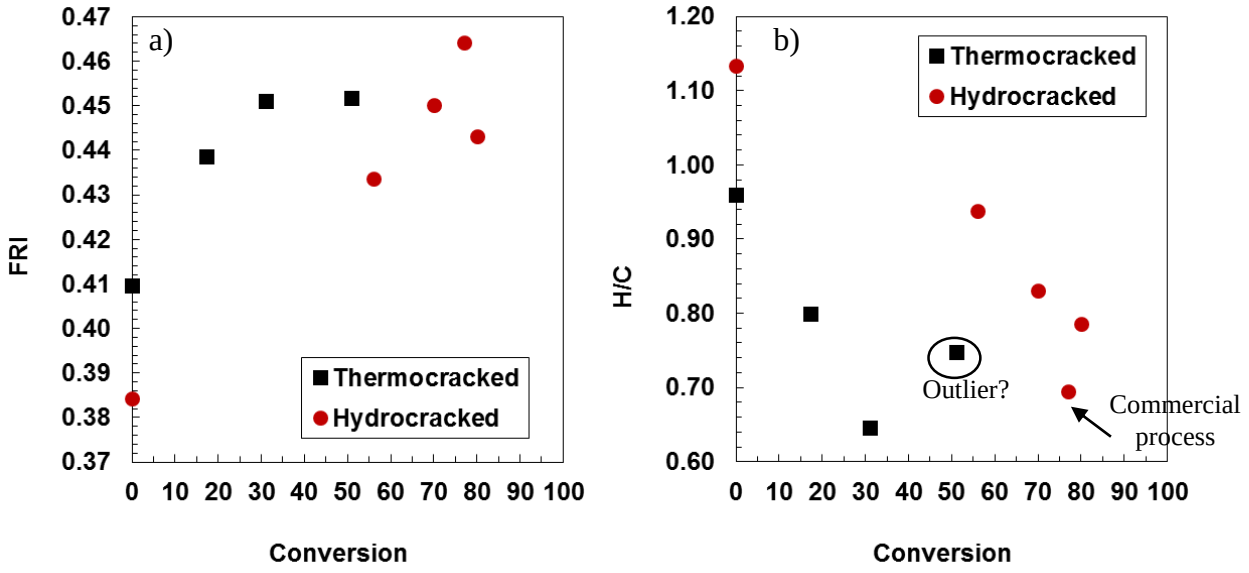

Figure G-8. FRI (a) and atomic H/C ratio (b) as a function of conversion for asphaltenes from thermocracked and hydrocracked samples.

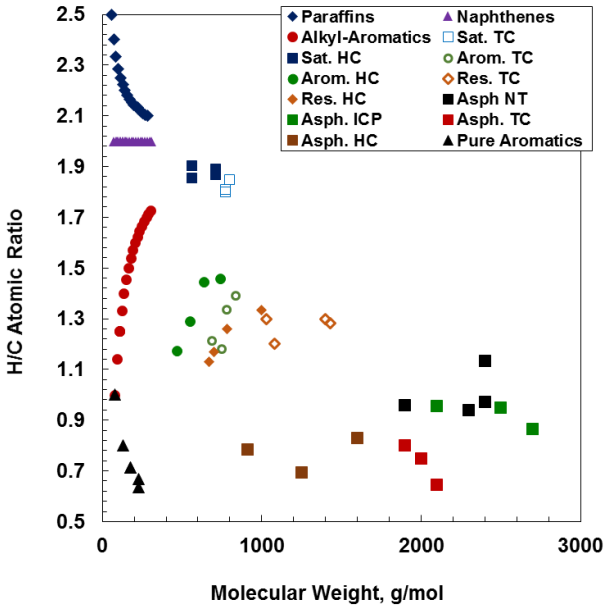

Figure G-9. H/C Atomic ratio as a function of molecular weight for hydrocarbon families and fractions.

Heteroatom content such as sulfur and nitrogen were also analyzed. Figures G-10 to G-11 show that there is no clear correlation between the heteroatom contents and molecular weight or FRI. Although not shown here, no correlation to density was observed either.

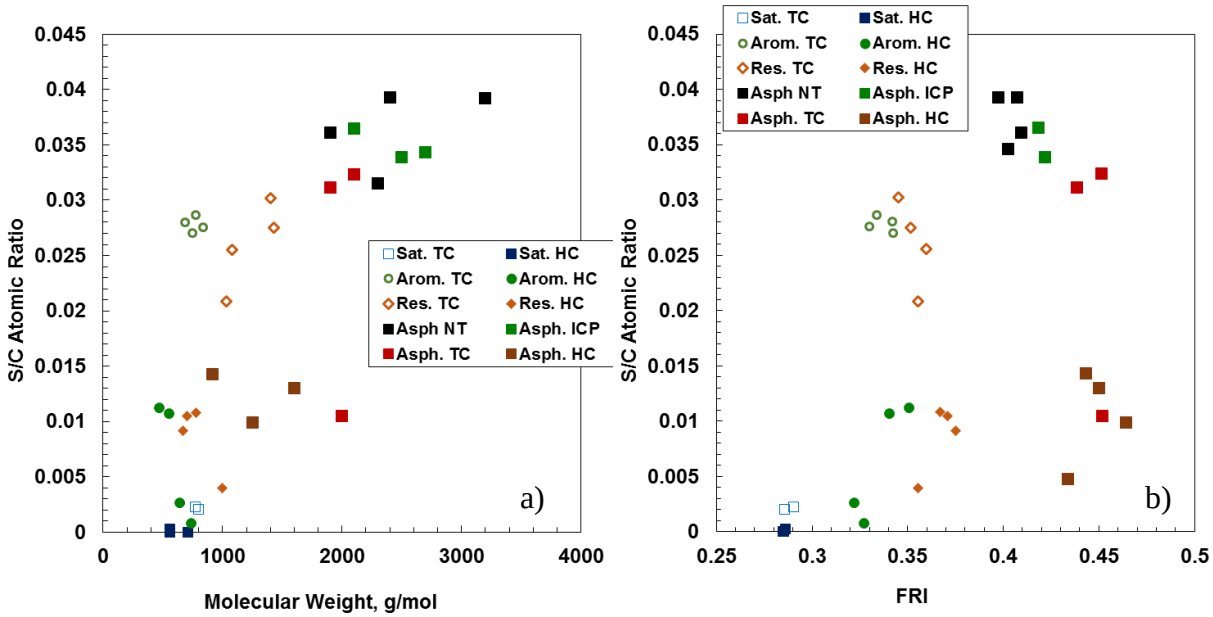

Figure G-10. S/C atomic ratio as function of molecular weight (a) and FRI (b) for SARA fractions.

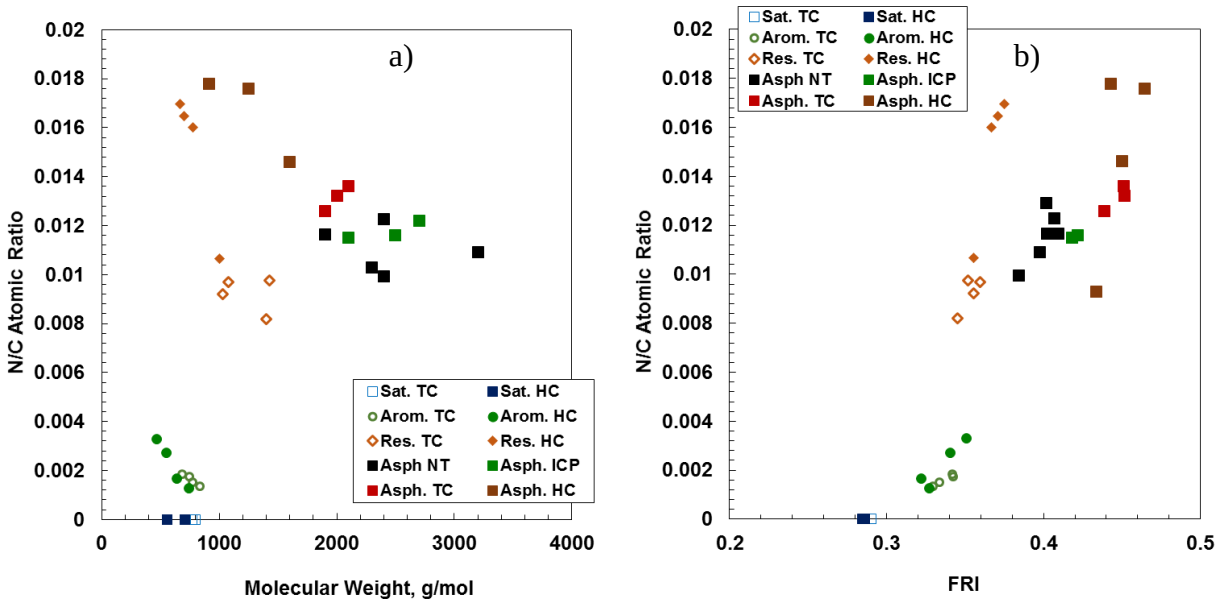

Figure G-11. N/C atomic ratio as function of molecular weight (a) and FRI (b) for SARA fractions.

G.3. Correlation of Asphaltene Solubility Parameter to Other Properties

This section focuses on the parameter *b* from the correlation for the apparent enthalpy of vaporization of asphaltenes (used to calculate the solubility parameter of asphaltenes). The b parameter is plotted against asphaltene density, RI, H/C ratio, resin molecular weight, and conversion in Figures G-12 to G-15, respectively. The b parameter correlates approximately to each of the other properties but not precisely enough for a useful correlation. It is recommended to evaluate a combination of property to build an accurate correlation.

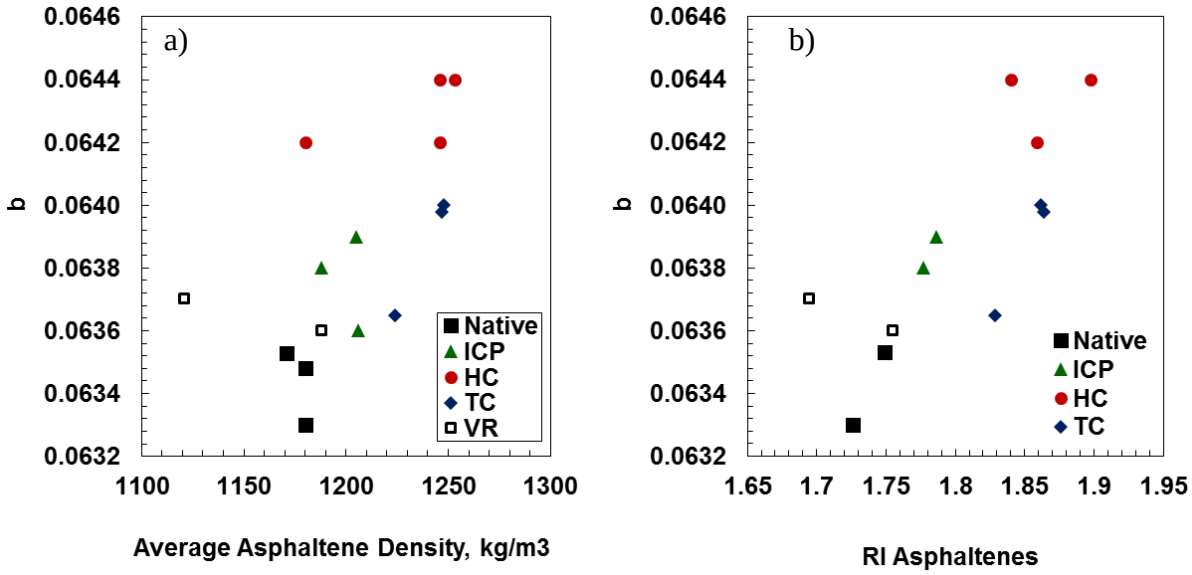

Figure G-12. Parameter *b* as function of: a) the average asphaltene density; b) refractive index.

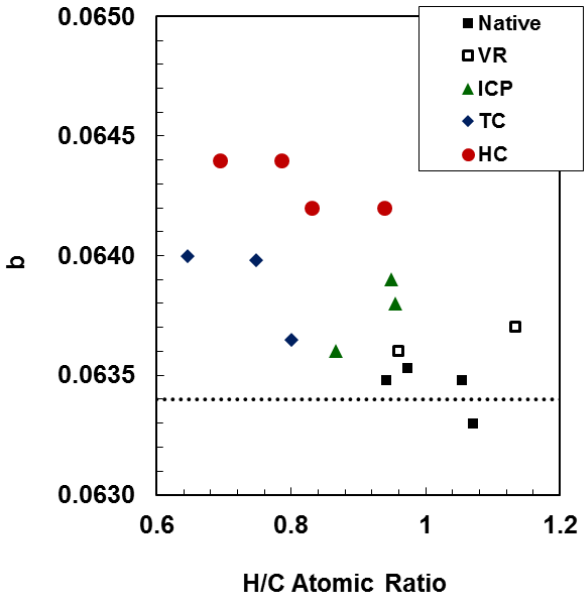

Figure G-13. Parameter *b* as a function of the asphaltene H/C atomic ratio.

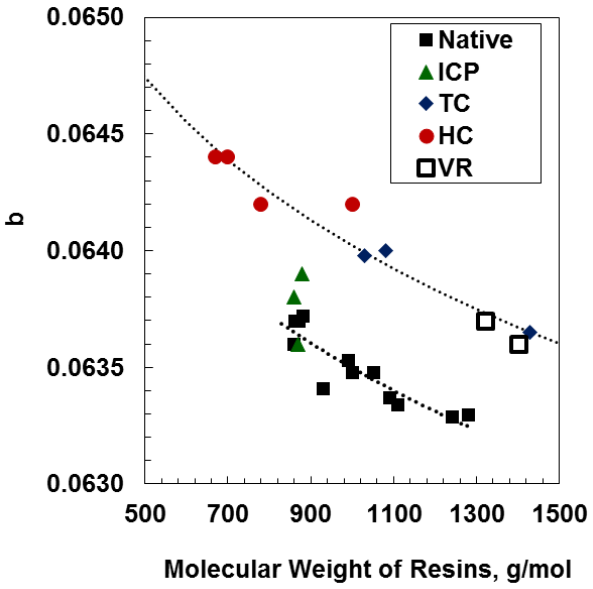

Figure G-14. Parameter *b* as a function of the molecular weight of the resins.

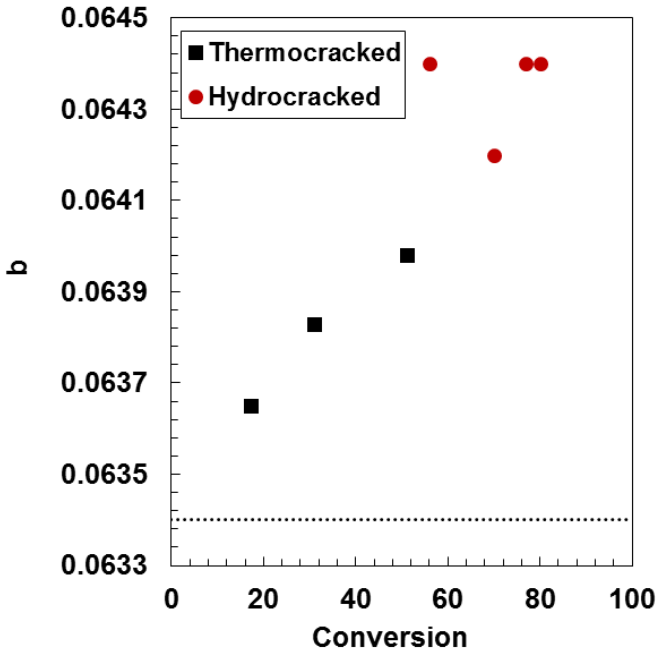

Figure G-15. Parameter *b* as a function of maltene conversion.

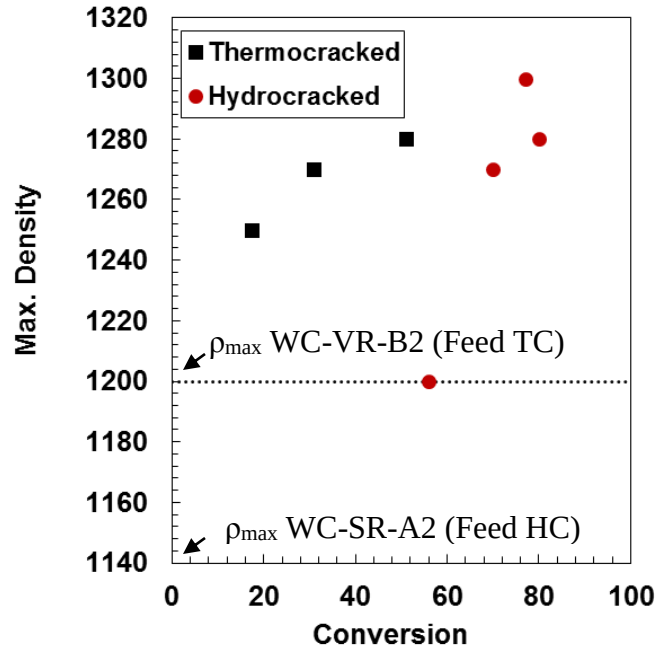

Figure G-16. Maximum density in asphaltene distribution as a function of maltene conversion.